Optimised investigation of radioactively contaminated land

By Peter D. Rostron

A thesis submitted for the degree of Doctor of Philosophy

School of Life Sciences
University of Sussex

Submitted June 2013.

Declaration

I hereby declare that this thesis has not been and will not be, submitted in whole or in part to another University for the award of any other degree.

The majority of the work presented in this thesis has been carried out by the author. The following exceptions apply:

a) Laboratory analysis of soil samples was carried out by trained personnel at a licensed laboratory on the case-study site.

b) In order to follow operational protocols, the acquisition of intrusive soil samples on the Dounreay site was carried out by certificated personnel, under direct supervision of the author.

Signature:…… (Peter Rostron)

UNIVERSITY OF SUSSEX
Peter D. Rostron

A thesis submitted for the degree of Doctor of Philosophy

"Optimised investigation of radioactively contaminated land"

Summary

Measurements of the radioactive content of environmental samples are potentially very costly, especially when these are made *ex situ* in a laboratory. A less expensive alternative is to acquire *in situ* measurements in the field. Both measurement types are subject to uncertainties, some of which arise from different sources depending on the measurement method used.

Surveys on radioactively contaminated land found that *in situ* measurements produced results that were as useful in satisfying the typical objectives of such surveys as *ex situ* measurements. The random component of analytical uncertainty estimated from duplicated *in situ* measurements was 2-4 times higher than would have been expected from Poisson statistics, however the sampling uncertainty (0-10 %) was found to be much lower than that for *ex situ* measurements (44-73 %). This resulted from the combined effects of high heterogeneity of the target radionuclide (^{137}Cs) in the ground, and the comparatively large primary sample mass associated with *in situ* measurements of gamma-emitting radionuclides. A large sampling mass also means that *in situ* measurements have an advantage in finding small hotspots of activity, although they may not provide sufficient resolution for spatially mapping lateral distributions of contaminants for remediation purposes. The degree of resolution can be readily changed in the field, however, by the simple expedient of changing the detector height. Experiments with an *in situ* detector close to the ground surface enabled the position of a small hotspot to be determined to within a few centimetres.

To evaluate activity concentrations in the soil, assumptions need to be made about the dimensions of the measured sample, and the distributions of activity within it. This requires some information that might be best obtained from *ex situ* measurements of excavated samples. However, well planned *in situ* surveys have the potential to significantly reduce the requirement for these expensive laboratory measurements. A new method of optimising the design of *in situ* surveys has been developed, based on a generic model for predicting the detector response to small particles of activity at different positions relative to the detector. The new mathematical model used by this method compares well with field measurements, and also with predictions made using a commercially available calibration program.

Acknowledgements

I would like to extend grateful thanks to the EPSRC and the Nuclear Decommissioning Authority for the joint funding of this project.

Thanks to my supervisors, Prof. Mike Ramsey of the University of Sussex and Dr. John Heathcote of Dounreay Site Restoration Ltd (DSRL). Particular thanks to Mike for his never ending academic support, great supervisory skills, and personal support when needed. A special thanks also to John for his patience while I have been on site, the use of his private property for some of my experiments, and his many suggestions of new avenues to explore.

Thanks to Dr. Patrick Chard of Canberra Inc. for his help with resolving computer modelling issues.

Thanks also to Prof. Tom Fearn of University College London, for his helpful advice on certain aspects of robust ANOVA calculations.

I would also like to thank the following staff at DSRL:

Tanya Favus, whose preparatory work, organisational skills, help and advice was absolutely essential to the project.

Simon Copsey, who put up with my many requests for logistical support during my three extended site visits to Dounreay.

Mark Alexander, Robert Spence, and Sanders MacDonald of the Non-Destructive Assay team, for their patience, technical support and advice, and for ensuring that I had the equipment that I needed.

Avril Cormack and Philip Ross, for their practical help in transporting and setting up of equipment and decontamination units.

Jason Bonniface and Nicky Moloney, for their assistance with positioning equipment and geographical mapping.

The Health Physics team, who not only checked me out of barriered areas twice a day, but who inspired me in my weekend explorations of the history of Caithness and Sutherland.

Dr Jeremy Andrew and the team at the Dounreay on-site laboratory facilities.

And the many others, too numerous to mention, who, through their friendly and invaluable assistance, made these experiments possible.

Thanks also to Dr. Katy Boon and Dr. Jacqui Thomas, who gave me great encouragement, support and inspiration throughout my final year as an undergraduate, and also in the early stages of this project.

Contents

Declaration ..... **ii**

Summary ..... **iii**

Acknowledgements ..... **iv**

Contents ..... **v**

List of figures ..... **xi**

List of tables ..... **xix**

List of acronyms ..... **xxiii**

Glossary of terms ..... **xxv**

Chapter 1 – Introduction **1**

1.1 Introduction to this research 1

1.2 Objectives of this research 5

1.2.1 Overall aim 5

1.2.2 Specific research objectives 5

1.3 Structure of the thesis 6

Chapter 2 – Literature review and introduction to radiation measurement **8**

2.1 Introduction to Chapter 2 8

2.2 Current legislation of radioactively contaminated land 8

2.2.1 Legislation in the USA 8

2.2.1.1 Data Quality Objectives (DQOs) 9

2.2.1.2 Multi-Agency Radiation Survey and Site Investigation Manual (MARSSIM) 10

2.2.2 European Legislation 11

2.2.3 Legislation in the UK 13

2.2.4 Threshold values of radionuclides (UK) 14

2.3 Characterisation of contaminated land 16

2.3.1 Defining the quantity to measure in investigations of radioactively contaminated land 16

2.3.2 Definitions of measurement uncertainty 19
2.3.3 The contribution of sampling uncertainty to the total uncertainty 20
2.3.4 Uncertainty estimation in contaminated land investigations 21
2.3.5 Evaluation of heterogeneity in contaminated land investigations 26
2.3.6 Fitness-for-purpose (FnFP) in contaminated land investigations 28
2.4 Introduction to the measurement of radiation 29
2.4.1 The origins of ionising radiation 29
2.4.2 Measurement of ionising radiation 31
2.4.3 Efficiency calibration of gamma detectors 37

Chapter 3 - Cost effective, robust estimation of measurement uncertainty from sampling using unbalanced ANOVA 39

3.1 Abstract 39
3.2 Introduction 39
3.3 Methods 44
3.3.1 Test 1 44
3.3.2 Test 2 45
3.4 Results 49
3.4.1 Test 1 results 49
3.4.2 Test 2 results 50
3.5 Conclusion 50

Chapter 4 - Advantages of *in situ* over *ex situ* radioactivity measurements for the characterisation of land on a decommissioning nuclear site. 53

4.1 Abstract 53
4.2 Introduction 53
4.2.1 Nuclear sites in the UK 53
4.2.2 Threshold values of radionuclides 54
4.2.3 Characterisation of radioactively contaminated land 54
4.2.4 Study objectives 56
4.3 Materials and methods 56
4.3.1The survey areas 56
4.3.2 Estimation of the random component of uncertainty 57

4.3.3 *In situ* measurement procedure 58
4.3.4 *Ex situ* measurement procedure 60
4.4 Results 62
4.4.1 Measurement uncertainty 62
4.4.2 ^{137}Cs Activity 62
4.5 Discussion 63
4.5.1 Comparison of *in situ* and *ex situ* samples 63
4.5.2 Random component of measurement uncertainty 66
4.5.3 Systematic differences between *in situ* and *ex situ* measurements 69
4.5.4 Shine from external sources 72
4.5.5 Identification of hotspots of activity 74
4.6 Conclusions 77
4.7 Colour photographs for Chapter 4 78

Chapter 5 - *In situ* detection of 'hot' particles by portable gamma-ray devices: modelling the effects of experimental parameters 79

5.1 Abstract 79
5.2 Introduction 79
5.2.1. Requirement for in situ particle detection in land areas 79
5.2.2 Optimisation of survey parameters for in situ particle detection 80
5.2.3 Developing a generic model for particle detection 83
5.2.4 Detection of a buried particle 85
5.2.5 Measurement uncertainty 87
5.2.6 Objectives 87
5.3 Methods 88
5.3.1 Field measurement apparatus and procedure 88
5.3.2 Uncertainty estimation 89
5.3.3 Source/detector geometry measurements 90
5.3.4 Interpretation of field measurements 90
5.3.5 Definition of ISOCS geometries 91
5.4 Results and discussion 91
5.4.1 Estimation of the random component of measurement uncertainty 91

5.4.2 Calibration of ISOCS and the generic model for zero offset 93
5.4.3 Calibration of the generic model for changing lateral offset..... 93
5.4.4 Determination of soil attenuation properties 96
5.4.5 Evaluation of the generic model and the ISOCS predictions of measured counts 97
5.4.6 Optimal source/detector geometry..... 101
5.5 Conclusions 102
5.6 Colour photographs for Chapter 5..... 103

Chapter 6 - Optimization of *in situ* measurement strategies for the characterisation of radioactively contaminated land that includes the presence of small particles..... 105

6.1 Abstract..... 105
6.2 Introduction 105
6.2.1 Survey design 105
6.2.2 Objectives..... 107
6.2.3 Detector coverage..... 107
6.2.4 Detector height 110
6.2.5 Particle depth..... 110
6.2.6 Estimation of counting time required to identify a small particle..... 111
6.3 Methods..... 116
6.3.1 The ROCLI program 116
6.3.2 Site background 117
6.3.3 Detection efficiencies..... 118
6.3.4 Standard inputs..... 119
6.3.5 Optimisation method..... 119
6.4 Results and discussion 121
6.5 Conclusions 125

Chapter 7 – Defining the test volume, and estimating the systematic component of uncertainty in *in situ* measurements. 126

7.1 Introduction to Chapter 7 126
7.2 Evaluating mass activity concentrations in land areas using portable *in situ* detectors 126
7.2.1 Evaluating mass activity concentrations: Introduction..... 126
7.2.2 Evaluating mass activity concentrations: Objectives..... 128

7.2.3 Evaluating mass activity concentrations: Methods 129
7.2.4 Evaluating mass activity concentrations: Results and discussion 129
7.2.5 Evaluating mass activity concentrations: Conclusions 131

7.3 High resolution surveys using portable *in situ* detection 132
7.3.1 High resolution surveys: Introduction 132
7.3.2 High resolution surveys: Objectives 132
7.3.3 High resolution surveys: Methods 132
7.3.4 High resolution surveys: Results and Discussion 135
7.3.5 High resolution surveys: Conclusions 137

7.4 Estimating the systematic component of measurement uncertainty in portable *in situ* measurements of land areas 139
7.4.1 Systematic uncertainty in *in situ* measurements: Introduction 139
7.4.2 Systematic uncertainty in *in situ* measurements: Objectives 140
7.4.3 Systematic uncertainty in *in situ* measurements: Methods 141
7.4.4 Systematic uncertainty in *in situ* measurements: Results 143
7.4.5 Systematic uncertainty in *in situ* measurements: Discussion 146
7.4.6 Systematic uncertainty in *in situ* measurements: Conclusions 148

Chapter 8 – Further discussion and synthesis of the experimental work in the context of the research objectives 150

8.1 Introduction to Chapter 8 150

8.2 Comparing the usefulness of *in situ* and *ex situ* measurement methods 150
8.2.1 Overview 151
8.2.2 Comparison of the random components of uncertainty 151
8.2.3 Heterogeneity of ^{137}Cs contamination 154
8.2.4 Uncertainty in the source characteristics of *in situ* measurements 155
8.2.5 Establishing traceability and bias in *in situ* measurements 158
8.2.5.1 Bias against a reference measurement target (RMT) 158
8.2.5.2 Bias against a reference point source 159
8.2.6 Systematic comparisons between *in situ* and *ex situ* measurements 160
8.2.7 Assessment of Fitness for Purpose (FnFP) of measurements 162
8.2.8 Standard error on the mean 163
8.2.9 Summary of comparison between *in situ* and *ex situ* measurement methods 165

8.3 Optimising the survey parameters of *in situ* investigations 166
8.3.1 Overview 166
8.3.2 Modelling the effects of experimental parameters 168
8.3.3 Optimisation of *in situ* surveys using the ROCLI method, and comparison with other methods. 169
8.4 Discussion of the findings of this project in a broader context 175

Chapter 9 – Conclusions and recommendations for further work 179

9.1 Introduction: innovative aspects of this research 179
9.2 Estimates of the random component of uncertainty. Effects of contaminant heterogeneity 180
9.3 Systematic differences between *in situ* and *ex situ* measurements 182
9.4 Reducing the cost of estimating the random component of uncertainty 183
9.5 Optimising the experimental parameters of full coverage *in situ* surveys 183
9.6 Evaluating the fitness for purpose (FnFP) of measurements 184
9.7 Comparisons between *in situ* and *ex situ* measurement methods 185
9.8 – Recommendations for future work 187
9.8.1 – Further development of the ROCLI method 187
9.8.2 – Characterisation of spatial distributions of radionuclides 187
9.8.3 – Traceability of *in situ* measurements 188
9.8.4 – Evaluation of uncertainty due to small scale heterogeneity in soil samples 190

References and bibliography 192

Appendix 1 (Table A1.1) - Raw data for U-RANOVA test 202

Appendix 2 (Tables A2.1 to A2.8) - Raw data from the Zone 12 and Barrier 31 surveys 207

Appendix 3 (Figs A3.1 to A3.3) – Regressions from detector modelling experiments 215

Appendix 4 (Tables A4.1 to A4.3) - Raw data from the RMT experiments 221

Appendix 5 – List of files on enclosed data disk. 224

Appendix 6 - List of presentations and publications 225

List of figures

Fig 2.1 Part of a gamma-ray spectrum obtained using a NaI 3”x3” detector on a land area at Dounreay (displayed using Genie 2000) and showing a clearly defined peak centered at an energy level of 662 keV (corresponding to the decay of ^{137m}Ba), with the associated Compton continuum. The Compton edge is not clearly seen in this spectrum, most likely because of the low resolution detector that was used. 35

Fig 3.1 The balanced experimental design, which can be used to estimate the sampling and analytical components of measurement uncertainty using the duplicate method. Two samples are taken at each primary sampling point, and each sample is chemically analysed twice (Ramsey and Ellison, 2007). 40

Fig 3.2 The unbalanced experimental design, where only one of the two samples from a duplicated primary sample undergoes duplicate analysis. This reduces the total number of chemical analyses required (Ramsey and Ellison, 2007). 42

Fig 3.3 Data extracts from the four trial populations used by Ramsey *et al.* (1992). For each trial the numbers shown represent measurements in μg g^{-1} of 15 out of a total of 100 sampling targets. The numbers were generated in such a way as to simulate measurements that might have been obtained using the balanced design (Fig 3.1). The boxed numbers are the outlying values, generated by adding a fixed number to the base population shown in Trial A. S1 = Sample 1, A1 = Analysis 1, etc. 46

Fig 3.4 Data extracts from a simulated population with analytical, sampling and between-target outliers. The boxed numbers (μg g^{-1}) are the outlying values, generated by adding a fixed number (100) to the base population. 48

Fig 3.5 Comparison of the means and standard deviations estimated by robust ANOVA for unbalanced (U-RANOVA) and balanced (RANOVA) experimental designs. The difference between estimates is shown as a percentage of the estimate calculated by the balanced design. Each % difference is the average % difference for 1000 simulated populations. Seed parameters are shown in Table 3.2. Total standard deviation is the square root of the sum of the component variances, e.g.√((Analytical s)^2 + (Sampling s)^2 + (Between-target s)^2). 52

Fig 4.1 Sample gamma spectra from *in situ* measurements, showing 662keV energy peaks: a) Zone 12, estimated ^{137}Cs = 0.04 Bq g^{-1}; b) Barrier 31, estimated ^{137}Cs = 0.14 Bq g^{-1}. 59

Fig 4.2 Dot maps (using equal divisions) for ^{137}Cs activity concentrations measured *in situ* using the collimated Canberra 3 x 3" NaI detector. a) measurements for Zone 12; b) measurements for Barrier 31. (Generated using ESRI ARCMAP^{TM} 9.3.1). 64

Fig 4.3 Dot maps (equal divisions) of ^{137}Cs activity concentrations measured in the on-site laboratory from *ex situ* soil samples for a) Zone 12; b) Barrier 31. Note that the measurement scales are different from those used in Fig 4.2. (Generated using ESRI ARCMAP^{TM} 9.3.1). 65

Fig 4.4 The geometric parameters used to estimate the shape of a soil sampling volume where a detector at position (*C*) is at height *h* above the ground surface. As this is a 2-dimensional representation of a 3-dimensional reality, it is assumed that the detector response to activity at point *A*, which is inversely proportional to the distance *AC*, is also directly proportional to the amount of gamma-emitting material at *A*, which would be expected to increase with the square of the distance *AC*, given a homogeneous medium with respect to radionuclide content. 68

Fig 4.5 Cross sections of the theoretical maximum sample volumes that would be defined if radiation path lengths through the soil were equalised to 500mm, for lateral offsets 0 to 3000 mm from the axis of an idealised *in situ* detector. An increasing 'ground collimation effect' can be observed as the detector height is reduced from 1000 mm (a), to 100 mm (b) and finally to 10 mm..... 70

Fig 4.6 Regressions of Canberra *in situ* against *ex situ* measurements of ^{137}Cs activity concentration for (a) Zone 12 and (b) Barrier 31. Note that in (a) only *ex situ* measurements from the 0-100 mm soil layer have been used. Error bars are shown for single points. 71

Fig 4.7 The regressions shown in Fig 4.6 with the single high values of activity concentration included. These were acquired at judgmentally positioned measurement locations. Comparison with Fig 4.6 shows that the significant rotational and translational biases have arisen due to the single high measurements in each survey..... 72

Fig 4.8 The Barrier 31 survey area, showing the location of the intermediate level radioactive waste store to the west of the area..... 73

Fig 4.9 Approximated measurements of shine from the ILW, measured from 11 measurement location along rows C (dotted line) and H (dashed line), plotted against estimated distance of each measurement location from the centre of the ILW store. These suggest that the *in situ*

measurements may have been affected by shine from the ILW, although some of the gradient seen could also be a result of increased radiation from the ground area surrounding the detector..... 74

Fig 4.10 Maps of measurements in Zone 12. In both cases, the small dots represent previous Groundhog measurements where local Moran's I has been calculated as more than 2.58 standard deviations from the mean. Clusters of such measurements imply localised hotspots of activity. The black crosses represent ^{137}Cs activity for a) Canberra *in situ* measurements; b) *ex situ* measurements from the 0-100 mm layer. Arrows indicate the higher measurement reported in the current surveys at location E11. 76

Fig 4.11 The collimated Canberra NaI 3" x 3" detector in position on the lower shelf of the detector trolley corresponding to a detector height of 280 mm. The Inspector 1000 recording unit is visible on the top shelf. This photograph shows the detector being used in the Zone 12 area (*Section 4.3.1*). 78

Fig 4.12 The Barrier 31 area (*Section 4.3.1*). The fence in the middle of the photograph had been removed at the time of the survey. The surveyed area was located between the building on the left (housing the ILW store) and the low-active drain which can be seen inside the fence on the right hand side of the photograph. 78

Fig 5.1 (a) The geometric components of single particle detection by *in situ* measurement with a portable gamma detector. (b) Showing an approximation of the solid angle representing the path of gamma rays from source (*P*) to the collimated detector (note that the edges will not be clearly defined as is depicted, due to collimator edge effects). All distances are assumed to be in units of millimetres. 84

Fig 5.2 Drawing (to scale) of the detector, collimator and collimator support used in these experiments. 89

Fig 5.3 Representation of the ISOCS geometry definitions used for a particle at depth (not to scale). This example shows the configuration of the geometry definition for the scenario where source depth = 200 mm, lateral offset r = 0.8, and detector height h = 215 mm. 91

Fig 5.4 Uncertainty estimation from replicate counts, showing that use of Poisson statistics (dashed line) would significantly underestimate the random component of uncertainty in the measurements. The standard deviations of the sets of experimental replicate counts are

plotted against predictions from Poisson statistics (√*N* where *N* = the average counts obtained)..... 92

Fig 5.5 (a) Regression of ISOCS predicted counts against measured counts for changing detector height. The rotational bias is significant suggesting a correction factor of 0.81 be used for ISOCS predicted counts. (b) Regression of field measurements and ISOCS predictions (corrected) against an inverse square model, showing a very good agreement between the measured/ISOCS counts and the model. 94

Fig 5.6 Fractional decreases in measured counts with changing lateral offset for the six detector heights used in the field experiments, shown as 5th order polynomial curves. Also shown is the polynomial curve for the mean fractional decrease in ISOCS predicted counts for the same 6 detector heights. Error bars on the ISOCS line represent the total spread between the 6 predictions for the different heights. Data points have been removed from the field-measurement curves for clarity. 95

Fig 5.7 (a) Fractional decreases in counts as lateral offset changes from *r* = 0 to *r* = 1, with fitted polynomial functions of the 5th order, for a detector height of 215mm; (b) Regression of the fractional counts calculated from ISOCS against those obtained from field measurements. 96

Fig 5.8 Regressions of counts predicted by the generic model against the field measurements for all detector heights, offsets and source depths defined in Table 5.2. In (a), the offset model used to define *f(r)* in equation 5.7 is based on ISOCS predicted counts at the height of 215 mm, while in (b), it is based on the measured counts at this detector height. 97

Fig 5.9 (a) Regression of counts predicted by individual ISOCS geometry definitions against the field measurements for all detector heights, offsets and source depths defined in Table 5.2. (b) Regression of counts predicted by the generic model against counts predicted by ISOCS geometry definitions..... 98

Fig 5.10 The regressions including residual plots for (a) the generic model (using an ISOCS generated offset model as in Fig 5.8a and (b) the ISOCS predicted counts as shown in Fig 5.9a, for field measurements up to the first quartile in the measurement results. Error bars based on estimates of the model errors from the ISOCS calculations and calibrations are shown for 25 % of the data..... 100

Fig 5.11 The experimental setup for the detector response modeling experiments described in Chapter 5 (See *Section 5.3*), showing the collimated Canberra NaI 3" x 3" detector supported at a height of 887 mm. The smaller photograph shows the source carrier (made from a piece of Oasis floral foam) inserted into the carrier pipe which was buried at an angle of 45°, and is just visible at the foot of the ladder on the right of the main photograph. 103

Fig 5.12 Photograph of the soil profile to a depth of approximately 150 mm, taken approximately 250 mm from the location of the source container pipe in the detector response modeling experiments described in Chapter 5. The soil appeared to comprise an organic-rich top layer approximately 100 mm thick, over a sandy subsoil. 103

Fig 5.13 Setting up for the detector response modeling experiments (See *Section 5.3*) and Photograph 3. ***Top***: a plumb line was used to position the supporting plank so that the detector would be at the correct offset, measured from the source container pipe, when it was moved into position over the aperture. ***Bottom:*** Prior to each measurement, the supporting plank was leveled in two dimensions. Leveling was maintained for the duration of each measurement by placing wooden spacers underneath the feet of the ladders (visible in the top photograph). 104

Fig 6.1 Two types of measurement grid that can be employed to yield 100 % coverage of the ground surface by the detector FOV with radius r_F. The measurement spacing of the square grid (a) can be expressed $d = \sqrt{2} \times r_F$, while for the triangular grid (b) $d = \sqrt{3} \times rF$, and the distance between rows $d' = d \times \sqrt{3}/2$..... 108

Fig 6.2 For a collimated *in situ* detector, the radius of the FOV subtended at the ground surface (r_F) is related to the height of the detector (h) multiplied by the tangent of one half of the collimator angle (tan (α/2))..... 108

Fig 6.3 The case where a particle *P* is buried at depth d_t beneath the ground surface, at a lateral displacement *s* from the axis of a detector at height *h*. In this case two soil layers with different attenuation properties are represented by the depths d_1 and d_2. The path lengths of radiation through each soil layer are shown as l_1 and l_2 respectively. 110

Fig 6.4 Two scenarios where the counting times used in the local site background survey are not optimal. The required probabilities of false positive errors and false negative errors are expressed in both cases as the z-scores z_{FP} and z_{FN} respectively. In (a), the counting time is too low for reliable particle identification, because any chosen setting of the decision level D_C within the region of overlap (shaded area) would result in increased probabilities of false

positive measurements and/or false negative measurements. In (b), the counting time is longer than necessary to identify a particle at the required probability settings. Any setting of the decision level in the region of overlap would result in probabilities of false measurements that were lower than required, leading to unnecessary cost. 112

Fig 6.5 Showing the coverage square for a single measurement in a full coverage survey that uses a regular square grid sampling pattern. The four corners of the square represent the "worst-case" particle positions for detection. 117

Fig 7.1 Showing possible paths that radiation from surrounding land areas (or other external sources) can take through the walls of the collimator. In the 'grey area', the path length through the lead walls is less than the 20 mm wall thickness. 129

Fig 7.2 Relative massimetric efficiencies calculated using ISOCS circular plane models with a soil density of 1.6 g cm-3, detector height of 920 mm, and an energy level of 661 keV, plotted against (a) Increasing source diameter for a fixed depth of 0.5 m; (b) Increasing soil depth for a fixed source diameter of 25m. The relative massimetric detection efficiencies are expressed in each case as proportions of the absolute efficiency at the assumed maximum source diameter (a) and at the maximum soil depth (b). 130

Fig 7.3 The relative massimetric efficiency model for increasing source diameter with a detector height of 37 mm. 133

Fig 7.4 Drawing (to scale) of the measurement setup used in the high resolution survey, showing the cone section that is defined by the nominal FOV in the top 100 mm soil layer. . 134

Fig 7.5 High resolution *in situ* survey in Barrier 31 around location C3 (See Figs 4.2 and 4.3). The values (in CPS) have been converted to units of Bq g^{-1}, using ISOCS^{TM} and Genie 2000 spectrum analysis software 135

Fig 7.6 The balanced design used in the high resolution survey conducted in Barrier 31. For each duplicate measurement location, the first measurement at the primary location was acquired singly, while the remaining three measurements were acquired together at a later date. 136

Fig 7.7 Uncertainty estimation using the unbalanced design for the high resolution experiment in Barrier 31. a) **Unbalanced design 1**, in which the original measurement from the primary

location was used; b) **Unbalanced design 2**, using the duplicate measurement from the primary location. 138

Fig 7.8 The RMT sampling scheme, showing the 20 *ex situ* measurement locations. 10 *in situ* measurements of 600 seconds each were taken at points 1,3,9,14 and 24 in order to evaluate the heterogeneity of the site with respect to ^{40}K activity concentrations. 142

Fig 7.9 Representation of the *ex situ* measurements acquired in the proposed RMT. The size of each dot is proportional to the mass activity concentration measured at that location. 144

Fig 7.10 The negative correlation between ^{40}K activity concentrations of *ex situ* measurements of core samples and the measured core depth in mm is not significant at $p < 0.05$ but is significant at $p < 0.10$. 145

Fig 8.1 Graphic representation of ROCLI optimisation, for Area 1 with a particle depth of 100 mm (See Table 6.4). Fig 8.1a shows the optimisation for minimum measurement cost, Fig 8.1b shows the optimisation for minimum expectation of loss. In each, the five detector heights used in the optimisation program are represented by different lines, plotted against increasing radius fractions. The curve for detector height = 250 mm in Fig 8.1a is incomplete because the program rejects scenarios which result in a measurement counting time of less than 10 seconds. 170

Fig 9.1 - Analysis protocol of soil samples for estimation of the random component of uncertainty due to internal heterogeneity. Each sample will be placed on the detector as received, and counted twice. The sample container will then be opened, the contents mixed, the lid replaced, and the sample container positioned in the same detector, and again counted twice. 191

Fig A3.1 Regressions of counts predicted by the generic model (graphs on left) and ISOCS predicted counts (graphs on right) against measured counts, for increasing LATERAL OFFSET for different detector heights and with the source at zero depth. 216

Fig A3.2 Regressions of counts predicted by the generic model (graphs on left) and ISOCS predicted counts (graphs on right) against measured counts, for increasing SOURCE DEPTH with fixed values of detector height and lateral offset. 218

Fig A3.3 Regressions of counts predicted by the generic model (graphs on left) and ISOCS predicted counts (graphs on right) against measured counts, for increasing LATERAL OFFSET

with fixed values of detector height, and with the source at a fixed depth beneath the ground surface..... 220

List of tables

Table 3.1 Seed distribution parameters of the 4 simulated populations used in the 1992 study. (Ramsey *et al.,* 1992). 45

Table3. 2 Seed distribution parameters used in *Test 2.* 47

Table3.3 The 4 different outlier types and 3 different outlier adjustments that were applied to each base population in *Test 2*, generating a total of 10 additional populations with outliers for each base population. 47

Table 3.4 Comparison of results of ROBUST ANOVA on an unbalanced experimental design (U-RANOVA), with previously published results for a balanced design, showing that the differences between the estimated component standard deviations are <6 %. The differences between estimates are shown as a percentage of the original estimate from the 1992 study (Ramsey *et al.,* 1992). 49

Table 4.1 Summary of survey parameters for the Zone 12 and Barrier 31 surveys. 61

Table 4.2 Summary of the random component of measurement uncertainty estimated using robust ANOVA on sampling and analytical duplicates. 62

Table 4.3 Summary statistics for the Zone 12 and Barrier 31 surveys, showing the means, medians and standard deviations for the entire population of activity concentrations measured across the whole site. Activity concentrations at the duplicate measurement locations have been calculated as the means of the four measurements (two analyses per sample, two samples per location) that were acquired at each. 63

Table 4.4 Comparison of means of Canberra *in situ* measurements with *ex situ* measurements, after exclusion of single judgmental measurement locations. 64

Table 5.1 Parameters for measurements acquired for the purpose of uncertainty estimation. Five replicate measurements were acquired for each of the parameter combinations shown. 90

Table 5.2 Parameter ranges of the field measurements. 90

Table 5.3 The maximum lateral offset (r <= 1.0) at which peaks in the spectra were observable and interpretable by Genie 2000 software, using a counting time of 600 seconds. 101

Table 5.4 Measurement spacings (in millimetres) that ensure 100 % coverage of the ground surface using a regular square grid survey, calculated from the *r* values in table 5.3. The maximum spacing has been highlighted for each source depth. 101

Table 6.1 Background parameters used in the optimisation examples. 118

Table 6.2 Standard input parameters to the ROCLI program for the example optimisations. 119

Table 6.3 Error probability ranges and error costs used in optimisation by expectation of loss. 121

Table 6.4 Optimised survey parameters for hypothetical 100m^2 surveys in the two areas. ... 122

Table 7.1 Random component of uncertainty estimates for the high resolution survey in Barrier 31, using both balanced and unbalanced designs. 138

Table 7.2 Averaged ISOCS calculated activity concentrations of *in situ* measurement at position C01 using different ISOCS depth models, showing the percentage difference from that calculated for the model based on the mean core depth of 111 mm. The variation in core depth from 60-170 mm introduces a source of uncertainty. This also shows that substantial amounts of activity (~11 %) may be acquired from below the mean depth of 111 mm, introducing yet another source of uncertainty..... 146

Table 7.3 Summary statistics of *in situ* measurements of ^{40}K activity concentration with the detector in position C01 (the centre point of the RMT) using an ISOCS circular plane model of diameter of 25 m, and two depths of 111 mm (the mean core depth) and 500 mm (the standard model depth). 147

Table 8.1 Overview comparison of *in situ* and *ex situ* measurement methods 152

Table 8.2 Comparison of Poisson uncertainty with random component of analytical uncertainty in the *in situ* measurements for the Zone 12 and Barrier 31 surveys. The Poisson uncertainty is based on a calculation of the peak counts that would be required to report the mean activity concentration..... 153

Table 8.3 Components of measurement uncertainty expressed as percentages of the total site variance..... 163

Table 8.4 Calculation of the standard error on the mean (SEM) for the Zone 12 and Barrier 31 surveys. Values for *in situ* measurements are calculated for the complete measurement set and also for the measurements acquired in the same location as the *ex situ* samples. The right hand column shows an estimate of the number of *ex situ* measurements that would be required to obtain the same SEM as the *in situ* measurement SEMs, assuming that the standard deviation does not change with different numbers of measurements. 164

Table A1.1 Original simulated data populations for testing of robust ANOVA, as used by Ramsey *et al.,* 1992. Both comprise of 4 columns of 100 random numbers drawn from a normal distribution: Trial 1 = no outliers, Trial 2 = 5 % of analytical duplicates overwritten with high-value outliers (highlighted). Used in U-RANOVA Test 1 (*Section 3.3.1*) 202

Table A1.2 Original simulated data populations for testing of robust ANOVA, as used by Ramsey *et al.,* 1992. Both comprise of 4 columns of 100 random numbers drawn from a normal distribution: Trial 1 = 5 %of sampling duplicates overwritten with high values; Trial 2 = 10% of between-target values overwritten with high-value outliers. Overwritten values have been highlighted. 204

Table A2.1 Zone 12 raw data for in situ measurements. Canberra detector measurements have been converted to mass activity concentrations using an ISOCS circular plane geometry definition of 25 m diameter and 0.2 m depth. Values for duplicate measurement locations have been averaged across all four measurements at each location. Pertains to *Section 4.4.2.* 207

Table A2.2 Zone 12 raw data for duplicate *in situ* measurements. Pertains to *Section 4.4.1*. 208

Table A2.3 Zone 12 raw data for *ex situ* measurements of soil samples, made in the on-site laboratory. Values for duplicate measurement locations have been averaged across all four measurements at each location. Pertains to *Section 4.4.2*. 209

Table A2.4 Zone 12 raw data for duplicate *ex situ* measurements for both the 0-100 mm and the 100-200 mm soil layers. Pertains to *Section 4.4.1*..... 210

Table A2.5 Barrier 31 raw data for *in situ* measurements. Canberra detector measurements have been converted to mass activity concentrations using an ISOCS circular plane geometry definition of 25 m diameter and 0.2 m depth. Values for duplicate measurement locations

have been averaged across all four measurements at each location. Pertains to *Section 4.4.2*. 211

Table A2.6 Barrier 31 raw data for *ex situ* measurements of soil samples, made in the on-site laboratory. Values for duplicate measurement locations have been averaged across all four measurements at each location. Pertains to *Section 4.4.2*. 212

Table A2.7 Barrier 31 raw data for duplicate measurements for the Canberra *in* situ detector, and the ex *situ* measurements for both the 0-100 mm and the 100-200 mm soil layers. Pertains to *Section 4.4.1*. 213

Table A2.8 Barrier 31 raw data for measurement of shine. Measured activity concentrations shown were obtained with the collimated Canberra *in situ* detector placed on the trolley (height 920 mm) on top of four lead bricks of total thickness 60 mm, and which completely obscured the collimator aperture. Pertains to *Section 4.5.4*..... 214

Table A4.1 West runway core (*ex situ*) measurements, showing GPS positions, depths, activities and uncertainties as reported by the external laboratory, including summary statistics. Pertains to *Section 7.4.4.* 221

Table A4.2 ANOVA of the five groups of *in situ* measurements from positions 1,3,9,14 and 21 (Fig 7.8), analysed using the 111 mm depth ISOCS model, and showing that there is no evidence of a significant difference between the mean measurements at each of the five locations ($p>0.05$). This suggests that the concrete area proposed as a RMT has no significant large-scale variation in ^{40}K activity. Pertains to *Section 7.4.4.*..... 222

Table A4.3 *In situ* measurements of ^{40}K activity concentration with detector in position 01 (the centre point of the reference site) using an ISOCS circular plane model of diameter of 25 m, and two depths of 111 mm (the mean core depth) and 500 mm (the standard model depth). Pertains to *Section 7.4.4.* 222

Table A4.4 *In situ* measurements of ^{40}K activity concentrations at the four measurement positions at the periphery of the proposed RMT (Fig 7.8), using an ISOCS circular plane model of diameter of 25 m and a depth of 111 mm. Pertains to *Section 7.4.4.* 223

List of acronyms

ALARA	**As Low As Reasonably Achievable** *In U.K. law, this means taking all reasonable steps to protect people. For example the costs of taking protection measures are weighted against the benefits obtained (NDA, 2013).*
ALARP	**As Low As Reasonably Practicable** *"To satisfy this principle, measures necessary to reduce risk must be taken until the cost of these measures whether in money, time or trouble, is disproportionate to the reduction of risk" (NDA, 2013)*
CPS	**Counts Per Second**
CRM	**Certified Reference Material**
DCGL	**Derived Concentration Guideline Level (USEPA)**
DQO	**Data Quality Objectives (USEPA)**
DST	**Decision Support Tool**
FFP	**Fit-For-Purpose**
FnFP	**Fitness-For-Purpose**
FOV	**Field-Of-View (of radiation detector)**
GUM	**Guide to the expression of Uncertainty in Measurement**
HSE	**Health and Safety Executive**
HPGe	**High Purity Germanium (a type of gamma detector)**
ILW	**Intermediate Level radioactive Waste**
ISO	**International Organisation for Standardisation**
ISOCS	***In Situ* Object Counting System**
IUPAC	**International Union of Pure and Applied Chemistry**
MARSSIM	**Multi-Agency Radiation Survey and Site Investigation Manual (USEPA)**
MCA	**Multichannel Analyser**
MDA	**Minimum Detectable Amount**
NDA	**Nuclear Decommissioning Authority**

NIA65	**Nuclear Installations Act 1965**
NORM	**(See glossary definition)**
OCLI	**Optimised Contaminated Land Investigation**
ONR	**Office for Nuclear Regulation**
RMT	**Reference Measurement Target**
RSD	**Relative Standard Deviation**
RST	**Reference Sampling Target**
SEM	**Standard Error of the Mean**
SEPA	**Scottish Environment Protection Agency**
SLC	**Site Licence Company**
SPT	**Sampling Proficiency Test**
STP	**Sampling Theory and Practice**
TEDE	**Total Effective Dose Equivalent**
TOS	**Theory Of Sampling**
VIM	**Vocabulaire international de métrologie (international vocabulary of metrology)**
US EPA	**United States Environmental Protection Agency**
WSOCLI	**Whole Site Optimised Contaminated Land Investigation**
XRF	**X-Ray Fluorescence**

Glossary of terms

(Terms that are defined elsewhere in the glossary are highlighted in bold)

Absolute efficiency	The number of pulses recorded (by a detector) divided by the number of radiation quanta emitted by the source (Knoll, 2000).
Absorbed dose	"A measure of the energy from ionising radiation deposited in a unit mass of any specified material" (Towler *et al.*, 2009) Units = Gray (Gy). 1 Gy = 1 J Kg^{-1}.
Action level	**Threshold** value that provides criterion for choosing between alternative actions.
Activity	For an amount of a **radionuclide** in a particular energy state at a given time, the number of spontaneous nuclear transformations in a given time interval. Unit = Bq (1 Bq = 1 disintegration per second) (ICRU, 1998).
Activity concentration	See **specific activity.**
Analyte	(In chemistry) "The component measured" (IUPAC, 1990).
Analytical bias	**Systematic effects** arising from an **analytical process** (Ramsey and Ellison, 2007). Also see **bias**.
Analytical process ***or*** Analysis	Used in this thesis to refer to the analytical component of a measurement procedure. Note that this would normally take place in a laboratory in the case of measurements made ***ex situ,*** or in the field in the case of ***in situ*** measurements. May also include sample preparation, e.g. drying and grinding in a laboratory, and interpretation of the measurement results into the units required for reporting.
Analytical uncertainty	The component of **measurement uncertainty** that arises from the **analytical process.**
Background (radioactivity)	"Radioactivity from naturally occurring **radionuclides** and anthropogenic **radionuclides** from manmade sources (such as global fallout as it exists in the environment from the testing of nuclear weapons or from accidents like Chernobyl) that are not under control of the owner/operator" (Towler *et al.*, 2009).
Balanced design	A particular case of the **duplicate method** for estimating overall **measurement uncertainty**, where the duplicated test samples are both analysed in duplicate (Ramsey and

	Ellison, 2007) (Contrast with **unbalanced design**).
Bias	"Estimate of a systematic measurement error" (JCGM, 2008a). Note – this refers to a numerical estimate of the systematic error.
Bottom-up	Method of estimating **measurement uncertainty** which aims to quantify all sources of uncertainty individually, and use a model to combine them (Ramsey and Ellison, 2007).
Bremsstrahlung	"Electromagnetic radiation resulting from the change in velocity of charged particles" (Longworth, 1998).
Certified reference material ***or*** CRM	**"Reference material,** accompanied by documentation issued by an authoritative body and providing one or more specified property values with associated uncertainties and traceabilities, using valid procedures" (JCGM, 2008a).
Channel	An individual window used in a **multichannel analyser**, corresponding to a change in the height of the voltage pulse from an energy discriminating detector.
Composite sample	"Two or more increments/sub-samples mixed together in appropriate portions, either directly or continuously, from which the average value of a desired characteristic may be obtained" (Ramsey and Ellison, 2007).
Compton continuum	"In gamma spectrometry, that part of the spectrum due to incompletely absorbed gamma-rays, and mostly devoid of useful information" (Gilmore, 2008).
Contaminant (Scotland)	"A substance which is in, on or under the land and which has the potential to cause harm or to cause pollution of the water environment." (Scottish Executive, 2006).
Coulomb forces	Forces between electrically charged objects (e.g. protons). The magnitudes of these forces follow an inverse-square relationship with increasing distance of separation.
Dead time	"The time that a signal processing circuit is busy processing a pulse, and during which is consequently unable to accept another pulse" (Gilmore, 2008). Although residual energy left over from detector interactions during the instrument's dead time may cause pile-up (i.e. interference effects between two or more pulses).
Delicensing (UK)	"The process of releasing a **nuclear licensed site** from regulation under the Nuclear Installations Act and of releasing the operator from his period of responsibility for any nuclear liability" (Towler *et al.,* 2009).

Detection limit	Measured quantity value, obtained by a given measurement procedure, for which the probability of falsely claiming the absence of a component in a material is β, given a probability α of falsely claiming its presence (JCGM, 2008a).
Dosimetry	The measurement and calculation of dose to matter and tissues resulting from exposure to ionising radiation.
Duplicate method	Method of estimating combined uncertainty (including **sampling uncertainty**) using duplicated analyses of duplicated samples for a proportion (e.g. 10 %) of the total number of **measurements**. Described in detail in the Eurachem guide (Ramsey and Ellison, 2007).
Effective dose (UK) ***or*** Effective dose equivalent (USA)	"A radiation dose quantity that is a modification of **equivalent dose**, which takes into account the susceptibility of different organs and tissues in the body to stochastic effects such as cancer induction" (Towler *et al.,* 2009) Units = Sieverts (Sv).
Equivalent dose	"A radiation dose quantity, which is a modification of the **absorbed dose** that takes into account the different amounts of damage done by different **radioactive decay** types" (Towler *et al.,* 2009) Units = Sieverts (Sv).
Expanded relative measurement uncertainty	The **measurement uncertainty** multiplied by a coverage factor *k* to give the required confidence level (e.g. *k* = 2 for ~95 % confidence), and expressed relative to the mean concentration, usually as a percentage. e.g. U % = 200 s_{meas} / $\bar{x}$ Where S_{meas} = the measurement standard deviation concentration, and $\bar{x}$ is the mean measurement concentration (Ramsey, 1998).
Exposure pathway	A route or means by which a **contaminant** can reach or affect a receptor, e.g. a living organism, ecological system, utility or controlled water which may be adversely affected as a consequence (Towler *et al.,* 2009).
Ex situ	Literally, "out of place". Used in the thesis to refer to a method of measurement in which samples (e.g. soil samples) are extracted and analysed out of place (contrast with ***in situ***).
False negative	Analogous to a **type 2 error**. Refers to a **measurement** which indicates that no action (or an alternative action) is required, when in fact a specific action is required.

False positive	Analogous to a **type 1 error**. Refers to a **measurement** which indicates that a certain action needs to be taken, when in fact no action (or an alternative action) is required.
Field-of-view (of detector)	In this thesis – For a collimated detector, the solid angle that is nominally defined by the dimensions of the collimator from which emitted radiation will impinge upon the detector volume. Note that in practice this angle is not well defined due to edge effects, and because of the lesser amount of radiation that passes through the collimator walls.
Final status survey	"Measurements and sampling to describe the radiological conditions of a site, following completion of decontamination activities (if any) in preparation for release" (USEPA, 2000b).
Fitness-for-purpose	"The degree to which the data produced by a measurement process enables a user to make technically and administratively correct decisions for a stated purpose" (Ramsey and Ellison, 2007).
Gamma radiation	"Highly energetic form of electromagnetic radiation in the approximate range keV-MeV, of nuclear origin emitted during **radioactive decay**, electron-positron annihilation and nuclear fission" (Longworth, 1998).
Grab-sampling	Process of obtaining a sample by convenience (e.g. ease of extraction) without any theoretical considerations (Gy, 2004). Also known as "convenience sampling". Strictly, no statistical inferences can be made from convenience samples (Thompson and Ramsey, 1995).
Heterogeneity Homogeneity	"The degree to which a property or a constituent is uniformly distributed throughout a quantity of material" (IUPAC, 1990). (Homogeneity refers to the degree of *uniformity*). (Heterogeneity refers to the degree of *non-uniformity*).
Hotspot	A small or localised area in which the **activity concentrations** of one or more **radionuclides** are elevated compared to their immediate surroundings.
In situ	Literally, "in place". Used to refer to a method of measurement in which the measurements are performed on samples that are in place, and so far as is reasonably possible, undisturbed. Contrast with ***ex situ***.
In situ object counting system ***or***	A proprietary calibration program, which uses a Monte-Carlo methodology to calibrate a gamma detector for a

ISOCS	user-defined combination of radiation source, collimated or un-collimated detector, and intervening radiation absorbing media.
Intermediate precision	Measurement **precision** under a set of **intermediate precision conditions of measurement** (JCGM, 2008a).
Intermediate precision condition of measurement	Condition of **measurement**, out of a set of conditions that includes the same measurement procedure, same location, and replicate measurements on the same or similar objects over an extended period of time, but may include other conditions involving changes (JCGM, 2008a).
Ion pair	"A positively charged ion together with the electron removed from the original atom by ionising radiation" (Longworth, 1998).
Massimetric efficiency (of detector)	**Absolute efficiency** expressed per unit mass (e.g. g^{-1}).
Measurand	"Quantity intended to be measured" (JCGM, 2008a).
Measurement	"Process of experimentally obtaining one or more quantity values that can reasonably be attributed to a quantity" (JCGM, 2008a).
Measurement error	"Measured quantity value minus a reference quantity value" (JCGM, 2008a).
Measurement uncertainty	See uncertainty (of measurement).
Minimum Detectable Amount	"The lowest activity in a sample that can be detected with a particular degree of confidence. It is the activity equivalent of the limit of detection. It is defined variously and is NOT the minimum activity measurable" (Gilmore, 2008). In this thesis, the term refers to the Currie **MDA**, which can be defined as "the minimum number of counts needed from the source to ensure a **false-negative** rate no larger than 5 % when the system is operated with a critical level (or "trigger point") of L_C that, in turn, ensures a **false positive** rate of no greater than 5 %." (Knoll, 2000).
Multichannel analyser	An electronic device that separates and counts voltage pulses into a number of windows, or **channels**, where each window corresponds to a change in height (amplitude) of the voltage pulse.
Non-targeted sampling	See **systematic sampling.**
NORM	Acronym for "Naturally Occurring Radioactive Materials", but used specifically to describe those where "human

	activities have increased the potential for exposure compared with the unaltered situation" (WNA, 2013).
Nuclear Decommissioning Authority	A non-departmental public body which is responsible for the decommissioning and clean-up of civil nuclear facilities in the UK, overseeing the management of radioactive waste, and implementing government policy on long-term strategies for dealing with radioactive waste (NDA, 2013).
Nuclear Installations Act 1965	Act of parliament relating to nuclear installations, the requirement for site licences, and the liabilities of **site licence companies** to third parties.
Nuclear licensed site (UK)	A site that is regulated by the UK Health and Safety Executive (**HSE**) under the provisions of the Nuclear Installations Act 1965 (as amended) with a nuclear site licence (Towler *et al.,* 2009).
Photon	A quantum of electromagnetic radiation (Gilmore, 2008).
Practice	"Any human activity that introduces additional sources of exposure or exposure pathways or extends exposure to additional people or modifies the network of exposure pathways from existing sources, so as to increase the exposure or the likelihood of exposure of people or the number of people exposed" (IAEA, 2004a).
Precision	"Closeness of agreement between indications or measured quantity values obtained by replicate measurements on the same or similar objects under specified conditions" (JCGM, 2008a).
Primary sample	The collection of one or more increments or units initially taken from a population (Ramsey and Ellison, 2007). (See **Primary Sampling**). In this thesis it is used to describe single measurements that represent a sub-area of ground within a surveyed area.
Primary sampling	The acquisition of one or more units that are initially taken from a population. The term "primary" refers to the fact that the sample was obtained during the earliest stage of measurement (e.g. soil samples in a field survey), as distinct from the process of sub-sampling which may be employed in a laboratory (Ramsey and Ellison, 2007; Ramsey, 1998).
Progeny (nuclide)	A nuclide that is produced following a **radioactive decay.**
Radioactive decay	"The spontaneous transformation of an unstable atom into one or more different nuclides accompanied by either the emission of energy and/or particles from the nucleus,

	nuclear capture or ejection of orbital electrons, or fission" (Towler *et al.,* 2009).
Radionuclide	"An unstable nuclide that undergoes **radioactive decay**" (Towler *et al.,* 2009).
Random effect	Effect which gives rise to variations in repeated observations of the **measurand** (JCGM, 2008b).
Random error	"Component of **measurement error** that in replicate measurements varies in an unpredictable manner" (JCGM, 2008a).
Reference material	"Material, sufficiently homogeneous and stable with reference to specified properties, which has been established to be fit for its intended use in **measurement** or in examination of **nominal properties**" (JCGM, 2008a).
Reference measurement target ***or*** RMT	Term used in this thesis to describe a **reference material** with dimensions which are fit for its intended use in estimating analytical bias.
Relative Standard Deviation	The standard deviation of a sample from a population expressed as a proportion of the mean. Often expressed as RSD % where RSD % = 100 * Standard Deviation / Mean.
Reference **sampling target** (RST)	"The analogue in sampling of a **reference material** or **certified reference material**" (Ramsey and Ellison, 2007). Used to estimate bias due to sampling.
Repeatability (of results of measurements)	"Closeness of the agreement between the results of successive measurements of the same measurand carried out under the same conditions of measurement" (JCGM, 2008b) (contrast with reproducibility).
Representative sample	"Sample resulting from a sampling plan that can be expected to reflect adequately the properties of interest in the parent population" (Ramsey and Ellison, 2007).
Reproducibility (of results of measurements)	"Closeness of the agreement between the results of successive measurements of the same measurand carried out under changed conditions of measurement" (JCGM, 2008b) (contrast with repeatability).
Risk assessment	"The formal process of identifying, assessing and evaluating the health and environmental risks that may be associated with a hazard" (Towler *et al.,* 2009).
Sampling bias	**Systematic errors** arising from sampling (Ramsey and Ellison, 2007). Also see **bias**.

Sampling target	"Portion of material, at a particular time, that the sample is intended to represent" (Ramsey and Ellison, 2007).
Sampling uncertainty	"The part of the total **measurement uncertainty** attributable to sampling" (Ramey and Ellison, 2007).
Sampling proficiency test (SPT)	A procedure in which two or more samplers independently acquire **primary sample**s from a parent population, and where measurements are made from these **primary sample**s in order to estimate the systematic component of **sampling uncertainty**.
Site Licence Company (SLC)	A company that owns permits for an individual nuclear site. These permits are non-transferrable, and an SLC has a parent body organisation which owns shares in that company and is responsible for managing the SLC for the duration of its contract with the **NDA**.
Specific Activity	Of a **radionuclide**, the **activity** per unit mass of that nuclide (IAEA, 2013).
Systematic effect	A recognised effect of an influence quantity on a measurement result which gives rise to a measurement error (JCGM, 2008b).
Systematic error	"Component of measurement error that in replicate measurements remains constant or varies in a predictable manner" (JCGM, 2008a).
Systematic sampling	Sampling that is performed using a non-judgmental systematic method of determining sampling locations (e.g. a regular grid). (Contrast with **targeted sampling**).
Systematic survey	Survey that employs **systematic sampling.**
Targeted sampling ***or*** Judgmental sampling	"Subjective selection of sampling locations at a site, based on historical information, visual inspection, and on best professional judgment of the sampling team" (IAEA, 2003). (Contrast with **systematic sampling**).
Threshold Value	A value of contaminant concentration above which some action is required (Ramsey *et al.,* 2002).
Top-down	Method of estimating measurement uncertainty which uses some replication of the measurement procedure to give a direct estimate of the final measurement uncertainty (Ramsey and Ellison, 2007).
Type 1 error	In statistics, an assertion that a null hypothesis is rejected when in fact it is true.

Type 2 error	In statistics, an assertion that a null hypothesis is true when in fact it is false.
Unbalanced design	A particular case of the **duplicate method** for estimating overall measurement uncertainty, where **only one** of the duplicate test samples is subjected to duplicate analysis (Ramsey and Ellison, 2007) (Contrast with **balanced design**).
Uncertainty (of measurement)	"Non-negative parameter characterizing the dispersion of the quantity values being attributed to a **measurand,** based on the information used" (JCGM, 2008a).

Chapter 1 – Introduction

Full definitions of terms and abbreviations are provided in the list of abbreviations and the glossary on pages xxiv - xxxiv. The first usages of abbreviations, words and phrases that appear in these sections are highlighted in bold. Italics are used for emphasis.

1.1 Introduction to this research

Several countries throughout the World face significant challenges with radioactive contamination, brought about by previous practices, uncontrolled disposal, weapons testing or as a result of accidents (IAEA, 1999; Beresford, 2006). In some cases this has left large areas of land permanently uninhabited or requiring extensive remediation (MARTAC, 2003). In the UK, there are no significant areas of radioactively contaminated land resulting from large-scale operations such as uranium mining and processing, or weapons testing. However, localised areas of contamination have been caused by the historical use of radioactive materials for various manufacturing activities, and also for power generation. These add to the natural and artificial **background** caused by deposition from the 1957 Windscale and 1986 Chernobyl incidents, and the fallout from atmospheric weapons testing worldwide. Nuclear power has been used commercially in the UK since the mid 1950s. Other civil and military applications have also added to the total inventory of radionuclides in this country. Examples are ore processing and luminizing, and some industrial processes that use naturally occurring radioactive materials (**NORM**) whether this be done deliberately (such as the use of thorium compounds in the production of gas mantles) or incidentally (Beresford, 2006; DEFRA, 2011).

As of 2012 there were a total of 36 **nuclear licensed sites** in England, Wales and Scotland (EA, 2012). **The Nuclear Decommissioning Authority** (**NDA**) is the public body with overall responsibility for the decommissioning of civil nuclear sites in the UK, and this organisation currently owns 19 nuclear sites, including three in Scotland (NDA, 2013; SEPA, 2009). The NDA achieves this by contracting out the delivery of site programmes to **Site Licence Companies** (**SLC**s), which manage individual sites and carry out the work required (NDA, 2013). Sites such as Sellafield, Dounreay and Harwell are known to have significant amounts of land that may have been contaminated by radionuclides (NDA, 2006).

Individual site licence holders are required to demonstrate that radioactively contaminated ground, which is considered to be an accumulation of radioactive waste, is being appropriately dealt with. This includes control and containment, recording of quantities and locations, and the maintenance of safe conditions (ONR, 2013). A prerequisite to fulfilling these requirements is the characterisation of land areas for radionuclide content, which is the subject of this research project.

A substantial body of literature already exists on the characterisation of chemically contaminated land. Many of the principles that apply to chemical contamination are equally applicable to radioactive contamination. There are some important differences, however, both in the characteristics of radioactive contamination, and also in the methods of measurement. An example of the former is a high degree of small-scale heterogeneity that is often found in the radionuclide content of land areas (IAEA, 2011). This presents particular challenges to characterisation, because heterogeneity can lead to high levels of **uncertainty** in the **measurements** of individual samples. If these uncertainties are not well understood, then they have the potential to result in decisions being made that are not of sufficient reliability to fulfil the original survey objectives.

An example of the differences in measurement methods is that whereas ***in situ*** measurements of chemical contaminants (e.g. by hand-held **XRF** instruments) only quantify concentrations in very small masses of substrate (~1 g), *in situ* measurements of gamma-emitting radionuclides can yield measurements of very large soil masses (~10 – 100 tonnes). This is because of the remote detection of penetrating **gamma radiation** over distances of 25m or more in air. In contrast, the masses of ***ex situ*** samples of soil or other substrate (e.g. concrete) that are removed and analysed in a laboratory, are typically in the order of 1 kg. This applies both to surveys of chemically and radioactively contaminated land. The differences in sample mass between the methods can be a significant advantage in the case of *in situ* measurements, as it potentially enables a relatively large area of ground to be investigated by a single measurement. However, remote detection can have drawbacks, especially if external sources of **activity** are in the vicinity of the site.

There is a lesser volume of scientific literature specifically concerned with the characterisation of radioactively contaminated land. With some exceptions, this is mostly based on measurements of environmental fallout deposit from the 1986 Chernobyl incident, or of the

fallout from global atmospheric weapons testing, although a number of legislative guidance documents exist that have been produced or commissioned by the regulatory authorities of countries with nuclear programmes. There are a relatively small number of published works in scientific journals dealing specifically with the subject of contaminated land at nuclear sites. This is probably partly a result of the comparatively small number of sites that have undergone, or are undergoing, decommissioning compared to the number of sites that are known to have been chemically contaminated. However, as the priorities of nuclear site licensees progress from the immediate 'making safe' and demolition of nuclear facilities, to the eventual deregulation of land areas, the demand for demonstrably reliable and cost-effective methods of land area characterisation seems likely to increase.

The quantification and interpretation of **measurement uncertainty** is central to the topics discussed in this thesis. All measurements are subject to uncertainty, which includes both systematic and random components, and this needs to be taken into account in any decision-making process that is based on measured values (Ramsey, 1998; Thompson, 1995). Unlike most measurements of chemical contaminants, those of radioactive contaminants are strongly affected by the stochastic process of **radioactive decay**. In theory, this component of uncertainty can be readily and reliably estimated by Poisson statistics, provided the half-life of the radionuclide of interest is long compared to the measurement acquisition time. However, other factors in all measurement techniques increase the total uncertainty of any analytical method. Importantly, uncertainty in the sampling process is a factor that is often not explicitly measured, or taken into consideration in subsequent decision-making (Thompson and Ramsey, 1995). This can lead to unreliable decisions, because the sampling component of uncertainty is often found to be large when compared to the analytical component (Ramsey and Argyraki, 1997).

Consideration of uncertainty in the decision-making process is important because of the possibility of misclassification when measurements are compared to a **threshold value**, e.g. a maximum **activity concentration**. A conceptual definition of the '**fitness-for-purpose**' (**FnFP**) of measurements was proposed by Thompson and Ramsey (1995). This definition requires measurements to be of sufficient quality to enable reliable decisions to be made for a stated purpose. An initial approach to evaluating FnFP was based solely on estimates of uncertainty (Ramsey *et al.*, 1992). It was later broadened to incorporate financial considerations. Methods were developed to balance the uncertainty in the measurements against the potential costs of

misclassification, as well as the costs of taking the measurements (Thompson and Fearn, 1996; Ramsey *et al.*, 2002).

In the case of chemically contaminated land, *ex situ* measurements obtained in a laboratory have traditionally been regarded as more reliable than measurements made *in situ* in the field. However, the acquisition of *in situ* measurements is usually substantially less expensive than the **analysis** of *ex situ* soil samples, and at least two previous studies have found that the fitness-for-purpose of *in situ* measurements compares favourably with that of *ex situ* measurements, when financial considerations are taken into account. Indeed, in some cases the use of *in situ* measurements has been found to result in a lower total expectation of financial losses when compared with the use of *ex situ* measurements (Ramsey and Boon, 2012; Taylor *et al.*, 2004). Typically, they are also subject to much lower turnaround times between conducting surveys and obtaining results. Reducing overall costs is likely to be of even greater importance in investigations of radioactive contamination, because of the relatively high measurement costs (e.g. ~£100 per gamma measurement in the laboratory), and also the potential costs of making erroneous decisions as a result of measurements that are not fit-for-purpose (**FFP**).

While there can be no doubt that it should be possible to obtain more reliable measurements of individual soil samples in the controlled conditions of a laboratory than *in situ* in the field, the eventual objective of a contaminated land survey is not to evaluate the radionuclide content of individual samples. Rather it is to use these measurements to build a picture of the types, distributions and intensities of radionuclides over the entire surveyed area. A broad contention of this thesis is that *in situ* measurements of radioactively contaminated land areas have advantages that make them at least as reliable, and in some cases more reliable, than *ex situ* measurements in fulfilling this objective. In practice, a comprehensive, integrated investigation will most likely require a combination of both *in situ* and *ex situ* methods, followed by an analysis that takes into consideration the advantages and disadvantages of each measurement method used. This study evaluates *in situ* and *ex situ* measurement methods in the particular case of characterising radioactively contaminated land on a decommissioning nuclear site. Part of this evaluation has depended on the development of a new approach to optimising the parameters of *in situ* surveys for cost-effective characterisation.

1.2 Objectives of this research

1.2.1 Overall aim

To devise and test generic methods for the optimised characterisation of radioactively contaminated land on a decommissioning nuclear site, based on measurements that can be considered fit-for-purpose.

1.2.2 Specific research objectives

1. Research the comparative usefulness of *in situ* and *ex situ* methods for the characterisation of radioactively contaminated land, where the aim is to achieve fitness-for-purpose of measurements:

a) Estimate the sampling and analytical uncertainties that arise from both *in situ* and *ex situ* measurements on radioactively contaminated land, and compare these to the uncertainties that would be expected to arise from the stochastic process of radioactive decay;

b) Model the relationships between activity concentration measurements made using *in situ* and *ex situ* techniques in the same area;

c) Investigate how the differences between these two measurement methods interplay with the characteristics of the contamination found, and how this impacts the quality of the measurements;

d) Investigate means of establishing systematic error and traceability in *in situ* measurements;

2. Devise and test statistical methods for the fit-for-purpose characterisation of radioactively contaminated land:

a) Evaluate and enhance existing statistical methods for the cost-effective estimation of the sampling and analytical components of measurement uncertainty;

b) Devise a prototype method for the optimisation of the survey parameters for *in situ* investigations of radioactively contaminated land;

c) Verify the assumptions and models used to construct this method, by comparison with measurements obtained in field trials;

d) Demonstrate the use of this new method as an aid to the design of systematic surveys in which the measurements can be considered fit-for-purpose;

e) Report on the advantages and limitations of the new method;

f) Propose further work to develop the method into a generic tool which can be used by the nuclear industry as a design aid for identifying optimal, fit-for-purpose investigation strategies.

3. Combine the results and conclusions obtained from these investigations to evaluate the relative advantages and disadvantages of using *in situ* and *ex situ* methods, where the objective is to identify the optimal approach for the characterisation of land areas for radionuclide content.

1.3 Structure of the thesis

This thesis is composed of nine chapters. The second chapter presents a general review of current legislation and issues considered to be relevant to the characterisation of radioactively contaminated land, where these are not covered by subsequent chapters. Chapters 3-6 are in the form of journal articles that have either been published or submitted for future publication. These four papers are presented largely as they have been submitted, with the following modifications: a) the reference lists have been removed from the individual papers and combined with the main reference section at the end of the thesis; b) the numbering systems for text sections, figures and tables have been standardised; c) the formats of the section headings, figure and table captions, have been standardised and made compatible with the rest of the thesis; d) where applicable, references have been made to relevant appendixes; e) Chapter 4 and Chapter 5 each has an additional section included at the end of the journal article. These sections contain figures with relevant colour photographs, which were not included in the submitted manuscript, and have been added as separate sections in order to preserve the format of the submitted articles. Additional references to these figures have been made in the text.

Chapter 3 introduces a refinement to a pre-existing statistical method, that enables empirical estimates of the random sampling and analytical components of measurement uncertainty to be carried out at reduced cost. This method was used in the experiments described in *Section 7.3* of this thesis. Chapter 4 presents the results of two surveys conducted at the case-study site, where the principal objective was to compare the usefulness of *in situ* and *ex situ* measurement techniques. Chapter 5 reports on the development of a generic approach to predicting detector response for *in situ* measurements of small radioactive particles. Chapter 6

introduces a novel method for the cost-effective optimisation of *in situ* surveys that use portable gamma-detecting equipment to characterise land areas. Chapter 7 presents the findings from some additional studies that are relevant to the research objectives, but which have not been submitted for publication. Chapter 8 provides a general discussion and synthesis of the experimental work described in Chapters 3-7, and Chapter 9 draws conclusions from all of the preceding chapters, and makes recommendations for future work.

Some additional figures and tables of raw data are provided in Appendixes 1 – 4. A disk containing all data in these appendixes, and some additional data in the form of data files or spreadsheets is enclosed with the thesis. A list of files that are on this disk is given in Appendix 5.

Chapter 2 – Literature review and introduction to radiation measurement

2.1 Introduction to Chapter 2

Four of the later chapters (Chapters 3 – 6) are written in the form of scientific papers which have either been published or submitted for publication. Each begins with an introduction that includes a specific literature review relevant to the subject of that chapter. This chapter (Chapter 2) provides an additional, preliminary review of the literature on radioactively contaminated land and its characterisation. In cases where further information is provided in the reviews contained in Chapters 3-6, this has been made clear in the text.

This chapter contains three main sections, each with a short introduction. First, a review of current legislation in the USA, Europe and the UK is given. Following this there is a discussion of the characterisation of land areas for **contaminants**. Finally, a brief introduction to the various methods of measuring the activity of **radionuclides** is given.

2.2 Current legislation of radioactively contaminated land

Legislation concerning radioactively contaminated land varies in different countries. Where specific legislation exists, it is often in the form of an extension to pre-existing legislation that was originally intended for chemically contaminated land. This section gives a brief outline of legislation in the United States and the United Kingdom. The case study site used for the experiments that are described in this thesis is Dounreay, which is located in Scotland, so there is a specific emphasis on Scottish legislation.

2.2.1 Legislation in the USA

In the USA, The Environmental Protection Agency (EPA), Nuclear Regulatory Commission (NRC) and Department of Energy (DOE) are responsible for the release of sites for restricted or unrestricted use. The release of a facility for unrestricted use requires facility licensees to demonstrate that the average member of a critical group will not be exposed to residual radioactivity levels (distinguishable from background) that will result in a total **effective dose equivalent** (**TEDE**) of more than 0.25 mSv per annum . The TEDE is calculated as the sum of the

effective dose equivalents for internal and external exposures. There is a further requirement to reduce levels so that they are as low as reasonably achievable (**ALARA**) below this threshold. What is considered ALARA is determined to a large extent on a consideration of the predicted cost-benefit ratios of remediation. In some situations where the 0.25 mSv criterion is not reasonably achievable, delicensing might still be carried out if the licensee can demonstrate that the total exposure from multiple sources will not exceed a TEDE of 1 mSv/annum (USNRC, 2013).

The effective dose equivalent (in units of Sieverts) is a measure of the probable effect on an organism resulting from exposure to radiation. For each type of radiation acting on a particular tissue or organ, it is calculated by multiplying the **absorbed dose** by a factor (known as a quality factor) which characterises the form of radiation (e.g. electrons or heavier charged particles), to give an **equivalent dose**. The equivalent dose is then further multiplied by a weighting factor that accounts for the radio-sensitivity of the affected tissue or organ, to give the effective dose (the term *effective dose equivalent* is used by the **US EPA**) (Knoll, 2000).

For the purposes of environmental investigations, regulatory dose limits need to be converted into **action levels**, in units of total activity or activity concentration. These are either already stipulated in regulation, or need to be calculated based on specific **risk assessments.** Risk assessments sum the potential effects of the target radionuclides, with consideration being given to the various **exposure pathways** (USEPA, 2000a).

2.2.1.1 Data Quality Objectives (DQOs)

Data Quality Objectives were developed by the US EPA as a guideline policy for quality assurance in environmental sampling. Applying the **DQO**s involves a 7 step process that is intended to provide a systematic method of determining the parameters of environmental data collection. The first six steps of the process assist the planner in establishing objective-driven parameters of the survey, such as the action level**,** the spatial and temporal boundaries of the survey, and the tolerable limits on decision errors. These parameters are then used as inputs to the final stage, which produces an optimised survey design that satisfies these requirements. Examples of outputs from the DQO process include the sample size and acquisition method, the placement and number of samples, and the analytical method to be used, among others (USEPA, 2000a). Various computer programs are also available, which can be used to examine the relationship between the numbers of samples, and the uncertainties

arising from random effects, in order to optimise these parameters for a particular confidence level (IAEA, 2004b).

2.2.1.2 Multi-Agency Radiation Survey and Site Investigation Manual (MARSSIM)

The Multi-Agency Radiation Survey and Site Investigation Manual (**MARSSIM**) has been prepared by four agencies within the United States government. It provides a nationally consistent approach to investigations at potentially contaminated sites (USEPA, 2000b). MARSSIM is probably the most comprehensive, standardised approach to the process of characterising radioactively contaminated land that is currently in use. It uses the DQO methodology to give a consistent approach to planning and conducting surveys, as well as the interpretation of survey data. The methodology of MARSSIM focuses on the need for a **final status survey**, which is considered necessary to demonstrate that each area of interest (termed a survey unit) complies with legislative requirements. Demonstration of compliance involves three interrelated processes:

a) The translation of release criteria into contaminant concentration levels (Derived Concentration Guideline Levels, or **DCGL**s);
b) The acquisition of scientifically sound and defensible data on distributions and levels of contamination, as well as any background levels;
c) The use of a statistically based decision rule to determine if the data support the assertion that the site meets the release criteria, with an acceptable degree of uncertainty.

Additional factors such as cost/stakeholder concern are recognised, but are outside the scope of MARSSIM. In brief, two types of statistical tests are used to evaluate data from the final status survey (Chapter 8 in USEPA, 2000b).

a) The non-parametric Wilcoxon Rank Sum (WRS) test is used for contaminants that are present in the background. This requires the setting up of a reference area on or near the site to establish background levels;
b) A *Sign Test* when contaminants are not in the background, or the background levels are considered to be insignificant.

For both of these methods, acceptable probabilities of **type 1 errors** and **type 2 errors** need to be established, and are determined at the planning stage, using the DQO methodology. Equations are provided for calculating the numbers of samples (*N*) that will be required to perform these tests at the stated probabilities of type 1 and type 2 errors. These calculations must be performed separately for each survey unit. The WRS test *N* value is based on the probability that a randomly selected measurement in the survey unit will exceed a randomly selected measurement from the reference area, by a value that is less than the DCGL. A standard (20 %) adjustment is added to *N* to allow for missing data, and the consequent uncertainty in the calculation of *N*. In the WRS test, *N* is split equally between the reference site and each survey unit. When the target contaminants are not present in the background, however, a Sign Test needs to be used. In this situation, a reference area is unnecessary, and *N* simply refers to the number of measurements that are required in the survey unit.

Further calculations are then applied to determine the measurement spacing (*L*) that is required in the survey unit in order to identify smaller areas of elevated activity. A revised value of *L* is subsequently determined, depending on whether the original value dictates a number of samples for the survey unit that is less than or greater than *N*/2 (WRS) or *N* (Sign test). In any case, it is recommended that any individual measurement results that are higher than the DCGL be subject to further investigation, regardless of the outcomes of the tests (USEPA, 2000b).

The MARSSIM approach has also been adopted by some countries outside the USA as part of their approach to the design of radioactively contaminated land surveys.

2.2.2 European Legislation

The primary legislative body in supranational Europe is the European Atomic Energy Community (Euratom). This was established alongside the EEC in the 1957 treaties of Rome, in order to further cooperation in research, set common safety standards, ensure equitable fuel supplies and to monitor the use of nuclear energy for peaceful means. It remains distinct from the European Union, but has the same state membership (Europa, 2007). Basic safety standards for the protection of workers and the public are set out in Council Directive 96/29/Euratom. This directive provides definitions of what would be considered as **practices** that may result in a significant increase in exposure to workers and/or members of the public, and which therefore come under state regulation and reporting requirements. The 96/29 directive specifies maximum permissible doses, exposure levels and fundamental principles of

health surveillance of workers. For example, the maximum effective dose limit for exposed workers is set down as 100 mSv in any consecutive five year period, not to exceed 50 mSv in any one year. Lower limits apply to special categories of workers e.g. pregnant women, apprentices and students. Effective dose limits to members of the public as a result of authorised practices are set at 1 mSv per year, except in special circumstances. There are also equivalent dose limits for specific parts of the body e.g. the lens of the eye. Determination of whether a practice is reportable or not is established on the basis of a list of maximum activity levels (or mass activity concentration levels) of specific radionuclides contained in Table A of Annex 1 of the directive. A summation rule applies when more than one radionuclide is produced (Euratom, 1996).

Member states are required to implement the Directive through national legislation, but methods of compliance are determined by individual member states. For example, the dose limit of 100 mSv over five years is implemented in the UK via the Ionising Radiations Regulations 1999, which imposed a dose limit of 20 mSv in any one year. A further example is the application of the concept of *clearance levels*, which may be used by competent authorities in order to permit the release of specific waste streams within a regulated practice from the requirements for reporting, allowing them to be disposed of, recycled or re-used without further regulation. Clearance must fall within with the same basic requirements that apply to exemption as set out in Annex 1. Deviations from the maximum activity levels in Annex 1 are permitted, but require that the additional effective dose to any individual member of the public as a result of the exempted practice does not exceed 10 μSv per year (other criteria also apply) (Euratom, 2000; Euratom, 1996).

Technical guidance documents are provided, e.g. the document ‘Radiation Protection 122’ sets out non-binding guidance intended to assist competent authorities in the dose calculations that are required in order to set clearance levels, based on an additional effective dose of less than 10 μSv per year (Euratom, 2000).

Other European legislation exists in specific contexts, e.g. the OSPAR Convention for the Protection of the Marine Environment of the North-East Atlantic which, following OSPAR decision 98/2, prohibits dumping in the maritime area of low and intermediate level radioactive substances (Ospar, 2007; Ospar,1998).

2.2.3 Legislation in the UK

In the United Kingdom, the Health and Safety Executive (**HSE**) is a non-departmental public body responsible for the regulation and enforcement of health and safety in the workplace. The body responsible for the regulation of radioactively contaminated land on nuclear licensed sites is the Office for Nuclear Regulation (**ONR**), which is an agency of the HSE. The ONR provides a legal definition of radioactively contaminated land as 'land containing radioactive contamination that would preclude ONR giving notice in writing that in its opinion there ceases/has ceased to be any danger from ionising radiations on site, or part of the site' (HSE, 2013; ONR, 2013).

Following a process of public consultation, the HSE formalised the use of the term "no danger", contained in the **Nuclear Installations Act 1965** (**NIA65**) (National Archives, 1965) to mean that the additional risk of death to an individual as a result of residual radiation levels above background will be less than one in a million per annum. If it can be demonstrated that this criterion has been met, then a site can usually be removed from regulatory control under NIA65 (HSE, 2005). There is also a general requirement under the Health and Safety at Work Act to reduce risks to as low as reasonably practicable (**ALARP**) (HSE, 2010).

Guidance for the management of radioactively contaminated land is provided as a series of revisions to Part IIA of the Environmental Protection Act, which deals with the subject of contaminated land generally (National-Archives, 1995). These modifications were created as separate regulatory documents for England, Wales and Northern Ireland in 2006 (National Archives, 2006a; National Archives, 2006b; National Archives, 2006c), and for Scotland in 2007 (National Archives, 2007). All guidance documents require that the benefits of any remediatory intervention are weighed up against the health detriment and cost of intervention, and that the perceived benefits are maximised. This is presumed to be in line with the stochastic effects of long term exposure to low levels of ionising radiation. In England and Wales, management of contaminated land is the responsibility of the Environment Agency and local authorities.

In Scotland, which is the focus of this project, the Scottish Environment Protection Agency (**SEPA**) is responsible for the identification of radioactively contaminated land, while the local authority is required to notify SEPA of areas of land which they suspect may be radioactively contaminated (National Archives, 2007). Radioactive Contaminated Land is defined in Scottish legislation as:

"any land which appears to the appropriate agency (SEPA) to be in such a condition, by reason of substances in, on or under the land, that –
(a) Significant harm is being caused or there is a significant possibility of such harm being caused; or
(b) Significant pollution of the water environment is being caused or there is a significant possibility of such pollution being caused" (Scottish Government, 2010).

Significant harm for humans is further defined in Chapter 3, Annex 3 of the Statutory Guidance to the Radioactive Contaminated Land (Scotland) Regulations, as maximum annual dose criteria (e.g. a maximum effective dose of 3 mSv per annum), and for non human species as maximum dose rates (e.g. 40 μGy hr^{-1} for terrestrial species) (Scottish Government, 2010).

In order to de-license part or all of a nuclear licensed site, the HSE must be satisfied that the "no danger" criterion has been applied. This requires the site license holder to demonstrate that any remaining residual radioactivity above background will lead to a risk of death to an individual for any reasonably foreseeable purpose of no greater than one in a million per year. This is interpreted as an additional effective dose of 10 μsV or less per year, based on European directives (see Section 2.2.2) and on international safety standards for the clearance and exemption of practices (and sources within practices) from the requirements for practices (Hill, 2010; IAEA, 2004a).

2.2.4 Threshold values of radionuclides (UK)

Risks from radioactive contamination can be considered in terms of long-term exposure to distributed material, and also acute exposure to concentrated material. This is to some extent reflected by the fact that two maximum contamination levels (thresholds) are commonly used in assessing whether remediation is required: first, an average activity concentration over a defined area; second, a maximum allowable activity within that area. In the latter case (referred to as a **hotspot** in this thesis), this might be defined either as activity per unit object, or as a maximum allowable activity concentration within a fraction of the total area (EA, 1999).

In the United Kingdom generally, a system of permitting is in place for the keeping and use of radioactive substances, and also for the accumulation and disposal of radioactive wastes. Legislation is provided by the Environmental Permitting Regulations 2010 and the Radioactive Substances Act 1993 Amendment (Scotland) Regulations 2011. Radioactively contaminated

land is not specifically covered by this legislation, because the radioactivity in contaminated land is not considered to be kept or used: however, once excavated, radioactively contaminated soil becomes waste, and this is under legislative control. Radioactive substances and wastes of activities below certain threshold concentrations are considered to be either out-of-scope or exempt from the permitting law. These thresholds are based on estimates of radiation dose which could be received by members of the public. For example, a maximum additional effective dose of 10 μSv/year, resulting from artificial radionuclides in radioactive materials or waste, is considered to be exempt or out-of-scope of regulation. This is based on international standards and guidance (DEFRA, 2011). In the case of ^{137}Cs, activity concentrations of less than 1 Bq g^{-1} are considered out-of-scope of the legislation, whereas activity concentrations of between 1 Bq g^{-1} and 10 Bq g^{-1} are considered to be radioactive materials, but may be exempt from permitting, provided other exemption criteria are met (DEFRA, 2011). The activity concentration limits are based on calculations of the expected effective dose under different exposure routes, e.g. ingestion, inhalation, external radiation, and skin contamination. Derivations of these dose levels are detailed in Annex 1 of the European Commission Guidance on General Clearance Levels for Practices (Euratom, 2000).

The thresholds previously described are based on estimates of exposure to members of the public to sources of radioactivity that are homogeneously distributed in the environment. The potential dose to a person is calculated from a combination of habit surveys and knowledge of the radiation levels. When a person is in a generally contaminated area it can be assumed that the probability of encounter with radiation is certain. However, a specific characteristic of some radioactive contamination is the presence of small, discrete, hotspots of activity (particles). These can present a relatively high hazard to members of the public, especially if they could (e.g.) be inhaled or ingested. In the case of particles, which may be too small to see with the naked eye, the probability of encounter is hard to establish. Various guidance documents for establishing the combination of potential dose and probability of encounter are provided by the International Commission on Radiological Protection (ICRP). For example, where an encounter could result in death, a probability of encounter of one in a million per annum is considered to be appropriate (Dale, 2008). The subject of setting workable thresholds for radioactive particles is discussed further in *Sections 5.2.1* and *4.2.2.*

In order to illustrate the general issues, the target radionuclide of interest in all of the experiments presented in this thesis is ^{137}Cs, for the reasons explained in *Section 4.2.3*. Tables

of the legislative scope and exemption criteria for other radionuclides are provided by Defra (2011).

2.3 Characterisation of contaminated land

Characterisation of radioactively contaminated land on a decommissioning nuclear site is carried out in order to determine what, if any, action is required. Data from investigations is an essential component of risk assessments to establish what hazards are present to personnel and the environment, now or in the future. An immediate objective is to protect site personnel, although the long term objective is to enable eventual **delicensing** of areas of the site. As has previously been stated (*Section 2.2.4*), this usually requires establishment of mean activity or activity concentration levels over a defined area, and also the maximum allowable activity in any part of that area. The latter is expressed either as a maximum activity per object, or maximum activity per unit volume (EA, 1999). This section begins by discussing the quantity which is to be measured in radioactively contaminated land investigations, and the measurement units that will be used in this thesis. The terms **sampling target** and **measurand** are also discussed. It then introduces the concept of measurement uncertainty, and provides definitions that are used in subsequent chapters. The contribution of **sampling uncertainty** to the total measurement uncertainty is considered, after which there is a discussion on the different approaches to uncertainty estimation. The method used here, known as the **duplicate method,** is introduced. A review of methods of evaluating levels of **heterogeneity** of contaminants is then given. Finally a discussion on the evaluation of the fitness-for-purpose (FnFP) of measurements is provided.

2.3.1 Defining the quantity to measure in investigations of radioactively contaminated land

The question of what quantity to measure in an investigation of radioactively contaminated land must be resolved, but is somewhat complex. Where the purpose of the survey is to satisfy the objective of avoiding harm to people, then this issue is complicated by the several stages involved in calculating the effective dose. Clearly this depends not only on the type and intensity of radiation, and the nature of the receptor, but also on the pathway that radionuclides take from source to receptor. For example, the exposure to radionuclides that an individual receives by consuming crops grown at a contaminated site will likely be significantly different from that which he or she receives by working at a location with ambient radiation

levels that are slightly above background. It further depends on the behaviour of specific radionuclides, regardless of the types and intensities of their emissions and their activity counts. Examples are provided by the two man-made radionuclides that are thought to pose the greatest risk to humans, caesium-137 and strontium-90 (Eisenbud and Gesell, 1997). The physical half-life of ^{137}Cs is approximately 30 years, and pathways to humans arise from ingestion of cow's milk, meat, grains, fruit and vegetables. However, as ^{137}Cs is well retained by clay soils, so much so that root uptake is minimal, the main source of exposure is thought to result from ambient environmental levels that have arisen from aerial deposition following nuclear tests and accidents. In the human body, ~80 % of ingested ^{137}Cs enters muscle tissue, while ~8 % enters bone. The residence time in the body depends on body weight, sex and dietary habits, with women having a more rapid turnover than men. It has been shown to have a biological half-life of 19 ± 8 days for infants, and of 105 ± 25 days for men. In contrast, ^{90}Sr (with a physical half-life of 28 years) is chemically similar to calcium, and so one of its prime pathways to the human body is through the ingestion of cow's milk, although some will also be ingested via plant products. When inside the body it predominantly enters bones, where it is very likely to remain until the death of the individual (Eisenbud and Gesell, 1997).

In the United States, regulatory limits for radioactive contamination are defined either in terms of dose (e.g. Sieverts), or of risk (e.g. of cancer mortality). For the purposes of site surveys, these units are converted into radionuclide-specific activity concentrations*,* or surface area concentrations of specific radionuclides, by modelling potential exposure pathways. Exposure pathway modelling is performed through an analysis of the various pathways and potential exposure scenarios, and can therefore be used to convert risk or dosage into activity concentration units, for example units of Bq kg^{-1} where 1 Bq (Becquerel) = 1 disintegration per second (USEPA, 2000).

The Radioactive Substances Act, as amended in Scotland by the Radioactive Substances Act 1993 Amendment (Scotland) Regulations (2011), defines the terms *radioactive materials* and *radioactive waste.* Different definitions apply depending on whether a *substance or article* arises from defined industrial activities involving NORM processes that are intended to use the radioactive properties of radionuclides of natural terrestrial or cosmic origin, or any material that contains radionuclides which are not of natural terrestrial or cosmic origin. In all cases the definitions apply only if the activity concentrations of individual radionuclides, in units of Bq g^{-1} (solid), Bq l^{-1} (liquid) or Bq m^{-3} (gas) exceed specified values (Scottish Government, 2011). All of the measurements described in this project pertain to levels of solid radionuclide

contaminants in the ground, and so where comparisons to these threshold levels (e.g. 1 Bq g^{-1} for ^{137}Cs) are implied or required, these are expressed in units of mass activity concentration (Bq g^{-1}). However, in order to convert measurements of raw activity to mass activity concentration units, it is necessary to define the portion of the material that each measurement is intended to represent.

The sampling target is defined as "the portion of material, at a particular time, that the sample (and therefore the measurement result) is intended to represent" (Ramsey and Ellison, 2007). In contaminated land investigations, it can therefore be used to represent the mass or volume of soil (or other substrate) that each primary sample is intended to represent. This term needs to be distinguished from the *primary sample mass (or volume)*, which is used to define the actual mass of a single **primary sample**. In the case of *ex situ* measurements of extracted soil samples, the latter is readily measureable and will almost always be smaller than the sampling target. It will be seen in Chapters 4 and 7 that because of the penetrating nature of gamma radiation, the primary sample mass of *in situ* measurements made with a gamma detector is less easily defined, and is often larger than the sampling target . Therefore some assumptions need to be made about its extent.

It is useful to define a further term, the *measurand*, in contaminated land surveys. A formal definition of measurand is provided by the International Organisation for Standardisation (**ISO**) as "the quantity intended to be measured" (JCGM, 2008a). A less formal definition, which expands on this concept for the purposes of analytical chemistry, has been given as "the true value of the **analyte** concentration in a specified segment of material" (Ramsey, 1998). In fact, the true value can never be known, but the measurand concept can be used as a reference point in other definitions, for example in the definition of measurement uncertainty given as: "non-negative parameter characterizing the dispersion of the quantity values being attributed to a measurand, based on the information used" (JCGM, 2008a).

The term 'analyte' is used in chemistry to refer to a particular chemical element or compound of interest. The definition of the measurand can be further refined as the value of the analyte concentration in the sampling target, or that within a sample of the sampling target, for example in a sub-sample that is extracted for laboratory analysis (Ramsey and Ellison, 2007). This thesis uses the term measurand to describe the true value of the analyte concentration in the sampling target. Where it is necessary to characterise activity concentrations, the

measurand is considered to be the true value of the mass activity concentration in the sampling target, in units of Bq g^{-1}. Where it is required to evaluate the activity of discrete objects (particles), then the measurand is considered to be the maximum activity of a point source within the sampling target.

2.3.2 Definitions of measurement uncertainty

All measurements are subject to uncertainties. An informal, but useful, definition of measurement uncertainty has been given as “an interval around the result of the measurement that contains the true value with a high probability” (Thompson, 1995). In contaminated land investigations, individual measurement values are usually compared to some type of action level. For example, measurements of the concentrations of a contaminant that have been obtained in a **systematic survey** on an area of soil might be compared to a threshold value. If all measurements results are found to be below this value, then it may be considered that no further action is necessary. However, if the measurement uncertainty is sufficiently high that the interval around the individual measurements is such that that in a worst case scenario one or more of them could exceed this limit, then the decision of whether or not any further action is required is ambiguous. It is therefore important to make decisions that take account of the uncertainty, as well as the measured values (Thompson, 1995).

A formal definition of measurement uncertainty is given by **VIM** as: “Non-negative parameter characterizing the dispersion of the quantity values being attributed to a measurand, based on the information used” (JCGM, 2008a). It is important, though, to recognise that this definition is not specific about the method of uncertainty estimation, nor the parameter used to express it. It also assumes that the measurement result is the best estimate of the value of the measurand, and that there are potentially many components of uncertainty, including **systematic effects**, that contribute to the dispersion of values around it (JCGM, 2008b).

A further guide (**GUM**) prepared by a joint working group that includes the ISO, defines **measurement error** as “the result of a measurement minus a true value of the measurand” (JSGM, 2008b). In this definition, the term ”a true value of the measurand” can refer to one of several different values, e.g. the value of a **certified reference material (CRM)**. Although it is not usually possible to know the true value, it can generally be assumed that one exists (Thompson and Ramsey, 1995). According to GUM, measurement error traditionally has two components, known as **systematic error** and **random error,** which arise due to systematic

effects and **random effects** (in the measurement method). GUM makes a distinction between the terms *uncertainty* and *error* in this context, because both systematic and random effects contribute to the distribution of measurement values around the measurand (JCGM, 2008b). However, the terms *systematic component of uncertainty* and *random component of uncertainty* are used in this thesis, as this usage is consistent with terminology found elsewhere in the scientific literature.

Where an empirical estimate is made of the uncertainty due to random effects, then this might be considered to be the **precision** of the measurement method**,** which describes characteristics such as the **repeatability**, **reproducibility,** or the **intermediate precision** of measurements (Ramsey and Ellison, 2007; JCGM, 2008a).

The word **bias** is often used (as in this thesis) to describe an estimate of a systematic measurement error (JCGM, 2008a). If a CRM is available, then the bias due to an analytical process can be calculated by subtracting the certified value of the analyte in the reference material from the value of a measurement made on that reference material. This is because it is assumed that the certified value is the best estimate of a true value (or measurand) that can be achieved (Thompson and Ramsey, 1995).

2.3.3 The contribution of sampling uncertainty to the total uncertainty

Measurement uncertainty arises from a number of different sources, and potentially at any stage throughout the measurement process, from the point of sample collection to the final reporting of measurement results. Much effort has been put into the reduction and evaluation of **analytical uncertainty** in laboratory measurements at the time of method validation, and the subsequent checking of its applicability to routine analysis using quality control and quality assurance procedures. However, there is increasing awareness that sampling uncertainty is often the largest component of the overall uncertainty of the measurement result. In the case of contaminated land, sampling uncertainty includes the uncertainty that derives from the spatial positioning of the measurement locations (Boudreault, 2012; IAEA, 2004b; Ramsey and Argyraki, 1997; Ramsey and Ellison, 2007; Taylor *et al.,* 2004). Sampling uncertainty can be considered to represent the uncertainty in measurements that arises when a primary sampling process (using the same nominal protocol) is repeated. Because the same protocol is assumed, one method of estimation of the sampling component of uncertainty can be made by acquiring duplicated primary samples, at a lateral displacement that is estimated to be the same as

could naturally occur if the protocol were repeatedly applied (Ramsey and Ellison, 2007). There may, therefore, be additional components of sampling uncertainty arising due to differences in interpretation of the sampling protocol, and also from processes inherent in the sample transport and preparation (note that uncertainties arising from the drying and grinding of primary samples are often included in the sampling uncertainty rather than the analytical uncertainty, even though these processes are carried out in a laboratory). However it is usually the case that heterogeneity of contaminants is the dominating factor in estimates of the random component of sampling uncertainty (Ramsey *et al.*, 2013).

It has been found that spatial heterogeneity of the target analyte in the soil within the sampling target is often the limiting factor in uncertainty reduction, and may contribute uncertainties of ~50 % or more to the total random component of measurement uncertainty (Ramsey and Argyraki, 1997). Land that is contaminated by radionuclides has often been found to exhibit high levels of contaminant heterogeneity (Dale *et al*., 2008; IAEA, 1998; IAEA, 2011). It is therefore likely that estimations of sampling uncertainty will have a significant impact on decisions that are made from the results of radioactively contaminated land investigations.

2.3.4 Uncertainty estimation in contaminated land investigations

Dealing with the potentially high levels of sampling uncertainty in contaminated land investigations is of high importance. Much has been written on the subject of materials sampling, notably by Pierre Gy. Gy's methods, termed *Theory of Sampling* (**TOS**), or *Sampling Theory and Practice* (**STP**) were developed in the field of mining science. They are rooted in the answers to two fundamental questions: how samples should be collected, and how much material should be sampled. A probabilistic approach is taken to obtaining **representative samples** from a batch (Gy uses the term *lot*) of material. Reliable samples are obtained by using a *correct* procedure that a) equalises the probabilities that the different constituents within the lot are selected; b) respects the integrity of the selected constituents (Gy, 2004). An advantage of this type of approach is that if the nature of the constituents of the lot, including their properties and respective dimensions, can be reasonably well predicted, then a theoretically optimal sampling strategy can be designed at the planning stage. Unfortunately, in contaminated land investigations, these factors are not likely to be well known prior to sampling (Kufurst *et al.*, 2004).

A comparison between procedures based on a) Sampling Theory and Practice, and b) non-probabilistic **grab-sampling**, carried out on chemically contaminated land, showed that using the STP approach to design the sampling strategy increased data reproducibility by an average factor of 10 when compared to grab sampling (Boudreault, 2012). However, empirical estimates of the variances due to sampling were found to be 2-4 orders of magnitude below the sampling variances predicted by the STP methodology. The author suggests that the primary reason for this was that the variances predicted by STP were based on an assumption that 100 % of all contaminants would be liberated from the soil matrix during analysis. A closer agreement was obtained by calculating a value for the *soil liberation factor*, based on mineralogical data. The author consequently recommends that the liberation factor be investigated prior to using STP equations to analyse and design representative sampling procedures (Boudreault, 2012). This may be difficult to establish reliably, and Ramsey (1998) points out that these kinds of fundamental factors may be subject to variation across the total survey area.

Contaminated land investigations are likely to be subject to more constraints than would be the case for many sampling tasks (e.g. a batch of material on a production line), due to the varied sizes and compositions of land areas, any obstructions, and also temporal conditions such as soil moisture content at the time of a survey. When samples are to be extracted for laboratory analysis, the available techniques, e.g. the use of a corer or digger, may affect the sample composition, and in the case of some *in situ* methods, it is not possible or practical to use a pre-determined sample size. For example, a hand-held XRF used in chemical investigations has a very limited (~1 cm^3) primary sample size, whereas in investigations of radioactively contaminated land that use a gamma-ray detector, the response of the detector to a gamma-emitting constituent (and therefore the probability of detection) depends on the position of that constituent with respect to the detector.

In practice, investigations of different land areas are most often carried out with standard equipment, and frequently combine a mix of **targeted sampling** and **non-targeted sampling.** Targeted sampling, or judgemental sampling, is employed when there is good information about the likely distributions of contaminants, e.g. there is a known potential source such as an historic leak from a pipe or drain. Non-targeted sampling, or non-judgmental sampling, is used when the purpose of an investigation is to characterise the distributions of contaminants, or evaluate the average or maximum contamination levels within a defined area. Techniques such as those prescribed by MARSSIM (USEPA, 2000) can be used to calculate the numbers of

samples that are needed to estimate an areal mean value with a defined confidence level. The varying size and nature of contaminated land sites also makes them more likely to be subject to financial constraints. Given the many factors that affect these types of investigations, it is important that the end user of the measurements acquired in a survey has sufficient information to be able to make reliable decisions. Although it is possible to use STP principles to calculate the variance due to sampling (e.g. Bordeault, 2012), the TOS approach makes an implicit separation of the uncertainties that arise due to sampling, and those that arise during the analysis of the samples. Ramsey and Boon (2010) suggest that it is more effective to report and consider both of these types of uncertainty explicitly and together, in order that the user is in a better position to make informed decisions based on the measurements.

In chemical analysis, there are two main strategies for estimation of the random component of measurement uncertainty. In the **bottom-up** approach, the overall uncertainty is calculated as a sum of the estimated variances of the random errors in each stage of the measurement process. The alternative **top-down** method uses some degree of replication of the measurement procedure, in order to be able to calculate an empirical estimate of the uncertainty in the final measurement (Ramsey, 1998; Ramsey and Ellison, 2007). Both methods have advantages and disadvantages. The bottom-up method enables each source of error to be considered individually, which may be useful in the control of overall uncertainty levels. However, it depends on reliable identification of all the potential sources of error, and in some cases, the main contributor to overall uncertainty might be missed (Ramsey, 1998). The top-down method has the advantage that overall measurement uncertainty can be estimated without needing to know each individual uncertainty component (Ramsey and Ellison, 2007). If an understanding of the individual uncertainty components is a priority, for example if it is desired to know the uncertainty contribution due to random effects that are caused by heterogeneity of a soil sample in a laboratory gamma detector, then it is necessary to take increasing numbers of replicated measurements to separate this uncertainty source from others. The two broad strategies described here are not mutually exclusive (Ramsey and Ellison, 2007). For example, the uncertainty due to random effects caused by sample heterogeneity could be estimated using replicates, and this information could then be used to improve an estimate of overall uncertainty by using the bottom-up approach.

It is possible to use geostatistical methods to account for some of the effects of the random component of measurement uncertainty in contaminated land investigations. In this approach,

the spatial (and potentially, temporal) locations of a sampling pattern are processed along with the measurements at those locations to produce a model of concentration levels at a site, using an interpolative process known as “Kriging”. The model can then be used to predict concentration levels at a given point, or the mean concentration within a given area. The predictions are obtained from a probability distribution of all possible realisations of the model (based on the measurements), and therefore the model incorporates some of the effects of the random component of measurement uncertainty at individual measurement locations, as well as the geochemical variance. As these models incorporate spatial data, they are particularly useful in the analysis of contaminated land, where point concentration levels tend to exhibit some degree of auto-correlation (Brus and Gruijter, 1997; Goovaerts, 1999). However, the measurement uncertainty is not specifically evaluated and included in the interpolation, and so Kriging tends to underestimate the random component of uncertainty, and any systematic component of uncertainty is not taken into account.

Published surveys of contaminated land vary considerably in their methods of dealing with measurement uncertainty. For example, de Zorzi *et al.* (2002) applied the principles described in the Eurachem guide (Ramsey and Ellison, 2007) to a bottom-up estimation of sampling uncertainty of trace elements in agricultural land. A bottom-up approach, based on recommendations contained in the GUM guide, was also used by Kurfurst *et al.* (2004) in a report on an inter-comparison exercise between the sampling protocols of 15 different European countries. However, where surveys on contaminated land have been published in the scientific literature, and in which uncertainty estimations, and the methods of estimation, have been reported, the authors have often devised their own methods of estimation. For example, Golosov *et al.* (2000) evaluated the use of *in situ* measurements for estimating the spatial variability of ^{137}Cs in a drainage basin in Russia. The authors used between 5 and 7 replicated measurements to estimate the random component of uncertainty in the analyses of the *in situ* measurements. The contribution of random effects due to sampling was also considered, in a comparison of the coefficients of variation between *in situ* and *ex situ* measurements, but was not evaluated explicitly for each measurement location. Other examples of bespoke methods of uncertainty estimation, used in surveys of chemically contaminated land, are provided by Buckzo *et al.* (2012) and Back (2007).

As the sampling uncertainty due to random effects in contaminated land investigations is often found to be much greater than the analytical uncertainty, it may be the limiting factor in uncertainty reduction. Ramsey (1998) suggests that when the sampling uncertainty is large,

then reductions in analytical uncertainty may make a negligible difference to the total uncertainty, and would not therefore be cost effective. He suggests an approach where **primary sampling** is considered to be the first stage in the overall measurement process. A method of uncertainty estimation due to random effects proposed by Ramsey, and also recommended by the Eurachem guide, is termed the *duplicate method***.** In this method, duplicated samples are taken at a proportion of the primary sample locations, and duplicated analyses are then carried out on each in a **balanced design** hierarchy. Where applicable, the spatial distance between the duplicated samples at the primary locations is determined by an estimate of the spatial separation that would have occurred had the same nominal sampling protocol been repeatedly applied (See *Section 2.3.3*). The results of the measurements from the duplicate samples and analyses can then be analysed by robust ANOVA (See *Section 3.2*) in order to separate the different contributions to the overall random component of uncertainty that are made by the sampling and the analysis. This is the method that has been used in this project, and is described in more detail in the introduction to Chapter 3 (*Section 3.2*). The magnitude of the random component of uncertainty is expressed as the **expanded relative measurement uncertainty**, in which the relative standard deviation of the measurement uncertainty is multiplied by a coverage factor of 2 to give a confidence level of approximately 95 %.

Systematic errors, as well as random errors, occur in all measurements. Estimation of the systematic errors in analysis (quantified as **analytical bias**) can be achieved by comparing measurements of certified reference materials (CRMs) with their known values. Ideally, these measurements are made over a range of analyte concentrations and with reference materials that have the same substrate composition and physical characteristics as the field samples. This procedure is relatively straightforward to carry out in the laboratory for chemical contaminants, provided suitable CRMs are obtained. Empirical estimations of the analytical bias in *in situ* measurements of penetrating gamma radiation is far more difficult, and is further discussed in Chapter 7.

Estimates of uncertainty arising from systematic errors in sampling (**sampling bias**) are generally harder to quantify than analytical bias. Ramsey *et al.* (2011) showed the effects of sampling bias in the food industry by analysing the results of a **sampling proficiency test** (**SPT**). Comparison of the uncertainty estimates *between-samplers* with the uncertainty estimates *within-samplers* showed that sampling bias was causing an approximately two-fold increase in

the overall estimate of measurement uncertainty. Two potential approaches for estimating sampling bias in contaminated land investigations are discussed by Ramsey (1998). They require the setting up of a **reference sampling target** (**RST**). The sampling bias can then be calculated by comparing the results of measurements from one or more samplers to a certified value for the RST. The problem is in establishing the certified value. The first of the proposed methods achieves this by taking a consensus from an inter-organisational sampling trial. The second method involves spiking the RST with known concentrations of the target analyte. The latter method has been successfully applied in the case of chemical contamination, by measuring the background levels in a defined area of ground, and then deliberately creating a hotspot of contamination within the area (Ramsey *et al.*, 1999). The applicability of this approach was demonstrated in a subsequent inter-organisational SPT, when the performances of nine different samplers were evaluated in the task of delineating the hotspot (Squire *et al.,* 2000).

2.3.5 Evaluation of heterogeneity in contaminated land investigations

It has been suggested (*Section 2.3.3*) that heterogeneity of contaminants is likely to be a significant factor in investigations of radioactively contaminated land. It may also be the single factor that makes the largest contribution to the overall random component of measurement uncertainty (Ramsey and Argyraki, 1997). Understanding contaminant heterogeneity and its potential impact is therefore an important part of understanding the characteristics of a site, and the uncertainties that might arise in the interpretation of measurements. According to Ramsey *et al.* (2013) there are three fundamental approaches to the issue of spatial contaminant heterogeneity:

1. Reduce effects of heterogeneity by taking larger samples (or **composite samples**);
2. Report the effects of heterogeneity as part of the uncertainty in each measurement;
3. Apply methods to explicitly evaluate heterogeneity over a range of spatial scales.

The last of these methods can be used both as an aid to the design of sampling surveys, and also to enable more reliable interpretation of the measurements obtained by a systematic survey. The most common approach to the evaluation of spatial heterogeneity of chemical contaminants in land areas is the production of variograms. Variograms model the variances in measurement results for groups of measurement pairs with similar spatial separations, as a function of the spatial separation distance. These models can then be used by methods such as Kriging to interpolate values of contaminant concentrations at un-sampled locations, by taking

into consideration the modelled variances between sampled and un-sampled locations at known separations. Quantitative estimates of the uncertainties at un-sampled locations due to heterogeneity of contaminants can also be made from the predicted variances, although these do not include the uncertainties at individual locations (Myers, 1997).

It has been found that patterns of geochemical data are often fractal in nature, i.e. the level of complexity does not decrease as the spatial scale decreases. Fractal or multi-fractal interpretations of geostatistical data have been used to determine threshold levels above which geochemical anomalies can be considered to exist (Li *et al.*, 2003), and also to characterise land area distributions of elements (especially trace elements) without the use of grid sampling techniques (Li *et al.*, 2004);

These methods of evaluating spatial heterogeneity are relatively complex and are usually only applied over relatively small ranges of spatial scales (e.g. 2 orders of magnitude). An alternative method used by Taylor *et al.* (2005) quantified heterogeneity as the **relative standard deviation** (**RSD**), estimated by the duplicate method when applied to *in situ* measurements. The contribution to the total measurement variance arising from random effects in the analytical method was first subtracted from the RSD to eliminate this component of variance from the heterogeneity estimate. Using this method, the heterogeneity in chemical contamination data was estimated from two different sites over spatial distances differing by 4.5 orders of magnitude (0.001m to 50m). It was shown to be a useful means of comparing heterogeneity between different contaminants in a single site, and also between the same contaminants in different sites.

Ramsey *et al.* (2013) proposed the use of the balanced design (*Section 3.2*) and robust ANOVA to estimate the standard deviation that arises from sampling (SD_{samp}). If it is then assumed that SD_{samp} arises due to heterogeneity alone, then a useful metric for evaluation of the heterogeneity in contaminated land investigations can be expressed either as the percentage relative standard deviation of sampling (RSD_{samp} %) or as a heterogeneity factor (HF), where HF = $10^{GSDsamp}$, and GSD_{samp}= the standard deviation of a log-transformed distribution. This approach was shown to be a better fit to experimental data than a variogram model in one case study site. It also enables direct comparisons of heterogeneity to be made between different contaminants on different sites.

2.3.6 Fitness-for-purpose (FnFP) in contaminated land investigations

The concept of fitness-for-purpose, in the context of a measurement process, has been defined as ”the property of data produced by a measurement process that enables a user of the data to make technically correct decisions for a stated purpose” (Thompson and Fearn, 1996).

One method of evaluating the FnFP of measurements is therefore to determine whether the magnitude of measurement uncertainty is appropriate, taking into consideration the use to which the measurements will be put. FnFP criteria are often based on professional experience. However, generic sampling protocols may not be well suited either to the purposes or to the financial sensitivities of particular investigations (Ramsey *et al.*, 2002). There is, therefore, a potential advantage to estimating the magnitude of uncertainty in measurements that could be considered fit-for-purpose (FFP) according to systematic criteria. An early method was proposed by Ramsey *et al.* (1992). If the analytical uncertainty contributed < 20 % to the total variance, then the measurement techniques would be considered FFP for describing the geochemical variation between different spatial (or temporal) locations.

However, implicit in the FnFP concept is consideration of the particular purposes of an investigation, which is likely to be subject to financial constraints. Consequently Thompson and Fearn (1996) proposed a refined definition in which an empirical economic loss function is used to minimise the expectation of financial losses of an investigation. This enables the costs of performing a survey to be balanced against the estimated potential costs of misclassification of individual measurements. The potential costs of misclassification are a direct consequence of the measurement uncertainty. The method was further developed into a decision theory approach to establishing FnFP by minimising the total end-user losses due to measurement costs, and the probable costs arising from measurement errors (Fearn *et al.,* 2002).

In a contaminated land investigation, misclassification can be of two types: a) **false positive** measurements (type 1 errors), which could lead to unnecessary remediation work; b) **false negative** measurements (type 2 errors), which may result in delays to development of the land and/or possible litigation costs. The new definition of FnFP, based on estimates of total financial losses, led to the development of the Optimised-Contaminated-Land-Investigation (**OCLI**) method. The rationale of this method is based on establishing whether a particular level of uncertainty is acceptable for achieving a particular objective. Estimates are made of the

expectation of financial losses that would be incurred at different levels of measurement uncertainty. The optimal level of uncertainty is the one which results in the lowest expectation of loss. Results from two case-study sites showed that increasing the cost of analysis in order to increase precision was not justified beyond a certain level, because the cost of the measurements became too high. However, reducing the cost of analysis had the effect of increasing the probabilistic consequential costs of misclassification of measurements, due to reduced precision (Ramsey *et al*., 2002; Taylor *et al.*, 2004). Using the OCLI method, the optimal uncertainty is dependent on the extent and severity of contamination on the site, as well as the threshold level to which these measurements are compared. For example, in a case where average concentration values are well below the action threshold, then a relatively high value of measurement uncertainty might be FFP (Ramsey *et al.,* 2002; Taylor *et al.*, 2004). A further use of the OCLI method is to make comparisons of the individual expenditures on sampling with those on the chemical analysis. This potentially enables resources to be directed where they will have the greatest benefit (Ramsey *et al.,* 2002).

OCLI was further development into the Whole-Site-Optimised-Contaminated-Land-Investigation (**WSOCLI**) method, which includes the effects of different sampling densities in the optimisation process. Using this method, it is possible to optimise measurements for the entire survey, instead of at individual measurement locations as in OCLI. The WSOCLI method comprises a loss function that optimises the number of samples acquired, as well as the measurement uncertainty (Boon *et al.,* 2011).

In summary, both the OCLI and WSOCLI methods enable better judgements of FnFP in contaminated land investigations, and also enable the direction of funds to where they are most appropriate (Ramsey *et al.,* 2002).

2.4 Introduction to the measurement of radiation

This section provides a brief introduction to the measurement of radiation, with specific emphasis on the measurement of gamma-emitting radionuclides.

2.4.1 The origins of ionising radiation

In experiments, the measured mass of an atomic nucleus is found to be slightly less than the mass sum of its nucleons (protons and neutrons). This difference (mass defect) comes about because of the energy required to bind the nucleus together against the repulsive **Coulomb forces** between protons. This binding force tends to increase as the atomic number increases,

because a greater number of protons means that greater Coulomb forces are needed in order to hold the nucleus together.

Of about 1700 known nuclides approximately 275 are stable. The stability of nuclides is governed by a) the N/Z ratio (where N = the number of neutrons and Z = the atomic number), which ranges from 1 for the lighter stable nuclei to 1.5 for the heavier stable nuclei; b) Nucleon pairing. Approximately 60 % of stable nuclides have even numbers of protons and neutrons, while the remainder have either an even number of protons or an even number of neutrons.

About 1400 known nuclides undergo spontaneous nuclear transformations, often through a series of intermediate, unstable product nuclei until they reach a stable state. For nuclides with an atomic mass of less than 230, two kinds of nuclear decay are possible (heavier nuclides may undergo spontaneous fission, which is not discussed here). Beta decay occurs when a neutron changes to a proton by emission of an electron. Rarer forms of beta decay sometimes occur in man-made nuclides, in which a proton changes to a neutron either by emission of a positron, or by electron capture. Beta decay is the dominant decay process in nuclei with Z numbers of less than ~80. For nuclei with Z numbers above 80, the dominant decay mode is spontaneous emission of an alpha particle (comprising two neutrons and two protons) due to the increase in Coulomb repulsive forces between protons in larger nuclei.

The difference in binding energies between the original and the product nuclei may be transferred to the alpha or beta particle in the form of kinetic energy, but nuclear transformations, especially of the heavier radionuclides, often result in nuclides which have different binding energies from the lowest energy state (ground state). These are known as isomers. Where these excited states last for longer than a microsecond they are termed metastable isomeric states**.** Isomers decay to the ground state, usually with the emission of gamma radiation, although in some cases this energy might be transferred to an atomic electron that is ejected from an inner shell of the atom in a process known as internal conversion. Often, several gamma rays at different energy levels are emitted in a cascade following decay (Longworth, 1998). Gamma rays are emitted as **photons** of electromagnetic radiation, which, unlike alpha or beta particles, are mass-less and so do not carry kinetic energy. They do, however, have a direction of propagation, and in some respects can be thought of as packets of electromagnetic energy that are capable of causing interactions over relatively long distances compared to alpha or beta particles.

2.4.2 Measurement of ionising radiation

In the late 19th and early 20th centuries, the work of physicists such as Henri Becquerel and Marie and Pierre Curie, advancing on the discovery of X-rays by Wilhelm Röntgen, showed that several elements emit penetrating radiation that will fog a photographic plate, or ionise the air surrounding a sample. These discoveries form the basis of some of the radiation detection equipment that is still in use today. For example, film badges, comprising a sealed piece of photographic film, can provide an estimate of long-term exposure to radiation when compared to an identical piece of film that has been exposed to a known source. This technique still sees widespread use in personal **dosimetry** (Knoll, 2000).

Although this method is useful for estimating total long-term exposure, the degree to which the photographic emulsion is affected by impacting radiation depends on two factors: a) the number of atomic decay processes that result in the emission of radiation; b) the energy levels of emitted radiation, which determines the penetrating power of radiation through intervening media (e.g. air and the film containment). Reliable, low cost quantification of the first of these factors was made possible by the invention of the Geiger-Müller (G-M) counter in 1928, which uses the ionisation properties (first discovered by Marie Curie) to permit an electrical current to flow through a gas-filled tube, thereby creating a voltage pulse. In a G-M tube, once ionisation has been induced by a high energy electron (beta particle) or an alpha particle, comparatively high voltages (e.g. ~10^3 V) applied between a cathode and anode result in an “avalanche” effect, in which electrons released by the ionisation of gas atoms induce further ionisation. Thus a chain reaction can be initiated by a single initial ionisation event. This makes them very sensitive to incoming alpha and beta particles, provided the tube walls are thin enough for alpha particles to penetrate, and the gas volume is sufficient that there is a high probability of beta particle interaction. However, for gamma radiation above low energy levels (~100 keV) it is necessary for electrons to be released into the gas by interactions of gamma photons with the material in the walls of the container. Some G-M tubes are designed specifically to enhance this effect. A disadvantage of G-M tubes is that the chain-reaction of ion avalanches is stopped by a build up of positive ions around the anode. These take time to clear and so G-M tubes are subject to significant **dead time** between each voltage pulse. To compensate for this, corrections must be applied in circumstances where the average detection count rate is over ~100 counts per second (Knoll, 2000).

When Alpha or Gamma radiation is emitted by a radioactive decay process, the energy of the alpha particle or photon is characteristic of the emitting radionuclide. A G-M counter cannot

be used to measure these energy levels, because the chain reaction initiated by a particle is essentially a runaway process that terminates as a result of interactions between the components (e.g. the gas and electrodes) within the ionisation chamber. G-M counters cannot therefore be used to discriminate between different radionuclide sources. Measurement of this second factor, the energy levels of emitted radiation, can enable identification of the radionuclide through the analysis of spectra that are generated by summing the numbers of events across a range of energy levels. Nuclide identification by discrimination between energy levels depends on a proportion of the radiation particles or quanta yielding all of their energy to the detector. This must be a sufficient proportion of the incident radiation that counts of pulses at these characteristic energy levels can be distinguished from single and additive counts from radiation at lower energy levels, and also from any residual energy left over from interactions during the instrument's dead time. In addition, the instrument must be sensitive enough to distinguish characteristic energy levels from those of other sources, and from background radiation. In all such detectors, this process relies on the production of information carriers (such as ***ion pairs*** in an ionisation detector) that induce a measurable effect, such as a charge of electrons in the detector volume, which is measured by electrical circuitry of which the detector is part. Broadly, there are three technological solutions, each using a particular type of information carrier within the detector volume:

1. Gas-filled ionisation detectors. In these types, electrons and positively charged ions (ion pairs) are produced in proportion to the energy level of the incoming particle or quantum of energy. The applied voltage is sufficiently high to ensure that an insignificant number of pairs re-combine before being collected by the electrodes, while being low enough to avoid the runaway chain-reaction that occurs in a G-M counter. Because of the lower applied voltages that have to be used, the output signal requires external amplification by electronic circuitry.

2. Scintillation counters. When radiation is incident on some substances, the excitation followed by de-excitation of their molecules results in the emission of detectable electromagnetic radiation of characteristic longer wavelengths, termed fluorescence. Thus in these devices the information carriers are photons of radiation which are detected and amplified by one or more photo-multipliers. Output from these detectors is proportional to incident radiation, so they can be used for energy spectroscopy. Scintillation detectors can be categorised into two encompassing types:

a) Liquid scintillators: Where the analyte is dissolved into a solution which includes an organic scintillator (e.g. 2, 5-diphenyloxazole). These are used for detection of alpha and

beta radiation. Because the analyte is in solution, nearly all of the energy from these types of short-range radiation is absorbed by the solvent/solute combination, thus achieving near 100 % efficiency. A special type of scintillation counter for the detection of high energy beta particles uses Cherenkov radiation, which occurs when these particles yield some of their energy as a result of a reduction in velocity as they make the transition into a medium where the speed of light is less than that *in vacuo.* This only occurs when the energy of the electrons is above a threshold value that is dependent on the refractive index of the Cherenkov medium, which does not need to include a scintillation component.

b) Activated crystal detectors (e.g. NaI): In a pure crystal, the outermost electrons of the atoms occupy the valance energy band. This energy level is separated from the conduction band by a zone of non-occupation termed the forbidden band. Ionising radiation imparts energy to the atoms of the crystal, allowing these valence electrons to jump into the conduction band. Addition of a small amount of impurity (known as an *activator,* e.g. thallium into sodium iodide) into the crystal structure results in the creation of additional energy states in the forbidden band, thus expediting the de-excitation of electrons and consequent release of photons. It also results in the emission of photons at an energy level which is lower than the energy level required to excite electrons in the crystal itself, so avoiding substantial re-absorption. NaI detectors are suitable for gamma spectroscopy, provided the detector is large enough that a significant proportion of the gamma photons yield their total energy within the detector volume.

3. Solid state detectors. These detector types depend on the potential difference that occurs across the junction between an n-type and a p-type semiconductor. The charge difference suppresses migration of electrons from the n-type to the p-type regions, which creates a *depletion zone* around the junction that is devoid of electrons. Ionising radiation passing through the depletion zone interacts with impurity atoms and causes some electrons to jump the energy gap between the valence and conduction bands, resulting in a temporarily lowered resistivity across the junction, and a consequent voltage pulse. Thus the information carriers in solid state detectors are electron-hole pairs. Very high purity germanium semiconductors are required to produce a depletion zone that is physically large enough to absorb all the energy from a significant number of high-energy gamma photons. In addition, they have to be cooled to cryostatic temperatures (< 100K) during operation, in order to reduce the leakage current across the junction that would otherwise be caused by thermally induced excitation of electrons.

Ionisation energy for electron-hole pairs in semiconductors such as Si or Ge is about 3eV, compared with about 30eV for ion-pair production in gas filled detectors. This results in two of the primary advantages of solid state detectors, being that:

a) The statistical fluctuation in the numbers of information carriers diminishes compared with the total number, allowing much higher resolution spectra;

b) A greater number of information carriers are created for a given particle or quantum of incoming radiation, which is important at low ionisation energies where resolution is limited by noise in the amplification system.

(Knoll, 2000; Longworth, 1998).

For most operating modes in an energy discriminating detector, a gamma-ray interaction results in a voltage pulse being created in the external circuitry which has an amplitude (height) that is proportional to the energy released by that interaction. To enable spectral analysis, these voltage pulses are separated into different windows corresponding to small increments in pulse height, and the number of pulses in each of these windows is recorded. This is usually performed in parallel mode using a **multi-channel analyser** (**MCA**). The output can then be displayed as the number of counts plotted against increasing **channel** number, which is an approximation of what is known as the differential pulse height distribution. This is the theoretical distribution of the differential number of pulses recorded with amplitude within a differential increase in amplitude, plotted against increasing amplitude (Knoll, 2000; Gilmore, 2008).

Over the time period of a single measurement (the counting time) a gamma detector records the total count of gamma photons that yield part or all of their energy into the detector volume. Spectral analysis is made possible when the detector is able to discriminate between different energy levels of the incoming photons. A proportion of these photons will yield all of their energy into the detector volume. As gamma sources emit photons with characteristic energy levels, spectral peaks occur that are centred on channels which correspond to these energy levels, provided the equipment has been calibrated using a source that emits gamma radiation at known energy levels. The energy calibration is assumed to be linear, and calibration data generally fit this model very well (Gilmore, 2008). The area of a peak then bears a direct relationship to the number of photons that have yielded their full energy into the detector from a specific radionuclide, within the limits of the resolution of the detector.

Not all gamma-ray photons will impart all of their energy into the detector volume. This is because more than one interaction may take place within the detector before all the energy of an incoming photon is absorbed. Compton scattering occurs when the photon is deflected by interactions with several electrons, imparting an amount of energy to these electrons which depends on the angle of deflection. All scattering angles are possible, and where these interactions occur near the surface of the detector, some photons will escape before all of their energy is released. In this case, the final electron kinetic energies do not correspond to the full energy of the original photon. As a result, a continuum of energy known as the **Compton continuum** exists across the detector response between zero energy and the energy level of a spectral peak. This is illustrated in Fig 2.1. The edge of the continuum is known as the Compton edge, and is clearly visible in some spectra as a marked drop in the Compton continuum, although this is not evident in Fig 2.1, most likely because of the comparatively low resolution achieved by the NaI detector that was used to record this spectrum. The Compton continuum must be subtracted by spectral analysis software in order to estimate the area of a particular peak (Knoll, 2000).

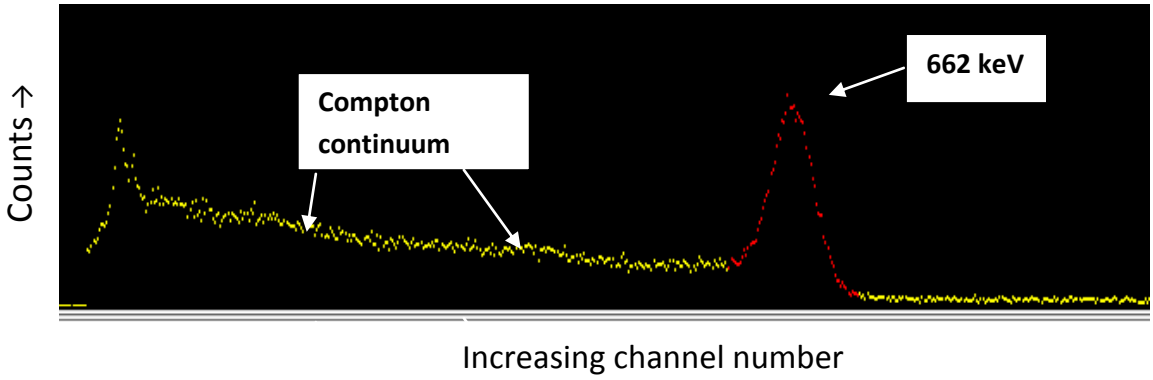

Fig 2.1 Part of a gamma-ray spectrum obtained using a NaI 3"x3" detector on a land area at Dounreay (displayed using Genie 2000) and showing a clearly defined peak centered at an energy level of 662 keV (corresponding to the decay of ^{137m}Ba), with the associated Compton continuum. The Compton edge is not clearly seen in this spectrum, most likely because of the low resolution detector that was used.

When spectral analysis is used to identify individual radionuclides from their characteristic energy lines in the spectra, the ability to distinguish individual energy lines depends on the widths of the peaks that are centred on these energy lines. These peak widths are determined by the resolution of the detector. In all detector types, various processes contribute to uncertainty in the strength of the pulse in the external circuitry that is produced by each gamma-ray interaction, and additional uncertainties are introduced by the electronic

amplification circuitry and the MCA. As the resolution is related to peak width, it is generally defined in terms of Full Width Half Maximum (FWHM), which is the width of the peak at one half of the maximum peak height. Because the resolution of a detector changes at different energy levels, the resolution of a detector is expressed by the FWHM as a percentage of the peak energy. Resolutions for a 3" x 3" NaI detector would typically be about 7.5 % at 661 keV (Gilmore, 2008). A comparison between the resolutions of a 3" x 3" NaI detector and a **HPGe** detector is given by Gilmore (2008) as 6 % for the NaI detector and 0.15 % for the germanium detector (both at 1332 keV). One of the key reasons for this difference is that a gamma photon at 661keV that is fully absorbed within the detector volume will produce approximately 1000 times more electron-hole pairs in germanium than it will produce photons in a sodium iodide crystal. Another reason for the relatively poor resolution of NaI detectors is a non-proportionality between light yield and absorbed energy in the detector volume. This is a result of imperfections in the crystal and also differences in light depending on whether gamma-ray interactions result in single photoelectric events, or a summation of smaller events produced by Compton scattering (Gilmore, 2008). A potential issue with *in situ* measurements made in the field where the target radionuclide is ^{137}Cs (identified by an energy line at 662 keV emitted with 85 % probability in the decay of its short-lived metastable **progeny** ^{137m}Ba) is interference from an energy line at 609 keV, which results from the beta decay of the naturally occurring radionuclide ^{214}Bi, with a gamma emission probability of 47 %. This potential interference is discussed further in *Section 4.3.3.*

While the spectral resolution of solid state detectors is much improved compared to ionisation or scintillation detectors, the volume of detection is significantly smaller than is achievable with the use of large (e.g. 3" x 3") NaI crystals. This results in lower detection efficiencies, especially for high-energy gamma radiation. In fact, NaI scintillation detectors have several advantages over ionisation and semiconductor detectors for field use:

a) They are relatively inexpensive compared to semiconductor detectors;

b) They are easier to handle: High purity germanium (HPGe) detectors require cooling in operation, either using liquid nitrogen or mechanical refrigeration;

c) The detection efficiency for high-energy gamma radiation is significantly better than that for HPGe detectors because of the larger detector volumes that are possible. Generally, it is desirable to use detector materials that have high *stopping power*, i.e. materials with high densities and atomic numbers. Ionisation detectors are of limited use in this case, because

a low proportion of photons will yield their full energy into the relatively low density gas within the ionisation chamber.

(Gilmore, 2008; Knoll, 2000; Longworth, 1998).

For these reasons, all of the *in situ* measurements acquired on radioactively contaminated land in the experiments described in subsequent chapters were made with NaI scintillation counters. Except in cases where an external laboratory was used (identified in the text), measurements of *ex situ* samples were made in the laboratory facilities at the Dounreay site. All laboratory measurements were made using HPGe detectors. More information is given on the detector types and procedures used in subsequent chapters, particularly in *Sections 4.3.3 – 4.3.4*.

2.4.3 Efficiency calibration of gamma detectors

As discussed previously (*Section 2.4.2*) spectral analysis to discriminate between different radionuclides requires that a gamma detector is first calibrated in order that the channel numbers correspond to specific energy levels of the photons that have yielded their full energy into the detector. The number of photon interactions that have occurred at specific energy levels can then be estimated by calculating the area of the spectral peak that is centred on the corresponding channel. However, these peak counts give no information about the dimensions or position of the radiation source with respect to the detector, and consequently are not a direct measure of the source activity. A further *efficiency calibration* is required in order to convert the peak counts into source activity levels. There are two generalised methods of doing this. In the first of these, a calibration source (or sources) with the same dimensions and approximate composition as the object to be measured (e.g. a sample pot) is made, and spiked with the radionuclide(s) of interest. Providing the detector response can be assumed to be linear, as is likely to be the case for environmental measurements (this is discussed further in *Section 6.4*), a single calibration source will suffice. Measurements of samples can then be related to the calibration. However, this method makes the assumption that the samples have similar physical properties to the calibration source, e.g. composition, heterogeneity and density.

In the second method, a computer program such as **ISOCS** (***In Situ* Object Counting System**) is used for the calibration. This program performs a computerised simulation, based on a Monte-Carlo n-Particle transport Code (MCNP) characterisation of the detector, to calculate **absolute**

efficiencies for user-defined source shapes and positions with respect to the detector. It removes the need for a calibration source of known activity with the same characteristics as the target source (although a source of sufficient activity for energy calibration is still required) and hence is a much faster and more cost effective means of detector calibration for different source and geometry characteristics. The user first builds a computerised geometry definition (or model) which defines an approximation of the positions, sizes and densities of the source and any intervening absorbers. ISOCS then simulates a repeated transmission of a photon, in a random direction, from a large number of volumes (termed voxels) within the source. The path of each photon is followed until it is lost within the system. ISOCS can therefore calculate the probability that each photon will yield its full energy into the detector volume. This entire process is repeated with an increasing number of voxels, until further increases have a minimal effect (at a user-defined level) on the result. The summed probabilities of photon detection are then translated into detection efficiency curves for a range of different energy levels (Gilmore, 2008; Canberra, 2013). The use of ISOCS for calibration of *in situ* detection is further discussed in relevant sections of the thesis, particularly in sections 4.3.3, 7.2, and 8.2.4.

Chapter 3 - Cost effective, robust estimation of measurement uncertainty from sampling using unbalanced ANOVA

This chapter comprises the manuscript of a paper that has been published in the Journal of Accreditation and Quality Assurance as follows:

Rostron, P., Ramsey, M.H. (2012) "Cost effective, robust estimation of measurement uncertainty from sampling using unbalanced ANOVA, *Accreditation and Quality Assurance*, **17,** 7-14.

3.1 Abstract

There is an increasing appreciation that the uncertainty in environmental measurements is vitally important for their reliable interpretation. However, the adoption of methods to estimate this uncertainty has been limited by the extra cost of implementation. A new program has been written and applied to a modified experimental design to enable the random component of measurement uncertainty, including that arising from the sampling process, to be estimated at 33 % less cost, whilst accommodating outlying values. This unbalanced robust analysis of variance (U-RANOVA) uses an *unbalanced* rather than the *balanced* experimental design usually employed. Simulation techniques have been used to validate the results of the program, by comparison of the results between the proposed unbalanced and the established balanced designs. Comparisons are also made against the seed parameters (mean and standard deviation) used to simulate the parent population, prior to the addition of a proportion (up to 10 %) of outlying values. Application to a large number of different simulated populations shows that U-RANOVA produces results that are effectively indistinguishable from the results produced by the accepted balanced approach, and are equally close to the true 'seed' parameters of the parent normal population.

Keywords

Uncertainty, unbalanced design, duplicate sample, robust ANOVA, accommodating outliers, optimised uncertainty.

3.2 Introduction

Characterisation of the intensity and distributions of analytes within a bulk of material usually requires the taking of a number of samples from discrete points within the parent volume,

where each sample represents a sampling target, which may either be the parent volume or a defined portion of material within the parent volume. This is because it is rarely possible to analyse the whole parent volume, for example it would be impractical to analyse the entire soil mass in an area of contaminated land. These primary samples are either analysed *in situ* or removed, processed, and analysed *ex situ*, in order to produce measurements which are intended to be representative of their respective sampling targets within the parent volume (Ramsey and Ellison, 2007).

These measurements are subject to uncertainties, which arise both at the sampling and at the analytical stages of the investigation. Uncertainties result from both systematic and random errors caused by the methods used. As the magnitudes of these errors affect the quality of the measurements, it is important to estimate these uncertainties before basing decisions on the characterisation of a parent volume (e.g. a plan for land remediation). Ramsey (1998) provides an overview of methods that can be used for the estimation of systematic and random errors in both the sampling and the analytical processes. Of the four methods for the estimation of the random component of uncertainty described in that review, the simplest is identified as the duplicate method, which uses a *balanced* experimental design. In this design, a number of duplicate samples are taken (from 10 % of the primary sampling locations, and a minimum of 8), and each of them chemically analysed twice (Fig 3.1).

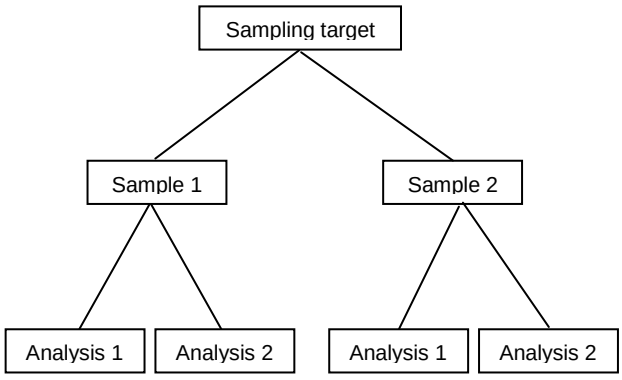

Fig 3.1 The balanced experimental design, which can be used to estimate the sampling and analytical components of measurement uncertainty using the duplicate method. Two samples are taken at each primary sampling point, and each sample is chemically analysed twice (Ramsey and Ellison, 2007).

When the analysis of primary samples is performed in order to characterise a number of sampling targets within a parent volume, the resultant set of measurements contains three components of variance: variance due to the actual variation of the particular property being

measured (e.g. analyte concentration), between the sampling targets (the between-target variance); variance due to uncertainty in the sampling method; and variance due to uncertainty in the analytical method . The first of these, the between-target variance, is the particular component of interest for characterization, as this is a parameter of the distribution of true values of the analyte within the sampling target. Therefore there is a need to separate this component from the total variance in the measurement set (Ramsey, 1998). Garrett (Garrrett, 1969) suggests that for geochemical data, where economic interests often rely on subtle changes in geochemistry, the total variance in the data should exceed the combined sampling and analytical variance by a factor of at least 4. When this is not the case, there is a greater than 5 % chance that observed variability could be due to variances inherent in the sampling and analytical processes.

These three components can be separated by the use of classical analysis of variance (ANOVA), which has been in use for determining the significance of areal variation in geochemical datasets since the 1960s. A drawback of the balanced design in geochemical surveys is that of increased cost, especially when several levels of variability are required. One way in which this cost can be reduced is to use the *simplified* design (not illustrated) as quoted in the Eurachem guide (Ramsey and Ellison, 2007), where only one analysis is performed on each duplicated sample, yielding an estimate of total uncertainty. If required, the sampling uncertainty can then be estimated by subtracting an external estimate of the analytical uncertainty from this total. An alternative approach is to modify the system of duplication so that each component of the variability is duplicated once only (Garrrett and Goss, 1980). Termed the ***unbalanced* design**, this design is also identified as being of potential use in the Eurachem guide (Ramsey and Ellison, 2007). The three-tier experimental design already described (Fig 3.1) can be modified to an unbalanced design by removing one analysis operation from one of the samples from each duplicated primary sample (Fig 3.2).

As the unbalanced design requires only 2 additional analyses per duplicated sample, instead of an additional 3 as for the balanced design, using the unbalanced design reduces the cost of analysing the 10 % subset of replicate locations by 33 %. As an example, a survey in which 100 primary samples are taken and chemically analysed, eight of which are designated as duplicate primary samples, would require the analytical procedure to be carried out a total of 124 times (i.e. 100 single samples + 8*3 duplicates) using the balanced design. This number would reduce to 116 (100 single samples + 8*2 duplicates) for the unbalanced design, equating to a saving of

6.5 % on the overall cost of analysis. This could be a significant saving particularly if the costs of chemical analysis were high.

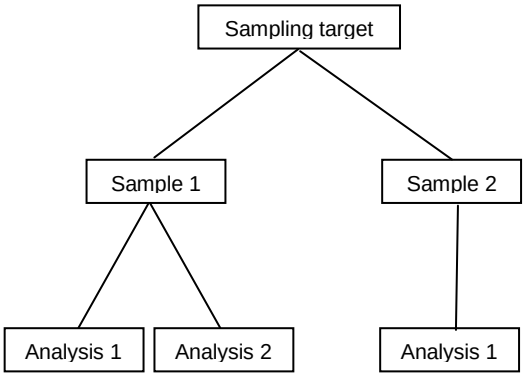

Fig 3.2 The unbalanced experimental design, where only one of the two samples from a duplicated primary sample undergoes duplicate analysis. This reduces the total number of chemical analyses required (Ramsey and Ellison, 2007).

It has been found in trials that 8 duplicate primary samples is typically a minimum number for the estimation of uncertainty by the duplicate method. Although increasing the number of these duplicates beyond 8 reduces the confidence interval on the uncertainty estimates, the marginal improvement so obtained may not justify the increased costs (Lyn *et al*., 2007). Performing the balanced design on 8 duplicate primary samples results in 8 sample duplicates and 16 analytical duplicates, whereas using the unbalanced design produces 8 sample duplicates and 8 analytical duplicates. One characteristic of the balanced design therefore is that there are fewer degrees of freedom in the estimation of sampling uncertainty than in the estimation of analytical uncertainty. Hence the confidence interval on the estimate of sampling uncertainty is larger than that on the estimate of analytical uncertainty. In the *unbalanced* design, the numbers of degrees of freedom on the sampling and analytical components of uncertainty are made more equal. As these components may be considered to be of equal importance, this enables an equal amount of effort to be applied to each level, instead of twice the effort being made to estimate analytical uncertainty as is made to estimate sampling uncertainty, which is the case for the balanced design. Therefore this method potentially enables a more efficient allocation of resources.

One of the assumptions of classical ANOVA is that the distribution of errors within each level of variance approximates to a Gaussian distribution. However, data from surveys (e.g. geochemical) often contain a small number of outlying values (i.e. values that are untypically far from the mean) and distributions may be heavily tailed (AMC, 2001; Ramsey *et al.*, 1992).

When classical statistics are used such outliers result in a biased mean and high standard deviation, which are not good representations of the main body of the data. A traditional approach to dealing with such outliers is to employ statistical significance tests in order to decide whether particular outliers should be excluded from the dataset (AMC, 2001). This method, however, leads to an underestimation of the variance achievable by a particular analytical method (AMC, 1989), and the same applies to sampling variance. An alternative approach is to use robust statistics (AMC, 2001). These methods accommodate, rather than reject, outliers, resulting in estimators of central tendency (e.g. the mean or median) and estimators of the variability in the data (e.g. variance or standard deviation) that are relatively unaffected by small populations of outliers (Ramsey *et al*., 1992). A number of different approaches to robust estimations of these parameters exist, e.g. those given by Rousseeuw and Verboven for very small datasets (Rousseeuw and Verboven, 2002). The methodology used in this current work is an iterative approach that can only practically be performed by a computer program. The robust mean μ_r is initially estimated as the classical mean, and the robust standard deviation σ_r as the median of the absolute differences between duplicated measurements. Any values that are found to exceed $\mu_r + c\ \sigma_r$ are replaced with $\mu_r + c\ \sigma_r$, and any values that fall below $\mu_r - c\ \sigma_r$ are replaced with $\mu_r - c\ \sigma_r$, where c is a factor between 1 and 2 (typically, as here, set to 1.5). The robust statistics μ_r and σ_r are then recalculated, and the process repeated multiple times, until μ_r stabilises (converges) at an acceptable level of accuracy (AMC, 1989; AMC, 2001).

The original robust ANOVA program for geochemical surveys (ROBCOOP) was based on a program listing published by the Analytical Methods Committee and uses the balanced design (Fig 3.1) (AMC, 1989). It was tested using simulated datasets, and the estimated robust means and standard deviations produced were shown to be very close to the seed distribution parameters used to create the simulated data. In contrast, classical estimates of these statistics were found to differ from the seed parameters by up to 1 order of magnitude in some cases (Ramsey *et al*., 1992). This FORTRAN program has since been partly re-written in Microsoft Visual Basic for Applications (Excel) so that it can be incorporated into Excel utilities, The new program RANOVA has been produced for the specific case of a two-stage nested design using the duplicate method, as quoted in the Eurachem guide (Ramsey and Ellison, 2007). It has been shown to produce identical results to the program ROBAN, which is also based on ROBCOOP, and is available free of charge from the Royal Society of Chemistry website.

However, no method has previously been devised for performing *robust* ANOVA on duplicate measurements obtained using the unbalanced design. Consequently the program RANOVA has been modified to perform robust ANOVA on the unbalanced design (Fig 3.2). As this reduces the number of additional measurements per duplicate primary sampling location from 3 to 2, this enables a 33 % reduction in the total costs of analysing the 10 % subset of replicate locations in order to estimate measurement uncertainty, as discussed above. The modified program has been named U-RANOVA. The aim of the following experiments was to verify that this program produces estimates of the robust mean and component standard deviations that are approximately equivalent to the robust statistics produced by ROBCOOP and RANOVA, and also to the seed parameters used to construct simulated datasets.

The objectives of this paper are as follows:

1. *Explain the advantages of using an unbalanced design for the empirical estimation of the random component of measurement uncertainty that arises from sampling.*
2. *Describe and validate a new computer program that can estimate uncertainty for population data with up to 10 % of outlying values using the unbalanced design.*

3.3 Methods

The new program U-RANOVA was tested in two stages. *Test 1* compared the variances estimated by U-RANOVA with the variances obtained by ROBCOOP in the 1992 study, using the same data as that study (Ramsey *et al.*, 1992). *Test 2* was performed on newly generated populations, comprising simulations of analyte concentration values. In this case the estimated variances were compared with the robust estimates made by the program RANOVA for balanced survey designs, as well as with the seed parameter values.

3.3.1 Test 1

The original FORTRAN program for robust ANOVA of balanced experimental designs (ROBCOOP) was tested using 4 simulated populations, to which outlying values were subsequently added as explained below. Each of the 4 populations was initially produced using the same seed parameters (Table 3.1).

Table 3.1 Seed distribution parameters of the 4 simulated populations used in the 1992 study. (Ramsey *et al.*, 1992).

Mean	100 µg g^{-1}
s (Analytical)	2 µg g^{-1}
s (Sampling)	5 µg g^{-1}
s (Between-target)	10 µg g^{-1}

s = standard deviation

These populations, designated A, B, C and D, each represent measurements of 100 sampling targets from a parent volume, with duplicated samples and duplicated analysis for each sampling target. Thus they comprise four columns of numbers, simulating sets of measurements that might be taken using a balanced experimental design (Fig 3. 1). In order to test the effects that outliers had on the estimations of variance, population B had 10 % of the analytical duplicates (10 % of column 4) were overwritten by simulated high values. Thus 2.5 % of the total population were set high, meaning that 5 % of the differences between analytical duplicates were replaced by outlying values in the ANOVA calculation. In the same way, population C had 10 % of the sampling duplicates (columns 3 and 4) overwritten with high values (5 % of the population), and population D had 10 % of the between-target values (all four columns, 10 % of the population) set high (Ramsey *et al*., 1992). An example showing simulated measurements for 15 sampling targets (including outliers) is shown in Fig 3.3. The original data were available to the author (*See Appendix 1*), and so could be input into U-RANOVA, and the estimated variances produced compared with the published results. As all four populations contained four columns of simulated measurements, and the unbalanced experimental design generates just three measurements per site (Fig 3.2), three columns were chosen for the test on each population. The columns were chosen to ensure that the simulated outlying values were included in the U-RANOVA estimations (Ramsey *et al.,* 1992).

3.3.2 Test 2

A more comprehensive set of tests was performed with the intention of comparing component standard deviations estimated by U-RANOVA with those produced by RANOVA. In total, 33 trials were performed, based on populations produced from a combination of three sets of seed distribution parameters (Table 3.2) and eleven outlier scenarios (Table 3.3). The three seed parameter combinations (Table 3.2) were chosen based on the following reasoning: Seed 1 is a repeat of the seed parameters used in the 1992 study (Table3. 1); Seed 2 equalises the

analytical and sampling standard deviation at 5 μg g^{-1}; Seed 3 uses parameters that are intended to be reasonable representations of the magnitude of variances that might be found during an investigation with a very high proportion of sampling variance (e.g. a contaminated land area) (Ramsey and Ellison, 2007).

Trial A – No outliers

S1A1	S1A2	S2A1	S2A2
106.45	103.34	117.64	117.09
106.27	100.47	104.1	106.43
117.92	118.72	112.87	110.7
92.919	89.953	93.136	92.373
102.36	99.469	111.14	112.43
81.423	82.055	90.477	87.235
76.779	74.422	87.253	88.654
107.41	106.3	99.763	101.1
62.89	67.339	77.66	81.813
100.91	95.623	98.088	97.658
105.55	104.19	106.34	103.94
112.76	110.54	98.468	101
96.147	97.735	116.55	112.9
122.27	122.84	114.82	119.92
91.665	95.648	104.58	105.62

Trial B – Analytical outliers X 10

S1A1	S1A2	S2A1	S2A2
106.45	103.34	117.64	117.09
106.27	100.47	104.1	106.43
117.92	118.72	112.87	110.7
92.919	89.953	93.136	92.373
102.36	99.469	111.14	112.43
81.423	82.055	90.477	**187.23**
76.779	74.422	87.253	**188.65**
107.41	106.3	99.763	**201.1**
62.89	67.339	77.66	**181.81**
100.91	95.623	98.088	**197.66**
105.55	104.19	106.34	**203.94**
112.76	110.54	98.468	**201**
96.147	97.735	116.55	**212.9**
122.27	122.84	114.82	**219.92**
91.665	95.648	104.58	**205.62**

Trial C – Sampling outliers X 10

S1A1	S1A2	S2A1	S2A2
106.45	103.34	117.64	117.09
106.27	100.47	104.1	106.43
117.92	118.72	112.87	110.7
92.919	89.953	93.136	92.373
102.36	99.469	111.14	112.43
81.423	82.055	**190.48**	**187.23**
76.779	74.422	**187.25**	**188.65**
107.41	106.3	**199.76**	**201.1**
62.89	67.339	**177.66**	**181.81**
100.91	95.623	**198.09**	**197.66**
105.55	104.19	**206.34**	**203.94**
112.76	110.54	**198.47**	**201**
96.147	97.735	**216.55**	**212.9**
122.27	122.84	**214.82**	**219.92**
91.665	95.648	**204.58**	**205.62**

Trial D – Geochemical outliers X 10

S1A1	S1A2	S2A1	S2A2
105.55	104.19	106.34	103.94
112.76	110.54	98.468	101
96.147	97.735	116.55	112.9
122.27	122.84	114.82	119.92
91.665	95.648	104.58	105.62
1437.7	**1563.8**	**1265.5**	**1370**
597.01	**627.2**	**707.98**	**720.11**
1106.8	**1170.1**	**1172.1**	**1036.9**
495.38	**489.73**	**692.58**	**643.48**
1605.2	**1694.6**	**1732.4**	**1522.3**
666.41	**607.45**	**528.7**	**506.31**
1702.4	**1768.4**	**1871.4**	**1759.2**
1108.8	**1130.4**	**931**	**946.38**
1046.9	**970.24**	**927.08**	**947.9**
940.91	**997.5**	**1079.7**	**1056.5**

Fig 3.3 Data extracts from the four trial populations used by Ramsey *et al.* (1992). For each trial the numbers shown represent measurements in μg g^{-1} of 15 out of a total of 100 sampling targets. The numbers were generated in such a way as to simulate measurements that might have been obtained using the balanced design (Fig 3.1). The boxed numbers are the outlying values, generated by adding a fixed number to the base population shown in Trial A. S1 = Sample 1, A1 = Analysis 1, etc.

Table3. 2 Seed distribution parameters used in *Test 2*.

	Seed 1	**Seed 2**	**Seed 3**
Mean	100 µg g^{-1}	100 µg g^{-1}	100 µg g^{-1}
s (Analytical)	2 µg g^{-1}	5 µg g^{-1}	5 µg g^{-1}
s (Sampling)	5 µg g^{-1}	5 µg g^{-1}	30 µg g^{-1}
s (Between-target)	10 µg g^{-1}	10 µg g^{-1}	50 µg g^{-1}

s = standard deviation

Table3.3 The 4 different outlier types and 3 different outlier adjustments that were applied to each base population in *Test 2*, generating a total of 10 additional populations with outliers for each base population.

Outlier Type	**Outlier adjustments (µg g^{-1})**	**Description of outlier adjustment procedure**
5 % analytical	**-90**	**10 different sampling targets selected at random throughout population. For each selected target, analytical outlier randomly assigned to either Sample 1 or Sample 2 with equal probability (Fig 3.2). Outlier adjustment then applied to either Analysis 1 or Analysis 2 of selected sample with equal probability.**
	+100	
	+200	
10 % sampling	**-90**	**10 different sampling targets selected at random throughout population. For each selected target, outlier randomly assigned to either Sample 1 or Sample 2 (Fig 3.1). Outlier adjustment applied to Analysis 1 and Analysis 2 of selected sample.**
	+100	
	+200	
10 % between-target	**-90**	**10 different sampling targets selected at random throughout population. For each selected target, outlier adjustment applied to Analysis 1 and Analysis 2 of both samples (Fig 3.1).**
	+100	
	+200	
10 % combined	**+100**	**3 between-target outller adjustments applied as described above (Outlier Type = 10 % between-target), followed by 3 sampling outlier adjustments applied as above (Outlier Type = 10 % sampling), followed by 4 analytical outlier adjustments as described above (Outlier Type = 10 % analytical).**

For each of the seed parameter combinations in Table 3.2, MS-Excel was used to randomly generate 1000 normally distributed "base" population of simulated measurements, each intended to simulate 4 measurements (see Fig 3.1) of each of 100 sampling targets. An additional ten simulated populations were then generated from each base population according to the outlier types and adjustments described in Table 3.3. In order to better represent measurements that might be obtained during real-life experiments, outliers were randomly distributed through each population. An example extract from a population with combined analytical, sampling and between-target outliers is shown in Fig 3.4. The 33,000 randomly generated test populations eventually generated were retained on computer disk and are available from the authors on request (*See Appendix 1*).

RANOVA nd U-RANOVA were used to estimate the robust statistics for each population. The mean and component standard deviations were then averaged across the 1000 populations for each of the 33 trials, thus producing an estimate of the bias between the results of the balanced and the unbalanced designs in each case.

114.5024	112.7102	111.1304	112.1127
106.1975	107.1449	114.7954	114.4674
89.21146	87.09401	**183.4472**	87.71243
85.22666	87.02409	97.79816	96.67791
85.1814	89.55124	91.58681	92.67708
191.8357	**190.852**	90.24191	87.63126
101.3663	100.5154	96.02608	93.94617
94.98708	98.21937	97.03501	99.37949
96.12857	92.51311	102.4799	104.2235
101.5718	101.2539	80.13705	80.51962
104.4135	101.6823	109.283	110.0088
94.20763	93.25907	99.05564	97.77308
209.0922	**206.9018**	**199.2465**	**201.2694**
97.96355	101.616	97.25568	100.7967
88.93586	91.92609	87.28093	94.46963

Analytical outlier

Sampling outlier

Between-target outlier

Fig 3.4 Data extracts from a simulated population with analytical, sampling and between-target outliers. The boxed numbers (μg g^{-1}) are the outlying values, generated by adding a fixed number (100) to the base population.

3.4 Results

3.4.1 Test 1 results

Comparisons of the variances estimated by U-RANOVA, expressed as standard deviations, are found to be within 6 % of the results originally obtained using robust ANOVA on a balanced design (Table 3.4). Identical values would not be expected as the estimates for the unbalanced design were made on three columns of data, whereas the estimates for the balanced design were made on all four columns. The U-RANOVA estimates are also better representations of the seed population parameters (Table3.1) than were obtained by classical ANOVA techniques, the most extreme difference being the estimate of 6.02 μg g^{-1} for the sampling standard deviation of population D. This is 20 % higher than the seed parameter of 5 μg g^{-1}. In comparison, the standard deviations estimated by Ramsey *et al.* (1992) using classical ANOVA differed by one order of magnitude in some cases.

Table 3.4 Comparison of results of ROBUST ANOVA on an unbalanced experimental design (U-RANOVA), with previously published results for a balanced design, showing that the differences between the estimated component standard deviations are <6 %. The differences between estimates are shown as a percentage of the original estimate from the 1992 study (Ramsey *et al.*, 1992).

Original population ID	Data source	Mean (μg g^{-1})	Standard Deviations (μg g^{-1})		
			Analytical (2.5% population outliers)	Sampling (5% population outliers)	Between Target (10% population outliers)
A (no outliers)	Ramsey *et al.* (1992)	100.13	1.92	5.24	9.62
	U-RANOVA (2011)	100.17	2.02	5.25	9.51
	Difference %	***0.04***	***5.21***	***0.19***	***-1.14***
B (analytical outliers)	Ramsey *et al*. (1992)	102.00	2.05	5.80	10.87
	U-RANOVA (2011)	102.30	2.02	5.85	11.17
	Difference %	***0.29***	***-1.46***	***0.86***	***2.76***
C (sampling outliers)	Ramsey *et al*. (1992)	102.67	1.92	5.82	11.88
	U-RANOVA (2011)	102.30	2.02	5.85	11.17
	Difference %	***0.01***	***5.32***	***0.5***	***0.04***
D (between-target outliers)	Ramsey *et al*. (1992)	102.28	2.23	6.02	11.83
	U-RANOVA (2011)	102.31	2.34	5.97	11.92
	Difference %	***0.03***	***4.93***	***-0.83***	***0.76***

3.4.2 Test 2 results

Comparison of the output from RANOVA and U-RANOVA on the 33 seed parameter/outlier type combinations (Fig 3.5), show that the average differences between the standard deviations for balanced and unbalanced designs are comparatively small, with all showing differences of <7 % averaged over 1000 trials. The maximum differences of -6.1 % are found in the sampling standard deviations for Seed 2. Some differences would be expected as the balanced design is using 4 columns of data whereas the unbalanced design is using only 3, and so the unbalanced design omits some of the randomly placed analytical outliers. The robust means are all very good approximations, with the means for the unbalanced design being within 1.0 % of the means for the balanced design. The means and component standard deviations are again much better estimates of the seed population parameters than are the classical ANOVA results obtained in the 1992 study (Ramsey *et al.,* 1992). In this case, the maximum differences are in the sampling standard deviations of the populations where sampling outliers have been added to Seed 2, which at 6.6 μg g^{-1} are 32 % higher than the seed population parameter of 5 μg g^{-1} (Table 3.2). That Seed 2 yields the highest percentage differences, both when the unbalanced design is compared to the balanced design, and also when the standard deviations are compared to the seed parameters, indicate that this method may not be optimal when the seed analytical and sampling standard deviations are equal in magnitude. Further experiments, where the seed analytical standard deviations have been set higher than the sampling standard deviations, have also shown progressively larger differences between estimates of standard deviations obtained from the unbalanced and the balanced designs. For example, in one case where the seed analytical standard deviation exceeded the sampling standard deviation by a factor of 4, the estimate of sampling standard deviation made by U-RANOVA was 18 % higher than that made by RANOVA, when averaged over 1000 trials. In most cases, e.g. chemical contamination of land areas, we consider it unlikely that the variance due to analytical uncertainty will often exceed that due to sampling uncertainty.

3.5 Conclusion

The unbalanced experimental design as described in the Eurachem guide (Ramsey and Ellison, 2007), can be used in the implementation of the duplicate method to estimate the random component of measurement uncertainty. However, it has not previously been possible to obtain these estimates using robust statistical methods, which accommodate a small proportion (<10 % of sampling targets) of outlying values. A computer program U-RANOVA has

been written to estimate the robust mean and component variances from data produced by an unbalanced design. This enables the random components of uncertainty to be estimated with fewer analytical measurements than are required by the balanced design. U-RANOVA was validated by inputting population data used in a previously published study, and comparing its output with that obtained in that study (Test 1) (Ramsey *et al.,* 1992). Additional trials were undertaken on datasets containing 1000 unique populations per set, and with 10 different outlier types (Test 2). Results of *Test 1* and averaged results from *Test 2* showed that estimates of population parameters from the balanced and unbalanced designs were much more representative of the seed population parameters than were produced by classical ANOVA (Ramsey *et al*., 1992). In both cases, the majority of estimates of component standard deviations from the unbalanced experimental design were found to be within 5 % of the estimates from the corresponding balanced design, and all were within 7 %. This demonstrates that the unbalanced experimental design can be used to obtain robust estimates of uncertainty with a 33 % reduction in the cost of analysing the 10 % subset of replicate locations required by the duplicate method.

The program U-RANOVA, written in Visual Basic for Applications (Excel) is to be made available at the Royal Society of Chemistry website.

		Percent difference U-RANOVA/RANOVA [(Unbalanced - Balanced)/Balanced %]					Population parameters estimated by URANOVA (μg g^{-1})			
Seed params (Refer to Table 2)	**Outlier type**	**Mean %**	**Total SD %**	**Between Target SD %**	**Sampling SD %**	**Analytical SD %**	**Mean**	**Between target SD**	**Sampling SD**	**Analytical SD**
Seed 1	Base (None)	0.0	0.2	0.2	0.1	0.0	100.0	10.0	5.0	2.0
	Analytical -90	0.3	-1.0	0.1	-5.1	0.1	98.5	11.3	5.7	2.2
	Analytical +100	-0.4	-1.8	-0.9	-5.1	0.1	101.6	11.4	5.7	2.2
	Analytical +200	-0.7	-5.5	-5.8	-5.1	0.1	101.7	11.5	5.7	2.2
	Sampling -90	0.1	-1.1	-1.5	0.4	0.0	97.8	12.0	6.1	2.0
	Sampling +100	-0.1	-0.6	-0.9	0.4	0.0	102.3	12.1	6.1	2.0
	Sampling +200	0.0	0.2	0.1	0.4	0.0	102.4	12.3	6.1	2.0
	Geochemical -90	0.0	0.2	0.2	-0.2	0.0	97.7	12.5	5.0	2.0
	Geochemical +100	0.0	0.2	0.2	-0.2	0.0	102.4	12.5	5.0	2.0
	Geochemical +200	0.0	0.2	0.2	-0.2	0.0	102.4	12.5	5.0	2.0
	Combined +100	-0.2	-0.8	-0.6	-1.9	0.0	102.0	11.9	5.6	2.1
Seed 2	Base (None)	0.0	0.0	-0.1	-0.1	-0.3	100.0	9.9	5.0	5.0
	Analytical -90	0.3	-0.8	0.5	-6.1	-0.2	98.5	11.2	5.8	5.4
	Analytical +100	-0.3	-1.5	-0.6	-6.1	-0.2	101.6	11.3	5.8	5.4
	Analytical +200	-0.7	-4.9	-5.8	-6.1	-0.2	101.7	11.5	5.8	5.4
	Sampling -90	0.1	-0.6	-1.8	2.9	-0.3	97.8	11.9	6.6	5.0
	Sampling +100	0.0	-0.2	-1.2	2.9	-0.3	102.4	12.0	6.6	5.0
	Sampling +200	0.0	0.6	0.1	2.9	-0.3	102.4	12.2	6.6	5.0
	Geochemical -90	0.0	0.4	0.6	-0.6	-0.3	97.6	12.6	5.0	5.0
	Geochemical +100	0.0	0.4	0.5	-0.6	-0.3	102.4	12.6	5.0	5.0
	Geochemical +200	0.0	0.4	0.5	-0.6	-0.3	102.4	12.6	5.0	5.0
	Combined +100	-0.1	-0.5	-0.4	-1.4	-0.3	102.1	11.9	5.8	5.1
Seed 3	Base (None)	0.0	0.2	0.3	0.0	0.2	100.0	50.2	30.0	5.0
	Analytical -90	0.1	0.5	0.4	0.7	0.3	97.8	50.2	31.6	5.4
	Analytical +100	-0.1	0.5	0.5	0.6	0.3	102.3	50.4	31.8	5.4
	Analytical +200	-0.3	0.3	1.7	-2.6	0.3	104.4	51.6	33.5	5.4
	Sampling -90	0.1	0.3	0.4	0.0	0.2	95.7	50.7	34.0	5.0
	Sampling +100	-0.1	0.3	0.5	0.0	0.2	104.7	51.0	34.4	5.0
	Sampling +200	-0.4	-0.3	-0.4	0.1	0.2	108.0	54.7	35.8	5.0
	Geochemical -90	0.0	0.2	0.2	0.0	0.2	92.1	55.9	30.0	5.0
	Geochemical +100	0.0	0.2	0.3	0.0	0.2	108.5	56.9	30.0	5.0
	Geochemical +200	0.0	0.2	0.3	0.0	0.2	111.6	62.6	30.0	5.0
	Combined +100	-0.1	0.3	0.4	0.2	0.2	104.8	52.4	32.0	5.2
	Median	***0.0***	***0.2***	***0.2***	***0.0***	***0.0***				
	Mean	***-0.1***	***-0.4***	***-0.4***	***-0.9***	***0.0***				

Fig 3.5 Comparison of the means and standard deviations estimated by robust ANOVA for unbalanced (U-RANOVA) and balanced (RANOVA) experimental designs. The difference between estimates is shown as a percentage of the estimate calculated by the balanced design. Each % difference is the average % difference for 1000 simulated populations. Seed parameters are shown in Table 3.2. Total standard deviation is the square root of the sum of the component variances, e.g. $\sqrt{(\text{(Analytical s)}^2 + \text{(Sampling s)}^2 + \text{(Between-target s)}^2)}$.

Chapter 4 - Advantages of *in situ* over *ex situ* radioactivity measurements for the characterisation of land on a decommissioning nuclear site.

This chapter comprises the manuscript of a paper that has been submitted for publication in the Journal of Environmental Radioactivity.

4.1 Abstract

Making measurements *in situ* has the advantages of a shorter turnaround time and reduced cost, when compared to the time and cost of analysing extracted soil samples. However, laboratory measurements potentially have the advantage of traceability, and are often stipulated by regulatory authorities. This study compares the results obtained by *in situ* gamma detectors, and *ex situ* soil sample analysis, on two areas of radioactively contaminated land on a decommissioning nuclear site. It is found that the random component of measurement uncertainty is dominated by analytical uncertainty in the *in situ* measurements, and by sampling uncertainty in the *ex situ* measurements. *In situ* measurements with a collimated detector produced estimates of mean activity levels that are not significantly different from those obtained by the analysis of extracted soil samples. When contamination is heterogeneous on a small spatial scale, high coverage *in situ* surveys are more effective at locating hotspots of activity, due to their larger primary sample size.

Keywords
Soil sampling
Measurement uncertainty
In situ measurements
Radioactive shine

4.2 Introduction

4.2.1 Nuclear sites in the UK

The use of nuclear material in industrial processes has left a legacy of radioactively contaminated sites in many countries around the World. In the United Kingdom, there are a total of 32 licensed nuclear sites in England and Wales, carrying out activities such as power production, nuclear fuel and waste processing, decommissioning, and site clean-up (EA, 2012). An additional 4 sites are in Scotland, the focus of this study. Land contamination at nuclear

sites can arise from a number of sources, such as leaks from facilities, activities associated with fuel processing, the dismantling of buildings which were previously used to process or store contaminating materials, and from authorised discharges. While this is not thought to pose a significant threat to the current workforce, further work is needed to determine what actions are necessary to avoid adverse effects to people and the environment in future (NDA, 2006).

4.2.2 Threshold values of radionuclides

Two maximum contamination levels (thresholds) are commonly used to assess whether remediation is required. The first of these is an average activity over a particular area, which is often defined in legislation as a threshold mass activity concentration. The second is a maximum allowable activity that results from a smaller hotspot of contamination within an area (EA, 1999). A particular source of hotspots is the presence of radioactive particles. Accidental or authorised emissions from nuclear power plants often result in the presence of particulate activity (Brown and Etherington, 2011; Dennis *et al*., 2007; IAEA, 2011; Poston *et al*., 2007; Salbu and Lind, 2005). Particles are important for two reasons: i) they may present risks to human health; ii) the sampling of bulk volumes with heterogeneous distributions of radioactive material can result in measurements that are not representative of the entire volume (Dale *et al*., 2008; IAEA, 2011). Consequently, there is a requirement to identify particles that might pose a hazard to human health, and which could also result in higher uncertainty in individual measurements. Classifications of radioactive particles do not exist in Scottish law, but have been provided by organisations such as the Dounreay Particles Advisory Group (DPAG). These definitions categorise radioactive particles at the Dounreay site based on their implications to public health (DPAG, 2006).

4.2.3 Characterisation of radioactively contaminated land

Characterisation of land areas is required to assess whether there is a need for remediation work. It also provides critical information during each step of the remediation process, e.g. planning, implementation, and post-remedial verification (IAEA, 1998). Both *in situ* and *ex situ* techniques are often used. Where there is a high probability of gamma-emitting radionuclides existing at or near the ground surface, then *in situ* gamma-ray detection can offer several advantages, compared to the *ex situ* analysis of soil samples. *In situ* measurements are taken in real time, and can be interpreted immediately. They are also less expensive to obtain. In addition, a larger sampling mass (due to remote detection capabilities) may give a more

representative picture of the extent and intensity of contamination. Various techniques have been proposed for characterising the depth distributions of radionuclides using *in situ* measurements (more details are given in Section 8.2.4), however, *ex situ* methods allow this to be done with greater confidence on individual samples. *Ex situ* measurements are usually required for the reliable quantification of alpha and beta emitters, and may also be prescribed by regulatory authorities for quantification of gamma emitters (IAEA, 1998).

Several studies have been undertaken where one of the objectives has been to compare *in situ* and *ex situ* measurements of radioactivity in land areas. These have been performed in several contexts. Some examples include: the use of distributions of fallout ^{137}Cs as a method of assessing soil erosion and deposition (He and Walling, 2000; Li *et al.*, 2010); assessment of existing or novel techniques for obtaining reliable *in situ* measurements, considering radionuclide variability with depth (Baeza and Corbacho, 2010; Kastlander and Bargholtz, 2005; Korun *et al.*, 1994; Korun *et al.*, 1991; Tyler *et al.*, 1996a); experiments to assess the reliability of *in situ* measurements when compared to *ex situ* (Golosov *et al.*, 2000; MacDonald *et al.*, 1996; Sadremomtaz *et al.*, 2010); and one inter-comparison exercise (Lettner *et al.*, 1996). Two of these studies investigated contamination in coastal environments, which was suspected to have arisen from discharges at the Sellafield (UK) nuclear power site (Macdonald *et al.*, 1996; Tyler *et al.*, 1996a). The other studies conducted measurements of natural radionuclides and atmospheric fallout from the Chernobyl incident and weapons testing. Some quote uncertainty in the measurements (both *in situ* and *ex situ*), but only one study (Golosov *et al.*, 2000) reports an empirical estimate of the random uncertainty in measurements made *in situ*. In contaminated land investigations, it is important to obtain estimates of the magnitudes of the uncertainties, in order to make reliable decisions. They can also be used to evaluate if the measurement methods are fit for their intended purposes (IAEA, 1998; Ramsey and Argyraki, 1997; Ramsey *et al.*, 2002).This study uses a published, empirical method to provide estimates of these uncertainties. The method has previously been applied to investigations of chemically contaminated land (Boon *et al.*, 2007).

Aerial deposition from radioactive fallout would usually be expected to result in relatively homogeneous contamination over small spatial scales. This study aims to extend the comparison of *in situ* and *ex situ* measurements to the particular case of a decommissioning nuclear site, where a much wider range of contamination sources would be expected. Caesium ^{137}Cs was chosen as the target radionuclide to illustrate the general issues. Although this

radionuclide does not occur naturally, it is widespread in the UK, following fallout from the 1986 Chernobyl incident. It is also a very important part of the contamination inventory from nuclear power generation. With a half-life of ~30 years, it is sufficiently long-lasting and radioactive to be present in measurable quantities more than one decade after its production. It is also fairly easy to detect and identify using gamma-ray spectroscopy. At Sellafield and Dounreay, ^{137}Cs is the target radionuclide for the monitoring of land, beaches and offshore environments for radioactive particles, through the use of wide-area search techniques such as Groundhog (Dennis *et al.*, 2007).

Two grassed areas of land that had potentially been contaminated by radionuclides were selected at the Dounreay site in Caithness, Scotland, in order to investigate the relative effectiveness of *in situ* and *ex situ* measurement methods. Dounreay was chosen because of its history of experimental and commercial power generation since the 1960s. Decommissioning of the site has been in progress since the last reactor was shut down in 1994.

4.2.4 Study objectives

1. Compare estimates of mass activity concentrations and uncertainty levels, made using *in situ* and *ex situ* measurements on radioactively contaminated land;

2. Evaluate the relative effectiveness of these measurement methods for the purposes of:
    i. Estimating mean activity concentrations in a surveyed area;
    ii. Identification of small areas of activity that are elevated compared to their surroundings.

4.3 Materials and methods

4.3.1The survey areas

The first site (Zone 12) was chosen on an unused area with no history of the processing or storage of nuclear materials, but which had potentially been exposed to aerial deposition from authorised discharges. Rubble from demolished buildings had also been stored on the site, but was no longer present at the time of the survey. Previous high-coverage *in situ* surveys had indicated the presence of a few spots of elevated ^{137}Cs activity, which were below regulatory concern. It was chosen to be representative of an area that might be supposed to be ‘clean’, but which requires demonstration of compliance with regulatory and local objectives. *In situ*

measurements were made using a Canberra 3” × 3” (3 x 3 inch) NaI detector with 20 mm 90° lead collimation, placed on a wheeled platform at a height above ground of 280 mm (*see colour photograph in fig 4.11 at the end of this chapter*). An additional set of *in situ* measurements was acquired using an Exploranium GR-135, a unit which is typical of portable, relatively inexpensive hand-held units with the ability to identify gamma-emitting sources. *Ex situ* measurements were made by excavating soil samples and analysing these in the Dounreay facility laboratory.

The second site (Barrier 31) was located alongside a subterranean storage tank containing intermediate level radioactive waste (**ILW**). Due to its location, this area was not thought to have been significantly affected by authorised discharges, however it was known that some ground contamination had resulted from historic leaks from an active drain located between the ILW store and the surveyed area. It may also have been contaminated during discharges of material to the ILW store. Previous *in situ* and *ex situ* surveys had indicated moderate levels of contamination by ^{137}Cs , including the presence of radioactive particles. When found, these had been removed for authorised disposal. *In situ* measurements were again made using a Canberra 3” × 3” NaI detector, with the same 20 mm 90° lead collimation, but this time at a height of 920 mm. This height was chosen so that 100 % of the ground was covered by the **field-of-view** (**FOV**) of the detector. *Ex situ* measurements were made at the on-site laboratory. *See colour photograph in Fig 4.12 at the end of this chapter.*

4.3.2 Estimation of the random component of uncertainty

The quantitative estimation of activities from specific radionuclides in subject to uncertainty due to Poisson variances in the source counts, and also other uncertainties e.g. uncertainty in the peak area analysis. For *in situ* measurements, uncertainties are also introduced by the model chosen to convert raw detector counts to activity per unit mass or volume, and for *ex situ* there are uncertainties in the masses and internal geometries of the samples. In addition, the responses of different detectors may vary in the laboratory, and for *in situ* measurements the response of a single detector might be significantly affected by environmental conditions. Finally, for the purposes of characterisation, there is likely to be significant spatial uncertainty, especially if the target radionuclides are heterogeneously distributed. This last component of uncertainty can theoretically be reduced by increasing primary sample size. In this study, an established protocol was used to estimate two encompassing components of uncertainty by empirical measurement: a) uncertainty due to the analytical process; b) uncertainty arising

from the sampling process, particularly that which results from the small-scale spatial heterogeneity of contaminants. Uncertainty estimates were made using the balanced design methodology, described in the Eurachem 2007 guide (Ramsey and Ellison, 2007). To achieve this, a number of the measurement locations were randomly assigned as duplicate measurement locations. For *in situ*, 10 % of the total measurement locations were so designated. This equated to 9 duplicate locations in Zone 12, and 12 duplicate locations in Barrier 31. However, only 8 duplicate measurement locations were assigned for *ex situ* measurements in Barrier 31, in order to reduce analysis costs. This number has previously been shown to be sufficient when using the duplicate method (Lyn *et al*., 2007). All *ex situ* duplicate soil samples were excavated at points which spatially coincided with *in situ* duplicate measurement locations. The sample mass of each *ex situ* measurement was approximately 300g (See Table 4.1) whereas the primary sample mass of *in situ* measurements can be estimated at 160 tonnes, assuming a circular model with a depth of 200 mm. An implication of this difference in sample mass is that individual measurements are not directly comparable between the two methods.

The question of where to acquire each duplicate measurement, with respect to the primary measurements, needs to be addressed. One approach is to take these at the extremity of the expected error in the positioning of the primary measurement. Positioning was carried out using a Trimble RGPS unit, with an expected absolute error of 2-3 cm, which was less than the diameter of the soil sampling device. It was therefore decided to take the duplicates at a distance from the primary measurement location equal to 10 % of the measurement spacing. The rationale of this approach was to assess the small-scale heterogeneity of contaminants, and its effect on the sampling component of measurement uncertainty (Ramsey *et al.*, 2002).

4.3.3 *In situ* measurement procedure

The Exploranium GR-135 was calibrated every morning using a ^{137}Cs source that is incorporated in its docking station, and transported to the site without the docking station so that this could not affect measurements made by either detector. When in use, it was placed on the ground surface so that the internal gamma detector was positioned directly over each measurement location. Reported counts of ^{137}Cs activity were recorded after each measurement, but these could not be converted to estimates of mass activity concentrations in the absence of an appropriate calibration. The Canberra 3×3” detector was mounted on a trolley which could be wheeled into position. Activity levels of ^{137}Cs can be inferred from

energy peaks located in the region of 662keV, this being a characteristic energy line in the decay of ^{137m} Ba, a short-lived progeny of ^{137}Cs. Energy calibrations were performed during acquisition, using a ^{137}Cs source at the start of each half day, or more frequently if significant drift in the 662 keV peak was seen to have occurred.

The spectra obtained from the Canberra detector were analysed using Genie 2000 software (Canberra, 2009a), Interferences from energy peaks of other radionuclides may occur, in particular from the naturally occurring radionuclide ^{214}Bi, which emits an energy line at 609keV. Laboratory analysis reported mean activity levels of ^{214}Bi at 0.018 Bq g^{-1} in Zone 12, and 0.023 Bq g^{-1} in Barrier 31. There is a potential uncertainty in these estimates due to different loss rates of ^{222}Rn in the laboratory samples, compared to these losses *in situ*. The effect of ^{214}Bi peaks on estimates of ^{137}Cs activity is less than would be implied by a comparison of their activity concentrations, due to the lower emission probability of the 609keV energy line (46.9 %) compared to the 662keV energy line (85.12 %), and also because the peaks may not fully overlap. The spectra were checked during analysis for possible interferences, but because of the difficulties of establishing a representative background in environmental measurements, a background spectrum was not subtracted during the analysis. Examples of spectra from the two surveys are shown in Fig 4.1. Peaks at 609 keV are not clearly distinguishable from background noise in either case. The measurements in Zone 12 (Fig 4.1a) were close to the **Minimum Detectable Amount** (**MDA**) of the analysis (0.026 Bq g^{-1}), and so were strongly affected by background noise. The levels of ^{137}Cs activity in this area were considered to be at the lower limit of the measurement capability of the equipment used.

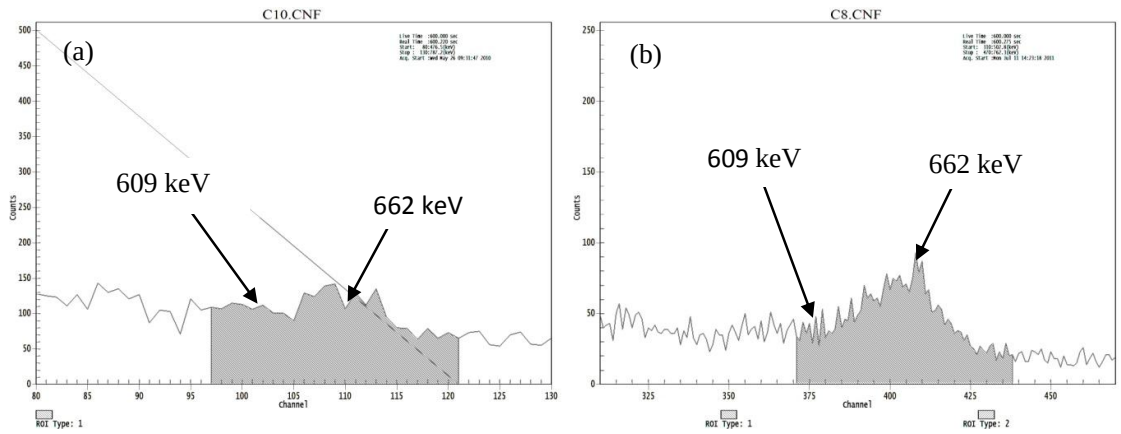

Fig 4.1 Sample gamma spectra from *in situ* measurements, showing 662keV energy peaks: a) Zone 12, estimated ^{137}Cs = 0.04 Bq g^{-1}; b) Barrier 31, estimated ^{137}Cs = 0.14 Bq g^{-1}.

Activity counts from these analyses were converted to estimates of mass activity concentration using ISOCS^{TM} calibration software, which requires the definition of an appropriate source model (Canberra, 2009b). The *ex situ* soil samples were acquired to a maximum 200 mm depth, and so a circular shaped ISOCS model of 25 m diameter and 200 mm depth was used to convert counts in the 662 keV peak to mass activity concentrations. Changing the depth model from 500 mm to 200 mm increased calculated activity concentrations by ~3.3 % (assuming homogeneity with depth) and so this could be considered an additional component of uncertainty in the *in situ* measurements. Model experiments showed that an insignificant amount of radiation at the 662 keV energy level would be recorded from depths of greater than 500 mm.

The soil in both surveys appeared to be a silty clay loam with organic content in the upper 10 centimetres (approximately). From knowledge of the local geology, the mineralogy was assumed to be non-calcareous, comprising mainly of quartz and feldspar. The ISOCS models were based on an assumed single homogeneous layer of density 1.7 g cm^3, with composition O=58 %, Si=26%, Al=9 %, Fe=5 %, H=2 %. A linear mass attenuation coefficient of 0.078832 cm^2 g^{-1} at 662 keV was assumed. Desk experiments using ISOCS showed that measurements acquired with the 20 mm lead collimator changed significantly depending on the source model dimensions, even when these extended beyond the nominal FOV of the collimator. Calculated activity concentrations were found to stabilise when a circular source model of 25m diameter was defined. This has significant implications for the *in situ* measurements. Changing the model dimensions from a cone shaped section of ground that would be theoretically defined by the nominal FOV, to the 25m diameter model that was used, reduced estimates of mass activity concentrations from the 662 keV energy peak by 42.5 % (Zone 12), and 40.7 % (Barrier 31). This implies that in contaminated land investigations, a significant proportion of the measured radiation can pass through the side walls of a 20 mm collimator. This additional radiation emanates from a ground area that is much larger than would be defined by the nominal FOV of the collimator.

4.3.4 *Ex situ* measurement procedure

In Zone 12, duplicate soil samples were extracted from soil depths of 0-100 mm and 100-200 mm at each of the 9 *in situ* duplicate locations. An additional 11 soil samples were then taken from the 0-100 mm layer at randomly assigned locations on the measurement grid. In Barrier 31, soil samples were extracted from both depths at 8 of the 12 *in situ* duplicate locations,

from location C3, and from a further 11 random locations. Soil samples of approximately 0.25 kg were extracted from each depth using a bulb planter and transferred to sample pots. A stony layer usually encountered between ~150-200 mm set the practical lower limit of 200 mm using this method. After extraction of the top layer, the bulb planter was wiped clean, however a small degree of contamination of the 100-200 mm samples from the top soil would be expected. Soil samples were analysed using HPGe detectors housed in 100 mm lead shielding with a quoted resolution of 2 keV (FWHM) at 1.33 MeV. Calibrations were performed using a geometry standard comprising a sample pot filled with soil, spiked with a certified mixed nuclide gamma standard. During the analysis, Q.C. checks were performed daily using a standard which included a known amount of ^{137}Cs. Background and interference corrections were applied by the counting software. Samples were analysed 'as received' with a counting time of three hours. Thus samples were measured in the laboratory at similar moisture contents to the field measurements. As part of other investigations, a subset of samples were dried and the loss on drying recorded. These measurements indicated a typical moisture content of 34 % in the 'as received' samples. Experimental parameters for both surveys are shown in Table 4.1.

Table 4.1 Summary of survey parameters for the Zone 12 and Barrier 31 surveys.

Parameter	Zone 12	Barrier 31
Area	Rectangular 20m x 14m = 280m^2	Irregular 206m^2
Measurement spacing	Square grid, 2m	Square grid, 1.3m
In situ (Detector 1)	Canberra 3×3" NaI, 90° 20 mm lead collimator	Canberra 3×3" NaI, 90° 20 mm lead collimator
In situ (1) Height	280mm	920mm
In situ (1) Coverage	6.2%	157% (100% of ground covered)*
In situ (Detector 2)	Exploranium GR-135 un-collimated	N/A
In situ (2) Height	Ground level	N/A
In situ (2) Coverage	N/A	N/A
In situ counting time	600 seconds both detectors	600 seconds
No. *in situ* locations	88	122
No. *in situ* duplicate locations**	9	12
No. e*x situ* primary samples	20 @0-100 mm, 9 @ 100-200 mm	20 @0-100 mm, 20 @ 100-200 mm
Ex situ average sample size	~ 500 cm^3, 330 g	~ 500 cm^3, 264 g
No. *ex situ* duplicate locations**	9	8
In/Ex situ duplicate spacing	20 cm	13 cm

*To achieve 100 % coverage of the ground surface by *in situ* measurements with a circular field-of-view, it is necessary to overlap a portion of each measurement.
**Duplicate locations for the purposes of estimating measurement uncertainty.

4.4 Results

All raw data is given in Appendix 2.

4.4.1 Measurement uncertainty

To estimate the random components of uncertainty (i.e. the repeatability of the measurements), the measurements obtained from the sampling and analytical duplicates were analysed using a robust ANOVA computer program, which down-weights the effects of outlying measurements, until the calculation of the robust mean stabilises (AMC, 1989). Using this method enabled apportioning of the total variance in the measurements between the sampling and analytical processes. The overall expanded relative measurement uncertainty (*U*) was then calculated from the component standard deviations:

$U = 2 * \sqrt{(s^2_{analytical} + s^2_{sampling})}$

The uncertainty for each of the components was estimated as (2 * standard deviation / robust mean) and quoted as a percentage (Ramsey, 2004). The estimates are shown in Table 4.2.

Table 4.2 Summary of the random component of measurement uncertainty estimated using robust ANOVA on sampling and analytical duplicates.

		Expanded relative uncertainty (%)		
		Sampling	Analytical	Measurement
Zone 12	Canberra *in situ*	0	42.6	**42.6**
	Exploranium *in situ*	34.5	31.8	**46.9**
	Ex situ 0-100 mm	31.5	20.3	**37.5**
	Ex situ 100-200 mm	56.8	17.2	**59.4**
	Ex situ 0-200 mm	43.6	18.7	**47.4**
Barrier 31	Canberra *in situ*	10.2	7.5	**12.6**
	Ex situ 0-100 mm	40.1	5.1	**40.4**
	Ex situ 100-200 mm	96.1	4.9	**96.2**
	Ex situ 0-200 mm	72.5	5.1	**72.6**

4.4.2 ^{137}Cs Activity

Summary statistics of the results of the two surveys are shown in Table 4.3. The mean and median activity concentrations in Barrier 31 were found to be approximately one order of magnitude higher than those in Zone 12. Dot maps of the Canberra *in situ* and the laboratory *ex situ* measurements are shown in Figs 4.2 and 4.3 respectively. Note that Fig 4.3 shows *ex situ* measurements for the 0-100 mm layer only in Zone 12 (because a full set of 100-200 mm

soil samples was not acquired), whereas individual measurements for the 0-100 mm and 100-200 mm layers have been averaged for Barrier 31.

Table 4.3 Summary statistics for the Zone 12 and Barrier 31 surveys, showing the means, medians and standard deviations for the entire population of activity concentrations measured across the whole site. Activity concentrations at the duplicate measurement locations have been calculated as the means of the four measurements (two analyses per sample, two samples per location) that were acquired at each.

		Number locations (N)	Mean activity conc (Bq g^{-1})	Median activity conc (Bq g^{-1})	Standard deviation (Bq g^{-1})	Range (Bq g^{-1})
Zone 12	Canberra *in situ*	88	0.043	0.043	0.015	0.01-0.148
	Ex situ 0-100 mm	20	0.047	0.043	0.013	0.033-0.098
	Ex situ 100-200 mm	8	0.081	0.047	0.090	0.033-0.318
	Average *ex situ* 0-200 mm	8	0.066	0.047	0.048	0.033-0.189
	Canberra *in situ* on *ex situ* locations	8	0.056	0.045	0.035	0.034-0.148
Barrier 31	Canberra *in situ*	122	0.49	0.37	0.35	0.06-1.92
	Ex situ 0-100 mm	20	0.67	0.54	0.83	0.03-3.94
	Ex situ 100-200 mm	20	0.53	0.39	0.46	0.06-2.04
	Average *ex situ* 0-200 mm	20	0.60	0.48	0.64	0.04-2.99
	Canberra *in situ* on *ex situ* locations	20	0.63	0.59	0.44	0.10-1.92

4.5 Discussion

4.5.1 Comparison of *in situ* and *ex situ* samples

The figures for *in situ* and *ex situ* measurements reported in Table 4.3 appear to suggest that the means of all Canberra *in situ* measurements (N=88 for Zone 12, N=122 for Barrier 31) underestimate those of the 20 *ex situ* measurements for both surveys. However, appying the non-parametric Mann-Whitney test for independent samples suggests there is no significant difference between the medians ($p>0.05$). As previously mentioned, *ex situ* measurements for both surveys included one judgmentally positioned location based on a high *in situ* measurement. Exclusion of these measurements from the data reduces the differences between the means, suggesting a closer agreement (Table 4.4).

Table 4.4 Comparison of means of Canberra *in situ* measurements with *ex situ* measurements, after exclusion of single judgmental measurement locations.

		No. of measurement locations (N)	Mean Activity Concentration (Bq g^{-1})
Zone 12	Canberra *in situ*	87	0.042
	Average *ex situ* 0-200 mm	19	0.046
Barrier 31	Canberra *in situ*	121	0.47
	Average *ex situ* 0-200 mm	19	0.47

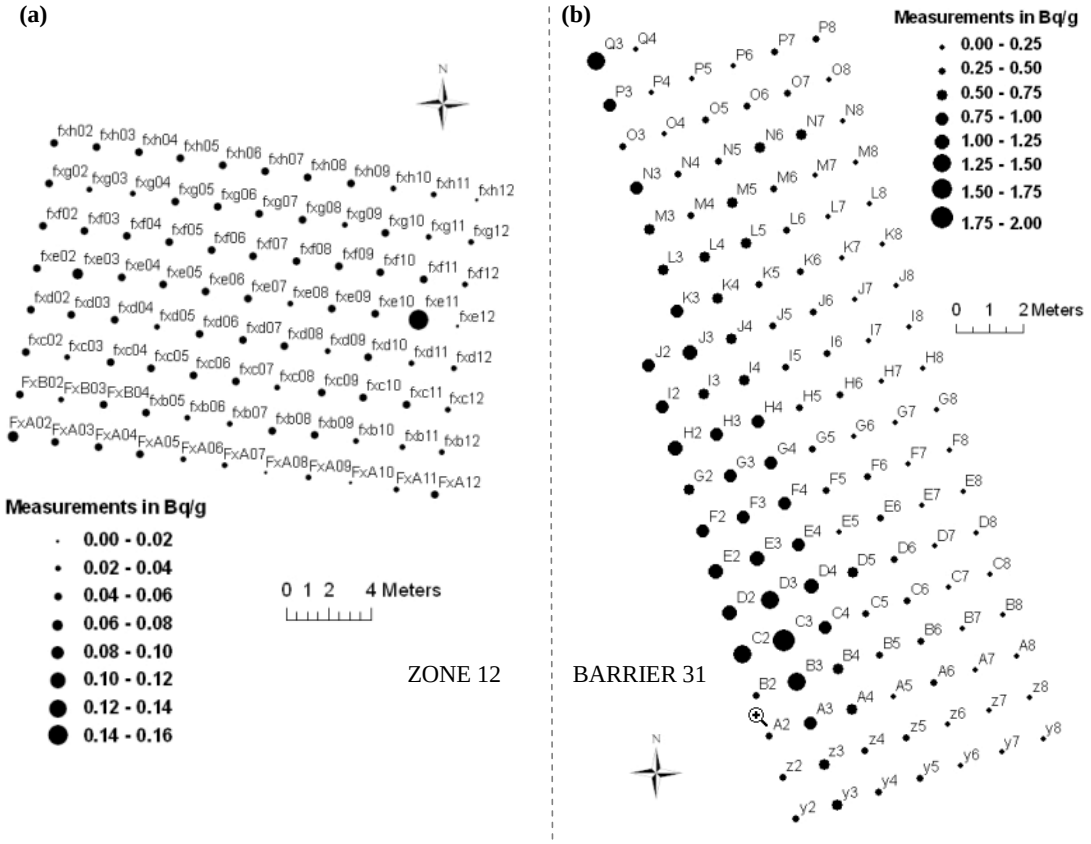

Fig 4.2 Dot maps (using equal divisions) for ^{137}Cs activity concentrations measured *in situ* using the collimated Canberra 3 x 3" NaI detector. a) measurements for Zone 12; b) measurements for Barrier 31. (Generated using ESRI ARCMAP™ 9.3.1).

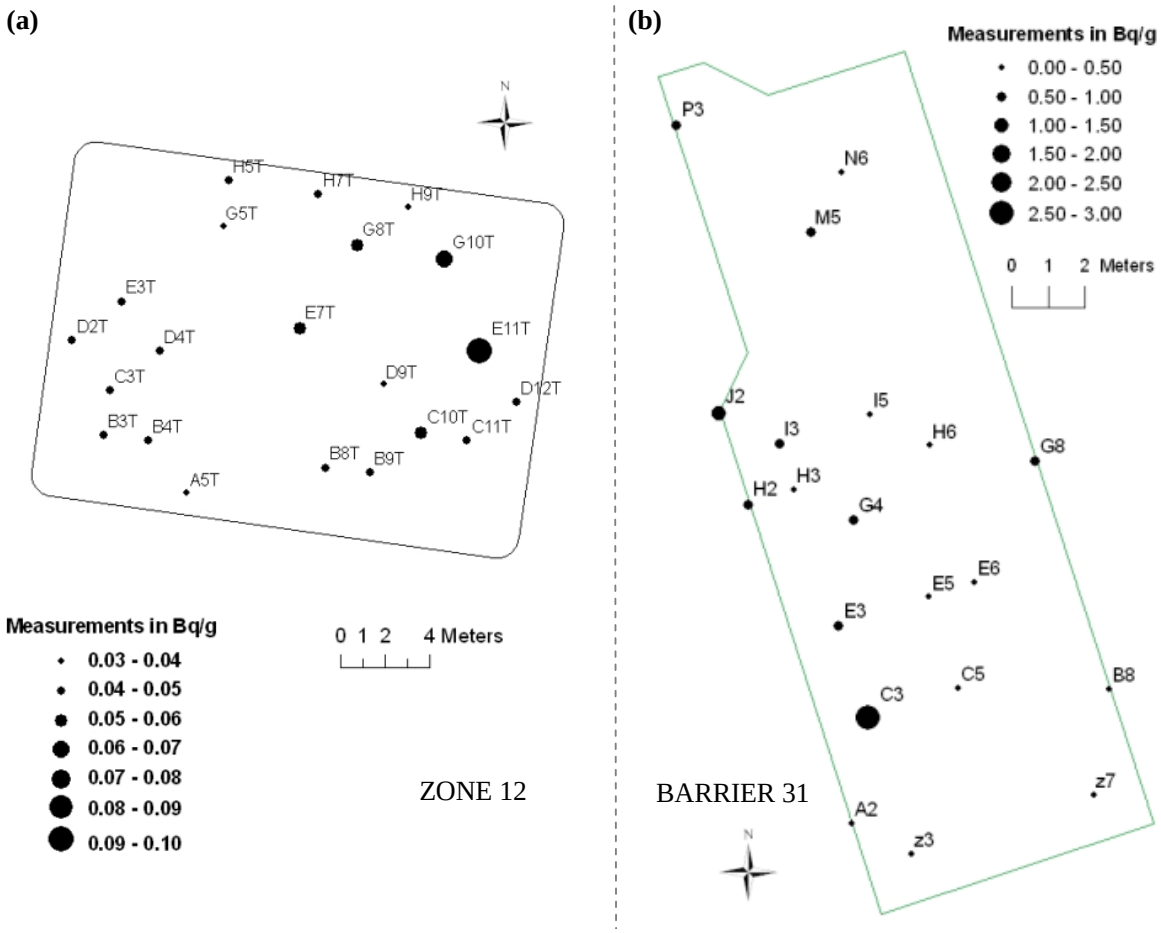

Fig 4.3 Dot maps (equal divisions) of ^{137}Cs activity concentrations measured in the on-site laboratory from <u>*ex situ*</u> soil samples for a) Zone 12; b) Barrier 31. Note that the measurement scales are different from those used in Fig 4.2. (Generated using ESRI ARCMAP™ 9.3.1).

Further statistical tests were performed to compare the 20 *ex situ* meaurements with the 20 *in situ* measurements acquired at the same locations. The measurement sets for Zone 12 and Barrier 31 were each affected by a single high measurement, at location E11 in Zone 12, and C3 in Barrier 31. None of these measurement sets are found to be good fits to normal distributions (Anderson-Darling, $p<0.05$) when these single high measurement points are included, but not significantly different from normality with them removed ($p>0.05$). Using the non-parametric Mann-Whitney test suggests that the medians of the *in situ* measurements at the *ex situ* locations, and the *ex situ* measurements themselves, are not significantly different ($p>0.05$) for either survey, when the high measurements are included. However, although the median is more robust with respect to outliers, it is a biased estimate of the mean if the distribution is skewed. Student's paired t-tests shows no significant differences between the means ($p>0.05$) when the single high measurements are excluded. This suggests that the

medians and means of the *in situ* measurements of activity concentrations are reliable estimates of the medians and means of the *ex situ* measurements.

4.5.2 Random component of measurement uncertainty

The relatively high uncertainty in the Canberra *in situ* measurements in Zone 12 (42.6 %, Table 4.2), is probably a result of the proximity of the measured activity concentrations (Table 4.3) to the MDA of 0.026 Bq g^{-1}. This uncertainty is entirely composed of analytical uncertainty (Table 4.2), suggesting that the measurements in Zone 12 are seriously affected by analytical noise. Uncertainties in *ex situ* measurements of the 0-200 mm layer have been estimated at 47.4 % in Zone 12 and 72.6 % in Barrier 31 (Table 4.2). In both cases the primary component is sampling uncertainty, which suggests significant small scale heterogeneity of ^{137}Cs activity concentrations in the soil. The analytical component of uncertainty in the *ex situ* measurements is 5.1 % for Barrier 31 and 18.7 % for Zone 12. The higher figure for Zone 12 is to be expected as the mean activity concentrations are one order of magnitude lower than those in Barrier 31, and thus much closer to the MDA of the analytical method.

The existence of significant sampling uncertainty (34.5 %) in the Exploranium measurements in Zone 12 may indicate that a smaller primary sample mass was measured than was the case with the collimated Canberra detector. It is suggested that soil attentuation of gamma radiation with this detector placed on the ground surface induced a “collimation effect” in the Exploranium measurements. As a consequence of this, less radiation was received from the surrounding ground surface than was the case for the Canberra detector which, as prevously stated in *Section 4.3.3,* was affected by radiation from outside the FOV of its collimation. If this were the case, then it also suggests that ^{137}Cs levels exhibit high heterogeneity on a small spatial scale.

The dimensions of the volume of soil from which radiation at a given energy level can be identified by an *in situ* detector depends on several factors, including the amount of radioactive material present, the energy of emitted photons, the radiation background levels, the detector height above the ground surface, and the level of attenuation by the intervening soil. The most practical method of accurately defining the shape of a source volume for a complex system such as is encountered in contaminated land surveys, where the potential source volume exceeds the practical upper limit of gamma radiation transmission through air, would be to use MCNP (Monte Carlo n-Particle) computer code. The philosophy behind such

an approach would be to randomly generate a large number of simulations of photons that could be emitted by a number of regions within a modelled mass of material. Once properly set up, MCNP code tracks the fates of each photon until its energy is lost to the system. During the entire process, the number of simulated photons from each region that would yield their full energy to the detector volume (and hence result in a detector count) could be calculated, and so a 3-dimensional map of the sample volume could be created.

If it is assumed that the total source volume is homogeneous with respect to composition, density and radionuclide content up to a maximum depth (beyond which any emitted radiation would be of an intensity that it would be attenuated to a negligible level) then a theoretical geometrical approximation of the shape of the source volume can be made. This approximation relies on the further assumption that the inverse square law pertaining to radiation density with increasing distance from a point source is balanced by an increase in the physical dimensions of the source volume from which radiation is received. The latter *increases* by the square of the distance between source and detector, and so the two effects effectively balance each other out, ignoring the additional factor of attenuation by any intervening air-space between each source and the detector.

Using this approach enables an approximation of the shape of the sample volume to be made from attenuation factors only. A gamma detector that uses a cylindrical NaI crystal would be expected to produce the same response to a point source that is positioned at the same distance from its centre and the same angle of offset from the detector axis, irrespective of its radial position. Some small differences in response are likely to arise with changing angle of offset from the detector axis, because radiation impinging on a non-spherical detector volume will have slightly different total path lengths through the crystal, and therefore different probabilities of yielding the full photon energy into the detector volume. In the case of a detector crystal that has equal dimensions (i.e. the length of the cylinder is the same as its diameter, as used in the field work) these differences would be expected to be very small, and so the model used here assumes that an un-collimated, ‘ideal’ detector (i.e. one that exhibits the same response to radiation arriving from any direction) is positioned at height *h* above the ground surface (Fig 4.4). An arbitrary depth *d* has to be chosen. This is considered to represent the baseline path-length of radiation from radioactive material that results in a discernible detector response when applied to the entire source volume. Clearly *d* actually depends on a) the attenuation coefficient of the soil; b) the absolute efficiency of the detector; c) the

counting time used; d) the background radiation levels and the resolution of the detector and its software; e) losses due to attenuation by intervening air space.

Given an assumed value of *d*, the theoretical shape of the sample volume can be defined by calculating the distance *y* for incremental steps of *x* from the ground surface to *d*, and where for each *x* the distance *AB* = *d* (Fig 4.4). The derivation is as follows:

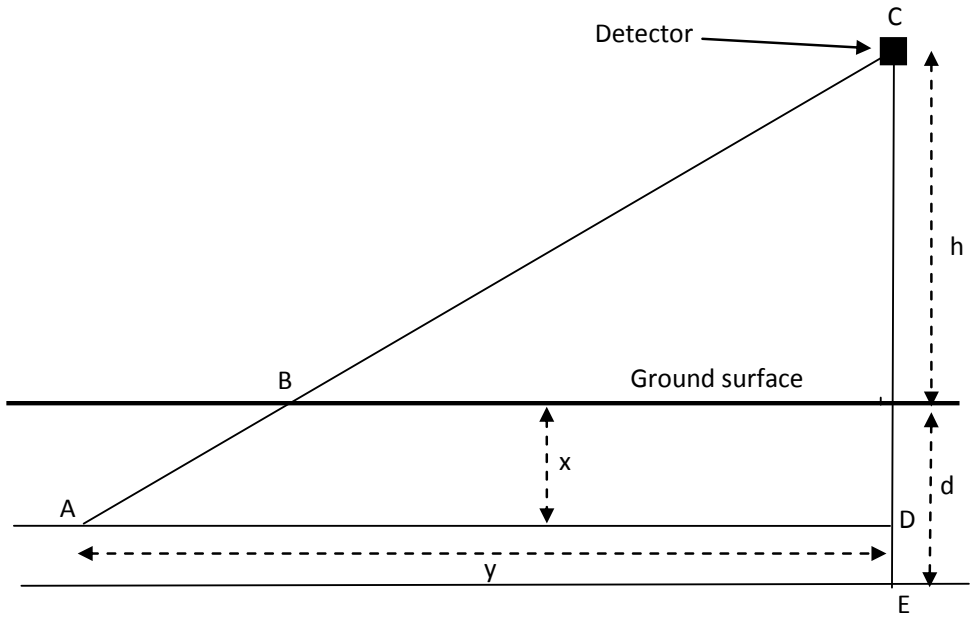

Fig 4.4 The geometric parameters used to estimate the shape of a soil sampling volume where a detector at position (*C*) is at height *h* above the ground surface. As this is a 2-dimensional representation of a 3-dimensional reality, it is assumed that the detector response to activity at point *A*, which is inversely proportional to the distance *AC*, is also directly proportional to the amount of gamma-emitting material at *A*, which would be expected to increase with the square of the distance *AC*, given a homogeneous medium with respect to radionuclide content.
The distance AB can be calculated for a given value of x by multiplying the length of the hypotenuse of the triangle ACD by the ratio x / (h + x).

From Fig 4.4:

$$AB = d = \sqrt{(y^2 + (h+x)^2)} \times \frac{x}{(h+x)}$$

$$d^2 = \frac{x^2y^2 + x^2(h+x)^2}{(h+x)^2} = \frac{x^2y^2}{(h+x)^2} + x^2$$

$$\frac{x^2y^2}{(h+x)^2} = d^2 - x^2$$

$$x^2y^2 = (d^2-x^2)(h+x)^2$$

$$y = \sqrt{\frac{(d^2-x^2)(h+x)^2}{x^2}} \quad (4.1)$$

Using (4.1), three theoretical sample volume shapes were calculated for detector heights of 10 mm, 100 mm and 1000 mm, based on an attenuation path length (*d = AB*, Fig 4.4) of 500 mm, and with 100 variations of *x* (from 5 mm to 500 mm). These are shown in Fig 4.5, note that the lateral offset from the detector axis has been truncated to 3000 mm in order to clearly show the effect on the sample volume close to the detector. Because of the assumptions and limitations of this approach as previously described, Fig 4.5 is intended only to illustrate the general effect of changing the detector height from 1m above ground level to the ground surface. The effect that variations in detector height have on the overall sampling mass of a collimated detector (using the MCNP approach as applied by ISOCS) is further discussed in *Sections 7.2* and *7.3*.

4.5.3 Systematic differences between *in situ* and *ex situ* measurements

Traditionally, *ex situ* measurements are considered to be more reliable than *in situ* measurements. This is because the primary samples are processed and measured in a controlled environment, because measurements are made on known masses of soil, and also because they are made using equipment that has been calibrated with standard, traceable reference sources. However, *in situ* measurements can have significant advantages in time and cost. In these experiments, where comparisons of individual *in situ* and *ex situ* measurements have been made, the large differences in mass between the primary samples must be taken into consideration. However, estimations of the systematic differences between them are useful in evaluating the relative effectiveness of these methods for the purpose of spatial characterisation. This is provided here through the use of a simple linear regression model. A constant difference between the two measurement sets across the entire range of activity concentrations is termed *translational* bias, and represented by the regression offset, whereas a difference that changes by a constant factor over the range of measurements is termed *rotational* bias and represented by the regression slope (Thompson, 1982).

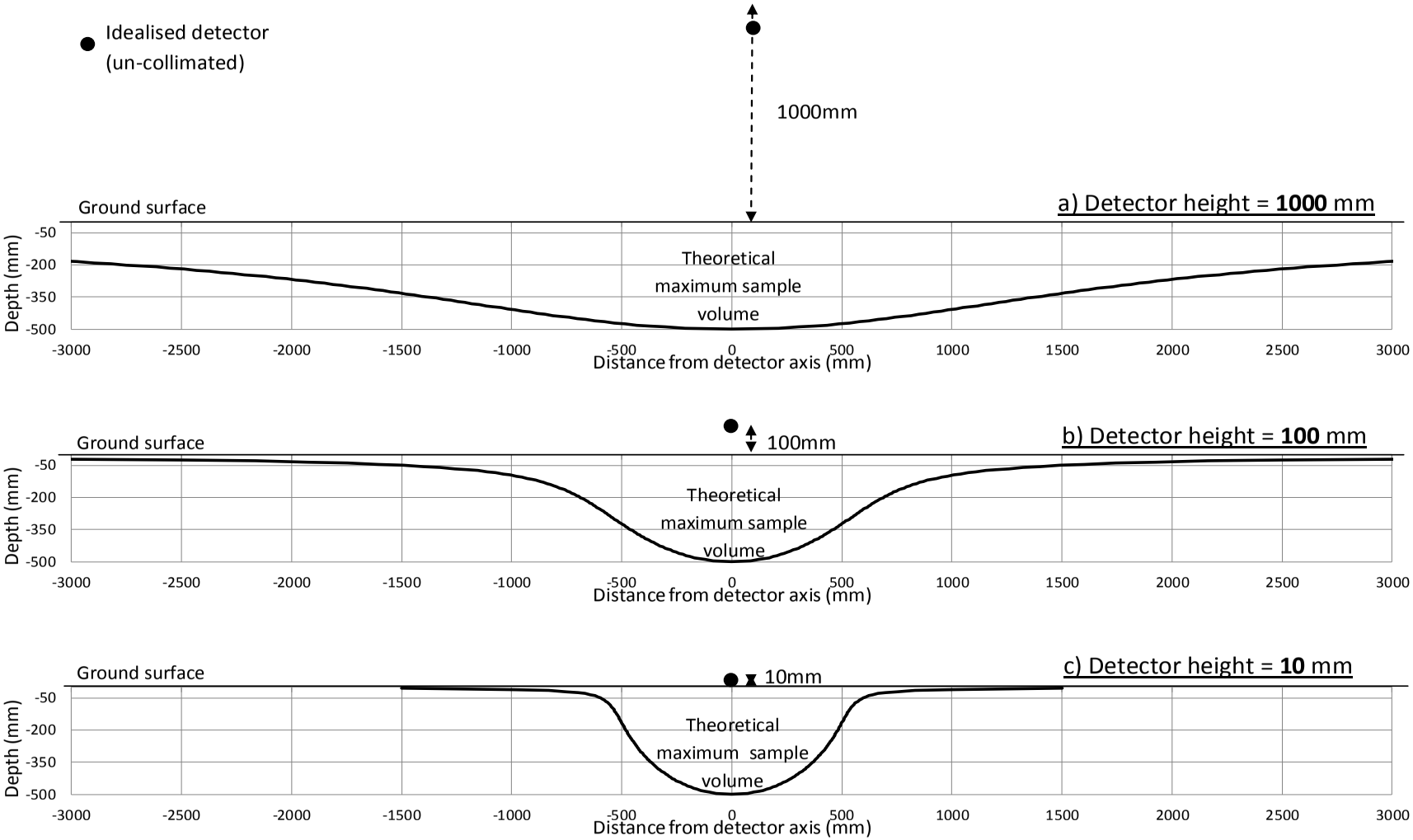

Fig 4.5 Cross sections of the theoretical maximum sample volumes that would be defined if radiation path lengths through the soil were equalised to 500mm, for lateral offsets 0 to 3000 mm from the axis of an idealised *in situ* detector. An increasing 'ground collimation effect' can be observed as the detector height is reduced from 1000 mm (a), to 100 mm (b) and finally to 10 mm

Regressions of *in situ* measurements against *ex situ* measurements are shown in Fig 4.6, with the single high-value outliers from the judgmental measurement locations excluded. The slope is not significantly different from unity, nor the intercept significantly different from zero ($p>0.05$) in either survey, suggesting that there is no translational or rotational bias between the two methods. The low correlation in the Zone 12 measurements (r^2 = 0.1405, Fig 4.6a) compared to that in the Barrier 31 measurements (r^2 = 0.635, Fig 4.6b) indicates that there is a poor spatial relationship between individual measurements obtained by the two methods in Zone 12. This is likely to be a result of the high levels of random measurement uncertainty for both methods (*in situ* = 42.6 %, *ex situ* = 37.5 %), and the differences in sampling mass. The situation improves in Barrier 31 (Fig 4.6b), where the uncertainty in the *in situ* measurements is lower (12.6 %), and there is also a greater degree of spatial variability in the estimated activity concentrations.

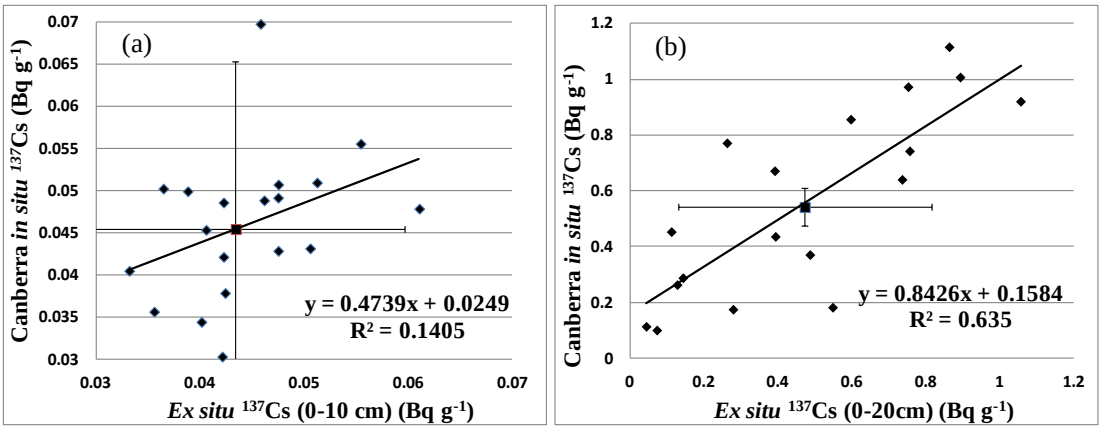

Fig 4.6 Regressions of Canberra *in situ* against *ex situ* measurements of ^{137}Cs activity concentration for (a) Zone 12 and (b) Barrier 31. Note that in (a) only *ex situ* measurements from the 0-100 mm soil layer have been used. Error bars are shown for single points.

Similar regressions with the single high-value measurements included are shown in Fig 4.7. In both cases, the intercepts are significantly different from zero, and regression slopes are significantly different from unity, suggesting that both translational and rotational biases exist between *in situ* and *ex situ* measurements. Rotational bias was found to be 56 % and -51 % for Zone 12 and Barrier 31 respectively. These differently signed bias values are thought to have resulted from small-scale heterogeneity and the difference in primary sample mass between the *in situ* and *ex situ* methods, which has particularly affected the higher measurements.

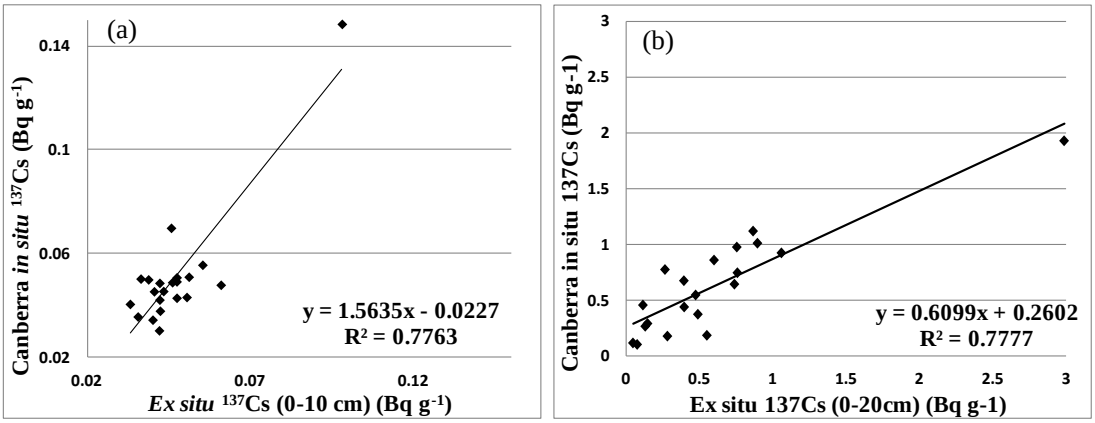

Fig 4.7 The regressions shown in Fig 4.6 with the single high values of activity concentration included. These were acquired at judgmentally positioned measurement locations. Comparison with Fig 4.6 shows that the significant rotational and translational biases have arisen due to the single high measurements in each survey.

One potential source of differences between *in situ* and *ex situ* measurements is variability of activity with depth. A number of methods have been proposed which take the depth of activity into account when processing spectra from *in situ* measurements of soil (MacDonald *et al*., 1997). These methods were not employed here, however, a Student's paired t-test showed no significant differences ($p>0.05$) between the mean activity concentrations of ^{137}Cs in the 0-100 mm and the 100-200 mm *ex situ* samples, in either survey. This result is consistent with results of surveys that have been previously conducted on the site. A possible explanation is that ^{137}Cs is strongly sorbed by the micas and clays that make up a substantial component of the soil in the area. However, the vegetative content of the topsoil has resulted in lower sorption per unit mass in the upper layer, because of the reduced concentration of sorbent. Assuming that this radionuclide has been deposited on the ground surface over a fairly long period of time, then these differential degrees of sorption at different depths may have resulted in an approximately even distribution of activity concentrations between the upper and the lower soil layers.

4.5.4 Shine from external sources

In situ measurements may be affected by radiation 'shine' from sources external to the survey area, such as buildings and drains. The Zone 12 survey was carried out on an unused piece of land close to the site perimeter, where no obvious external sources of radiation were present. However, the Barrier 31 area was adjacent to both active drains and buildings. The most probable source of any significant radiation shine from external sources was from an

intermediate level waste storage tank located immediately to the west of the survey area (Fig 4.8). This comprised a subterranean tank partially filled with intermediate level radioactive waste. It is clear from Fig 4.2 that *in situ* measurements of activity concentrations show an increasing trend from east to west towards the ILW store, although this effect could also be explained by higher activity concentrations in the ground, possibly caused by historic leaks from a drain that runs along the west side of the survey area. *Ex situ* measurements made in a remote laboratory will clearly not be affected by the radiation field from the ILW store, but would be expected to show any gradient in mass activity concentrations of ^{137}Cs in the soil itself.

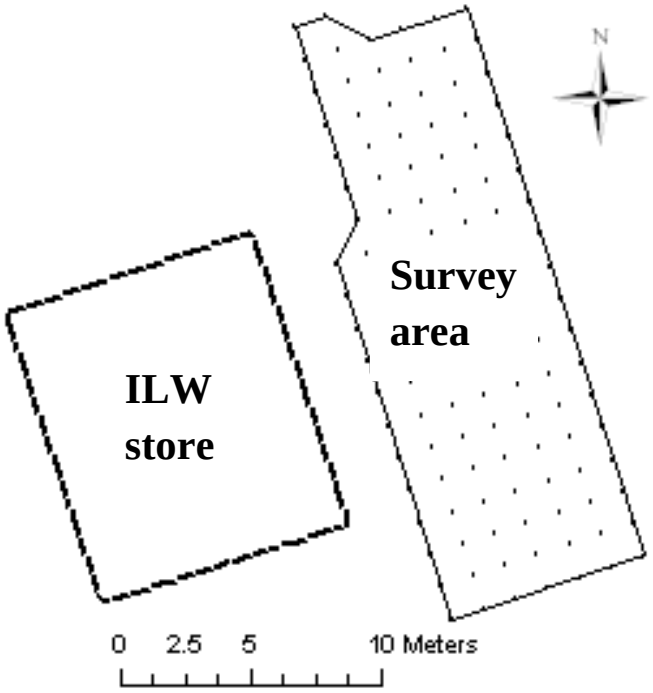

Fig 4.8 The Barrier 31 survey area, showing the location of the intermediate level radioactive waste store to the west of the area.

The shine received by a detector that is near to a large source, such as a building, will vary with distance between the source and the detector. This variation will contain both exponential and geometric components. In order to show the effects of shine, the detector/collimator assembly was placed on four lead bricks, so that the FOV of the detector was completely obscured by a layer of lead with a total thickness of 60 mm. *In situ* counts were then acquired at a total of 12 measurement locations along rows C2-C8 and H2-H8 (Fig 4.2). These measurements have been plotted in Fig 4.9, and show a decreasing trend with distance from

the centre of the ILW store. The lead bricks obscured a greater angle than was defined by the FOV of the collimator, and a more reliable method would be to use a "zero degree" collimator, which was not available at the time of the survey. In either of these methods, estimated shine would be increased if greater levels of ^{137}Cs activity existed in the ground close to the ILW, because this would also result in increased levels of radiation passing through the side walls of the collimator (see *Section 4.3.3*). There does appear to be an increasing trend in activity concentrations of the *ex situ* samples as distance from the ILW store decreases (Fig 4.3). A better approach to reducing the effects of shine in contaminated land investigations would be to use more effective shielding, although this may introduce handling problems, particularly on rough ground or in less accessible locations. For example, a proprietary 50 mm lead collimator for the Canberra 3"×3" detector would weigh approximately 70 kg.

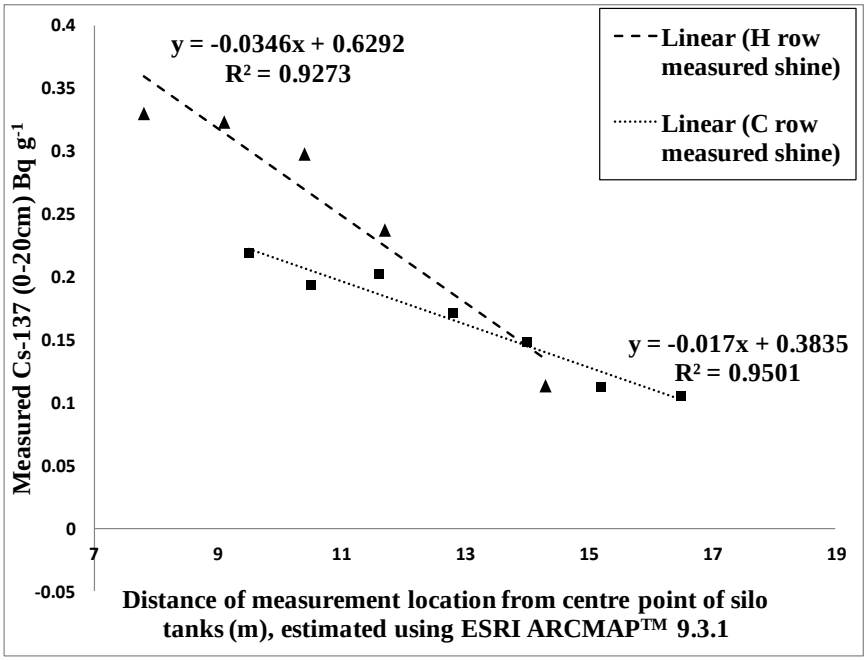

Fig 4.9 Approximated measurements of shine from the ILW, measured from 11 measurement location along rows C (dotted line) and H (dashed line), plotted against estimated distance of each measurement location from the centre of the ILW store. These suggest that the *in situ* measurements may have been affected by shine from the ILW, although some of the gradient seen could also be a result of increased radiation from the ground area surrounding the detector.

4.5.5 Identification of hotspots of activity

Identification of areas of higher activity than the average local background may be required for the purpose of identifying hotspots (e.g. particles) with activity concentrations exceeding a

certain threshold. Assessment of the techniques used in these surveys could best be achieved by comparing the measurements obtained with previous knowledge of hotspot locations. This information was available for the Zone 12 survey from Groundhog continuous coverage data. The Groundhog system is a vehicle mounted detector array which records counts per second (**CPS**) as the vehicle moves slowly across an area in overlapping swathes. Counts are recorded in three spectral windows, the centre window including the energy level 662 keV. Thus the Groundhog survey was primarily aimed at locating hotspots of ^{137}Cs activity, although it does not give estimates of activity concentrations.

The Groundhog system takes many measurements per unit area, and so some means of identifying areas of raised activity was required. In this study, 'hotter' areas have been identified using Arcview software to produce maps based on Anselin local Moran's I with inverse distance weighting, a technique which can be used for the identification of spatial clusters (Anselin, 1995). Fig 4.10 shows two maps of Zone 12: a) Canberra *in situ* measurements; b) *ex situ l*aboratory measurements from the 0-100 mm soil layer. On both maps, Groundhog data are shown where Moran's I exceeds 2.58 standard deviations from the mean (corresponding to a probability p = 0.01 of higher values occurring by chance), thus there is justification for regarding these areas as localised hotspots of activity. Both techniques identified higher activity levels around measurement location E11 only, with the Canberra *in situ* giving a strong indication of higher activity at this point. This appears to be a result of relatively small hotspots being missed by the sampling grids used in both the *in situ* and *ex situ* surveys. In the case of the *in situ* measurements this is also a consequence of the low coverage factor (6.2 %) that was used in the Zone 12 survey.

No Groundhog data were available for the Barrier 31 site, however it is reasonable to assume that the high coverage (>100 %) by the FOV of the Canberra detector would be the most likely of the methods to locate spots of higher activity. A caveat here is that, due to differences in source/detector geometry, a very small spot of activity (e.g. <10 % of the FOV area) would yield a significantly lower count within the detector volume if it was positioned at the periphery of the FOV, compared to the same activity spot positioned at the centre of the FOV. Two areas where *in situ* measurements suggested areas of raised activity were investigated following the main survey, by performing sub-surveys with the Canberra detector at ground level. The first sub-survey used a 0.25 m grid spacing close to measurement location C3, while the second used a 0.365 m grid spacing between the locations N6, N7, O6, O7 (Fig 4.2). In the

first case, a stone that was excavated 0.35 m to the North East of location C3 was measured by the on-site laboratory at ~8 kBq of ^{137}Cs activity.

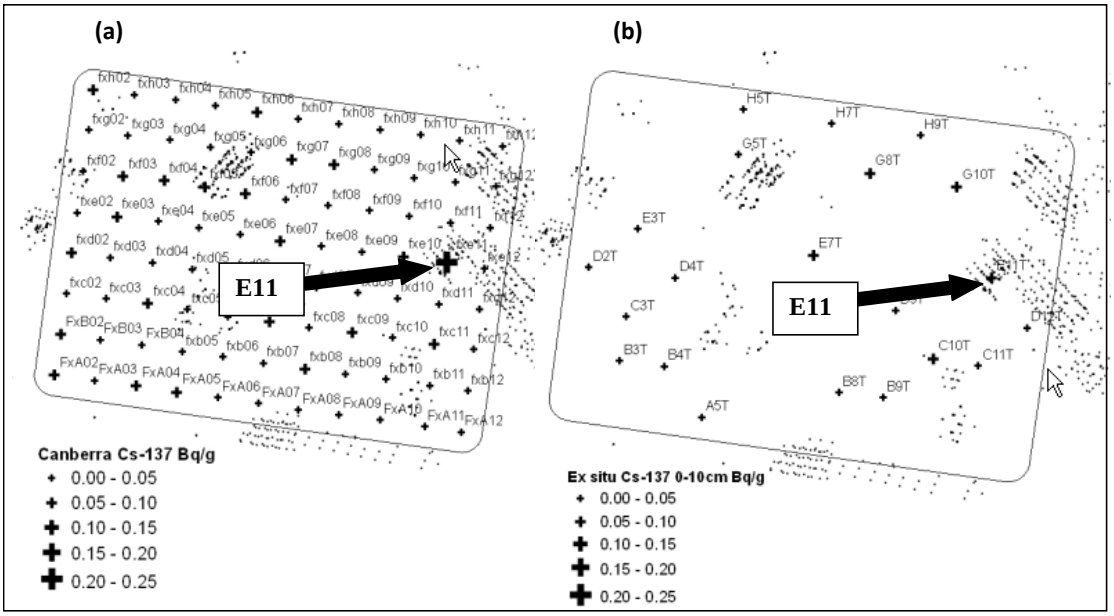

Fig 4.10 Maps of measurements in Zone 12. In both cases, the small dots represent previous Groundhog measurements where local Moran's I has been calculated as more than 2.58 standard deviations from the mean. Clusters of such measurements imply localised hotspots of activity. The black crosses represent ^{137}Cs activity for a) Canberra *in situ* measurements; b) *ex situ* measurements from the 0-100 mm layer. Arrows indicate the higher measurement reported in the current surveys at location E11.

Site rules require any particle with ^{137}Cs activity exceeding 10,000 Bq to be formally reported. In the second case, a diffuse area of higher activity was found centred on a point approximately 0.4 m north of the centre of a line drawn between measurement locations N6 and N7. The seemingly elevated concentration at point Q3 was not investigated due to time constraints. By comparison, it is unlikely that the *ex situ* measurements as shown in Fig 4.3 would have prompted investigations of the area around N6 or Q3, but may have initiated investigation at location C3, as this was the highest *ex situ* measurement recorded. This was also one of only two *ex situ* measurements (the other being J2) that exceeded the 1 Bq g^{-1} criterion for ^{137}Cs that is within the scope of the radioactive substances regulation in the UK (DEFRA, 2011). However, it has to be taken into consideration that only 20 *ex situ* measurements were acquired compared with 122 *in situ,* due to the cost of laboratory analysis of soil samples. It is not known whether the outcome would have changed had the same number of *ex situ* samples been acquired on the same regular sampling grid as was used for the *in situ* survey. It should be noted that if high coverage of a ground area is required in order

to locate small spots of activity, it is more efficient to use grids that are based on a triangular sampling pattern.

4.6 Conclusions

In situ measurements made with gamma detectors are less expensive, and have a faster turnaround time, than *ex situ* analyses of soil samples. Results from two surveys on radioactively contaminated land showed no significant differences in estimates of mean mass activity concentrations between the two methods, when single outlying values were excluded. Differences at individual measurement locations occured due to the effects of random uncertainty, and also because of the large difference in sampling mass between the excavated samples and the volume of soil that was measured *in situ*. Because of a larger sampling mass, *in situ* measurements are less affected by small-scale heterogeneity of contaminants.

Potential radiation shine from outside the survey area needs to be considered in an *in situ* investigation. Also, improved methods would be needed if depth distributions of radionuclides were either non-uniform, or not sufficently well understood to be modelled in the calibration. Within these constraints, well designed surveys using *in situ* methods are suitable for estimating activity concentrations over averaging areas.They are also the most reliable method for locating small hotspots of activity.

4.7 Colour photographs for Chapter 4

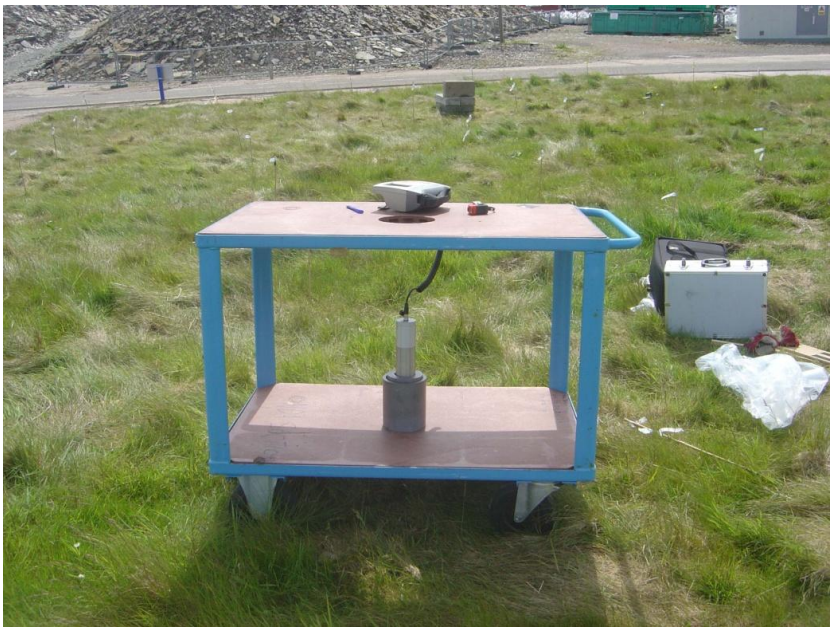

Fig 4.11 The collimated Canberra NaI 3” x 3” detector in position on the lower shelf of the detector trolley corresponding to a detector height of 280 mm. The Inspector 1000 recording unit is visible on the top shelf. This photograph shows the detector being used in the Zone 12 area (*Section 4.3.1*).

Fig 4.12 The Barrier 31 area (*Section 4.3.1*). The fence in the middle of the photograph had been removed at the time of the survey. The surveyed area was located between the building on the left (housing the ILW store) and the low-active drain which can be seen inside the fence on the right hand side of the photograph.

Chapter 5 - *In situ* detection of 'hot' particles by portable gamma-ray devices: modelling the effects of experimental parameters

This chapter comprises the manuscript of a paper that has been submitted for publication in the Journal of Radiological Protection.

5.1 Abstract

Surveys of land areas for the purposes of identifying small particles of activity can be an important part of a decommissioning strategy. For γ-emitting particles, this can best be achieved using *in situ* methods. Confidence in a survey strategy can be greatly enhanced if an estimate can be made of the detector response to particles at different positions relative to an *in situ* detector. This is already possible through the use of calibration programs that use a Monte-Carlo methodology to calculate detection efficiencies for different source/detector geometries. However, each calibration is only valid for a defined combination of detector height, particle offset, and particle depth beneath the ground surface. For the purpose of optimization, there is therefore a potential advantage to the development of a generic mathematical model that is able to give reliable approximations of detector response with varying values of these parameters. The primary aim of this study is to develop such a model and test it against measurement results obtained in the field, and also against results predicted by a commercially available calibration program (ISOCS). It is found that both the generic model and the ISOCS predictions give good approximations of the field measurements, and that the generic model is in close agreement with ISOCS. A preliminary estimate of the optimal detector height and measurement spacing that would enable identification of a relatively low activity (40kBq) particle is made, using a detector that might typically be used in the field. It is shown that for a pre-defined counting time (e.g. one that is determined by cost considerations) there is an optimal combination of detector height and measurement spacing.

5.2 Introduction

5.2.1. Requirement for in situ particle detection in land areas

Surveys of land areas and artificial surfaces on decommissioning nuclear sites can include a requirement to identify small (<1 mm) particles with activity levels that are high compared to background activity. In addition to possible risks to human health, the presence of particles

adds to the heterogeneity of radioactive material. When land areas are sampled, this heterogeneity may result in measurements that are not representative of the target mass or volume that they are intended to represent (Dale *et al.,* 2008; IAEA, 2011). Radioactive particles have been associated with both fallout from nuclear weapons testing, and authorised emissions from industrial processes (IAEA, 2011). They have also been identified as a consequence of previous activities at specific sites, where they can make a significant contribution to the overall cost of ground area monitoring (Brown and Etherington 2011; Dennis *et al.,* 2007; Poston *et al*., 2007). It is therefore desirable to optimise methods of particle detection, enabling it to be performed at known levels of confidence, and for minimum overall cost.

Legal thresholds of unacceptable particle activity have not been defined in many jurisdictions, such as in Scotland, where this study was undertaken. Thresholds have been suggested by local organisations, however. The Dounreay Particles Advisory Group (DPAG) categorises radioactive particles based on their implications to public health (DPAG, 2006). According to these definitions, a particle of activity below 10^5 Bq would be considered to be a minor particle, a particle of activity $10^5 – 10^6$ Bq would be categorised as relevant, and a particle with activity $>10^6$ Bq is categorised as significant. The latter is considered to be the minimum activity that has the realistic potential to cause harm to the public. It is recommended by DPAG to monitor and remove particles with activities > 10^5 Bq. There is also a general requirement under the Health and Safety at Work Act to reduce risks to as low as reasonably practicable (ALARP) (HSE, 2010). At the Dounreay site in Caithness, Scotland, this principle has been applied to on-site particle detection for activities of ~10^4 Bq of ^{137}Cs (Goss and Liddiard, 2007).

5.2.2 Optimisation of survey parameters for in situ particle detection

Optimisation of survey parameters (detector choice, detector height and counting interval) for locating discrete sources through the use of systematic scanning surveys has previously been discussed in the scientific literature. Such methods involve passing a gamma detector over the ground, either by hand or mounted on a vehicle, along parallel tracks at a steady speed. The detector is kept at a constant height above the ground surface. Measurements are made by recording the numbers of counts received during consecutive time intervals. The presence of a particle is then indicated by any measurement with a count rate that is elevated above that of adjacent measurements. It has been found that there is an advantage to setting the counting interval of each measurement as a running sum of three or more sub-intervals. Using this

method reduces the maximum offset that the source particle can be from the centre-line of the detector, in the direction of travel. The threshold at which a particle is assumed to be present can then be set at a higher level than would be the case if no sub-intervals were used. Using a higher threshold reduces the probability that statistical fluctuations in the γ-emissions from the background will falsely indicate the presence of a particle (Long and Martin, 2007).

Although these types of scanning survey continue to see widespread use throughout the nuclear industry, they can be limited in their ability to reliably identify the presence of particles with low activity levels. The time interval during which counts are acquired for each measurement is typically of the order of a few seconds. This may not be enough to allow the particle detection threshold to be set sufficiently high to reduce the probability of false positive measurements to acceptable levels. In the particular case of vehicle mounted surveys, using multiple large detectors improves the sensitivity of the system. Vehicle mounted systems are not suitable for all areas of potentially contaminated land, however. For example, the floor-slabs of demolished buildings may not be accessible because of structures on or around the survey area. Also, scanning surveys are not able to give good estimates of activity concentrations, due to uncertainties in the source geometry. There can therefore be an advantage to the use of hand-portable *in situ* detectors that can easily be moved between measurement locations, in which each measurement is acquired over a pre-determined counting interval. Surveys using this methodology may be based on **systematic sampling** patterns, with the dual objectives of characterising average activities (or activity concentrations), as well as the location of discrete hotspots of activity. They will often be backed up by the acquisition of targeted and/or randomly positioned core samples, which are subsequently analysed in a laboratory. Survey design methodologies have previously been established for these objectives where less than full coverage of the ground surface is required. For example, calculation of the optimal number of randomly positioned samples to obtain statistical significance for average activity is described in the U.S. MARSSIM guide (USEPA, 2000). There are also published methods for establishing the numbers of samples that are needed to identify hotspots of a defined size, e.g. the method described by Ferguson (1992) in the context of chemically contaminated land. For small (<1 mm) particles, these methods result in requirements for extremely high sampling densities.

Site de-licensing requires the licensee to demonstrate that there is “no danger” from ionizing radiations on the site. Because of the stochastic nature of the risk to human health from exposure to radiation, it is accepted that in practice a small, tolerable hazard may still be

present after site characterisation and cleanup, if this would necessitate a disproportionate amount of effort and expense to identify and remove. However, it is necessary to show that any residual radiological hazard does not pose a significant ongoing risk to any person, regardless of any foreseeable use to which the site may be put (HSE, 2005). While methods of calculating the risks to humans from average activity levels are fairly well established (e.g. possible contamination of ground water or the agricultural food chain) the risks posed by radioactive particles are less so. In this case, the risk is a combination of the potential harm to a person encountering a particle, and the probability of such an encounter occurring. Being able to demonstrate that land is free of spatially small radioactive particles, within tolerances of defined probability levels, can therefore contribute significantly to the body of evidence that will ultimately be used to demonstrate that site de-licensing criteria have been met.

In the particular case of detecting the presence of small, γ-emitting particles, high coverage *in situ* surveys have a considerable advantage over low coverage *in situ* or *ex situ* investigations, because these are likely to overlook any particulate activity that occurs between measurement locations. There is, therefore, a requirement to improve the confidence in the ability of high coverage *in situ* surveys of land areas to locate small particles, wherever they happen to be located in the surveyed area. When *in situ* surveys are employed to estimate the total radionuclide inventory in an area of land as well, a further potential benefit of improving confidence in their use is that it may result in a reduction in the requirement for relatively expensive laboratory measurements of core samples.

The number of counts that is recorded by a particular *in situ* gamma detector when exposed to a particle containing a radionuclide of given activity depends on the length of time for which the measurement is taken, and also on the efficiency of the detector. The detection efficiency is in turn dependent on the energy level of the gamma radiation that is used to identify the particle, and on the relative positions of the particle, detector, and any absorbing media in between. The efficiency can be predicted for any individual scenario by a program such as Canberra's ISOCS (Canberra, 2009), which uses a Monte-Carlo methodology to estimate efficiencies from repeated simulations of the eventual fate of photons emitted by the source. After a definition of the relative positions of the source, detector and absorbers has been created, ISOCS converges on estimates of the absolute detection efficiencies across a range of energy levels. An advantage of ISOCS is that it can calculate detection efficiencies relatively quickly, which makes it suitable for use in the field. However, because of the Monte-Carlo

methodology that is used, it is necessary to create an individual definition of every possible source/detector/absorber geometry scenario that could be encountered. An alternative approach is to use a generic, mathematical model that is based on continuous functions of the various geometry components, and takes account of the attenuation by intervening absorbers. Such a model would be suitable for incorporation into optimisation algorithms for determining the optimal survey parameters under particular circumstances.

5.2.3 Developing a generic model for particle detection

There is a significant advantage to the use of a collimated detector for the identification of particles of relatively low activity. This is because the reduction in background radiation levels improves the probability of detection of a particle within the field-of-view (FOV) of the collimator. The number of counts received by an *in situ* detector from a particle positioned within the FOV of the collimator depends on: a) its position relative to the detector axis; b) the height of the detector above the particle; and c) attenuation due to overlying soil (or other media). These three factors are considered separately below.

The situation where a particle is displaced from the detector axis is illustrated in Fig 5.1a. As a particle (*P*) on the ground surface moves away from the detector axis at *B*, the proportion of emitted radiation that impinges upon the detector volume diminishes, as a result of the increased distance *AP*, and also because of the change in source/detector geometry. For the purposes of these experiments, a means of standardising the lateral displacement *BP* for different detector heights was needed. One method would have been to use equal increments of the angular displacement of *P* from the detector axis, however this would result in a non-linear increase in the distance *BP* with increasing equal divisions of this angle. It was therefore decided to define the term *lateral offset (r)* as the ratio between the distance *BP* and the total radius (r_F) of the FOV of the collimator, subtended to the ground surface (Fig 5.1a). This has the additional advantage that it is more easily calculated and measured in the field. An adjustment to *r* is then required for a particle that is buried vertically beneath position *P*. In this case the lateral offset of the particle P_D is considered to be the same as that for a hypothetical particle at position *C* on the ground surface, given by:

$$r = \frac{sh}{r_F(h + d_t)} \tag{5.1}$$

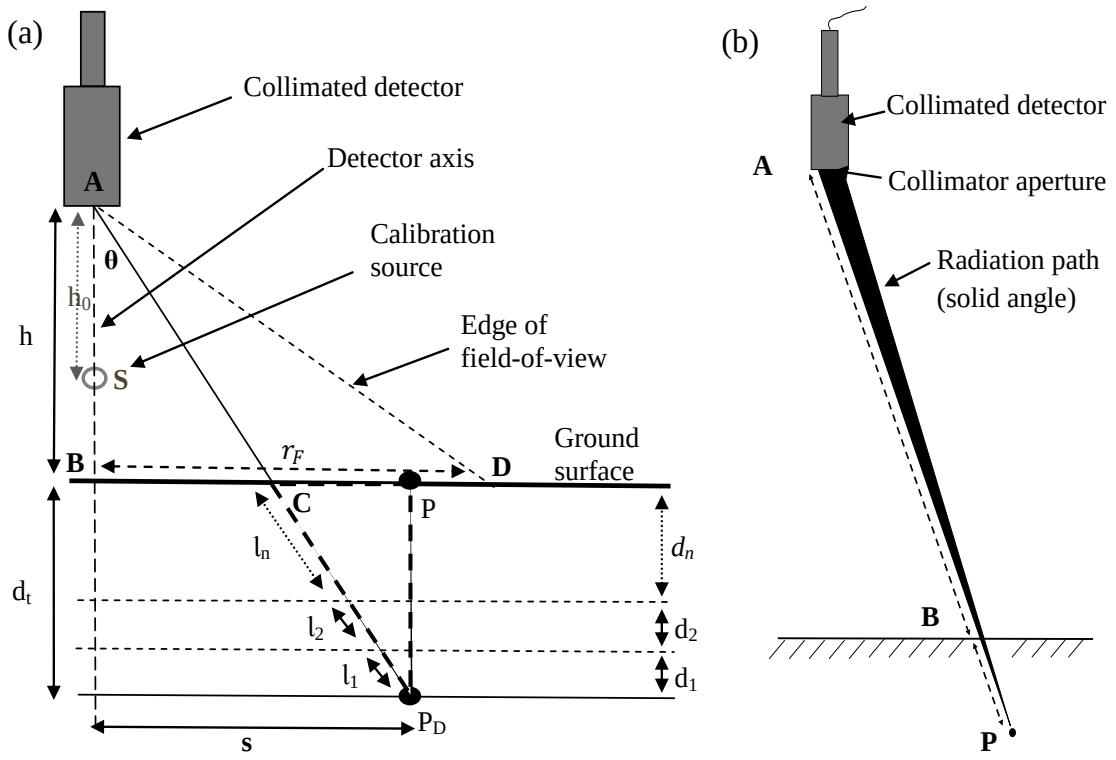

Fig 5.1 (a) The geometric components of single particle detection by *in situ* measurement with a portable gamma detector. (b) Showing an approximation of the solid angle representing the path of gamma rays from source (*P*) to the collimated detector (note that the edges will not be clearly defined as is depicted, due to collimator edge effects). All distances are assumed to be in units of millimetres.

The change in detector response with increasing *r* is complex, because it not only involves changes in the geometry between the source and the detector volume, but also with the different components of the collimator. It would be expected that if r_F is large compared to the dimensions of the detector, then the counts detected (*N*) at lateral offset *r* would tend to decrease compared to the counts at *r* = 0 (N_0), according to some function of *r* so that:

$$N = f(r) \times N_0 \qquad (5.2)$$

The absolute detection efficiency (ε_0) for a calibration source (*S*) that is positioned on the axis of a detector at height h_0 (Fig 5.1a) is given by:

$$\varepsilon_0 = \frac{Number\ of\ pulses\ recorded\ by\ detector}{Number\ of\ radiation\ quanta\ emitted\ by\ source}$$

(Knoll, 2000).

This can be calculated by obtaining a single measurement using a physically small source of known activity at a fixed distance along the centre-line of the detector, provided the expected number of radiation quanta emitted by the source can be estimated for the duration of the measurement. Given a value for ϵ_0, the number of counts N that would be expected to be recorded by the detector for a particle P of activity A_p at detector height h and lateral offset r can be calculated (using the inverse square law):

$$N = f(r)\, A_p\ \ \varepsilon_0\, p_\gamma\, t\, \frac{h_0^2}{h^2} \tag{5.3}$$

Where p_γ is the probability of emission of gamma photons from the source at the energy level of the measured radiation, and t is the counting time. This equation makes the assumption that attenuation of radiation by air is negligible, and that the detector response is linear with increasing source activity. These are considered to be reasonable assumptions for measurements on land that are made using ground-based detectors.

5.2.4 Detection of a buried particle

In a report on the management of particles at the Dounreay site up to 2005, Goss & Liddiard (2007) give an average depth of 72 mm for all the particles located over a period of 10 years. The maximum average depth in any single year was 130 mm. It is therefore important to consider the possibility of a particle being buried beneath the ground surface. In this case, the effective detector height becomes $h + d_t$ (Fig 5.1a), and the lateral offset r needs to be adjusted according to *Equation 5.1*. In addition, gamma radiation that is emitted by the particle on a vector that could intercept the detector volume is subject to attenuation by overlying material. The actual path of gamma radiation emitted by a physically small particle can be defined as a solid angle, originating at the particle and subtending to the detector volume (Fig 5.1b). However, for a collimated detector, the greater part of received radiation can be expected to arrive through the collimator aperture. The 90˚ collimator used in these experiments had an internal aperture of 25 mm diameter. Providing this aperture is small compared to the distance between source and detector, a reasonable approximation can be made by assuming parallel attenuation through the material existing on a line between the particle and the intercept of the detector axis with the detector face. This can readily be calculated using the Beer-Lambert law:

$$I\ =\ I_0\, e^{\left(-\mu l/_{10}\right)} \tag{5.4}$$

Where I = radiation intensity after travelling through thickness l of the soil (mm), I_0 is the original intensity of radiation on a path that will intercept the detector volume, and μ is the linear attenuation coefficient, which is conventionally given in units of cm^{-1}.

As the Beer-Lambert law assumes that the radiation will travel along parallel paths through the attenuating media and can be expressed as a ratio of I/I_0, an approximation of the total attenuation can be made by applying a correction to the total counts that would be received at the detector as defined by the source/detector geometry. Fig 5.1a shows a particle P_D buried at depth d_t beneath the ground surface, where the subsurface is made up of layers of thickness $d_1, d_2 \ldots d_n$. Gamma radiation follows a path P_DA to the detector, which is at a height h above the ground and at lateral displacement s from the particle. Total attenuation will be the product of the attenuation due to each successive layer, given by:

$$I = I_0 \times e^{\left(-\mu_1 l_1/_{10}\right)} \times e^{\left(-\mu_2 l_2/_{10}\right)} \times \ldots\ldots \times e^{\left(-\mu_n l_n/_{10}\right)} \tag{5.5}$$

Where μ_i = the linear attenuation coefficient (in units of cm^{-1}) of layer d_i, and l_i is the path length through each layer, given by:

$$l_i = d_i / \cos(\Theta).$$

and

$$\Theta = \tan^{-1}(s / (h+d_t))$$

It is known that $\cos(\tan^{-1} x) = 1 / \sqrt{(1+x^2)}$, so the thickness of each source layer can be calculated:

$$l_i = d_i \sqrt{1 + \left(\frac{s}{h + d_t}\right)^2} \tag{5.6}$$

Using (5.1 – 5.6), a combined generic model for particle detection can be expressed:

$$N = f\left\{\frac{s\,h}{(h + d_t) r_F}\right\} \times A_p\, p_\gamma \varepsilon_0 t \times \frac{h_0^2}{(h + d_t)^2} \times \exp\left(\sqrt{1 + \left(\frac{s}{h + d_t}\right)^2} \times \sum_{i=1}^{n} \left(\frac{-\mu_i d_i}{10}\right)\right) \tag{5.7}$$

5.2.5 Measurement uncertainty

A known random component of uncertainty in measurements of radionuclide activity arises from the stochastic process of atomic decay. This is well known and described by Poisson statistics. Where measurements are made in the controlled conditions of a laboratory, on dried, ground and homogenised samples of known masses, it can be expected that this will be the predominant random component of uncertainty in individual measurements. However, other uncertainties will arise, e.g. uncertainty in the identification, resolution, and quantification of peak areas above background radiation levels. In the case of *in situ* measurements made in the field, additional random factors will contribute to the overall uncertainty in the measurements, for example:

a. Variability in detector response. A particular cause of this is expected to be changes in temperature. The light output of a NaI(Tl) is reasonable constant over the normal range of room temperatures (Gilmore, 2008). However, when used in environmental conditions, temperature changes can cause fluctuations in the light yield and decay times within the crystal itself, and also in the electronics, leading to peak shifts in the recorded spectra (Casanovas *et al*, 2012).
b. Where a particle is beneath the ground surface, the proportion of radiation emitted by the particle that is geometrically "receivable" by the detector will be attenuated by overlying material. The degree of attenuation will vary with soil moisture content as well as any other factors that influence the soil characteristics, e.g. compaction.
c. Uncertainty in source/detector geometry can be expected to be a much more significant factor than it would be in a laboratory. Some uncertainty will be introduced by errors in detector positioning, additionally there is a much larger component of uncertainty because the actual mass of the primary sample is not clearly defined.

5.2.6 Objectives

1. Evaluate the ability of the generic mathematical model to predict the response of an *in situ* detector to small particles of activity. Also evaluate this model against individual predictions that are made using a commercially available calibration program (ISOCS).

2. Use the experimental results to identify the optimal detector height and measurement spacing that would enable reliable identification of the existence of a particle with an activity

level in the 10^4 – 10^5 Bq range, by a systematic, full-coverage *in situ* survey with a fixed counting time.

5.3 Methods

5.3.1 Field measurement apparatus and procedure

All field measurements were made using a NaI 3"x3" (76 mm x 76 mm) scintillation detector, enclosed in a 90 degree lead collimator with a wall thickness of 20 mm. Gamma energy spectra were recorded and downloaded onto a PC where they were analysed using Genie-2000 Gamma Acquisition and Analysis software (Canberra, 2009). In order to permit measurements over a range of detector heights and at different lateral offsets of the source, a wooden support was fabricated with a bevelled circular aperture in its centre. This was sized so that it offered an unobstructed 90^o field-of-view (FOV) when the collimator was positioned centrally over the aperture. For each measurement, the support was suspended on an aluminium frame which allowed a total of six different detector heights between 215 mm and 1325 mm. The support was constructed of wood of thickness 44 mm and with a density of 0.53 g cm^{-3}. This was sturdy enough that there was no noticeable distortion when supported at each end with the detector in position. Although the structure of the aluminium framework would have resulted in a small degree of attenuation of the radiation background, it was ensured that in each experiment the path between the source and the collimator aperture was completely unobstructed. A scale drawing of the detector, collimator and part of the wooden support is given in Fig 5.2.

A location was selected for the experiments on private land. An experimental area of dimensions 4.5 m x 4.5 m was marked out. A set of nine background measurements were acquired in a 3 x 3 grid pattern across this area, using a detector height of 1080 mm, and a measurement spacing of 1527 mm. This detector height was thought to approximate to that which might typically be used during an *in situ* survey, and the spacing ensured full coverage of the work area by the FOV of the collimated detector. A counting time of 600 seconds was used, which had previously been found to be sufficient to identify (although not to reliably quantify) the presence of ^{137}Cs at average activity concentrations of ~0.01Bq g^{-1}. Analysis of the acquired spectra for this background characterisation revealed no discernible peaks in the energy range 604 keV - 750 keV. This energy range was chosen to encompass the energy band

661.65 keV, which is characteristic of the decay of ^{137m} Ba, a short-lived progeny radionuclide of ^{137}Cs.

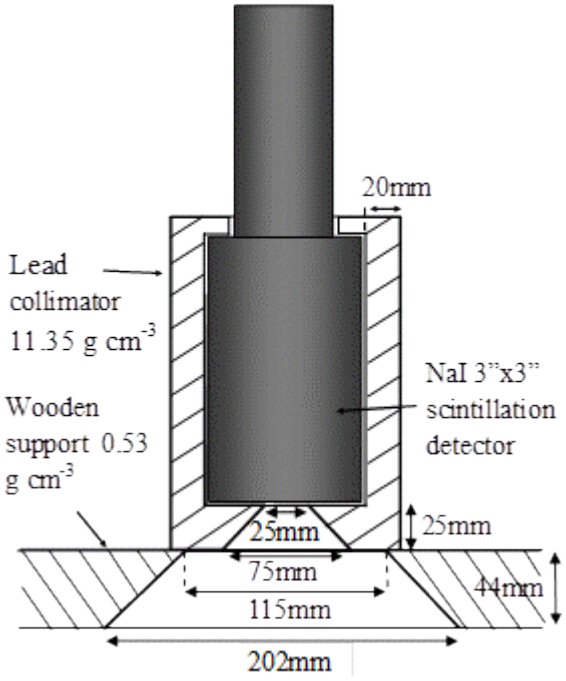

Fig 5.2 Drawing (to scale) of the detector, collimator and collimator support used in these experiments.

In order to permit repeatable positioning of the source at a range of depths beneath the ground surface, a square plastic pipe of cross-section 65 mm x 65 mm and with a wall thickness of 1.5 mm was buried at an angle of 45^{o} in the centre of the work area. During the experiments, a sealed source of ^{137}Cs (considered to be a point source), embedded into a plastic disk of dimensions 25 mm x 1.5 mm, was positioned at the required depth inside the pipe. The activity of the source was measured at the National Physics Laboratory and found to have an activity of 40.6 kBq +/- 1.5 %. During operations, the source was placed on a carrier to ensure that it was firmly held against the top surface of the pipe.

5.3.2 Uncertainty estimation

Five replicate measurements were made for each combination of parameters (detector height, lateral offset, source depth and counting time) that are shown in Table 5.1. The random component of measurement uncertainty was estimated as a factor of the relative standard deviation of the replicated measurements.

Table 5.1 Parameters for measurements acquired for the purpose of uncertainty estimation. Five replicate measurements were acquired for each of the parameter combinations shown.

Detector height (mm)	Lateral offset	Source depth (mm)	Counting times (seconds)
661	0	0	15, 30, 60, 120, 300, 600, 1200
664	0	10	30, 60, 120, 210, 300, 600
889	0.7	0	30, 60, 120, 210, 300, 600

5.3.3 Source/detector geometry measurements

To enable comparisons of the detector counts predicted by the generic models with measured detector counts, a number of measurement sets were acquired with the detector at different heights, and with the source at different lateral offsets and depths. The ranges of the parameters that were used are shown in Table 5.2. Additional measurements were acquired to establish the approximate limits of detector height and lateral offset beyond which a ^{137}Cs peak was no longer discernible in the spectra. This was carried out for source depths of 0 mm, 100 mm and 200 mm at each of the six different detector heights.

Table 5.2 Parameter ranges of the field measurements.

Parameter	Parameter ranges (all measurements = 600 s counting time)
Lateral offset	Lateral offset (r) range 0.0 - 1.0 in steps of 0.1, for detector heights h=215 mm, h=445 mm, h=661 mm, h=887 mm, h=1115 mm, h=1325 mm.
Source depth	Depth (d_t) range 0 – 240 mm, in steps of 50 mm, for detector height 215 mm, offsets 0.0, 0.3, 0.5, 0.8. 1.0 and for detector height 445 mm, offsets 0.5 and 1.0.
Lateral offset (with source at depth)	Lateral offset (r) varied 0.0 – 1.0 in steps of 0.1, for detector height 215 mm, depths 50 mm, 100 mm, 150 mm and 200 mm. Also for detector height 661 mm, source depth 100 mm.

5.3.4 Interpretation of field measurements

Acquired spectra from the field measurements were analysed using Genie-2000 software (Canberra, 2009). The numbers of ^{137}Cs counts for each measurement were inferred from the

peak area in the region of interest, by using the standard Genie 2000 Peak Locate and Peak Area utilities with a nuclide library that included a key line for ^{137}Cs at 661.65 keV.

5.3.5 Definition of ISOCS geometries

To obtain ISOCS predictions of counts from a particle at depth, a standard ISOCS "complex box" geometry definition was used. The source itself was represented by an internal box of dimensions 5 mm x 5 mm x 0.1 mm (material = caesium), and the container box was split so as to define two absorbing ground layers of thickness 0-100 mm and 100-250 mm. Estimates of the soil types and densities of these layers are described later in *Section 5.4.4*. An additional PVC absorber of thickness 2.85 mm was defined in order to represent an approximation of the attenuation caused by the material of the source container pipe and the plastic casing that contained the deposited ^{137}Cs source. An example representation of the ISOCS geometry for detector height = 215 mm, particle depth = 200 mm and r = 0.8 is shown in Fig 5.3.

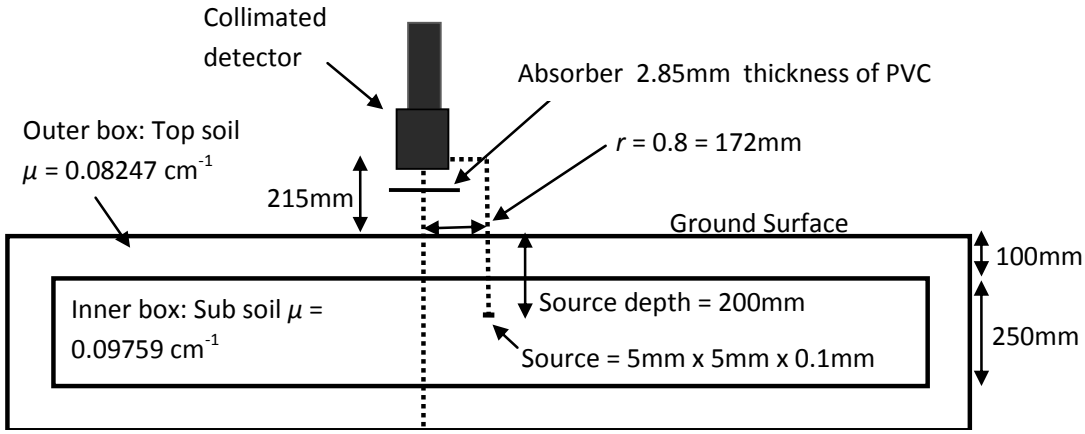

Fig 5.3 Representation of the ISOCS geometry definitions used for a particle at depth (not to scale). This example shows the configuration of the geometry definition for the scenario where source depth = 200 mm, lateral offset r = 0.8, and detector height h = 215 mm.

5.4 Results and discussion

5.4.1 Estimation of the random component of measurement uncertainty

Results of all of the uncertainty measurements have been combined for the three different source/detector geometries described in Table 5.1. These are summarised in Fig 5.4, which shows the calculated standard deviation of the replicate measurements plotted against the standard deviation expected by Poisson statistics (equal to $\sqrt{n}$, where n is the average number of counts for each replicate set). There is considerable scatter in the measured values. This

may be partly a result of using only five replicates per measurement set. Error bars are shown based on a calculation of the standard error (ε) on the standard deviation where $\varepsilon = s / \sqrt{(2 \times n)}$ and n = 5. Least-squares linear regression analysis on the complete data shows a significant rotational bias (i.e. the proportional bias, represented by the slope of the fitted line) of +74 % (i.e. a multiplication factor of 1.74) compared to the Poisson case. The offset of +4.2 was not statistically significant in the regression. The rotational bias implies that there are additional sources of random uncertainty in the field measurements over and above Poisson variability. Estimates of the random uncertainty in the field measurements (with a coverage factor of 2) can therefore be expressed:

$$U = 2 \times 1.74 \times \sqrt{N} = 3.48\sqrt{N}. \quad (5.8)$$

Where *N* is the number of counts at the detector, extracted from spectral analysis.

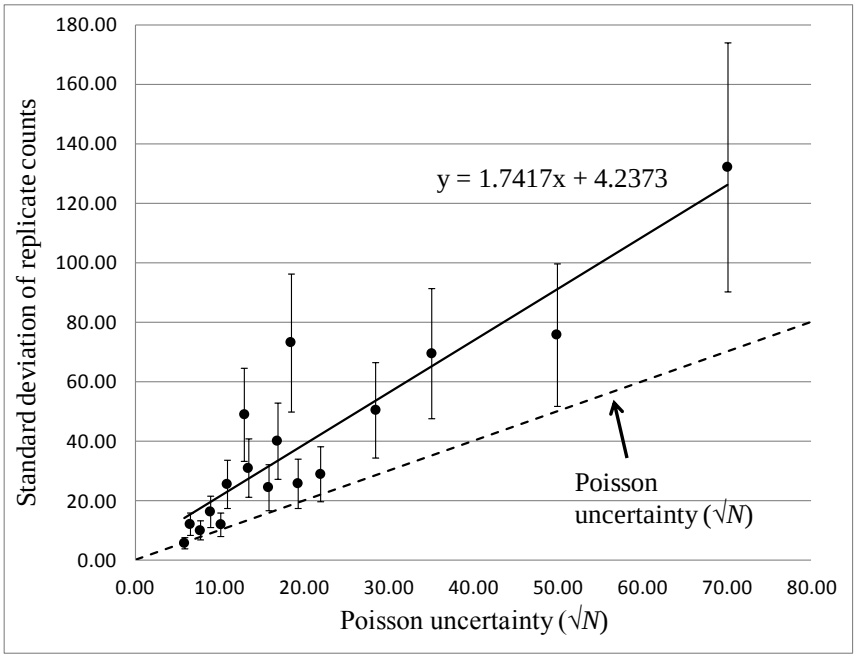

Fig 5.4 Uncertainty estimation from replicate counts, showing that use of Poisson statistics (dashed line) would significantly underestimate the random component of uncertainty in the measurements. The standard deviations of the sets of experimental replicate counts are plotted against predictions from Poisson statistics ($\sqrt{N}$ where N = the average counts obtained).

5.4.2 Calibration of ISOCS and the generic model for zero offset

The detector used in the field experiments had not been individually characterised for ISOCS use, so some differences between the ISOCS count predictions and the measurements would be expected. These differences arise from non-uniformities in the NaI crystal, and deterioration of the quality of the crystal with increasing age and use. It would be expected that the number of counts recorded by the detector would decrease according to an inverse square relationship with increasing distance from the source. It should therefore be possible to use ISOCS to predict the detector counts that would be obtained using an uncharacterised detector with varying source-detector distances, provided a suitable correction is applied. For these experiments, this correction was obtained by creating ISOCS geometry definitions for each of the six detector heights defined in Table 5.2. Detection efficiencies calculated from these definitions were used to predict the expected detector counts for each detector height. These are plotted against the corresponding field measurements in Fig 5.5a. Linear regression produces a significant rotational bias (represented by the slope factor of 1.23) and a non-significant translational bias (represented by the offset of 174 counts). This implies that a correction factor of 0.81 should be applied to the ISOCS predicted counts. Further regressions of the measured counts and the corrected ISOCS predictions against the idealised inverse square model show good agreements to this rule (Fig 5.5b). In this case bias is non-significant for the field measurements, and while the rotational bias is significant for the ISOCS predictions, it is extremely small (-0.5 %). In the case of the generic model (*Equation 5.7*), a single measurement at a known distance between source and detector is required for the zero-offset calibration, which can then be converted into a value for the absolute detection efficiency ε_0 as described in *Section 5.2.3.* The single measurement at the lowest detector height (215 mm) was used to calculate a value of $\varepsilon_0 = 1.061 \times 10^{-3}$.

5.4.3 Calibration of the generic model for changing lateral offset

The effect that increasing lateral offset has on the recorded counts can be represented as a fraction of the counts at each offset compared to those obtained at offset 0. This is shown for the six detector heights in Fig 5.6. The fractional count information for ISOCS, obtained by calculating detection efficiencies from ISOCS geometry definitions for each detector height and offset combination, is also shown. For ISOCS, the mean value of the fractional counts has been plotted for each offset increment, with error bars representing the total spread between the

predicted counts for the different detector heights. It can be seen from Fig 5.6 that the measured counts decrease more rapidly with increasing offset than is predicted by ISOCS, which is almost certainly the result of using a detector that has not been characterised for ISOCS use. The ISOCS models for the different detector heights are in very good agreement, with the maximum deviations in individual models (shown by the error bars in Fig 5.6) occurring at the low offsets (r = 0.2 – 0.3). This again implies that the offset model is independent of detector height. With the exception of the curve for the maximum detector height 1325 mm, the measured offset curves are in fairly good agreement. The special case of the 1325 mm curve is probably a result of high uncertainty due to the low count levels obtained at this height. Fig 5.6 confirms the assumption that the response to increasing offset between source and detector is similar at all detector heights, and can be summarised by a function that depends on r alone.

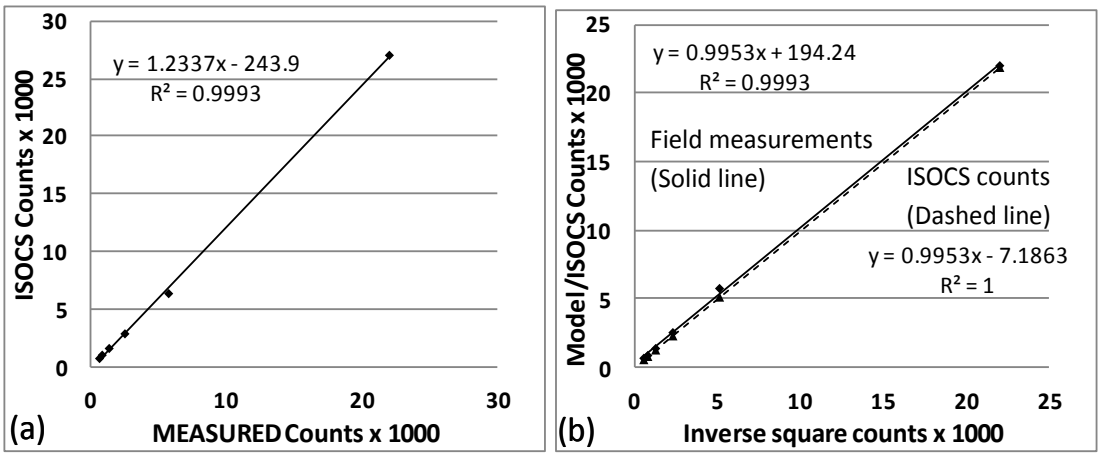

Fig 5.5 (a) Regression of ISOCS predicted counts against measured counts for changing detector height. The rotational bias is significant suggesting a correction factor of 0.81 be used for ISOCS predicted counts. (b) Regression of field measurements and ISOCS predictions (corrected) against an inverse square model, showing a very good agreement between the measured/ISOCS counts and the model.

Where single field measurements at each offset increment are to be used to describe the change in counts with increasing r, it is suggested that the measurements are obtained at low values of the detector height (e.g. 200-250 mm). This reduces the uncertainty in the model. The particular case of the (lowest) detector height 215 mm is shown in Fig 5.7a, where the fractional counts have been produced both by measurement and by ISOCS geometry definitions. A linear regression of the fractional counts for the ISOCS case against those for the field measurements is shown in Fig 5.7b. Neither the rotational bias (slope) nor the

translational bias (offset) are significant at the 95 % confidence level, however, there seems to be some structure in the residual values in Fig 5.7b which suggests a slightly non-linear relationship. Although the measured counts appear to decrease more rapidly than predicted by ISOCS in this uncharacterised detector, the ISOCS case appears to be a reasonable approximation of the results from the field measurements at this detector height. This relationship between fractional counts and lateral offset is equivalent to the *f(r)* term in *Equation 5.7*, and can be described by a polynomial function. It is considered here that a polynomial function provides a sufficient characterisation of the change in counts with changing lateral offset, provided a good fit to the data is obtained, and that the function includes the full offset range from r = 0.0 to 1.0 in increments of 0.1r. The 5th order polynomials shown appear to ft the data well, and a calculated R^2 value of 0.9999 is shown for the ISOCS case.

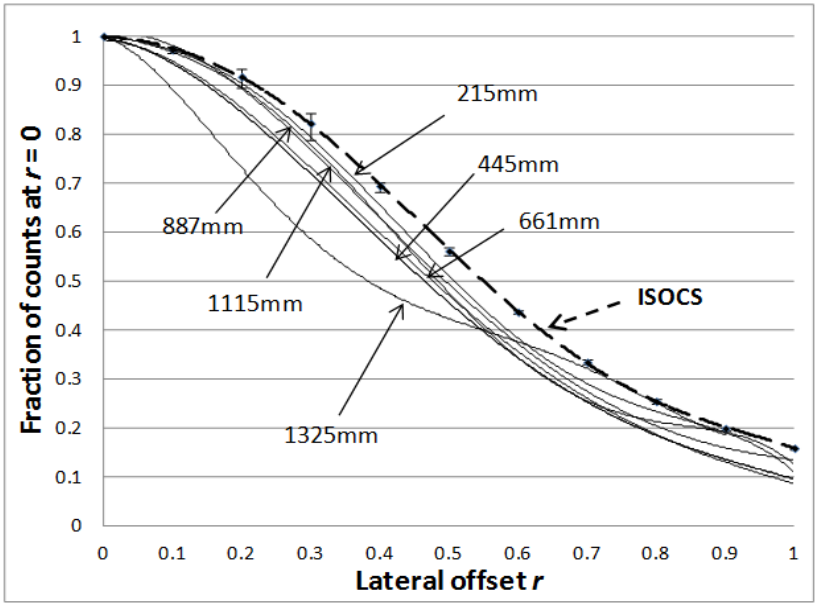

Fig 5.6 Fractional decreases in measured counts with changing lateral offset for the six detector heights used in the field experiments, shown as 5th order polynomial curves. Also shown is the polynomial curve for the mean fractional decrease in ISOCS predicted counts for the same 6 detector heights. Error bars on the ISOCS line represent the total spread between the 6 predictions for the different heights. Data points have been removed from the field-measurement curves for clarity.

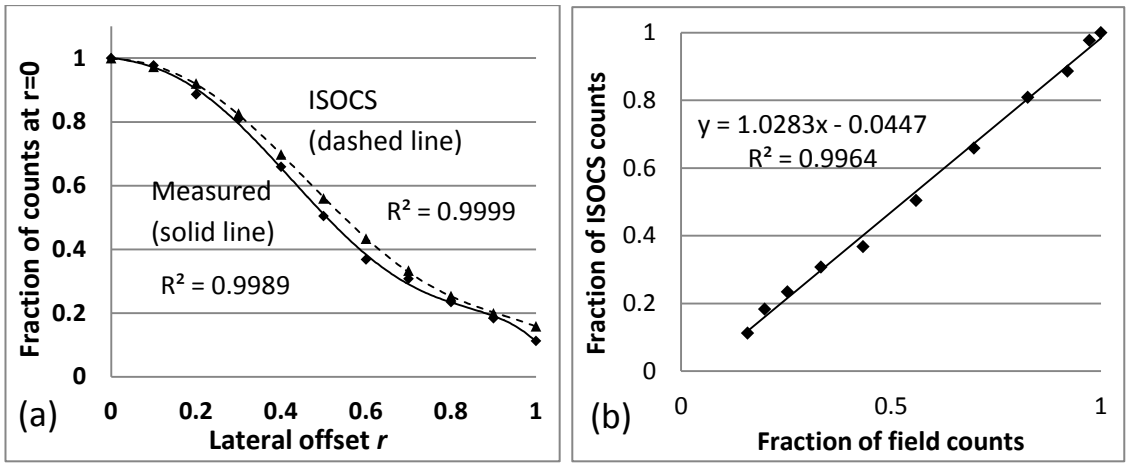

Fig 5.7 (a) Fractional decreases in counts as lateral offset changes from $r = 0$ to $r = 1$, with fitted polynomial functions of the 5th order, for a detector height of 215mm; (b) Regression of the fractional counts calculated from ISOCS against those obtained from field measurements.

5.4.4 Determination of soil attenuation properties

Visual inspection of the soil profile in the experimental area showed that it comprised an organic-rich top layer approximately 100 mm thick, over a sandy subsoil which extended at least as far as the maximum depth (240 mm) achieved in the experiments. The attenuation properties of the 0-100 mm layer can be estimated from the replicated measurements for zero offset at a detector height of ~661 mm (Table 5.1). Using these data, the average counts per second can be calculated for the full range of counting times used. After adjustment for the different detector heights (661 mm for zero depth, 664 + 100 mm for 100 mm depth) the ratio I/I_0 can be calculated (See *Section 5.2.4*) as equal to 0.438354. This can then be converted to a linear attenuation coefficient (μ) :

$$\mu = \frac{-\ln(0.438354)}{10} = 0.08247\ cm^{-1}$$

Replicated measurements at zero offset were not acquired for depths greater than 100 mm, and so single measurements at depths of 100 mm and 240 mm at the detector height of 215 mm have been used for the deeper layer. Using the same method as above results in a value of μ for the 100-240 mm layer of 0.09759 cm^{-1}.

Mass attenuation coefficients for the energy level 662 keV were then estimated at 0.0754 $cm^2\ g^{-1}$ and 0.0788 $cm^2\ g^{-1}$ for the two layers respectively, using definitions of an organic soil type

and a mineral soil type contained in the "Materials Editor" program provided by Canberra Industries Inc. (Canberra, 2009). Using these values for the mass attenuation coefficients, the individual linear attenuation coefficients would be consistent with a dry soil of bulk density 1.0 – 1.2 g cm^{-3}, and 15-30 % saturation. These are thought to be reasonable assumptions for the soil in the experimental area.

5.4.5 Evaluation of the generic model and the ISOCS predictions of measured counts

Evaluation of the generic model was carried out using *Equation 5.7* to predict the expected detector counts for all of the various source/detector geometries specified in Table 5.2. Both of the polynomial functions discussed in *Section 5.4.3* (and shown in Fig 5.7a) were used to calculate the change in counts with increasing values of *r*. Regressions were then performed of these predictions against the measured counts obtained by experiment. These are shown graphically in Fig 5.8. Neither the rotational nor the translational biases are significant at the 95 % confidence interval in either case.

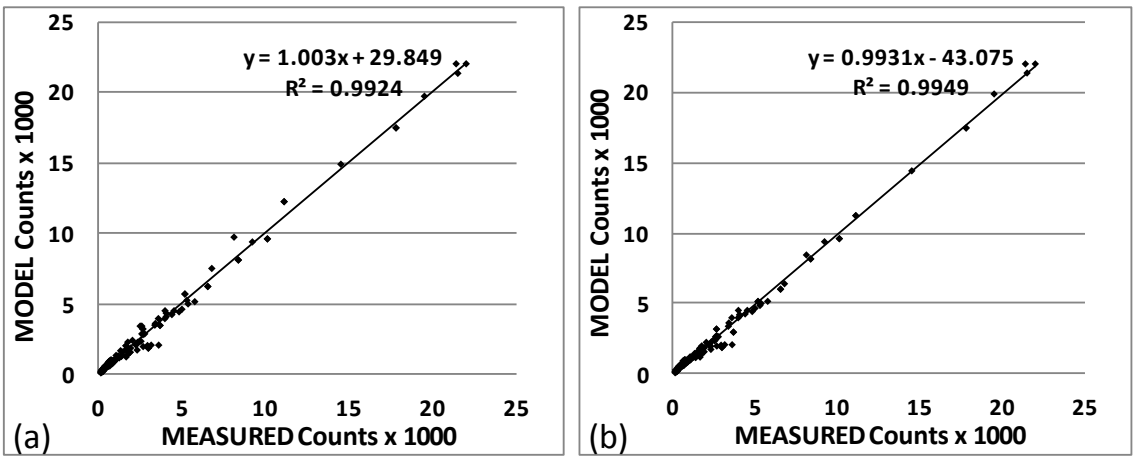

Fig 5.8 Regressions of counts predicted by the generic model against the field measurements for all detector heights, offsets and source depths defined in Table 5.2. In (a), the offset model used to define *f(r)* in equation 5.7 is based on ISOCS predicted counts at the height of 215 mm, while in (b), it is based on the measured counts at this detector height.

Fig 5.9a shows a similar graph for the count predictions made using individual ISOCS geometry definitions, for each of the same source/detector geometries. Again, neither translational nor rotational biases are significant at 95 % confidence. Finally, a comparison of the counts predicted by the generic model with predictions made by the individual ISOCS geometry

definitions is given in Fig 5.9b. The rotational and translational biases are significant in this case, but both are very low (0.5 % and 17 counts respectively).

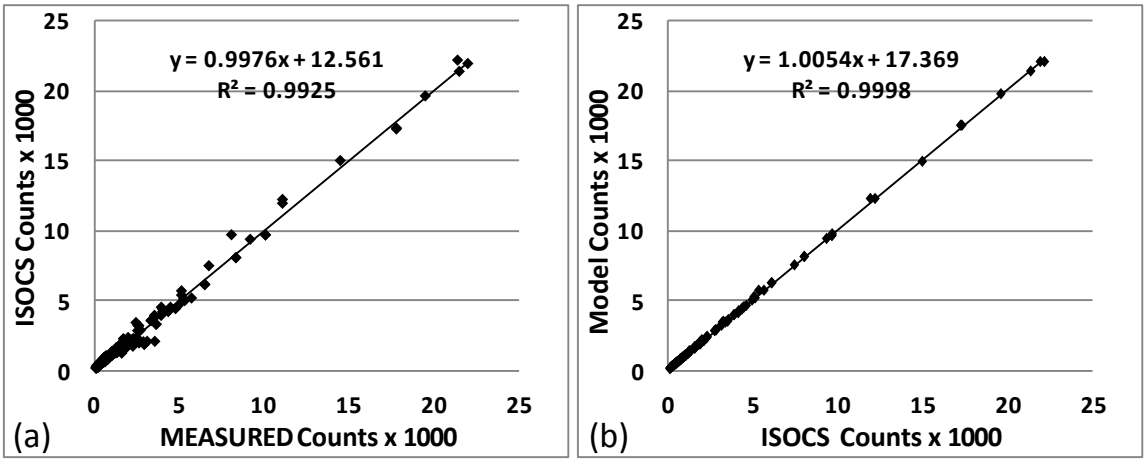

Fig 5.9 (a) Regression of counts predicted by individual ISOCS geometry definitions against the field measurements for all detector heights, offsets and source depths defined in Table 5.2. (b) Regression of counts predicted by the generic model against counts predicted by ISOCS geometry definitions.
(Additional regression graphs are shown in Appendix 3, Figs A3.1 – A3.3).

The regressions shown in Fig 5.8 and Fig 5.9a suggest that both the generic models and the individual ISOCS geometry definitions (after adjustment for measured detector sensitivity) are good predictors of the activity levels recorded by the detector in field experiments. Regressions performed on the data from the individual experiments detailed in Table 5.2 (See Appendix 3, Figs A3.1 – A3.3) do reveal some significant biases. In 12 out of the total of 18 experiments, rotational biases were less than 10 %, for both the generic model and the ISOCS predictions, and in all but one case were less than 23 %. In the single case of increasing lateral offset with a fixed source depth of 150 mm, large rotational biases were found for both methods (-49 % for ISOCS, -45 % for the generic model, see Fig A3.3). The underlying reason for this apparent anomaly is not clear, but occurs as a result of an underestimation of the counts predicted by both the generic model and by ISOCS when compared to the measured values for lateral offset values of 0.0, 0.3 and 0.5. These three measured values are between 1.3 and 1.6 times greater than those predicted by the models. It may be that some local anomaly in the attenuation characteristics of the soil was an influencing factor.

Generally, the results suggest that both the generic model and the adjusted predictions from individual ISOCS geometry definitions give reasonable predictions of the results obtained by

measurement in the field. Some differences between the generic model and experiment would be expected, as the generic model is an approximation only, for the reasons described in *Section 5.2.4.* The integrity of the generic model approach is supported by the comparisons of the counts predicted by this method with those calculated from the efficiencies generated using ISOCS geometry definitions (Fig 5.9b). The small rotational bias of 0.5 % between the generic model and ISOCS may be because the Monte-Carlo method used by ISOCS takes additional factors into account, such as attenuation of radiation by the intervening air space. However, these experiments suggest that the generic model is capable of giving predictions of detector response that are very close to the predictions obtained by individual ISOCS geometry definitions. Differences between counts predicted by ISOCS and counts predicted by the generic model are small compared to the uncertainties that are likely to be encountered in field measurements.

Differences between the predicted counts and experiment will have resulted from a variety of different sources of uncertainty, including uncertainty in the estimation of the soil attenuation properties, and positioning errors during the field experiments. An additional source of error in the experimental counts would have resulted from limitations inherent in the experimental apparatus. The wooden support that was used (Fig 5.2) was designed so as not to obstruct the nominal 90˚ field-of-view of the collimator, however some radiation will also have passed through the collimator walls and the variable thicknesses of lead near the collimator aperture. This component of radiation will have been subject to additional attenuation by the wooden support. Total attenuation by 44 mm of soft wood can be calculated as equivalent to that of less than 1.5 mm of lead, and so this additional source of error is considered to have been insignificant in these experiments. The ISOCS predicted counts were calculated using geometry definitions that were based on a source particle that was defined as a box section of dimensions 5 mm x 5 mm x 0.1 mm. This approximated to the actual dimensions of the source, but a small component of uncertainty will have been introduced by this assumption.

Gilmore (2008) suggests that error levels of up to 10 % have been identified in the laboratory version of ISOCS (LabSOCS). An approximation of the uncertainties in the predicted counts has been made based on this estimate, and also on estimates of the uncertainties in the calibration measurements for both the generic model and the ISOCS predictions. For the ISOCS predictions, this has been estimated as the root sum square of the uncertainties in ISOCS geometry modelling (10 %) plus the standard error (at 95 % confidence) in the calibration (Fig

5.5a). In the case of the generic model, a ratio of counts predicted by ISOCS for different offsets is used, and so the overall uncertainty has been estimated based on the root sum square of two ISOCS models (10 % each) and the estimated uncertainty in ε_0 which has been calculated by applying *Equation 5.8* to the count that was used to estimate this figure. Uncertainties are more likely to affect the relationships between modelled and measured counts at the low range, due to the increased Poisson uncertainty in low counts. For this reason, Fig 5.10 shows the same regressions as Fig 5.8a and Fig 5.9a, with the same slopes and offsets, but only for the data points below the first quartile in the measured values datasets. For clarity, corresponding error bars have been shown for one in four of these data points only. This is sufficient to see that these are an underestimate of the actual uncertainties, which would have included the uncertainties in the experimental geometries and soil attenuation properties previously discussed.

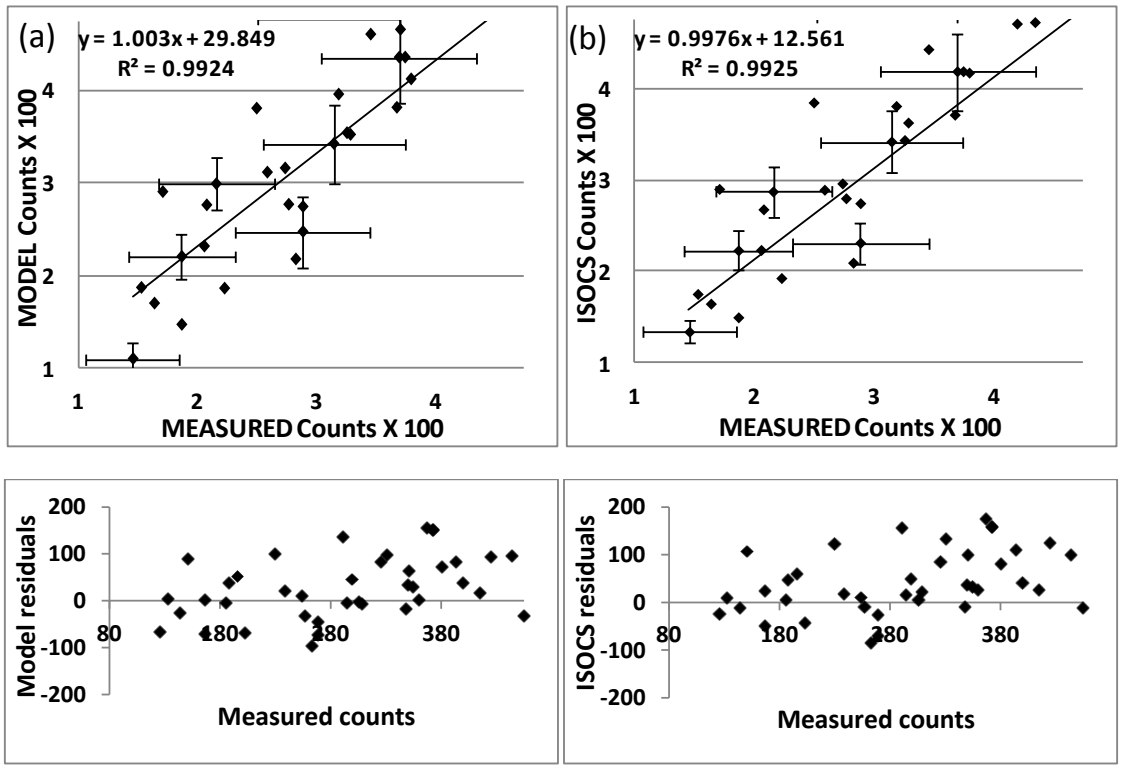

Fig 5.10 The regressions including residual plots for (a) the generic model (using an ISOCS generated offset model as in Fig 5.8a and (b) the ISOCS predicted counts as shown in Fig 5.9a, for field measurements up to the first quartile in the measurement results. Error bars based on estimates of the model errors from the ISOCS calculations and calibrations are shown for 25 % of the data.

The residual plots shown in Fig 5.10 suggest that both the generic model and the ISOCS predictions have a tendency to overestimate detector response at these low count ranges, as is also apparent in Fig 5.8. This could be of importance in the design of optimum survey strategies where detector counts are compared to a fixed action level, as potentially it could result in a reportable particle not being detected. This problem may need to be addressed by applying a safety factor to any design strategy for particle detection.

5.4.6 Optimal source/detector geometry

The maximum lateral offsets beyond which a ^{137}Cs peak was no longer discernible in the spectra during analysis are shown in Table 5.3. These are given for the six detector heights and the three different source depths. As would be expected, these maximum values decrease with increasing detector height, and also with increasing source depth. The data in Table 5.3 can be geometrically converted into inter-measurement distances (i.e. measurement spacings) that will ensure 100 % coverage of the ground surface. The results of these calculations are given in Table 5.4, for a regular square grid survey. The approach used here could easily be adapted for triangular grid surveys, which provide greater coverage for a given number of measurements (USEPA, 2000).

Table 5.3 The maximum lateral offset (r <= 1.0) at which peaks in the spectra were observable and interpretable by Genie 2000 software, using a counting time of 600 seconds.

Source	Detector height (mm)					
depth (mm)	215	445	654	887	1115	1325
0	1.0	1.0	1.0	1.0	0.9	0.8
100	1.0	1.0	0.8	0.6	0.5	0.4
200	1.0	0.5	0.2	0.1	0.1	n/a[a]

[a]No spectrum peak resolved

Table 5.4 Measurement spacings (in millimetres) that ensure 100 % coverage of the ground surface using a regular square grid survey, calculated from the r values in table 5.3. The maximum spacing has been highlighted for each source depth.

Source	Detector height (mm)					
Depth (mm)	215	445	654	887	1115	1325
0	304	629	925	1254	1419	**1499**
100	304	629	740	753	**788**	750
200	304	**315**	185	125	158	n/a

5.5 Conclusions

It has been shown that the response of a non-characterised, “off-the-shelf” detector to a small particle of activity can be reasonably well predicted from individual ISOCS geometry definitions, after a correction has been applied based on a small number of measurements with a calibration source. A more generalised method of prediction uses a single field calibration plus a characterisation of the changing detector response with different lateral offsets of the source from the detector axis. This characterisation needs to be performed at one detector height only, and can either be based on measurements at a low detector height (~0.2-2.5m), or on simulated measurements from ISOCS geometry definitions. Adjustments can then be made to this relationship for other detector heights and source depths, using basic principles of geometry and linear attenuation. This generic approach gives results that are effectively as good as using individual ISOCS geometries. As it can be applied to any source/detector geometry, it has the advantage that it could potentially be used in the development of methods of identifying optimum survey strategies for particle detection.

The effective design of an *in situ* survey for particle detection is not straightforward. In some cases it is more efficient to overlap the coverage area defined by the field-of-view of the detector/collimator combination. Uncertainty in the field measurements also needs to be taken into account when designing optimum strategies. Uncertainties in the measurements obtained in these experiments were estimated empirically by acquiring replicated measurements at different counting times, and were found to be approximately 75 % higher than would be expected from Poisson counting statistics alone. There is some evidence that both ISOCS and the generic model may tend to overestimate detector response at low count ranges, and this should be taken into consideration when designing surveys.

The mathematical generic model described here has been further applied to the design of strategies for optimising the parameters of full coverage *in situ* surveys (Rostron *et al.,* submitted-a). A possible avenue for further study is the potential use of the generic model *Equation 5.7* to estimating particle depth from two or more measurements with an *in situ* detector. Such an approach might be particularly applicable to surveys performed on hard standings (e.g. concrete floor slabs).

5.6 Colour photographs for Chapter 5

Fig 5.11 The experimental setup for the detector response modeling experiments described in Chapter 5 (See *Section 5.3*), showing the collimated Canberra NaI 3" x 3" detector supported at a height of 887 mm. The smaller photograph shows the source carrier (made from a piece of Oasis floral foam) inserted into the carrier pipe which was buried at an angle of 45^{o}, and is just visible at the foot of the ladder on the right of the main photograph.

Fig 5.12 Photograph of the soil profile to a depth of approximately 150 mm, taken approximately 250 mm from the location of the source container pipe in the detector response modeling experiments described in Chapter 5. The soil appeared to comprise an organic-rich top layer approximately 100 mm thick, over a sandy subsoil.

Fig 5.13 Setting up for the detector response modeling experiments (See *Section 5.3*) and Photograph 3. ***Top***: a plumb line was used to position the supporting plank so that the detector would be at the correct offset, measured from the source container pipe, when it was moved into position over the aperture. ***Bottom:*** Prior to each measurement, the supporting plank was leveled in two dimensions. Leveling was maintained for the duration of each measurement by placing wooden spacers underneath the feet of the ladders (visible in the top photograph).

Chapter 6 - Optimization of *in situ* measurement strategies for the characterisation of radioactively contaminated land that includes the presence of small particles.

This chapter comprises the manuscript of a paper that has been submitted for publication in the Journal of Radiological Protection.

6.1 Abstract

High-coverage *in situ* surveys with gamma detectors are the best means of identifying small hotspots of activity, such as radioactive particles, in land areas. Scanning surveys with vehicle-mounted arrays of detectors can produce rapid results, but do not generally satisfy other criteria, such as evaluation of the average mass activity concentration over a defined area. They can also be limited by accessibility issues and the nature of the terrain. The alternative is to use portable gamma-detectors. This type of survey is typically carried out with settings of detector height, measurement spacing and counting time that are based on convenience, rather than being pre-determined in order to meet requirements. This paper introduces the Radioactive Optimised Contaminated Land Investigation (ROCLI) method for setting these parameters at the outset of a survey, using a recently described generic model to estimate the detector counts that would be expected from a particle at different positions relative to the detector. The optimal parameters are identified as those which minimise the measurement costs, with the option to also minimise the potential consequence costs of false positive and false negative results. Example survey designs have been produced for two sites with different background levels for the radionuclide of interest. These demonstrate the advantages of the ROCLI method for designing measurement strategies that minimise overall costs.

6.2 Introduction

6.2.1 Survey design

Characterisation of radioactively contaminated areas is an essential requirement at most stages of the remediation process. It is also used to demonstrate to regulatory authorities that the risk in a particular area is within acceptable limits (IAEA, 1998; IAEA, 1999; Towler *et al.,*

2009). A combination of both *in situ* and *ex situ* methods is often used, where the latter involves acquiring samples that are later analysed in a laboratory. If survey objectives can be satisfied by the detection of gamma-emitting radionuclides, then *in situ* methods are less expensive, and quicker to employ (IAEA, 1998). When possible, therefore, it is advantageous to maximise the use of *in situ* measurements, and to minimise the need to acquire and analyse *ex situ* samples.

The design of a characterisation survey should provide a balance between expected costs, survey objectives, and feasibility. It must also incorporate knowledge of the uncertainty in the measurements (IAEA, 1998). A particular component of radioactive contamination is often found to be the presence of small (<1 mm diameter) particles of activity. Radioactive particles have been associated with many nuclear activities, such as releases into the environment via effluents from civil facilities (Salbu and Lind, 2005). Particles can cause particular problems with characterisation, because their presence significantly increases the heterogeneity of activity in a sampled area. This heterogeneity results in higher levels of measurement uncertainty (IAEA, 2011).

Statistical methods for designing optimal contaminated land surveys, where the objectives are to determine a) the average concentration of activity in defined areas, and b) the extent and location of hotspots of a few metres or more in extent, are well established (USEPA, 2000; Ferguson, 1992). These methods assume that a number of *in situ* or *ex situ* samples will be acquired at discrete locations. There will therefore be spaces between adjacent samples, where no information is collected. If the survey objectives can be satisfied by characterisation of the extent and concentrations of gamma-emitting radionuclides, then it is possible to investigate an entire survey area using gamma detection equipment. This full coverage capability is frequently exploited in wide-area scanning surveys, for example by the Groundhog system (Dennis *et al.,* 2007). Such scanning surveys have the advantages that they are very quick to implement, however they are subject to a number of limitations:

i) The ability to detect small particles of relatively low activity, or higher activity particles at depth, can be limited by short counting times over discrete areas;
ii) The source geometry is hard to characterise, and so they do not give reliable estimates of activity concentrations;
iii) Vehicle mounted systems can be restricted by terrain or limitations of access;

Where any of these limitations apply, an alternative approach is to use portable gamma detection equipment, which can be manually set up at a sequence of points in a systematic survey design. The counting times to be used at each measurement location can be pre-determined in order to satisfy survey objectives. If collimation is used, this enhances the ability to estimate activity concentrations in discrete areas, and also increases the resolution of the characterisation.

The aim of this paper is to investigate methods of optimizing these types of surveys, when full coverage of a land area is required to satisfy survey objectives. The method is based on the worst-case scenario, where the existence of spatially small hotspots (particles) of activity may be missed by *ex situ* sampling, or by lower coverage *in situ* surveys. In this method, the existence of particulate activity is inferred from activity levels that are elevated compared to the average activity over the survey area.

6.2.2 Objectives

1. Devise a method of optimizing *in situ* experimental parameters, where the primary objective is to identify small particles of activity through the use of full coverage surveys.
2. Demonstrate the use of this optimisation method, by applying it to two case study surveys of radioactively contaminated land.

6.2.3 Detector coverage

Interpretation of *in situ* measurements of gamma-emitting radionuclides in contaminated land is simplified if the detector is partially enclosed by a purpose-built collimator. This allows definition of the area covered by each measurement, and also reduces interference from any nearby sources (IAEA, 1998). In order to have high confidence in the ability of a particular measurement strategy to locate small particles, it is necessary to cover 100 % of the ground surface with the collimator's field-of-view (FOV). If the lower face of the collimator is parallel to the ground surface, then it will subtend a circular FOV on the surface. Two types of systematic measurement grid can be used to define the location of each measurement that will ensure 100 % coverage: square grids (Fig 6.1a) and triangular grids (Fig 6.1b). Of these, the triangular grid is the more efficient method of covering the ground surface, while the square grid is easier to calculate and mark out, and so is less prone to operator errors in the field.

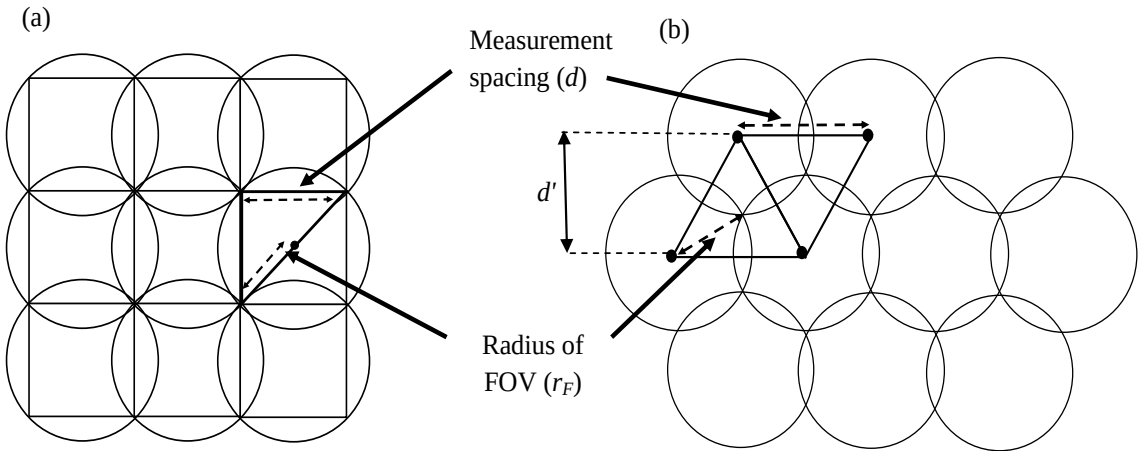

Fig 6.1 Two types of measurement grid that can be employed to yield 100 % coverage of the ground surface by the detector FOV with radius r_F. The measurement spacing of the square grid (a) can be expressed $d = \sqrt{2} \times r_F$, while for the triangular grid (b) $d = \sqrt{3} \times r_F$, and the distance between rows $d' = d \times \sqrt{3}/2$.

The case of a collimated detector at height *h* above the ground surface, subtending a circular FOV of radius r_F, is shown in Fig 6.2.

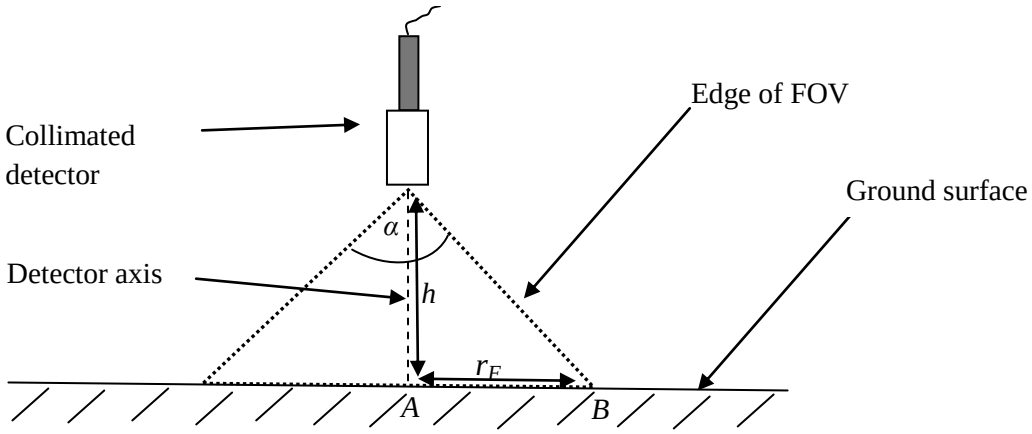

Fig 6.2 For a collimated *in situ* detector, the radius of the FOV subtended at the ground surface (r_F) is related to the height of the detector (*h*) multiplied by the tangent of one half of the collimator angle (tan (α/2)).

From Fig 6.2, for any collimator angle α, r_F can be calculated as:

$$r_F = h \times tan\left(\frac{\alpha}{2}\right)$$

And so for a regular square grid survey (Fig 6.1):

$$d = \sqrt{2} \times h \times tan\left(\frac{\alpha}{2}\right) \quad (6.1)$$

A particle of given activity that is on the ground surface (buried particles are considered in *Section 6.2.5*), at different positions along the radius of the FOV (along line *AB* in Fig 6.2) will yield different count rates within the detector body, due to differences in the geometry of the source and detector. Additionally, as a particle moves towards the periphery of the FOV, the numbers of counts reaching the detector will be reduced because of the increased distance between the source and the detector. The net result is that for a given particle, the activity recorded by the detector drops off fairly rapidly as the particle moves away from the detector axis towards the periphery of the FOV. Longer counting times then become necessary in order to identify the existence of the particle with the same level of confidence.

It is possible to estimate detector efficiency figures for small particles at different radial distances from the centre of the FOV, either through experiment or by using calibration software such as ISOCS (supplied by Canberra Industries Inc). These values can then be used to calculate the number of counts that would be measured by the detector for a particle of given activity, located at different radial positions. The radial position is expressed here as the *lateral offset r* where:

$$r = \frac{Radial\ distance\ of\ particle\ from\ detector\ axis}{Radius\ of\ FOV}$$

It has been found, by modelling and experiment, that for any given value of *r* between *r* = 0.0 and *r* = 1.0, the proportional decrease in efficiency relative to the efficiency at *r* = 0.0 is approximately the same for all detector heights (Rostron *et al.,* submitted-b). This is an approximation that does not take account of attenuation by the intervening air volume, which can be considered negligible when using detectors at heights of a few metres above the ground surface. From *Equation 6.1,* when a regular square grid design (Fig 6.1) is used:

$$d = \sqrt{2} \times h \times tan\left(\frac{\alpha}{2}\right) \times r \quad (6.2)$$

6.2.4 Detector height

Greater detector heights will extend the coverage of each measurement, but this comes at a cost, because the resolution over the survey area is reduced (IAEA, 1998). Increased detector heights also reduce the probability of particle detection above background levels in each measurement. For a given value of *r*, the number of counts received at the detector approximates to an inverse square relationship with increasing detector height (Rostron *et al.,* submitted-b).

6.2.5 Particle depth

When a particle is buried beneath the ground surface, the number of counts that are recorded by the detector changes because of the differences in source/detector geometry, and also because of attenuation by the overlying soil layers (Fig 6.3).

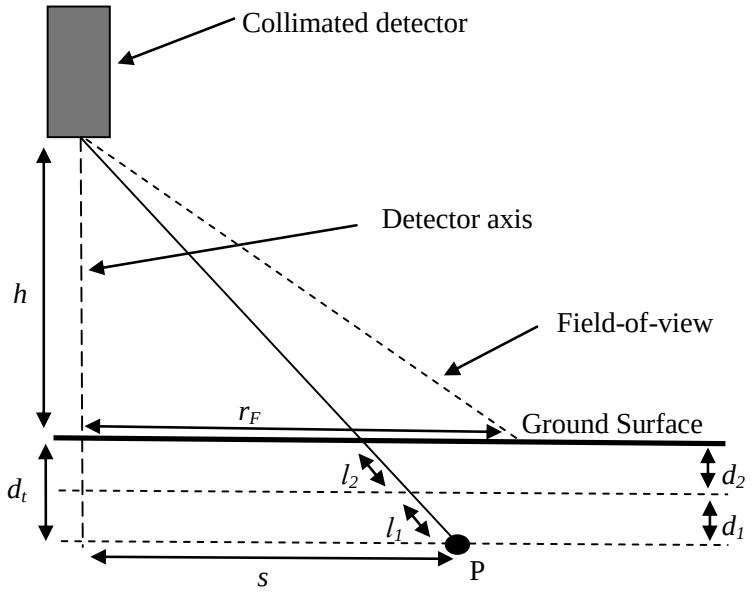

Fig 6.3 The case where a particle *P* is buried at depth d_t beneath the ground surface, at a lateral displacement *s* from the axis of a detector at height *h*. In this case two soil layers with different attenuation properties are represented by the depths d_1 and d_2. The path lengths of radiation through each soil layer are shown as l_1 and l_2 respectively.

The following three adjustments need to be made to obtain an approximation of the counts received by the detector from particle *P* (Fig 6.3):

1. The effective detector height above the particle is increased to $h + d_t$.

2. The lateral offset *r* used to estimate the detection efficiency is adjusted to:

$$r = \frac{sh}{r_F(h + d_t)} \tag{6.3}$$

3. An approximation of the attenuation by the two soil layers can be made by assuming that the collimator aperture and the particle *P* are both small compared with the height of the detector ($h + d_t$).

The gamma photons that travel from the source to the detector can then be assumed to follow a parallel path through the intervening soil layers. From the Beer-Lambert law:

$$\frac{I}{I_0} = e^{\left(-\mu_1 l_1/_{10}\right)} \times e^{\left(-\mu_2 l_2/_{10}\right)} \tag{6.4}$$

Where I/I_0 is a factor representing the proportional attenuation of gamma radiation intensity by the intervening soil layers, the coefficients μ_1 and μ_2 are the linear attenuation coefficients of the two soil layers d_1 and d_2 in units of cm^{-1}, and the path lengths l_1 and l_2 (in mm) are given by:

$$l_i = d_i \sqrt{1 + \left(\frac{s}{h + d_t}\right)^2} \tag{6.5}$$

Using *Equation 6.3* to calculate *r* for a given particle depth, the detection efficiency for a particle at a defined lateral offset from the detector axis can be estimated using the method described in *Section 6.2.3*. This can then be adjusted for detector height (using the inverse square rule) and linear attenuation (*Equations 6.4, 6.5*) in order to estimate the number of counts that would be received by the detector from a particle at any position with respect to the detector.

6.2.6 Estimation of counting time required to identify a small particle

The decision of whether a single measurement indicates the existence of a particle requires interpretation based on a threshold number of counts. This is termed here as the *decision level*

counts D_C, above which a particle will be assumed to exist in the area of ground assessed by that measurement. Two types of measurement error are possible. A *false positive* error occurs when statistical fluctuations in the number of counts from the local site background cause the measurement to exceed D_C, even though no particle is present. A *false negative* error occurs when a particle does exist, but the statistical fluctuations in the summed counts of the background and the particle are such that the measurement is below D_C. These false positive/negative scenarios are illustrated by the shaded areas in the hypothetical distributions shown in Fig 6.4.

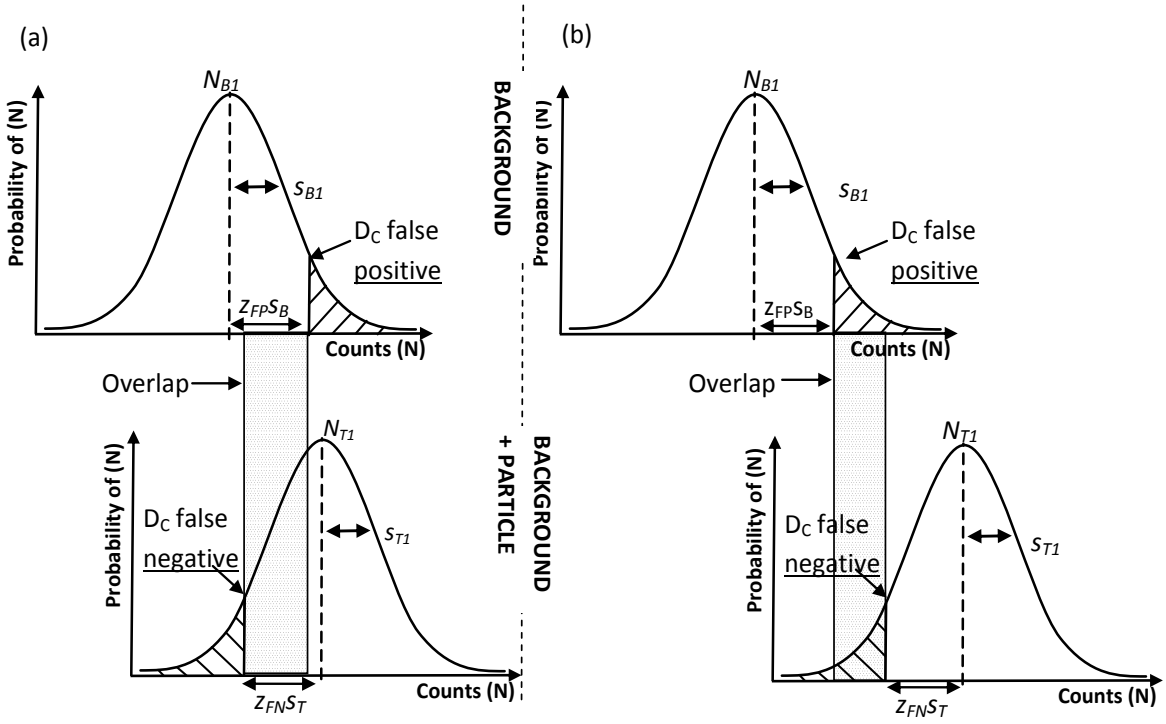

Fig 6.4 Two scenarios where the counting times used in the local site background survey are not optimal. The required probabilities of false positive errors and false negative errors are expressed in both cases as the z-scores z_{FP} and z_{FN} respectively. In (a), the counting time is too low for reliable particle identification, because any chosen setting of the decision level D_C within the region of overlap (shaded area) would result in increased probabilities of false positive measurements and/or false negative measurements. In (b), the counting time is longer than necessary to identify a particle at the required probability settings. Any setting of the decision level in the region of overlap would result in probabilities of false measurements that were lower than required, leading to unnecessary cost.

When the number of counts recorded in a measurement is large enough (e.g. $N > 30$), the count distribution approximates to Gaussian. To be able to compare the local site background distribution with the hypothetical distributions that include the presence of a particle, estimates must be made of the standard deviations of these distributions. It is then possible to

estimate the numbers of counts that would be required to achieve different levels of variance, using estimates of the activity and variance of the local site background counts. These may be obtained either by performing a pilot survey, or alternatively they may be estimated from previous surveys that have been carried out in the local area. In either case, the detector height at which the local site background counts have been estimated, as well as the counting time *(T_1)* that was used in these measurements, must be known. While we can expect the counts received by a detector from a source under ideal conditions to conform to Poisson statistics, other uncertainties are introduced. These uncertainties cause deviations from Poisson statistics, both during single counts, and also between successive counts in the same position. A possible factor causing random uncertainty is drift in the response of the detector or its electronics over time, brought about by variations in the ambient temperature. Other factors may cause additional variance between measurements taken at different times, e.g. variations in soil moisture content. Spectral interpretation (e.g. peak area analysis) is yet another potential source of uncertainty. We can therefore expect there to be components of uncertainty in the detector counts that are separate from, and additional to, the uncertainty of counting statistics alone. If an estimate of background uncertainty can be made, and some assumption is also made about the change in uncertainty with increasing *N*, then it is possible to fully characterise the hypothetical Gaussian distributions of counts that would be obtained if a particle were present on the measured background. The assumption made here is that the variance s^2 of the number of counts is proportional to *N*, i.e. *s* is proportional to $\sqrt{N}$ where *s* = the standard deviation of repeated background measurements. From this it can be shown that the standard deviation of the distribution where a particle exists (s_{T1}) is given by:

$$s_{T1} = \frac{s_{B1} \times \sqrt{N_{T1}}}{\sqrt{N_{B1}}} \tag{6.6}$$

Where N_{B1} and s_{B1} are the number of counts and the standard deviation of the background distribution, and N_{T1} is the predicted total number of counts when a particle exists at a certain location on that background. This number is estimated by adding the predicted counts from the particle (using the methods described in *Sections 6.2.2-6.2.4*) to the original background counts N_{B1}.

Using this method, it is possible to fully characterise the frequency distributions of counts (as measured by the detector) of the local site background activity, and also of the hypothetical

distribution that would occur were a particle to be present (assuming the same detector height). The latter can be repeated for a range of values of *r*, provided detection efficiency figures have been estimated for different *r* values as described in *Section 6.2.3*. It is then possible to establish whether the counting time that was used to obtain the background measurements would be optimal for particle identification, at probability levels that have been expressed here as z-scores. Two sub-optimal scenarios are possible (Fig 6.4). A case where the counting time is too low to reliably identify a particle at probabilities of false results represented by the z-scores z_{FP} and z_{FN}, is shown in Fig 6.4a. An alternative scenario where the counting time is longer than necessary is shown in Fig 6.4b.

An optimal scenario can be considered one in which the decision levels for false positive and false negative measurements, at defined probabilities, occur at the same value of *N*. The concept behind this methodology could be considered analogous to evaluating the counting time that would be required to obtain a given **detection limit** for a particle of given activity and position. **IUPAC** recommends the probabilities of obtaining false positive and false negative measurements to be set to default values of p = 0.05 (JCGM, 2008a). However for the purposes of optimisation, and also in making a case for site clearance, it may be useful to be able to evaluate counting times for other probability values. It also has parallels with the derivation of the Currie equation for evaluating the Minimum Detectable Amount (MDA) of activity that is measurable when monitoring for the presence of radioactive contaminants (Currie, 1999; Knoll, 2000).

The counting time that was used to obtain the measurements of the site background can then be used as a basis to calculate a new counting time T_2 that will result in this optimal scenario. The number of counts recorded by the detector is directly proportional to the counting time, and so the counting time is directly related to the relative increase (or decrease) in counts between the background distribution (counting time T_1) and the optimal distribution (counting time T_2):

$$\frac{T_2}{T_1} = \frac{N_{B2}}{N_{B1}} = \frac{N_{T2}}{N_{T1}} \qquad (6.7)$$

Where N_{B2} and N_{T2} are the background and the total (background + particle) counts at time T_2. As T_1, N_{B1} and N_{T1} are either known or have been estimated, it is only necessary to calculate N_{B2} in order to solve the remaining terms in (6.7).

The decision level (Fig 6.4) for false positive (D_{cfp}) and false negative (D_{cfn}) results can be expressed:

$$D_{cfp} = N_{B2} + (z_{FP} \times s_{B2})$$

and

$$D_{cfn} = N_{T2} - (z_{FN} \times s_{T2}).$$

So for the optimum scenario:

$$[N_{T2} - (z_{FN} \times s_{T2})] - [N_{B2} + (z_{FP} \times s_{B2})] = 0$$

If it is assumed that the variance is directly proportional to N ($s \propto \sqrt{N}$), then:

$$\left[N_{T2} - \left(z_{FN} \times s_{T1} \times \frac{\sqrt{N_{T2}}}{\sqrt{N_{T1}}}\right)\right] - \left[N_{B2} + \left(z_{FP} \times s_{B1} \times \frac{\sqrt{N_{B2}}}{\sqrt{N_{B1}}}\right)\right] = 0$$

Substituting for s_{T1} (6) and simplifying the first term:

$$\left[N_{T2} - \left(z_{FN} \times s_{B1} \times \frac{\sqrt{N_{T2}}}{\sqrt{N_{B1}}}\right)\right] - \left[N_{B2} + \left(z_{FP} \times s_{B1} \times \frac{\sqrt{N_{B2}}}{\sqrt{N_{B1}}}\right)\right] = 0$$

Using (7) to express N_{T2} in terms of N_{B2}:

$$\left[\left(N_{T1} \times \frac{N_{B2}}{N_{B1}}\right) - \left(z_{FN} \times s_{B1} \times \frac{\sqrt{N_{T1} \times \frac{N_{B2}}{N_{B1}}}}{\sqrt{N_{B1}}}\right)\right] - \left[N_{B2} + \left(z_{FP} \times s_{B1} \times \frac{\sqrt{N_{B2}}}{\sqrt{N_{B1}}}\right)\right] = 0$$

This can be solved for N_{B2}:

$$N_{B2} = \left[\frac{\left(\frac{Z_{FN} \times S_{B1} \times \sqrt{N_{T1}}}{N_{B1}}\right) + \left(\frac{Z_{FP} \times S_{B1}}{\sqrt{N_{B1}}}\right)}{\left(\frac{N_{T1}}{N_{B1}} - 1\right)}\right]^2 \quad (6.8)$$

Equation 6.8 can then be solved by substituting the parameters of the local site background distribution (N_{B1} and s_{B1}), an estimate of the total (background + particle) counts (N_{T1}), calculated as described in *Sections 6.2.3 – 6.2.5*, and the required probabilities of false results converted to z-scores (z_{FP} and z_{FN}). The optimal counting time T_2 can then be calculated:

$$T_2 = T_1 \times \frac{N_{B2}}{N_{B1}} \tag{6.9}$$

6.3 Methods

6.3.1 The ROCLI program

A computer program (Radioactive Optimised Contaminated Land Investigation, ROCLI) was written in Excel Visual Basic for Applications, which uses these equations to identify an optimised measurement strategy for small particle detection. This was then applied to background measurements from two areas that were recently surveyed on the Dounreay experimental reactor site in Caithness, Scotland. The first of these areas (Area 1) was on an unused field adjacent to a reactor building that is currently undergoing decommissioning. The second of these (Area 2) was on a small grassed area, which is known to have been subject to low levels of contamination, as a result of aerial deposition from authorised discharges elsewhere on the site. Investigations of the Dounreay site had already identified ^{137}Cs as a major component of the contamination. This radionuclide can be identified by the 662 keV gamma emission associated with its short-lived progeny ^{137m}Ba. A NaI 3" x 3" (76.2 mm x 76.2 mm) scintillation detector was used for the background measurements. This was fitted with 90^{o} lead collimation, and a counting time of 600 seconds was used. The measurements were analysed using Genie 2000 gamma acquisition and analysis software. Hardware and software were supplied by Canberra Industries Inc (Canberra, 2009). The optimisations are intended for regular square grid surveys, but could be adapted for a triangular grid design.

A worst-case scenario is one in which a single particle exists on one of the corners of the coverage square that is defined by the FOV of the detector (Fig 6.5). However, the probability of a randomly positioned particle existing at one of these points is very low. As *r* decreases from 1.0 to ~0.7, this probability rapidly increases. It then decreases more slowly until *r* = 0.0. The probability of detection, however, increases non-linearly throughout the range *r* = 1.0 to *r* = 0.0. The ROCLI program takes the probability of particle existence into account by splitting

the FOV of the detector into 100 concentric 'probability bands', defined by equal values of r (r = 0.0 - 0.01, r = 0.01 - 0.02 ….. r = 0.99 - 1.0). For any given counting time, it calculates the probability of missing a particle (termed p_{fn}, the probability of a false negative error) in each band from the predicted detection efficiency of a particle in the band at the defined depth (assuming that variance is proportional to N). A conservative approach has been applied by using the predicted detection efficiency for a particle at the outer edge of each band. This value for p_{fn} is then multiplied by the probability of a single randomly positioned particle existing within the probability band. The sum of these products is an estimate of the probability that a single particle that is randomly positioned within the coverage square will be missed. The program then uses an iterative method to converge on the required value of p_{fn} for the entire coverage square, to the nearest 100th of a percent.

Sections 6.3.2 – 6.3.4 explain the inputs to the ROCLI optimisation program that are required, and include details of the specific inputs that were used for these example sites.

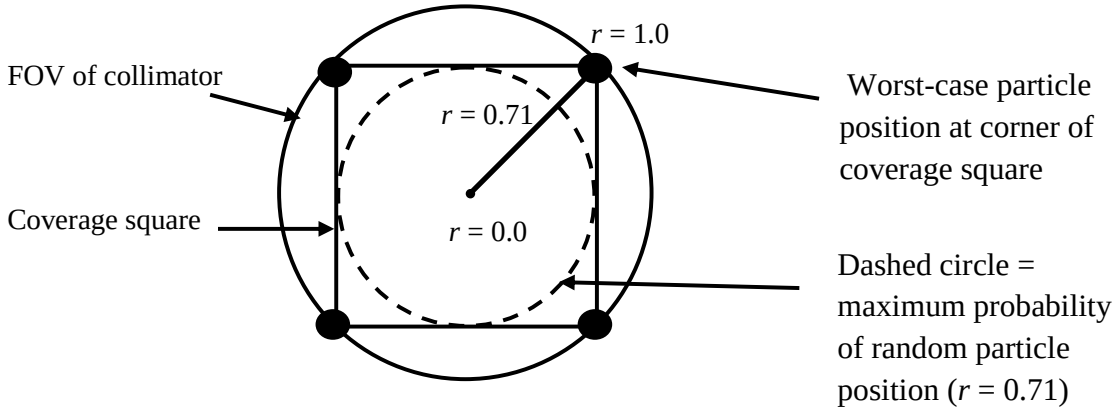

Fig 6.5 Showing the coverage square for a single measurement in a full coverage survey that uses a regular square grid sampling pattern. The four corners of the square represent the "worst-case" particle positions for detection.

6.3.2 Site background

For each optimisation, an estimate of the background distribution must be entered as a number of counts (N_{B1}) and its standard deviation (s_{B1}). These were evaluated by using the *duplicate method* for estimating the random component of measurement uncertainty in a sampling process (Ramsey and Ellison, 2007; IAEA, 2004). This method uses robust statistics to provide estimates of uncertainties in individual measurements, which are subsequently used in

the process of site characterisation. Sampling and analytical duplicates were acquired for this purpose from eight random locations in each area. The analysis also provides an estimate of the robust mean and standard deviation of the activity levels across these eight locations. This was considered to be representative of the distributions of the general background levels.

The 662 keV energy level associated with the decay of ^{137}Cs was present in all of the spectra in Area 2. The area of each peak in the duplicated measurements was calculated using proprietary Genie 2000 software (Canberra, 2009), and these results used to calculate the background mean and standard deviation. However, no peaks at this energy level were evident in the spectra for Area 1. When this is the case, the background distribution must be evaluated as the mean and standard deviation of the total counts within a spectrum window. The window was defined as a channel range corresponding to the energy levels 580-725 keV, following an initial detector calibration that used a source of ^{137}Cs. These two methods of background evaluation require different interpretation in the final optimisation, which is explained later.

The detector height and counting time that was used in the background estimation must also be entered. A summary of the background inputs to the optimisation program used in the examples is shown in Table 6.1.

Table 6.1 Background parameters used in the optimisation examples.

	Detector Height (mm)	Detector count evaluation method	Mean (counts)	Standard deviation (counts)
Area 1	280	Window	2006	90
Area 2	920	Peak	365	78

The ROCLI program also incorporates a background correction for different detector heights. For these examples, this was achieved by modelling the change in background counts that occurs as detector height changes, using ISOCS geometry modelling software.

6.3.3 Detection efficiencies

The detection efficiencies for a small particle at various lateral offsets from the axis of the detector need to be entered. These are used to estimate frequency distributions of counts that would be expected when the hypothetical counts from a particle are added to the background counts. These efficiencies were evaluated using ISOCS, but they could alternatively be

calculated from experimental results. This process need only be performed at one specified detector height for a particular detector /collimator configuration. It would also be possible to apply a correction based on experimental measurements of a calibration source, using a defined source/detector geometry. This was not carried out in these experiments, because it is not necessary in order to demonstrate the general method. The program prompts the user to enter coefficients of a polynomial function (up to 5th order) which are generated using standard Excel functions. Efficiencies should be entered for $r = 0.0$ and $r = 1.0$ in order that these extreme values of r are included in the function, and for sufficient intermediate values between $r = 0.0$ and $r = 1.0$ that the fitted polynomial is a good fit to the data points. This has been easily achieved with example efficiencies generated using ISOCS. The efficiencies used in the following examples were generated for 10 values of r from 0.1 to 1.0 in equal intervals of $r = 0.1$. A simple inverted "S" curve was fitted with a reported correlation coefficient of $r^2 = 0.99997$.

6.3.4 Standard inputs

Standard inputs to the optimisation program are shown in Table 6.2. Costs have been estimated from previous surveys at the Dounreay site. The target particle activity level was chosen because it is the minimum activity considered to be "relevant" by the Dounreay Particles Advisory Group (DPAG, 2006).

Table 6.2 Standard input parameters to the ROCLI program for the example optimisations.

Parameter	Value used in the example optimisations
Target particle activity	10^5 Bq
Particle depths to optimise	0 mm and 100 mm
Soil attenuation coeff.	0.126131 cm^{-1} at 662 keV
Range of possible detector heights	250 mm, 500 mm, 750 mm, 1000 mm, 1250 mm
Setup time between measurements	2 minutes
Site area	100m^2
Cost per site, e.g. mobilisation, management and reporting	£600
Cost per measurement, e.g. cost of spectrum analysis	£2.00
Cost per acquisition minute, including setup time	£0.50

6.3.5 Optimisation method

The optimised scenario identified by the program is the one which would result in the minimum cost. The first method used is to minimise the total measurement cost, calculated at

fixed probabilities of false positive and false negative errors per measurement. In these examples, the probability of a false positive result has been set to p_{fp} = 0.05, and the probability of a false negative to p_{fn} = 0.01.

An alternative optimisation is obtained by minimising the *expectation of (financial) loss*. This is based on a method that has been proposed for evaluating the fitness-for-purpose of measurements in contaminated land investigations (Boon *et al.,* 2007, Ramsey *et al.,* 2002, Thompson and Fearn 1996). The total expectation of financial loss (E_L) is defined where:

$$E_L = (Measurement\ cost) + (Probabilistic\ cost\ of\ false\ positive\ errors) + (Probabilistic\ cost\ of\ false\ negative\ errors)$$

The optimisation program permits entry of a range of the probabilities of each of the two error types, and the estimated costs that would be incurred in the event of these errors. The probabilistic costs of false positives (C_{fp}) and false negatives (C_{fn}) are calculated where N = the number of measurements:

$$C_{fp} = (Cost\ of\ false\ positive\ per\ unit\ area) \times (area\ covered\ per\ measurement) \times p_{fn} \times N \quad (6.10)$$

$$C_{fn} = (Cost\ of\ false\ negative\ per\ site) \times \left[1 - \left(1 - p_{fn}\right)^N\right] \quad (6.11)$$

C_{fn} and C_{fp} are added to the measurement costs to yield a total expectation of financial loss for each scenario. This method requires ranges of the probabilities of false positive and false negative errors to be entered into the optimisation program. The ranges used, and the associated costs of each error type, are shown in Table 6.3. The cost of a false positive error is expressed per square metre of land area, and is intended to represent an estimate of the cost for an operative to conduct a follow up survey to verify that no contamination exists. The cost of a false negative error makes the conservative assumption that a single particle will exist at every measurement location, and calculates the probabilistic cost based on the probability that one of these particles will be missed in the entire survey area. The cost value that has been used here (£50,000) is only intended to illustrate the use of the ROCLI method, and is an estimate of the cost that would be incurred if a subsequent verification survey located a particle which had previously been missed, and this resulted in an unplanned particle recovery.

It therefore makes the implicit assumption that such a follow-up survey will take place. These examples are intended to show that the ROCLI tool provides a way to consider the implications of the costs of possible consequences, which might be estimated very differently in other circumstances.

Table 6.3 Error probability ranges and error costs used in optimisation by expectation of loss.

Parameter	Value used in the example optimisations
Probability of false positive error	0.01 - 0.1, in steps of + 0.01
Probability of false negative error	$1.0E^{-6}$ - 0.1, in increasing factors of 10
Cost of false positive error (£)	£15.00 / m^2
Cost of false negative error (£)	£50,000 / site

6.4 Results and discussion

The optimised parameters for hypothetical characterisation surveys in the two background areas are shown in Table 6.4. The cost values in bold text are the values that have been minimised in each optimisation method, i.e. measurement cost or expectation of loss. The values given for the decision level D_C in Table 6.4 are the threshold numbers of counts at which a particle should be considered to exist, and further investigation would be required at those measurement locations. During analysis of the spectra acquired during the characterisation surveys, the measured counts for comparison with the decision levels must be extracted in the same way as the background counts were extracted for entry into the optimisation program. So for Area 1, these values must be the total counts in the 580-725 keV spectrum window (See *Section 6.3.2*). The Area 2 counts, however, must be obtained from the net peak area of the peak centred in the 662 keV region. In the latter case, if it were found that some measurements did not show a peak at the relevant energy level, then it would be reasonable to assume that no particle was present at these locations. An alternative optimisation of *window counts* for Area 2 at zero particle depth (not shown), resulted in an increase in measurement time of 17 %, and a 12 % increase in measurement cost for the minimum measurement cost optimisation.

Table 6.4 Optimised survey parameters for hypothetical 100m^2 surveys in the two areas.

Area 1	***Optimisation method 1*** ***Min measurement cost***		***Optimisation method 2*** ***Min expectation of loss***	
	Particle Depth		*Particle Depth*	
	0 mm	*100 mm*	*0 mm*	*100 mm*
Probability (False positive)	0.05[a]	0.05[a]	0.02	0.1
Probability (False negative)	0.01[a]	0.01[a]	10^{-5}	10^{-5}
Detector height *h* (mm)	1250	750	1250	750
Measurement spacing *d* (mm)	1768	849	1414	743
Counting time (seconds)	273	303	533	605
Decision level **(window counts)**	1038	1104	2004	2114
Number of measurements *N*	32	156	50	181
Total time (hours)	3.5	16.3	9.1	36.6
Est. measurement cost (£)	**769**	**1367**	972	2060
Expectation of loss (£)	14595	39061	**1027**	**2300**

Area 2	***Optimisation method 1*** ***Min measurement cost***		***Optimisation method 2*** ***Min expectation of loss***	
	Particle Depth		*Particle Depth*	
	0 mm	*100 mm*	*0 mm*	*100 mm*
Probability (False positive)	0.05[a]	0.05[a]	.02	0.1
Probability (False negative)	0.01[a]	0.01[a]	10^{-5}	10^{-5}
Detector height *h* (mm)	1250	500	1250	750
Measurement spacing *d* (mm)	1591	707	1414	742
Counting time (seconds)	207	185	636	732
Decision level **(peak counts)**	205	181	562	550
Number of measurements *N*	40	200	50	181
Total time (hours)	3.6	17	10.5	43
Est. measurement cost (£)	**787**	**1509**	1015	2251
Expectation of loss (£)	17247	44885	**1070**	**2492**

[a]Probabilities are pre-defined in minimum measurement cost optimisation

For optimisation method 1 (minimum measurement cost), total survey times increase by a factor of five when the particle depth is increased from 0 mm to 100 mm (Table 6.4). The corresponding two-fold increase in measurement costs is dependent on the estimated unit costs (Table 6.2) and would clearly be different for other operators. When potential consequence costs are taken into account (optimisation method 2), then the total expectation of loss decreases by ~93-94 % in all cases. This comes with an increase in both measurement cost and the total survey time, but suggests that in all cases it would be advantageous to reduce the probability of obtaining a false negative measurement from $p_{fn} = 10^{-2}$ to $p_{fn} = 10^{-5}$. This is a reflection of the relatively high consequence cost of a false negative occurring (£50,000). The probability of obtaining a false positive when the maximum particle depth is 100 mm has increased to $p_{fp} = 0.1$, due to the low consequence cost of this error type (£15.00 m^{-2}). In this case, it would be likely to result in approximately 18 false positive measurements

during the course of the survey, which would need to be further investigated by repeat measurements or (e.g.) ground level scanning. Operators may wish to increase this cost or set a lower limit on the maximum value for p_{fp}. The long survey times calculated for buried particles, up to 43 hours for 100 mm depth and optimisation method 2 (Table 6.4) may not be practical to implement, and if performed in areas where the existence of higher activity particles is expected then implications to human health might need to be considered. For example, preliminary scanning surveys could be employed to evaluate the overall risks to field workers.

For comparison, a survey that used a non-optimal scenario, with a fixed counting time of 30 seconds and a detector height of ~1m, produced an estimated p_{fn} of 0.7 in the outer band when tested using the same parameters for a 10^5 Bq particle at 0 mm depth. This would result in a total expectation of loss in excess of £50,000 using the method as applied in these examples.

The price to be paid for optimising the survey design is a substantial increase in both the measurement cost and the total survey time, especially for buried particles. These factors could be significantly reduced by using more than one detector. Where counting times exceed a few minutes, it is possible for a single person to operate two detectors simultaneously. This can be achieved by recording the measurements from one detector, then re-positioning it and staring a new measurement, during the time that the other detector is in acquisition mode. This approach not only halves the recording time, but also effectively eliminates setup times. It may result in substantial long-term cost savings, especially in the case of relatively inexpensive NaI scintillation detectors.

Estimation of the cost of a false negative error is a complex issue, and is potentially controversial. If it were used to aid the design of a final-status survey, then setting a price for missed contamination encompasses ethical, as well as legislative and financial concerns. One approach would be to set the false negative cost at a sufficiently high level that would ensure that there is a very low probability of a false negative occurring. However, this approach could be more transparently addressed by fixing the probability of a false negative at a required level (e.g. 10^{-6}) and optimising the false positive cost only.

The ROCLI method depends on an assumption that there is a linear increase in detector counts with increasing activity levels of the background and the particle. It therefore ignores the effects of coincidence summing. However, it is unlikely that true coincidence summing would have a significant impact on measurements on radioactively contaminated land, because of the relatively large distances between the source and detector (e.g. at least 0.25m). It is expected that the minimum particle activity levels that would normally be specified in the optimisation would be sufficiently low that there would also be negligible errors due to random summing.

The optimisations described have been based on a range of discrete detector heights (Table 6.2). The program calculates a counting time for each combination of height and lateral offset. It is often found that the optimum value of the lateral offset *r* is less than 1.0 (where *r* = 1.0 represents the full field-of-view of the collimator). This implies there is an advantage to overlapping the contiguous square areas that are defined by the size of the field-of-view (Fig 6.1). Using the optimisation program to set progressively finer variations in the detector height ranges suggests that a height can be found at which there is no significant advantage to using values of *r* that are less than 1.0, for a particle at 0 mm depth. If an adjustable detector mount (e.g. an adjustable tripod) with continuously variable detector heights were used, then it is likely that an optimum strategy could always be found for this detector/collimator combination with *r* set to 1.0. This observation may not apply to different detectors and/or collimators.

The optimisations are based on probabilities of particle detection by single measurements. However, it is necessary to overlap the circular FOV of the detector in adjacent measurements in order to achieve full coverage (Fig 6.1). The overall probabilities of detection in a survey are therefore increased somewhat, as a particle that is missed near the edge of the coverage square (Fig 6.1) may be picked up by the overlap from an adjacent measurement. Finally, it should be stated that the intention of this paper is to introduce a method that can assist in the design of an optimal strategy for high-coverage *in situ* surveys. Of necessity, this depends on the definition of a threshold decision level (D_C) above which the presence of a particle is indicated. Interpretation of the results of such a survey also requires consideration of the spatial patterns of results from contiguous measurements, whether this is carried out by judgment or through the use of statistical methods.

6.5 Conclusions

Remote detection of gamma-emitting radionuclides *in situ* has the advantage that full areal coverage is possible, so this technique is more suitable than *ex situ* methods for the purpose of locating small (<1 mm) hotspots, or particles, of activity. Individual measurements are also substantially less expensive than laboratory analysis of soil samples, and the results can be available almost immediately.

The parameters of an *in situ* survey can be considered to be the detector height, measurement spacing and counting time. It is possible to use quantitative methods to optimise these parameters at the outset of a survey in which the reliable identification of small particles of activity is a priority. This approach has advantages over the use of standardised settings, which are often based on convenience (IAEA, 1998). Using a quantitative methodology that is based on the statistical probabilities of obtaining false results is likely to be advantageous financially. It also enables increased confidence in the ability of *in situ* methods to demonstrate that fit-for-purpose measurements have been used as a basis to satisfy regulatory and site requirements.

Chapter 7 – Defining the test volume, and estimating the systematic component of uncertainty in *in situ* measurements.

7.1 Introduction to Chapter 7

In order to be able to apply the results of *in situ* field measurements to the reliable characterisation of radioactively contaminated land, it is necessary to be able to estimate the spatial characteristics of the volume of soil (test volume) from which radiation is received. It is also desirable to be able to compare estimated activity concentrations with a certificated reference source CRM), in order to provide an estimate of the systematic component of the uncertainty and traceability to that source.

This chapter is composed of three sections, each of which is written in the form of a scientific article. The first of these (*Section 7.2*) describes desk experiments that were performed to estimate the physical dimensions of the test volume that was measured in the field experiments described in Chapter 4. *Section 7.3* details an additional field experiment that was performed to test the ability of an *in situ* detector to perform a high-resolution survey of a localised area, when that detector was positioned close to the ground surface. The final section (*Section 7.4*) reports on an approach to estimate the systematic component of uncertainty of *in situ* measurements in land areas, by comparison with laboratory measurements that were calibrated against a nationally traceable reference source.

7.2 Evaluating mass activity concentrations in land areas using portable *in situ* detectors

7.2.1 Evaluating mass activity concentrations: Introduction

A particular issue that affects *in situ* measurements of land areas by gamma spectroscopy is uncertainty in the geometry (and hence the mass) of the primary sample (see *Section 2.3.1*). This is because photons that impart part or all of their energy into the detector volume are counted at the imparted energy level, regardless of their point of emission.

When a source of discrete dimensions (e.g. a 40 gallon drum) is measured, then the average activity concentration of the source can be evaluated accurately, at least in theory. An initial evaluation of the background radiation is made with the source absent, and then a further measurement made with the drum positioned close to the detector. Subtracting the former from the latter gives the balance of detector activity that is due to the proximity of the drum. The use of a calibration program such as ISOCS then enables an average activity concentration to be calculated, providing an accurate model of the type and density of materials comprising the drum and its contents is defined, and its position and orientation with respect to the detector. The former is important because a source the size of a 40 gallon drum will be subject to significant internal attenuation. This is taken into account by the ISOCS Monte-Carlo methodology.

In measurements of contaminated land, however, the dimensions of the source are not discretely definable. Assuming that the energy levels of the radionuclide(s) of interest only emanate from the land and surrounding structures, then a theoretical volume of emission comprises the entire Earth and structures (a theoretical 3-dimensional source in which all dimensions greatly exceed those of the extent of the test volume for practical purposes is sometimes termed an 'infinite source'). A practical upper limit is set by the inverse-square law and the path length of gamma radiation through air. This can be assumed to have an approximate upper limit of ~100m for gamma radiation emanating from ground contamination. In this case, a background measurement as described above cannot be carried out.

The nominal FOV of the collimated detector used in the field work defines a conical section of soil. The diameters of the upper and lower boundaries of this section depend on the height of the detector above the ground surface. Assuming a soil density of 1.6 g cm^{-3}, the total soil mass to 200 mm depth that would be defined by the nominal FOV can be calculated as 40 kg for Zone 12 (detector height = 280 mm), and 269 kg for Barrier 31 (detector height = 920 mm). However, desk experiments with ISOCS models of the detector and collimator that were used in the field experiments (Fig 7.1) revealed that a significant amount of radiation was being received from outside the FOV of the 20 mm lead collimator. There are, broadly, two different effects here, illustrated in Fig 7.1. First, there is a 'grey area' around the edges of the nominal FOV, because of differential path lengths that radiation can take through variable thicknesses of lead. In this case the thickness of lead ranged between 0 mm and 25 mm, the latter being the thickness of the base of the collimator. This results in what are often called 'edge effects',

because the edge of the FOV of the collimator is not clearly defined. A second effect is that a small proportion of radiation emanating from greater distances and impacting the sidewalls of the collimator will pass through the side walls and into the detector volume. Based on a density value for lead of 11.35 g cm^{-3}, and a mass attenuation coefficient of 0.10432 cm^2 g^{-1} (Canberra, 2009b) for radiation with an energy level of 662 keV, it can be calculated that approximately 9.3 % of incident radiation normal to the external surface will pass through a 20 mm lead wall. With the detector at a height of 1m, the diameter of the FOV subtended at the ground surface by a 90° collimator should be 2m, equating to a ground area of 3.1 m^2. However, the total radiation arriving at the walls of the collimator emanates from a very much larger surface area that this. Assuming an upper limit of transmission through air of 100 m, this is potentially equal to an area of nearly 8000 m^2. So although any radiation that passes through the 20 mm sidewall of the collimator will be attenuated to less than 10 % of the intensity with which it intercepted the wall surface, this component of the detector response emanates from a much larger area than is defined by the nominal FOV. A published study that used a more effective 90° collimator with 44 mm lead sidewalls found that 22-27 % of the instrument response came from beyond the nominal FOV (Kalb *et al.*, 2000). It is therefore important to have an understanding of the area of ground that is 'seen' by a collimated detector during *in situ* measurements on land areas. In order to be able to express activity levels as mass activity concentrations, it is also important to have an estimate of the maximum depth in the soil from which radiation is likely to contribute to the detector response.

7.2.2 Evaluating mass activity concentrations: Objectives

1. Establish the minimum source dimensions from which at least 95 % of the detector response is received by a 3" x 3" NaI scintillation detector fitted with 90° 20 mm lead collimation (as used in these experiments).

2. Compare these dimensions with the dimensions of the ISOCS geometry definition that was used to represent the primary sample dimensions in the field experiments described in Chapters 4 – 6 and *Sections 7.3 - 7.4.*

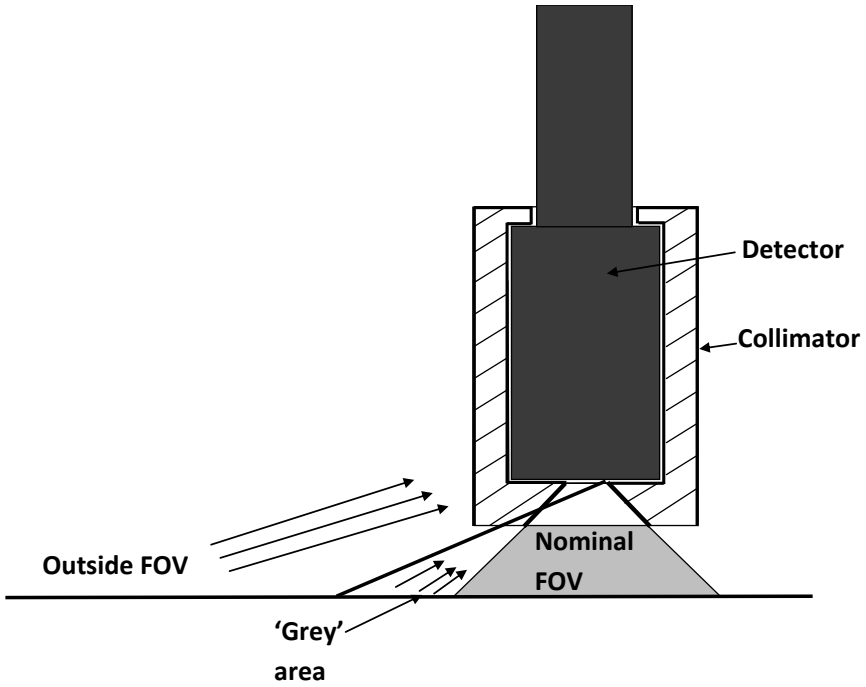

Fig 7.1 Showing possible paths that radiation from surrounding land areas (or other external sources) can take through the walls of the collimator. In the 'grey area', the path length through the lead walls is less than the 20 mm wall thickness.

7.2.3 Evaluating mass activity concentrations: Methods

The field experiments described in Chapter 4 used a NaI 3"x 3" detector enclosed in a 90° 20 mm lead collimator. ISOCS geometry definition models for a range of source diameters (2 m – 100 m) and soil depths (0.1 m - 1.0 m) were created. The standard ISOCS 'circular plane' model was used to represent the ground area, with the plane at 90° to the axis of the detector. The detector height was set to the 920 mm height used in the Barrier 31 survey. Genie-2000 Gamma Acquisition and Analysis software was then used to calculate **massimetric** detection efficiencies for each geometry model, at an energy level of 662 keV. This energy level was chosen as it can be used to identify ^{137}Cs, which was the target radionuclide in the field experiments. The results of these desk experiments are shown graphically in Fig 7.2.

7.2.4 Evaluating mass activity concentrations: Results and discussion

It can be seen from Fig 7.2 that approximately 95 % of the detector response results from radiation that emanates from a source diameter of 22.5 m, and approximately 95 % of the detector response is due to radiation from the top 0.18 m of soil.

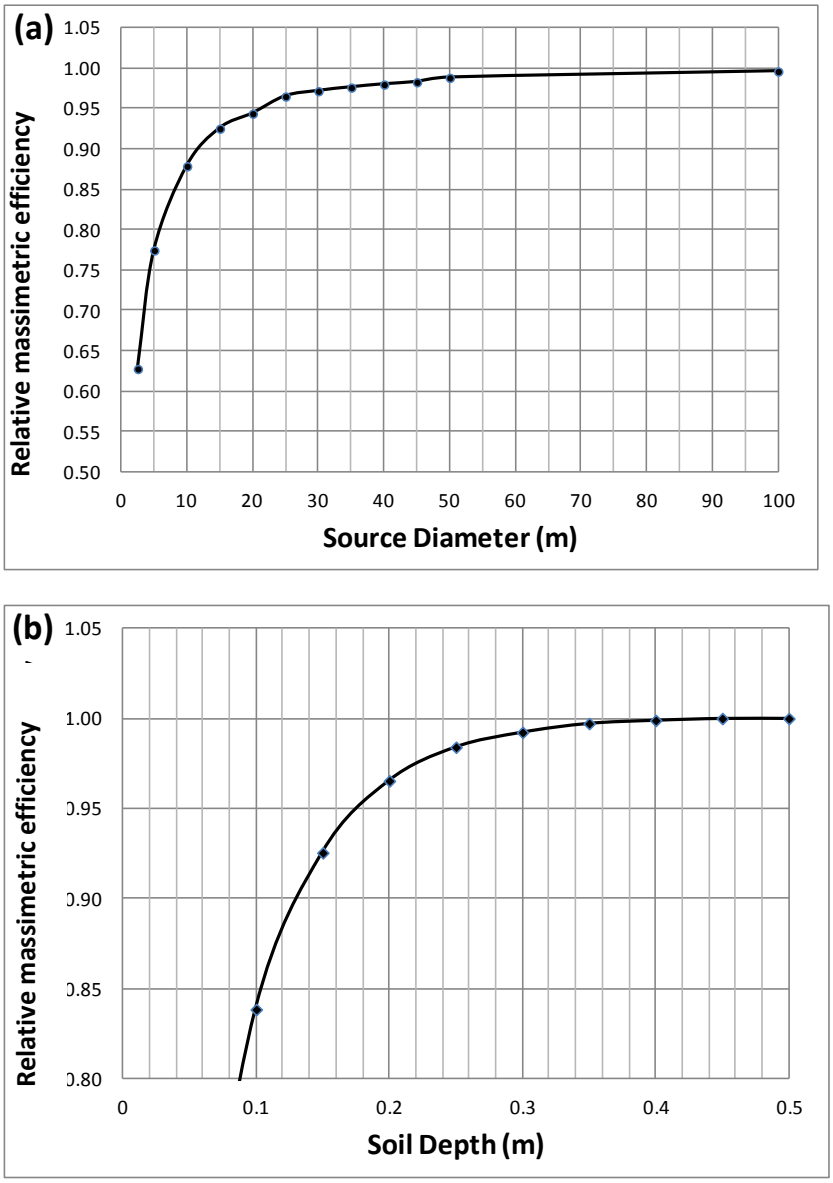

Fig 7.2 Relative massimetric efficiencies calculated using ISOCS circular plane models with a soil density of 1.6 g cm-3, detector height of 920 mm, and an energy level of 661 keV, plotted against (a) Increasing source diameter for a fixed depth of 0.5 m; (b) Increasing soil depth for a fixed source diameter of 25m. The relative massimetric detection efficiencies are expressed in each case as proportions of the absolute efficiency at the assumed maximum source diameter (a) and at the maximum soil depth (b).

In order to convert mass raw activity counts to estimates of activity concentrations, it is important to understand the approximate dimensions of the ground area that is being measured by an *in situ* detector. If it is assumed that a relatively homogeneous distribution of radionuclides is present within that area, then underestimation of the source dimensions would produce results that were positively biased.

The geometry model used to convert measured activities to mass activity concentrations in the field experiments was defined as a circular plane of 25m diameter and 200 mm thickness. It can be seen from Fig 7.2 that if a homogeneous distribution of radionuclides exists over the land area and surroundings then approximately 3 % of the detector response would be expected to arise from areas of ground beyond the 25 m model, and a further 3 % from beneath the 200 mm soil depth. The actual soil depth obtained in these surveys ranged from 150 -200 mm, with an average of 168 mm. No attempt was made to investigate the soil depth at the 6 % of measurement locations where the full 200 mm depth was achieved. Soil extraction beyond the depths obtained at the majority of the locations was prevented by a stony layer. It is not known whether concentrations of ^{137}Cs extended into this layer. The limitations of the geometry model dimensions chosen to interpret these measurements may cause an additional component of uncertainty in some of the measurements in both the Zone 12 and the Barrier 31 surveys.

A highly active hotspot in the ground (or an external source such as described in *Section 4.5.4*), that is located outside of the test volume that is defined by the dimensions of the geometry model used in the interpretation, will potentially have some impact on the measurement results. In this case, a higher mass activity concentration than actually exists within the defined test volume would be reported. This emphasises the need for careful consideration of all measurements in a survey for the purposes of spatial mapping. If such a source exists then it will affect more than one measurement in a systematic survey, unless the measurement spacing is much larger than the diameter of the primary sample. Careful study of the pattern of elevated measurements would then prompt further investigation to establish the reason for the pattern of raised activity levels seen.

7.2.5 Evaluating mass activity concentrations: Conclusions

1. Approximately 95 % of the detector response of the NaI 3”x3” detector and 90° collimator used in these experiments is due to radiation emanating from a source diameter of 22.5 m. Given a source diameter of 25 m, approximately 95 % of the detector response is due to radiation from the top 0.18 m of soil.

2. The ISOCS geometry models used to represent the dimensions of the primary sample in the *in situ* field experiments were constructed assuming a circular ground area of 25 m diameter and 0.2 m depth. If a very large soil volume with homogeneous levels of contamination were assumed, approximately 3 % of the detector response would be expected to arise from a

diameter greater than 25 m, and a further 3 % from depths below 200 mm. This represents an additional source of uncertainty in the measurements.

7.3 High resolution surveys using portable *in situ* detection

7.3.1 High resolution surveys: Introduction

One characteristic of *in situ* detection of gamma-emitting radionuclides is the remote detection that is made possible by the penetrating abilities of gamma radiation. As has been seen in Chapter 4, this has advantages for the estimation of mean activity concentrations, and also for the detection of activity hotspots. A potential drawback is that the unknown source geometry (*Section 7.2*) makes spatial mapping of the activity concentrations from individual measurements problematic. The use of more effective collimation than was used in these experiments would assist in this, by defining a smaller ground area from which a high proportion (e.g. 95 %) of the radiation was received. This would equate to a smaller primary sample mass. Collimators with side walls of 50 mm thickness are commercially available. The weight of such a collimator is in the region of 70 kg, however. Such equipment would be difficult to handle in most field situations, other than where a trolley-mounted detector was used on a hard, level surface.

Analysis of the results from the hand-portable Exploranium detector (*Section 4.5.2*) suggested that a significant collimation effect is induced when a detector is placed very close to the ground surface. It was surmised that this was due to attenuation of gamma radiation by the components of the soil. It was further surmised that it may be possible to use this effect to improve the resolution of *in situ* gamma surveys.

7.3.2 High resolution surveys: Objectives

Test the ability of a collimated *in situ* detector positioned as close as practicable to the ground surface to characterise spatial distributions of contaminants with a resolution of 0.25 m.

7.3.3 High resolution surveys: Methods

Further field experiments in the Barrier 31 area were conducted in a small area of ground around measurement location C3 (Fig 4.2). This location had the highest recorded activity concentration in the main survey (see Figs 4.2, 4.3). Initially, a 5 x 5 square grid pattern was

marked out using DGPS, with a measurement spacing of 0.25 m and centred on the main survey location C3. This was later extended west and south In order to investigate a raised activity level in the southwest corner of the grid. In each measurement, the detector was placed on top of a piece of 12 mm plywood with a 110 mm diameter circular hole cut into the centre, so that the collimator aperture was unobstructed. The plywood was first positioned directly on the ground with the hole centred on the measurement location. A counting time of 600 seconds was used (as in the main survey). The total detector height of 37 mm was calculated from the thickness of the plywood (12 mm) plus the thickness of the lower face of the collimator (25 mm). An ISOCS model of 25 m diameter and 0.5 m depth was used to convert activity levels to activity concentrations, however, ISOCS estimations of the massimetric efficiencies plotted against increasing source diameter for this arrangement (Fig 7.3) suggest that 95 % of the radiation comes from a source diameter of ~2 m using this arrangement. This supports the suggestion that attenuation of radiation by the components of the soil effectively results in a "collimation effect" (*Section 7.3.1*).

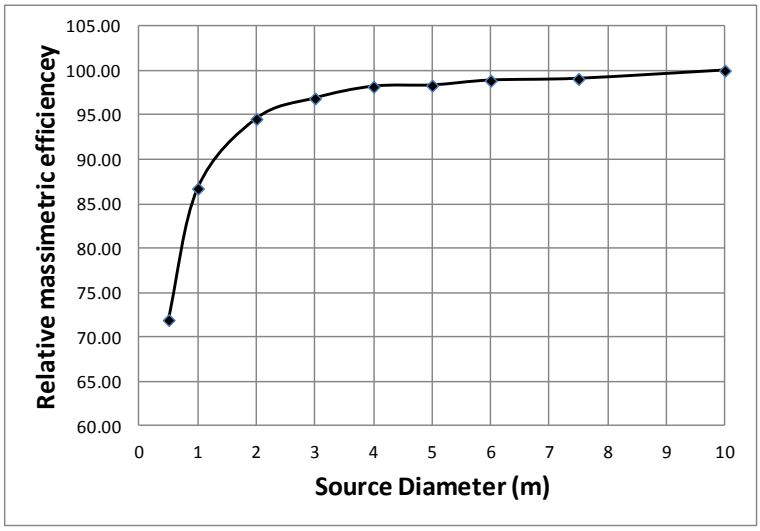

Fig 7.3 The relative massimetric efficiency model for increasing source diameter with a detector height of 37 mm.

The actual soil volume defined by the nominal FOV of the collimator defines a cone section in the ground. This is illustrated in Fig 7.4, from which it can be seen that the nominal FOV of the detector subtends a circular area of diameter 99 mm on the ground surface. This diameter increases to 299 mm at a depth of 100 mm. Radiation from within the FOV of the detector will cause a relatively greater detector response than radiation from outside, which will be partially attenuated by the components of the collimator, and will also be reduced by increasing

distance and angular offset from the detector volume. The actual resolution ability of this type of survey would therefore be expected to decrease with increasing soil depth.

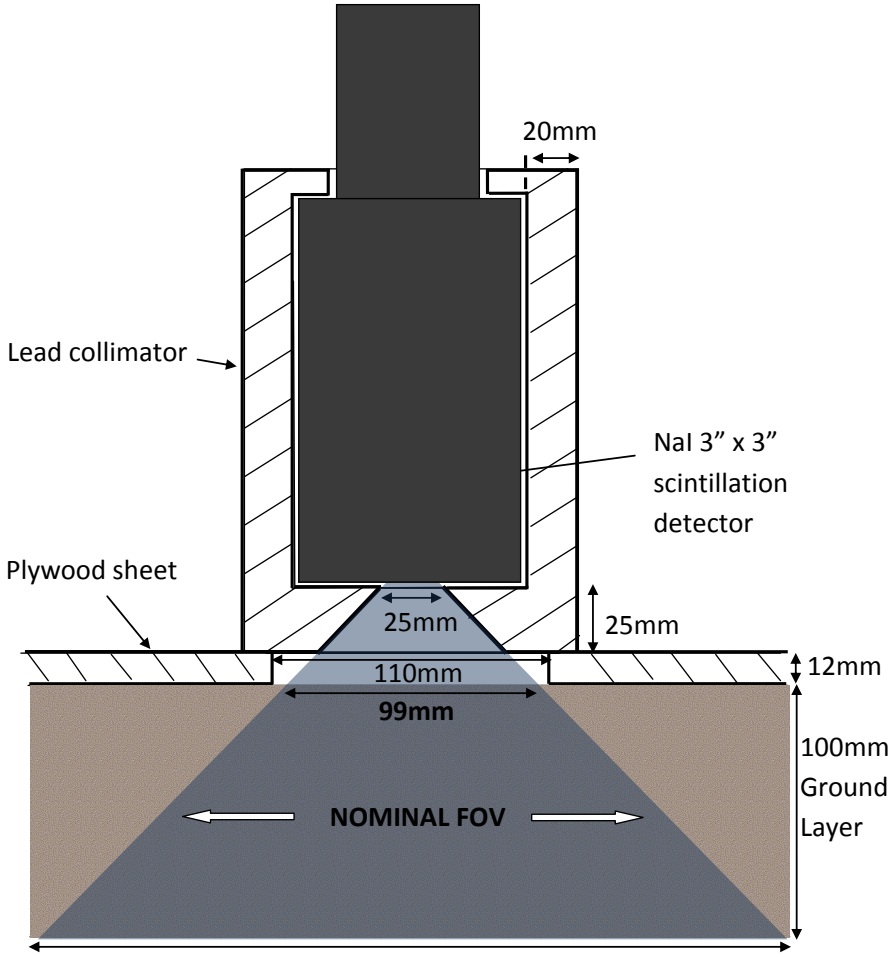

Fig 7.4 Drawing (to scale) of the measurement setup used in the high resolution survey, showing the cone section that is defined by the nominal FOV in the top 100 mm soil layer.

For practical reasons, duplicate measurement locations were not assigned until a single measurement had been acquired at each of the 36 measurement locations. Eight duplicate measurement locations were then assigned. These included the high measurement at location C3EC35 (Fig 7.5) plus seven other locations that were selected at random. Duplicate measurements were made using a full balanced design (*Section 3.2*). This meant that the duplicate analysis at each of the primary locations was made 2 – 13 days after the primary measurement, and therefore necessitated repositioning of the detector over each location. Each of the sample duplicates was positioned 2.5 cm from the primary location, in a random direction corresponding to N, S, E or W. The duplicated analyses at the sample duplicate locations were acquired consecutively, and without moving the detector (Fig 7.6).

7.3.4 High resolution surveys: Results and Discussion

The results of the high-resolution survey are shown in Fig 7.5. Further measurements were made using a 100 mm measurement spacing in a systematic pattern around the high measurement (10 Bq g^{-1}) at location C3EC35. This resulted in the extraction of a soil sample that was found by the on-site laboratory to have an activity of > 8,000 Bq ^{137}Cs. The sample was retained for authorised disposal.

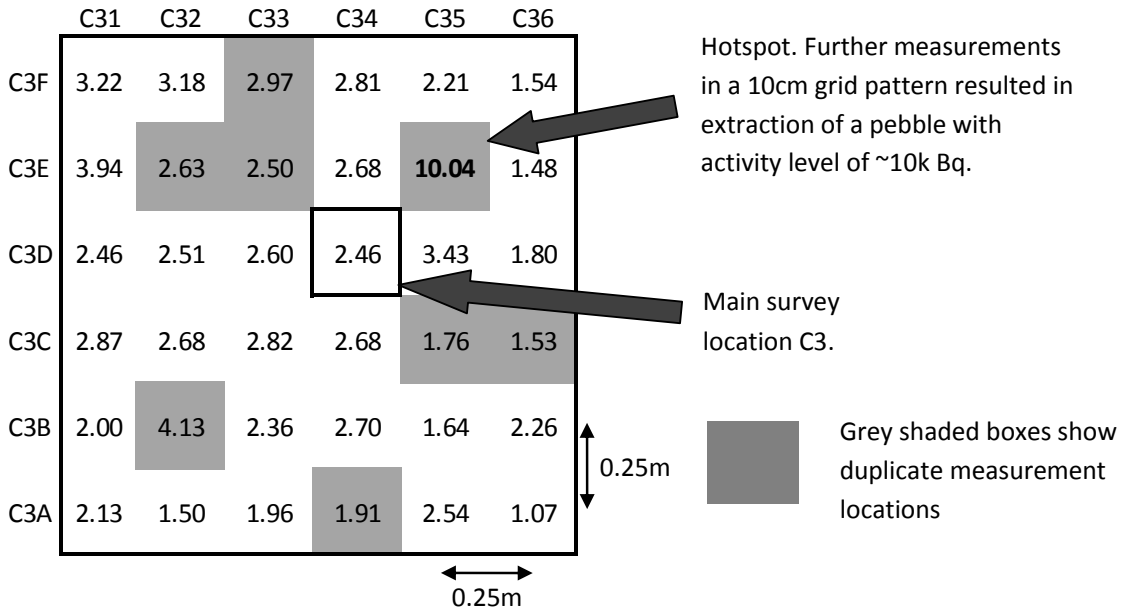

Fig 7.5 High resolution *in situ* survey in Barrier 31 around location C3 (See Figs 4.2 and 4.3). The values (in CPS) have been converted to units of Bq g^{-1}, using ISOCS^{TM} and Genie 2000 spectrum analysis software.

Analysis of the duplicates by robust ANOVA (*Section 3.2*) gave estimates of 17.4 % and 13.1 % for the expanded relative sampling and analytical uncertainties respectively, when using the balanced design. Using the method proposed by Ramsey *et al.* (2013) as described in *Section 2.3.5,* a quantification of the heterogeneity of contaminants can be expressed as the relative sampling standard deviation, which is in effect one half of the expanded relative uncertainty given in Table 7.1. For this high resolution survey, RSD_{samp} % = 8.7 % for a duplicate spacing of 0.025 m, compared to RSD_{samp} % = 5.1 % for a duplicate spacing of 0.13 m in the main survey (*Table 4.2*). A similar estimate of the heterogeneity from the *ex situ* sample duplicates in the main survey results in RSD_{samp} % = 21.8 %. The estimates of heterogeneity from the *ex situ* measurements would be expected to be higher because of the much smaller test volume. However, heterogeneity estimates from *in situ* measurements of gamma-emitting

radionuclides are not directly comparable to the estimates made from *ex situ* data, because of the uncertainty in the dimensions of the source volume in the *in situ* measurements, and also because of the differential detector response to activity at different positions with respect to the detector axis (See *Section 5.2.3*). In both the main survey and the high-resolution survey conducted in Barrier 31, the measurement spacing was much smaller than the estimated total diameter of the primary sample. In the high-resolution survey, the measurement spacing was 0.25 m, whereas it has been estimated that 95 % of the detector response arose from a sampling target of ~2 m diameter (*Section 7.3.3*). Therefore estimates of the heterogeneity of contaminants in the ground will have been underestimated by the *in situ* measurements. It is, however, possible to draw the broad conclusion from these results that significant heterogeneity of ^{137}Cs contamination exists on a scale of a few centimetres.

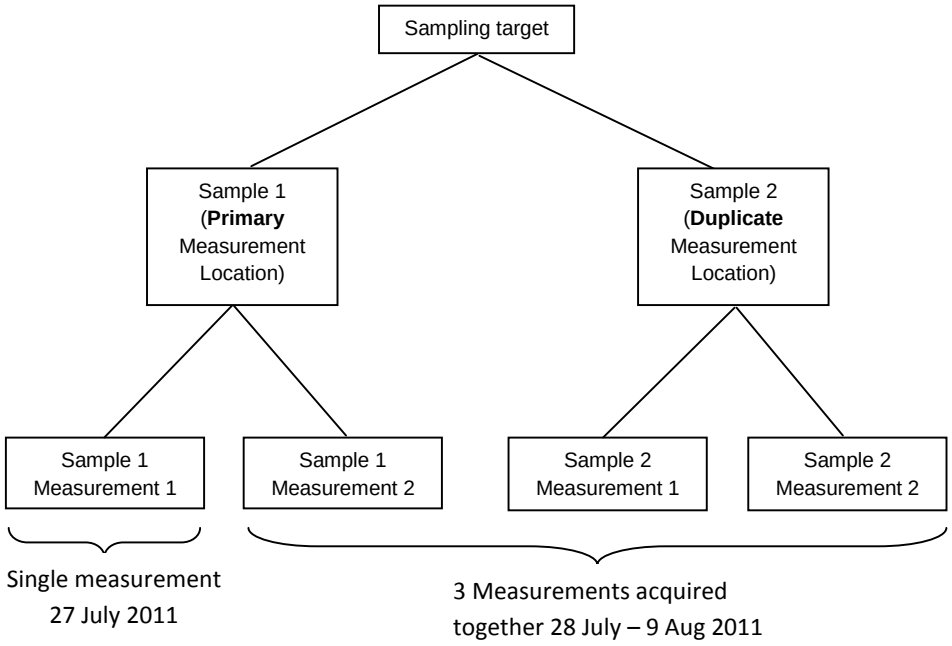

Fig 7.6 The balanced design used in the high resolution survey conducted in Barrier 31. For each duplicate measurement location, the first measurement at the primary location was acquired singly, while the remaining three measurements were acquired together at a later date.

The figure of 13.1 % for the analytical uncertainty is nearly double the estimate of 7.5 % from the main survey (Table 4.2). This would not be expected. A possible explanation is that it is an artefact of repositioning the detector in order to acquire the analytical duplicate counts at the primary measurement locations (*Section 7.3.3*). It could also be due to the time interval (2-3 days) between acquiring the initial measurement and its analytical duplicate. To investigate

further, analysis was repeated using the unbalanced design (See *Section 3.2,* Fig 3.2). This method enabled the analytical uncertainty estimate to be made using only the two analytical measurements that were made at each duplicate measurement location, which had been acquired consecutively without moving the detector between measurements. Sampling uncertainty was then estimated between the means of these measurements and a) the original measurements at the primary location; b) the duplicate measurement at the primary location. This is illustrated in Fig 7.7. The results of these trials and comparisons against the balanced design are shown in Table 7.1. In both of the unbalanced designs the analytical uncertainty is reduced from ~13 % to ~2 %. This strongly suggests that the high level of the analytical component of uncertainty that was obtained when using the balanced design was a result of acquiring the duplicate measurements at the primary locations non-consecutively. The fact that there is close agreement between the estimates for the two different unbalanced designs suggests that this did not result from the time interval between the two measurements, but from the repositioning of the detector.

By making repetitions of the measurement positioning protocol in the field, it was estimated that a maximum error of 20 mm would have been made in repositioning the detector. The relatively large difference in estimates of the analytical component of uncertainty between the balanced and the unbalanced designs therefore suggests that there was significant heterogeneity of ^{137}Cs contamination over a very small scale (i.e. <=20 mm).

7.3.5 High resolution surveys: Conclusions

This experiment supports the suggestion made in *Section 4.5.2* that there is a significant "ground collimation" effect when using *in situ* gamma detectors very close to the ground surface, enabling a much improved resolution. The use of a collimated NaI 3" x 3" scintillation detector at a height of 12 mm above the ground surface enabled significant spatial variation of ^{137}Cs contamination to be observed in a localised area of less than 2 m^2, with a resolution of 0.25 m. These experiments also suggest that significant heterogeneity of ^{137}Cs contamination was present in the Barrier 31 survey area on a spatial scale of <= 20 mm.

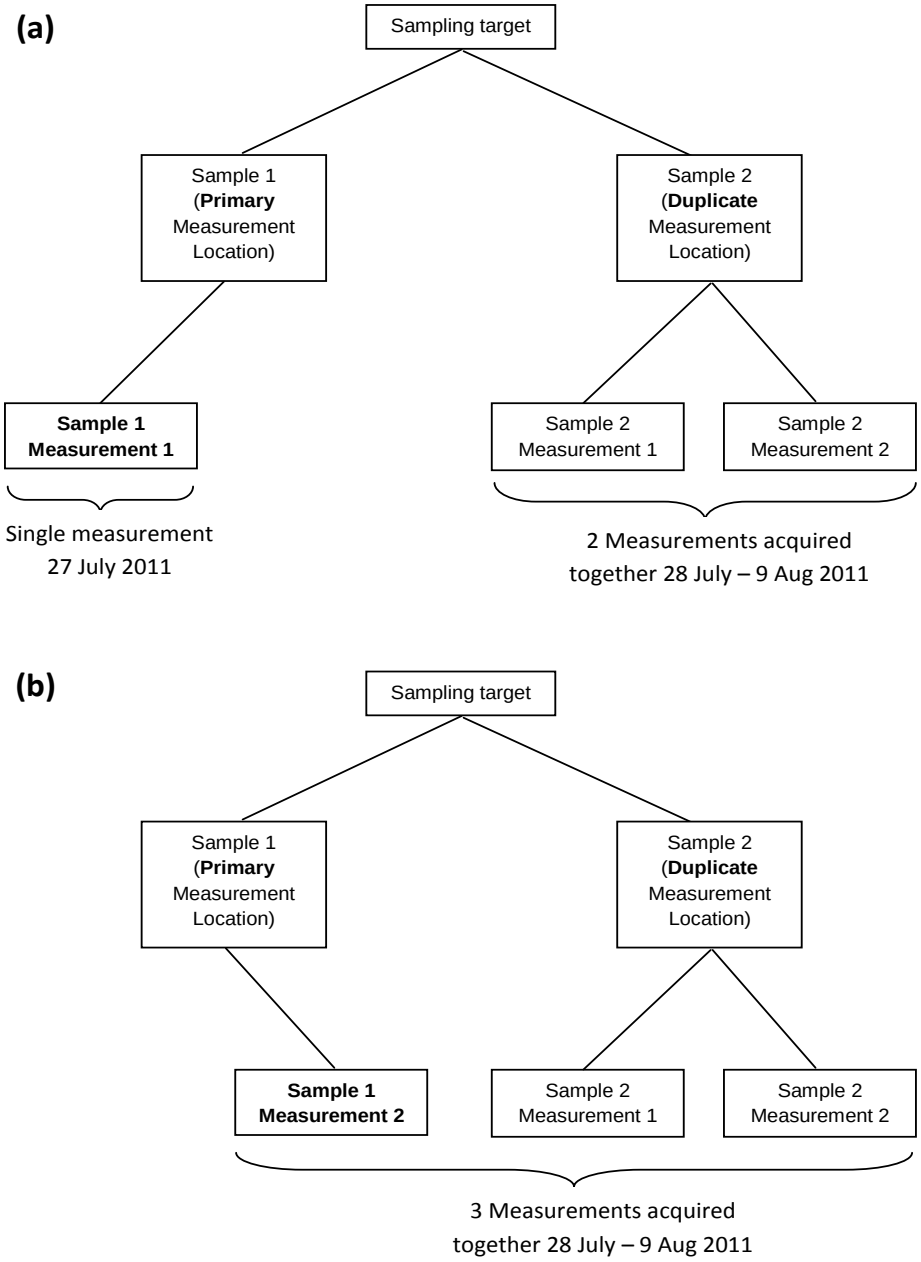

Fig 7.7 Uncertainty estimation using the unbalanced design for the high resolution experiment in Barrier 31. a) **Unbalanced design 1**, in which the original measurement from the primary location was used; b) **Unbalanced design 2**, using the duplicate measurement from the primary location.

Table 7.1 Random component of uncertainty estimates for the high resolution survey in Barrier 31, using both balanced and unbalanced designs.

RANOVA type	Sampling U%	Analytical U%	Measurement U%
Balanced Design (Fig 7.6)	17.4	13.1	21.8
Unbalanced Design 1 (Fig 7.7a)	20.2	1.9	20.3
Unbalanced Design 2 (Fig 7.7b)	20.6	2	20.7

7.4 Estimating the systematic component of measurement uncertainty in portable *in situ* measurements of land areas

7.4.1 Systematic uncertainty in *in situ* measurements: Introduction

Measurement uncertainty arises from two effects: a random effect, and a systematic effect (Ramsey, 1998). The systematic component of uncertainty in the analysis results in bias between measured values and true values (analytical bias). In laboratory experiments, this component of uncertainty can be estimated by comparing measurements of samples of known concentration (e.g. reference sources) to their known values. The use of certificated reference sources (CRMs) as the reference materials adds traceability to the laboratory measurements of field samples.

This type of procedure is usually much more difficult to apply to measurements that are taken *in situ* in the field. In the case of measurements of chemical contamination by hand-held XRF, a reference source can be taken to the site, and measurements made of that source at periodic intervals during the survey. Ideally, these additional measurements should be randomly assigned in the measurement sequence, to minimise any bias that could be caused by changes in instrument response over time, or by operator procedure. However, such methods typically do not take account of the nature of the substrate in which contamination exists, e.g. differences in the particulate size, moisture content and density between the field substrate and the reference source. These factors can be more easily controlled in laboratory conditions.

The remote detection of gamma rays by *in situ* measurements on land areas means that the mass of the primary sample is potentially very large (e.g. ~400 tonnes for a circular area of 25 m diameter and 0.5 m depth). The use of progressively heavier collimation reduces the source diameter from which the majority of radiation is received. With the 90° 20 mm lead collimator used in these experiments, ISOCS modelling indicates that ~95 % of the detector response (at 662 keV) comes from radiation emanating from within a circular plane of ~25 m diameter and ~0.2 m depth (*Section 7.2*).

The term **Reference Measurement Target** (**RMT**) has been used here to refer to a volume of soil or other substrate with sufficient dimensions to act as a reference source for estimating the analytical bias in *in situ* measurements of land areas. This should not be confused with a Reference Sampling Target (RST), which is an area of ground that has been created in order to estimate the bias due to sampling (See *Section 2.3.4*). An RST may be specifically designed to be heterogeneous, in order to be able to assess the performance of different samplers and

sampling protocols in the task of characterising the spatial distributions of contaminants, using multiple measurements. An RMT, however, would ideally be homogeneous with respect to contaminant content, because the purpose of an RMT is to estimate the analytical bias in measurements of a single primary sample. Creation of a true RMT for gamma *in situ* measurements, therefore, would necessitate construction of a volume of the required dimensions, which could be evenly spiked with known quantities of one or more radionuclides. Assuming that the RMT would be intended for long-term use, then the obvious substrate material to use would be concrete. However, a source of these dimensions would require ~100 m^3 of concrete (for perspective, a typical concrete mixer transport carries 6 m^3). The difficulties of site location, ensuring sufficient mixing of the materials, and subsequent decontamination of equipment, make the construction of such a site logistically problematic, and very costly. The use of calibration programs such as ISOCS is therefore a much less expensive method of instrument calibration for large source dimensions. However, this does not provide traceability to a 'standard', such as a certified reference source.

In order to be able to provide traceability for *in situ* measurements of ground areas it was decided to identify a pre-existing area which could be used as a RMT. Providing the site was of sufficient dimensions and the substrate was well-mixed, a naturally occurring radionuclide could then be used as the reference material.

7.4.2 Systematic uncertainty in *in situ* measurements: Objectives

1) Designate an area of concrete of sufficient dimensions that it could potentially be used as a reference measurement target for estimation of the systematic uncertainty in *in situ* measurements of ground areas. Establish a reference value for the RMT using *ex situ* measurements with traceability to a certified reference source in the laboratory.
2) Test the hypothesis that the concrete is relatively homogeneous with respect to radionuclide content, e.g. less than 10 % relative standard deviation between measurement locations.
3) Test the usefulness of this site as a reference site, by making comparisons of *in situ* measurements with the traceable *ex situ* measurements that were performed on extracted concrete cores.

7.4.3 Systematic uncertainty in *in situ* measurements: Methods

The case study site (Dounreay) has a disused concrete runway which was built during the early 1940s, and is a short distance from the site perimeter. It is currently in use as a car park for site personnel. The western end of this runway has been sectioned off and designated as a bus turning area. It was decided to identify a portion of this part of the runway as the potential RMT.

Previous experiments with ISOCS suggested that with a 3" x 3" NaI detector fitted with 20 mm lead collimation, more than 95 % of the detector response comes from radiation within a circular area of 25 m diameter (See *Section 7.2*). The actual reference site was selected according to the following criteria:

a) The centre of the reference point would be at least 25 m from the edge of the concrete in any direction;
b) A circular area of 25 m diameter was defined which, on visual inspection, appeared to exhibit the most uniform concrete surface (i.e. the least cracks and holes).

Measurements were made using two methods:

a) *In situ* measurements using a Canberra 3"x3" NaI detector, fitted with 90°, 20 mm lead collimation, at a height of 920 mm.
b) *Ex situ* measurements were made by extracting concrete cores and analysing them for gamma-emitting radionuclides in an external, accredited laboratory.

The sampling scheme is shown in Fig 7.8. A total of 50 *in situ* measurements were made. Initially, 10 were acquired at the proposed centre of the RMT, for comparison with the *ex situ* measurements. The latter were made on cores that were extracted after all *in situ* measurements had been completed. An additional 10 *in situ* measurements were also made at the hypothetical edge of the reference site at each of the locations 3, 9, 14 and 23 (Fig 7.8). Measurements were made at these additional four locations with the objectives of:

a) Ensuring that no substantial external sources (external to the reference site) would affect the *in situ* measurements;
b) Support the hypothesis that the radionuclide content of the concrete is homogeneous on a large scale.

Ten measurements were made at each of the *in situ* measurement locations in order to achieve an estimate of uncertainty in the *in situ* measurements. The naturally occurring radionuclide ^{40}K was selected for the comparison between *in situ* and *ex situ* measurements, because this was the only radionuclide that consistently showed peaks when the *in situ* spectra were analysed. Twenty *ex situ* measurements were made on cores extracted from 20 randomly selected locations within the reference site. The locations of all measurements are shown in Fig 7.8.

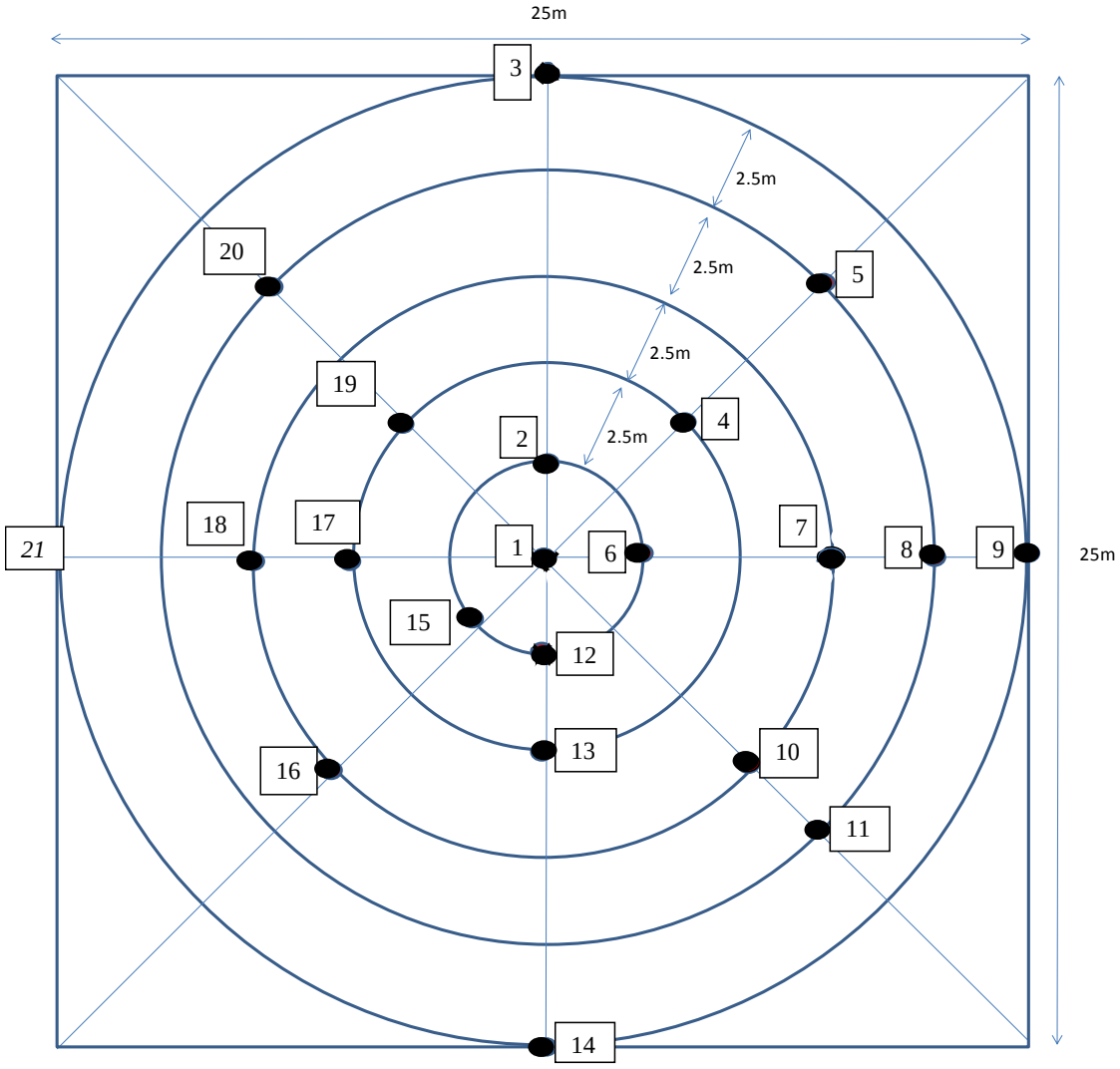

Fig 7.8 The RMT sampling scheme, showing the 20 *ex situ* measurement locations. 10 *in situ* measurements of 600 seconds each were taken at points 1,3,9,14 and 24 in order to evaluate the heterogeneity of the site with respect to ^{40}K activity concentrations.

Ex situ measurements of the concrete cores were made in an external laboratory. Each core (~60 mm in diameter and an average 111 mm in length) was first crushed and ground and passed through a 1 mm sieve. A measured amount was then transferred to a container in order to produce a standard sample geometry, prior to measurement by high-resolution gamma spectrometry. This was conducted using high-purity germanium detectors, coupled to computerised multi-channel analysers, with peak search and peak shape functions and a validated radionuclide library. System calibration was undertaken for standardised geometries using a nationally traceable "mixed gamma" reference solution, in the energy range 60 keV - 1836 keV.

7.4.4 Systematic uncertainty in *in situ* measurements: Results

Ex situ measurements and summary statistics are provided in Appendix 4 (Table A4.1). The mean value of ^{40}K activity concentration was found to be 0.73 Bq g^{-1}. A visual representation of the results of the *ex situ* measurements is also shown in Fig 7.9. The full range of measurements varies between 0.52 and 1.05 Bq g^{-1}, however Fig 7.9 suggests general heterogeneity of ^{40}K activity with no particular hotspots of activity in the proposed reference area.

The mean depth of concrete was found to be 111.5 mm across all 20 measurements. This will be a cause of uncertainty when comparing *ex situ* measurements *with in situ* measurements, because previous (ISOCS) experiments have suggested that a significant amount of radiation will be received at the detector from depths greater than 111.5 mm (*Section 7.2*).
The *ex situ* measurements are not significantly different from a normal distribution (Anderson-Darling, SPSS v 21, $p>0.05$). The relative standard deviation of the measurements is 19 %. Subtraction of the average analytical uncertainty estimated by the laboratory (expressed as an expanded uncertainty of 0.056 Bq g^{-1}) reduces this to 18.6 %, significantly higher than the criteria of 10 % (Objective 2). This level of heterogeneity of ^{40}K activity concentrations is higher than was originally expected, and may be too high for the area to be reliably used as a reference measurement target.

To investigate whether measured activity is uniform throughout the depth of concrete, activity concentration is shown plotted against core depth in Fig 7.10. There does appear to be an overall decrease in ^{40}K activity as core depth increases, although the correlation is not significant ($p>0.05$).

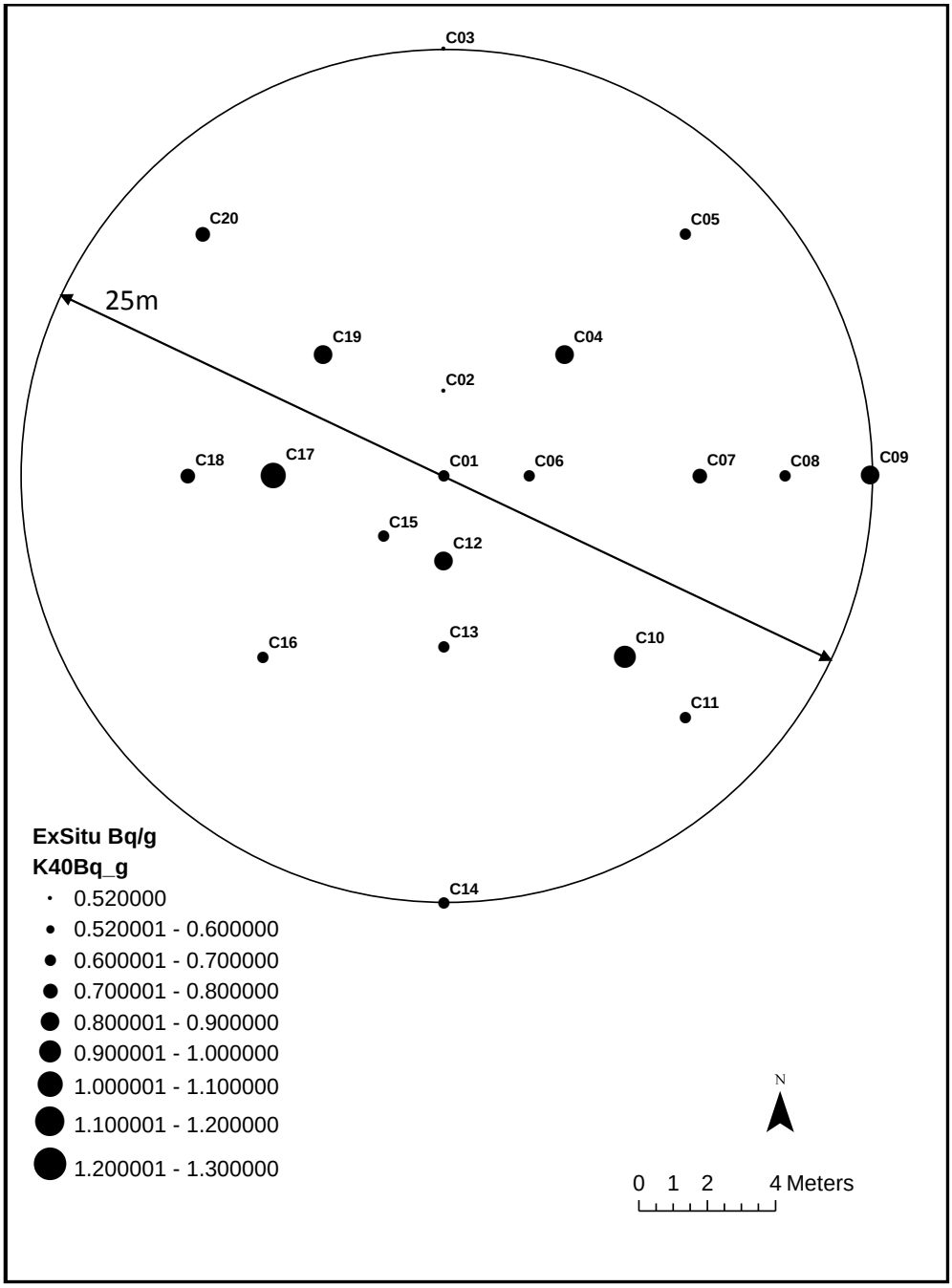

Fig 7.9 Representation of the *ex situ* measurements acquired in the proposed RMT. The size of each dot is proportional to the mass activity concentration measured at that location.

None of the sets of 10 *in situ* measurements acquired at the 5 different locations were found to deviate significantly from normality (Anderson Darling test, $p>0.05$). The mean values of these activity concentrations for the 5 groups acquired at positions C01, C03, C09, C14 and C21 were tested by ANOVA and found to be not significantly different (Appendix 4, Table A4.2). There also appears to be much less difference between the mean values of the *in situ* sets than

there was for the *ex situ* measurements, with a range of 0.55-0.58 Bq g^{-1} for the mean activity concentrations at each location, and 0.47-0.62 Bq g^{-1} for the 50 individual measurements.

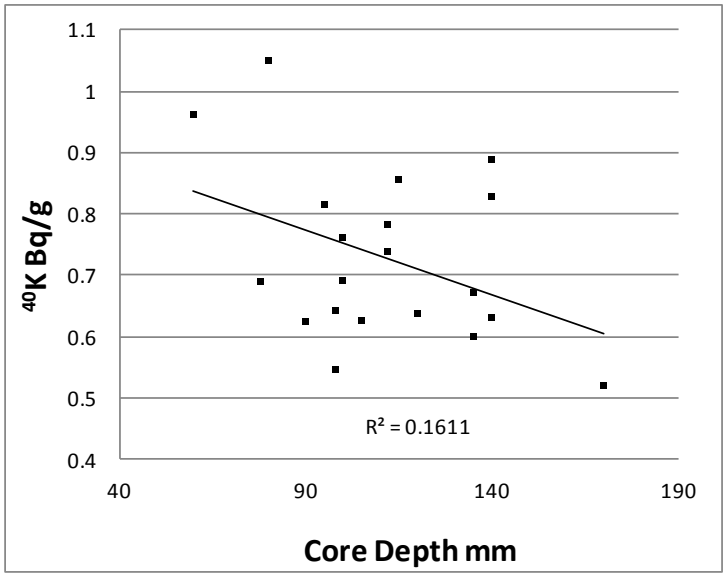

Correlations

		K40_Bq_g	Depth_mm
K40_Bq_g	Pearson Correlation	1	-.401
	Sig. (2-tailed)		.079
	N	20	20
Depth_mm	Pearson Correlation	-.401	1
	Sig. (2-tailed)	.079	
	N	20	20

Fig 7.10 The negative correlation between ^{40}K activity concentrations of *ex situ* measurements of core samples and the measured core depth in mm is not significant at $p < 0.05$ but is significant at $p < 0.10$.

Expanded relative uncertainty for the *in situ* measurements was estimated using ANOVA on the 5 measurement sets. There was found to be an analytical uncertainty of 11.7 % and a between-target variance of 2.3 % (between the 5 measurement locations). As the *in situ* detection method acquired measurements over a much larger surface area than the *ex situ* measurements, this tends to suggest that heterogeneity in ^{40}K activity is on a relatively small scale, thus affecting the *ex situ* measurements to a much greater degree than the *in situ* measurements.

The ten *in situ* measurements acquired at position C01 (Fig 7.8) at the centre of the RMT were analysed using various different ISOCS geometry model depths. Averages for the ten measurements at the different model depths are shown in Table 7.2. The differences between the estimates for each geometry model compared to the geometry model for the actual average depth of 111 mm are also shown. It can be seen that significant uncertainty arises due to a) the variability in core depth from 60 mm to 111 mm; b) an assumed component of radiation emanating from depths greater than 111 mm. Each core was drilled until further drilling was prevented by pebbles, either embedded in the concrete or from an apparent aggregate of pebbles beneath the concrete itself. The potassium content of the pebbles might vary significantly from the concrete, and no measurements of ^{40}K activity were acquired from this underlay. Previous data suggests a figure of about 0.7 Bq g^{-1} for soils around the Dounreay site (Heathcote, 2013), which is consistent with the mean of the ex situ measurements of 0.73 Bq g^{-1}. Thus for comparison with *ex situ* measurements, the *in situ* measurements have been analysed using an ISOCS model of 111 depth (corresponding to the mean core depth) and also with a 500 mm depth model. The latter was chosen because the results shown in Table 7.2 suggest that minimal activity would be recorded from depths greater than 500 mm.

Table 7.2 Averaged ISOCS calculated activity concentrations of *in situ* measurement at position C01 using different ISOCS depth models, showing the percentage difference from that calculated for the model based on the mean core depth of 111 mm. The variation in core depth from 60-170 mm introduces a source of uncertainty. This also shows that substantial amounts of activity (~11 %) may be acquired from below the mean depth of 111 mm, introducing yet another source of uncertainty.

	Model depth (mm)	^{40}K activity conc. (Bq g^{-1})	% difference from mean
Minimum depth	60	0.72	20.04
Mean depth	**111**	**0.60**	**0**
Maximum depth	170	0.56	-6.74
Standard depth	500	0.54	-10.71
Large depth	2000	0.54	-10.72

Summary statistics of the results of the analyses for the 10 *in situ* measurements acquired at position C01 are shown in Table 7.3. The full data sets are provided in Appendix 4 (Tables A4.2 - A4.3).

7.4.5 Systematic uncertainty in *in situ* measurements: Discussion

The seemingly high level of heterogeneity of ^{40}K activity concentrations of the *ex situ* measurements, as shown by the relative standard deviation of 19 % and overall range of 0.52-

1.05 Bq g^{-1} (*Section 7.4.4*), suggests that the hypothesis that the concrete is relatively homogeneous with respect to radionuclide content is not well supported (Objective 2). This would make the site less useful as a RMT than one that was purposely designed with a known amount of a target radionuclide in well-mixed concrete. However, comparison of these levels of uncertainty with the *in situ* heterogeneity (between-target uncertainty of 2.3 %, range 0.55-0.58 Bq g^{-1} for the mean activity concentrations at each of 5 *in situ* locations) suggests that the heterogeneity seen in the *ex situ* measurements exists on a relatively small spatial scale. If this is the case, then it is reasonable to compare the mean activity concentration of the *ex situ* measurements with the *in situ* measurements at position C01 (Objective 1), because the large primary sample mass of the *in situ* measurements means that they would be expected to be less affected by this small-scale heterogeneity. For traceability of the *in situ* measurements to the laboratory reference source, the assumption has to be made that the *ex situ* measurements are representative of the radionuclide levels in the proposed RMT.

Table 7.3 Summary statistics of *in situ* measurements of ^{40}K activity concentration with the detector in position C01 (the centre point of the RMT) using an ISOCS circular plane model of diameter of 25 m, and two depths of 111 mm (the mean core depth) and 500 mm (the standard model depth).

Source depth (mm)	Mean (Bq g^{-1})	Std deviation (Bq g^{-1})	Minimum (Bq g^{-1})	Maximum (Bq g^{-1})	Std error (Bq g^{-1})
111	0.55	0.029	0.49	0.58	0.0091
500	0.50	0.026	0.44	0.52	0.0081

Based on these assumptions, the mean of the ten *in situ* measurements taken at the centre of the RMT appears to underestimate the mean of the *ex situ* measurements when interpreted using either the 111 mm depth model or the 500 mm depth model (0.55 and 0.50 Bq g^{-1}, Table 7.3 compared with 0.73 Bq g^{-1} for *ex situ*). Both the student's t-test and the non-parametric Mann-Whitney test suggest that the *in situ* results differ significantly from the *ex situ* measurements ($p<0.05$). Confidence limits on the mean values of *in situ* and *ex situ* measurements show no overlap, also indicating a significant bias, equal to -25 % for the *in situ* measurements using the 111 mm depth model.

The limited depth of concrete (mean = 111 mm) may have severely affected the estimate of bias, as the ^{40}K content of the underlying hardcore and soil could have differed significantly from that in the concrete. Such a difference would have affected the *in situ* measurements but

not the *ex situ* measurements of laboratory samples, as these comprised of concrete only. The bias between *in situ* and *ex situ* measurements might therefore not have been representative of the general bias between the two methods.

Some uncertainty may have been introduced because a much larger proportion of the counts received at the detector (per unit ground area) would be expected to emanate from within the FOV than from outside it, as radiation received from outside the FOV has to pass through 20 mm of lead. Only the core acquired at position C01 (Fig 7.9) would have been part of the concrete within the FOV of the *in situ* detector. Fig 7.9 also shows that four out of the five cores taken from positions closest to C01 had measured activity concentrations that were below the mean activity concentration of 0.73 Bq g^{-1}. The mean activity concentration of these five points is found to be 0.65 Bq g^{-1}. This suggests that the figure of 0.73 Bq g^{-1} may be an overestimate of the activity that is within the FOV of the detector at this point, if some heterogeneity of activity existed on a scale of ~1.5-2.5 m. Based on an accepted value of 0.65 Bq g^{-1} the bias can be re-calculated as -15 % for the *in situ* measurements using the 111 mm depth model. However, it is unlikely that most of the apparent bias in the *in situ* measurements results from this effect, because no significant differences were found between the *in situ* measurements taken at five different positions at the centre of the RMT and on its perimeter (*Section 7.4.4* & Appendix 4, Table A4.2). A single measurement suggested that the particular *in situ* detector that was used in this experiment may have had a bias of approximately -29 % when measuring a point source on the axis of the detector. This matter is discussed further in *Section 8.2.5.2.*

7.4.6 Systematic uncertainty in *in situ* measurements: Conclusions

A circular area of concrete was designated as a Reference Measurement Target. *Ex situ* measurements established a reference value of 0.73 Bq g^{-1} of ^{40}K. These measurements were linked to a nationally traceable mixed-gamma solution.

The relative standard deviation of ^{40}K activity concentrations between the measurement locations was evaluated at 18.6 %, and so the hypothesis that the site was homogonous with respect to ^{40}K activity was not supported according to the criteria of < 10 % RSD.

Comparison of the *in situ* and *ex situ* measurements made on the proposed RMT suggest that there was a significant difference between the mean activity concentrations, with the *in situ* measurements underestimating the *ex situ* measurements by ~25 %. This difference was

reduced to ~15 % when the 5 *ex situ* measurements closest to the centre of the RMT were used. It may be that heterogeneity of ^{40}K activity on a smaller scale than the proposed 25m diameter RMT was a cause of some of this bias, however the -25 % bias found in the *in situ* measurements is consistent with the level of bias also found in a comparison to a point source of known activity (*Section 8.2.5.2*).

A further potential source of error would have been introduced by the incorrect assumption that the depth of concrete was about 500 mm. The true depth was found to average 111 mm across the 20 concrete cores that were extracted for the *ex situ* measurements. The concrete was embedded with pebbles, and more pebbles of varying sizes were found beneath the concrete. Variable potassium content in these may have caused a systematic error in the average activity concentration of ^{40}K estimated from the laboratory measurements.

The location of a site which would better fulfil the requirements of a RMT, i.e. correct source dimensions (radius and depth) and lower levels of heterogeneity of the target radionuclide, would be the subject of future work.

Chapter 8 – Further discussion and synthesis of the experimental work in the context of the research objectives

8.1 Introduction to Chapter 8

This chapter provides a general discussion of the findings of the experimental work described in Chapters 4-7 and serves the following purposes:

1. Extend the discussion sections of these chapters beyond that which was possible in the papers that were submitted for publication;

2. Synthesise the findings of some of the experiments in order to address research objectives;

3. Consider the findings of the field experiments in a broader context, e.g. comparison of the suitability and costs of the measurement methods with surveys conducted by vehicle mounted detectors, and the applicability of the studies to radionuclides other than ^{137}Cs.

The chapter is divided into three main sections. *Section 8.2* addresses research objective 1. *Section 8.3* addresses research objective 2 (See *Section 1.2* for the research objectives). Finally, a section (*Section 8.4*) is included to discuss the work presented in this thesis in a broader context, e.g. the characterisation of alternative types of land areas (such as concrete slabs), and applicability to different target radionuclides.

8.2 Comparing the usefulness of *in situ* and *ex situ* measurement methods

Section 8.2 relates to Objective 1. It acts as a synthesis between the results of the two surveys of radioactively contaminated land areas (Chapter 4), and the three additional desk and field experiments described in Chapter 7. The overall purpose of this section is to draw on the findings of all these experiments in order to evaluate the relative effectiveness of *in situ* and *ex situ* measurement methods.

8.2.1 Overview

The two primary methods of measurement that have been used and discussed in this thesis are the *ex situ* analysis of extracted core samples and the *in situ* measurement of gamma-emitting radionuclides. Any useful comparison between these methods (Objective 1) depends on consideration of a number of factors, including the costs and practicalities of implementation. An overview of these factors, which is based on the findings of the experiments, and also on the author's experience of working on a decommissioning nuclear site, is presented in Table 8.1. The first of these relates to the relative costs of measuring equipment and costs per measurement, and is somewhat generalised. Although the purchase cost of a portable NaI scintillation detector and collimator (a few thousand pounds) might compare favourably with the analysis of a set of 30 samples by a commercial laboratory (e.g. ~£6000), clearly the cost of setting up a vehicle mounted system with large volume scintillation detectors would be much higher. Individual operators would need to consider the relative capital and operating costs of equipment, and the amount of characterisation work that is required, alongside the potential advantages and disadvantages of each method with respect to individual aspects of characterisation.

8.2.2 Comparison of the random components of uncertainty

The first detailed research objective of this project (Objective 1.a) was to make estimates of the sampling and analytical components of uncertainty in the measurements obtained by *in situ* and *ex situ* methods. Empirical estimates of the random components of uncertainty were made in all the experiments, and where possible this was achieved by using a method that is well established in measurements of chemically contaminated land. This 'balanced design' method (as well as the 'unbalanced design' described in Chapter 3) enables separate quantification of estimates of the random components of sampling and analytical uncertainty (Ramsey and Ellison, 2007). In all cases it was found that the random component of analytical uncertainty in the *in situ* measurements was higher than that which would be expected due to statistical fluctuations in the radioactive decay process. A comparison of the estimated random components of analytical uncertainty for the *in situ* measurements in Zone 12 and Barrier 31 with the predicted uncertainty from Poisson variance on the mean values is given in Table 8.2.

Table 8.1 Overview comparison of *in situ* and *ex situ* measurement methods

***Ex situ* gamma spectroscopy of extracted samples**	**Gamma spectroscopy of *in situ* measurements**
High capital cost of equipment and/or relatively high cost of analysis per sample (e.g. £100 per measurement).	Lower capital equipment cost and lower cost of individual measurements (e.g. £5.00 per measurement).
Long turnaround times, especially if using a commercial laboratory.	Measurements can be interpreted and available almost immediately.
Costs/admin associated with transporting and shipping of samples.	Personnel may be working in controlled areas for extended periods, leading to additional costs of decontamination and health physics.
Traditionally regarded as more reliable. Measurements made in controllable conditions (e.g. temperature, background).	Measurements made in environmental conditions. Environmental factors (e.g. temperature change) increase analytical component of uncertainty.
Small sampling size (volume or mass) per measurement (~1 kg).	Large sampling size (volume, mass or area) per measurement (e.g. up to ~400 tonnes).
Quantifiable sampling size. Not affected by external sources of radiation (shine).	Sampling size has to be estimated. Estimate is susceptible to errors due to external sources of radiation (shine) or heterogeneity of contaminants on a similar scale to the sampling size.
Measurements can be traced to certificated reference materials (when available).	Hard to establish traceability, principally due to large mass of the primary sample (See *Section 7.4*).
Highly susceptible to sampling uncertainty due to *in situ* analyte heterogeneity on a small (i.e. centimetres) scale.	Less susceptible to sampling uncertainty from small-scale heterogeneity. Potentially more reliable estimates of activities within averaging areas.
Easy to implement longer counting times to reduce random component of analytical uncertainty.	Random component of analytical uncertainty harder to reduce by increasing counting times, due to (e.g.) unattended equipment, may be hampered by weather conditions.
Sample processing can be carried out (e.g. drying, grinding), but less representative of actual site conditions.	Measurements affected by variable environmental conditions, e.g. soil moisture content.
Potential for uncertainties caused by sample extraction and transportation (e.g. soil compaction, loss of ^{222}Rn).	Measurements are more representative of site conditions at the time of measurement.
High-coverage surveys are practically unachievable. Highly likely to miss small hotspots of activity.	High coverage surveys are achievable, and with careful planning are able to reliably identify small hotspots with stated confidence levels.
Reliable depth profiling is possible for individual measurement locations.	Depth distributions of contaminants are harder to establish, and may be impossible without excavation.

Table 8.2 Comparison of Poisson uncertainty with random component of analytical uncertainty in the *in situ* measurements for the Zone 12 and Barrier 31 surveys. The Poisson uncertainty is based on a calculation of the peak counts that would be required to report the mean activity concentration.

Survey	Mean activity concentration (Bq g^{-1})	Uncertainty calculated (2s) from Poisson variance on peak counts	Random component of analytical uncertainty (2s) estimated from analytical duplicates
Zone 12	0.043	10.8 %	42.6 %
Barrier 31	0.49	3.2 %	7.5 %

The empirical estimate of uncertainty is higher than the prediction from Poisson variance by a factor of approximately 4 in Zone 12 and a factor of approximately 2 in Barrier 31 (Table 8.2). A similar conclusion was drawn from the results of the modelling experiments described in Chapter 5.

These results suggest that there are additional factors that make a significant contribution to the total uncertainty budget, even when replicated measurements are taken consecutively and without moving the detector in between. Two primary contributory factors are suggested here. First, changes in temperature affect the response of the detector, and secondly, uncertainty in estimation of the peak areas occurs during spectral analysis. Temperature changes could be a result of environmental influences. The weather was very changeable during the field work at Dounreay, and although the air temperature would not be expected to change significantly over the time period (~25 minutes) that it took to obtain two consecutive measurements, there were often periods of variable sunshine over short timescales. A second possible cause of temperature change may be a “warming-up” effect of the detector over time. It was noticed during field work that drift in the energy levels between detector channels was most pronounced during the first 10-15 minutes of detector operation, especially in the case of the un-stabilised detector that was used in Barrier 31. For this reason, the detector was allowed a “warming up” period prior to use. This suggestion is supported by the analysis of data from *in situ* measurements that were made on a floor-slab by site personnel during the project period. This suggested that greater variances in detector counts arose from consecutive measurements that were made at the start of the survey (an un-stabilised detector was used in this case).

8.2.3 Heterogeneity of ^{137}Cs contamination

Evaluation of the heterogeneity of contaminant concentrations in contaminated land investigations has been discussed in *Section 2.3.5*. A primary finding of the *in situ* and *ex situ* surveys performed in Zone 12 and Barrier 31 (Chapter 4) is that levels of ^{137}Cs activity concentrations were heterogeneous on a small scale in both areas. A previous study has noted that spatial variation in environmental radioactivity levels occurs at all scales, and affects both *in situ* and *ex situ* measurements (Tyler *et al.*, 1996b). In the Zone 12 and Barrier 31 surveys, variability on small spatial scales is indicated by the relatively high levels of the sampling uncertainty estimated from the duplicate *ex situ* measurements, compared to the analytical uncertainty, shown in Table 4.2. Sampling duplicate locations were separated by spatial distances of 200 mm (Zone 12) and 130 mm (Barrier 31). These results therefore show that heterogeneity of ^{137}Cs activity exists over a spatial scale of 130-200 mm in these areas. The high-density *in situ* survey reported in *Section 7.3* suggests that there may also be significant heterogeneity even on a scale of 20-30 mm. Heterogeneity on this scale might be expected to have a lesser impact on the sampling uncertainty of *ex situ* measurements, because this distance is less than the ~80 mm diameter of the bulb planter that was used to acquire the soil samples. However, when soil samples are measured without prior processing (e.g. drying and grinding) as they were in these experiments, heterogeneity in the sample may result in an additional component of uncertainty, if the majority of activity in the sample emanates from a small number of discrete sources that are randomly positioned within the sample volume. This is because of the different degrees of attenuation that would occur if, for example, a particle of elevated activity were positioned in the centre of the sample, instead of near the periphery of the sample. This possible source of uncertainty is further discussed in *Section 9.8.4*. The choice of the distances of the sampling duplicates from the primary measurement locations was made on the basis of an estimate of the positioning error that might typically be incurred when laying out a survey grid with measuring tapes. This has previously been estimated at 10% of the measurement spacing (Ramsey *et al.,* 2002). In the field experiments reported here, positioning was carried out using DGPS with a reported precision of < 30 mm. Consequently the estimates of the random component of sampling uncertainty presented in Table 4.2 may be an overestimate of those that would have been obtained had it been possible to separate the primary and duplicate measurement locations by this small positioning error.

Nevertheless, the high sampling uncertainty in the site surveys on a 130 – 200 mm scale has the potential to have a significant effect on the reliability of mean activity concentration values

within an averaging area. This problem was largely overcome in the case of the *in situ* measurements, which produced measurements of average activity concentrations over a much large soil volume, e.g. ~100m^3 based on the ISOCS model defined in *Section 7.2.* This equates to a soil mass of ~160 tonnes. Quoting this large mass in the current context presents a somewhat distorted picture of the actual situation, because a relatively high proportion of the detector response (50-60 %) emanates from the soil volume that is defined by the FOV of the collimator (Fig 7.2). However, even if the collimator were perfect, i.e. if all of the detection response was due to radiation emanating from within the nominal FOV, then the mass of *in situ* measurements would be approximately 40 kg and 269 kg in Zone 12 and Barrier 31 respectively. In contrast, the average mass of the soil samples was measured to be 330 g in Zone 12 and 264 g in Barrier 31, and so the masses of the primary samples in the *ex situ* measurements are smaller than those of the *in situ* measurements, by at least 2-3 orders of magnitude.

When a single, small spot of elevated activity is present, the large sampling target mass of an *in situ* measurement will result in 'dilution' of the recorded activity from this spot by the local site background activity. When it is necessary to identify maximum activity levels of small hotspots of contamination (e.g. radioactive particles), then any single *in situ* measurement in a systematic survey that appears to be elevated compared to surrounding measurements requires further investigation. This may be achieved by one or a combination of three methods: a) a scanning type survey performed *in situ*; b) a high resolution *in situ* survey such as described in *Section 7.3*; c) a set of *ex situ* measurements acquired in a systematic sampling pattern. Where this can be achieved by a scanning survey, and perhaps backed up by one or a few measurements made with a portable, collimated gamma detector placed close to the ground surface, this is likely to be the least expensive option. *Ex situ* surveys cannot practically be designed to be certain, or even highly confident, of locating small hotspots. However, because of the much larger soil volume that is analysed, i*n situ* surveys can be designed so that there is a low risk of missing small hotspots.

8.2.4 Uncertainty in the source characteristics of *in situ* measurements

In situ measurements of gamma-emitting radionuclides in land are prone to two potential drawbacks. First, there is significant uncertainty in the geometry of the test volume, and therefore in the definition of the primary sample mass or volume of any individual measurement, which results in uncertainty in the calculated activity concentrations.

Uncertainty in the test volume results not just from uncertainty in the area of ground covered by each measurement, but also from the effects of external sources of radiation, such as shine from nearby structures. The issue is further complicated by the differential response of the detector to radiation from sources at different positions relative to the detector. One potential method of reducing these effects is to use more effective collimation (or additional shielding if measurements are affected by shine). Heavy collimation reduces the effect that radiation from outside the FOV of the detector has on the measurement, but even with 44 mm lead collimation, it has been found that around 25 % of the instrument response from a land area with homogeneous radionuclide content comes from beyond the nominal FOV (Kalb *et al.*, 2000). One method that might be used to establish the extent to which radiation from outside the FOV affects each measurement would be to also take measurements with a 'zero degree' collimator, i.e. a collimator with no aperture. These are commercially available for the purpose of establishing background radiation levels. Once the background radiation levels have been established, further measurements with the 'aperture collimator' theoretically enable the radiation levels received from the area that is defined by the FOV to be determined. Some uncertainty will still be present, because the shielding effect of the additional components of the zero degree collimator will not be perfect. Therefore some radiation from the area that would be within the nominal FOV of the aperture collimator will act to increase the background measurement. There are also operational difficulties, as it either involves changing the collimator at every measurement location (a time consuming and laborious process), or using two identical detectors fitted with different collimators, which would introduce an additional source of uncertainty due to the different responses of the two detectors. In the latter case, it would also be necessary to take each of the two measurements with the non-active detector and collimator removed to a position from which it would not influence the measurement being taken. Either method, therefore, involves taking two measurements at different times, and the need to re-position the detector(s), again introducing uncertainties.

A second potential drawback of *in situ* measurements on land areas is a lack of information about the depth of radionuclide activity. In contrast, *ex situ* soil samples that have been extracted from clearly defined depth ranges can be analysed separately, giving direct information about the depth profiles of radionuclide activity at individual measurement locations. For *in situ* measurements, there are two broad approaches to dealing with the issue of depth variability. The first of these is to make assumptions about the depth profile, and build these into the calibration model. This is fairly easy to do using ISOCS (*Section 2.4.3*), which allows the definition of different layers within an encompassing source 'container'.

ISOCS then permits the user to assign relative activity concentrations to each source layer. The Monte-Carlo convergence process used by ISOCS takes account of these relative values, and also of the attenuation factors of each source layer and its overlying layers, which are defined in terms of density and atomic composition. This was the approach that was used in the Zone 12 and Barrier 31 field surveys described in Chapter 4. Initially, the ISOCS geometry models were based on databases of previously obtained *ex situ* measurements around the site, which revealed no statistically significant differences between measurements of ^{137}Cs activity concentrations between soil samples extracted from depths of 0-100 mm and 100-200 mm. Subsequent analysis of the soil samples obtained from the Zone 12 and Barrier 31 surveys supported this hypothesis. More information is given in *Section 4.5.3*, which includes a possible explanation for this apparent homogeneity between the different soil layers. The ISOCS calibration model that was built for analysis of these results therefore assumed a single, homogeneous layer of 200 mm depth.

A second approach to depth profiling with *in situ* measurements is to attempt to infer radionuclide depths from the measurements themselves. Different methods of achieving this have been previously described, and a useful comparison of three of these methods is given by MacDonald *et al.* (1997). Two of the methods described in this study depend on the differential penetrating abilities of radiation with different energy levels through the attenuating overlying layers. The use of this property of radiation is the most common approach to interpretation of *in situ* measurements for depth profiling purposes. Other examples are cited in *Section 4.2.3*. The third method depends on making two consecutive measurements, but in one of these measurements part of the FOV of the detector is obscured by a circular lead plate. This obscures radiation from a definable area on a plane surface at right angles to the detector axis. The proportional difference between the obscured and un-obscured areas changes as the hypothetical plane is assumed to be at different distances from the detector. This effect can be used to estimate the depth of radionuclide activity (MacDonald *et al.*, 1997). The successful application of any of these methods depends on there being a uniform distribution of radionuclide activity at each depth within the ground area that is defined by an individual measurement. In the case where there is a heterogeneous distribution of activity on a small scale, these methods are likely to be limited in their ability to reliably infer the depths of small hotspots of activity that are at different horizontal and vertical positions with respect to the detector.

8.2.5 Establishing traceability and bias in *in situ* measurements

8.2.5.1 Bias against a reference measurement target (RMT)

The issue of providing traceability of *in situ* measurements of a ground area to a known reference source has already been discussed in *Section 7.4* (traceability of *in situ* measurements to a single point source is discussed in *Section 8.2.5.2*). Statistical analysis of the data from the RMT experiments described in *Section 7.4* showed significant differences between the means of the *in situ* and the *ex situ* measurements on the proposed site of the RMT. A significant bias of -25 % in the *in situ* measurements was suggested. This may be an overestimate, however, for the reasons discussed in *Section 7.4.5*. However, two basic assumptions that had been made about the proposed site itself were not supported by the results of the *ex situ* measurements. These assumptions were that radionuclide activity would be homogeneous across the area, and that the concrete was of sufficient depth. The practical problems that would be involved in constructing a site with these characteristics are considerable. Purpose built 'calibration pads' have been constructed for the calibration of both ground and airborne *in situ* measurements, but these are generally of limited size, e.g. 1 m^2 (Jones, 2012). Concrete pads of 3 m diameter and 500 mm thickness, spiked with known quantities of radionuclides, are available for the calibration of geological and environmental survey instruments at the Risø National Laboratory in Denmark (Potts, 2013). A possible approach to estimating the systematic uncertainty of a collimated detector would be to use a 3m diameter pad with the detector at very low level, thus limiting the sample volume to within the boundaries of the reference target (See *Section 7.3)* .

Wide area calibrations of airborne surveys have been carried out over sites which have first been characterised by *ex situ* methods (Tyler *et al.,* 1996b). These methods include a spatial weighting of the sampling pattern in order to be able to estimate expected mean values and random uncertainty levels at different detector heights. Ground-based *in situ* measurements are limited by practicality to detector heights of about 1.5 m. There would be an advantage to constructing or identifying a RMT of sufficient dimensions, with relatively homogeneous levels of radionuclide activity, and where the concentrations of radionuclides would be expected to change only by radioactive decay, and not any other process, over time. This would enable improved confidence in the use of calibration software such as ISOCS to convert raw activity counts to units of activity concentration. Additionally, this approach could provide a level of traceability to *in situ* measurements, and also improve confidence in the use of detectors that

have not been individually characterised, or for which a significant time period has elapsed since characterisation. Identification of such a site would need to be the subject of future work. Due to the problems of construction, such a site would most likely need to be a pre-existing area of land with sufficient levels of naturally occurring radionuclides, or of artificial radionuclides which can be determined to have been distributed uniformly throughout the area.

8.2.5.2 Bias against a reference point source

A single measurement was made of the activity of the field source (treated as a point source) during the field measurements described in Chapter 5. This was carried out with the detector at a height of 630 mm, and with the source placed on a hard, level surface, precisely on the detector axis. This measurement was then analysed using Genie 2000 software calibrated with an appropriate ISOCS geometry definition, and resulted in a reported activity level of 35.5 kBq. The ^{137}Cs source that was used in these experiments was subsequently characterised at the National Physics Laboratory (NPL), using a HPGe detector that was first calibrated with an NPL certified reference source with an activity level of 11.95kBq. Eight replicate measurements were acquired using a 90 second counting time. Uncertainty was estimated at 2 times the standard deviation of the eight measurements. The measured activity of the field source was found to be 40.6kBq +/- 1.5 %.

This indicates that there was a systematic error of -12.6 % between the measured counts and those predicted by ISOCS. This difference between measured counts using an ISOCS calibration and counts from a source with known activity is most likely a result of using a detector that had not been characterised for ISOCS use. Although a different detector was used in the RMT experiments (*Section 8.2.5.1*), it may also have been affected by systematic differences between the sensitivity of the detector and the sensitivity of the hypothetical “generic” detector that was used in the ISOCS geometry definitions.

Due to operational protocols at the case study site, it was not possible to use the same reference source to estimate the bias in the different detector that was used for the RMT characterisation and the Barrier 31 experiments. However, the response of this detector to a point source was investigated by measuring a small ^{137}Cs source of known activity (2.699×10^5 Bq) that was available on site. Bias between the measured counts (calibrated with an appropriate ISOCS geometry definition) and the known value in this case was estimated at -7 % (un-collimated) and -29 % (collimated). The latter figure appears to be approximately

consistent with the -25 % bias suggested by the *in situ* measurements (*Section 8.2.5.1*). This further suggests that the bias in the RMT experiments could have been a result of using a non-characterised detector. It also suggests that a significant bias might have been present in the *in situ* measurements obtained in Barrier 31. However, this finding must be treated with some caution, because a) the source that was used was not certificated; b) the bias was calculated from a single measurement of 5 minutes duration; c) the bias in measurements of a point source may be different from any bias that exists in measurements of activities from the much larger test volumes that are applicable in the case of land areas.

8.2.6 Systematic comparisons between *in situ* and *ex situ* measurements

One of the primary objectives of the Zone 12 and Barrier 31 field experiments described in Chapter 4 was to compare *in situ* measurements with *ex situ* measurements, in order to identify any systematic differences between areal means, and also between the measurement results at individual locations. An assumption that is often made in such comparisons is that measurements carried out on extracted soil samples in a laboratory are the most reliable (Ramsey and Boon, 2012). This is not without some justification, as these can be conducted in controlled conditions (e.g. at a standard temperature and humidity) and are performed by an accredited analytical method using equipment that is maintained, calibrated and verified in position. An additional factor for measurements of radiation is that background levels can be established on a regular (e.g. daily) basis, and influences from other man-made sources can be controlled. The detectors used in these experiments were calibrated using standard sample pots filled with soil, and spiked with a certificated mixed gamma source, providing a level of traceability to the measurements. Dry soil was used, that had been shown to have no significant content of the radionuclides of interest. This procedure will have introduced some uncertainty into the laboratory results, however, because the field samples were measured 'as received', and will therefore have had different internal characteristics from the reference sources (e.g. water content). Geometric uncertainties will also have been present in the air-spaces within the sample containers.

Potential problems with comparisons of measurements at individual measurement locations have already been discussed in *Section 4.5.3*. These arise due to the large differences in source geometry, and hence the masses of the primary samples, between the measurements obtained by the two methods. However, it might be expected that mean measurements over averaging areas would be comparable, providing sufficient measurements were obtained by

each method to give a representative picture of the site. In the Zone 12 and Barrier 31 surveys described in Chapter 4, statistical comparisons of the means were only possible after removal of single high measurements that were obtained in locations that were sampled judgmentally. Once these measurements were removed from the data, there were found to be no significant differences in either case. Inclusion of the judgmentally positioned measurements makes a substantial difference to the means of the *ex situ* measurements, because these were only obtained at 20 locations in each survey. In contrast, *In situ* measurements were acquired at 87 locations in Zone 12, and 121 locations in Barrier 31. The conclusion was that the *in situ* measurements gave results for site mean values that were not significantly different from those obtained by the soil sampling surveys. The difference in results between the two measurement methods at the outlying locations (*Section 4.5.3*) is explained as a combined result of the small-scale heterogeneity of ^{137}Cs activity, and the differences in source geometry (i.e. differences in primary sample mass).

Although no statistically significant differences were found between the means of the *in situ* and *ex situ* measurement sets in the Zone 12 and Barrier 31 surveys, taking the results presented in Tables 4.3 and 4.4, and Figs 4.6 and 4.7 into consideration along with the findings of the experiments to establish traceability discussed in *Section 8.2.5*, there is some combined evidence that the *in situ* measurements were underestimating *ex situ* measurements. This is indicated both at individual locations and over averaging areas, and also for measurements of the activity of a point source. For the field surveys and the RMT, this may be an artefact of the limitations of the experiments, e.g. the high random component of uncertainty in Zone 12 (42.6 % for *in situ*, 47.6 % for *ex situ*), and the rejection of critical assumptions about the nature of the RMT, as described in *Section 7.4*. It may also be that the laboratory measurements were over-estimated, due to differences in composition between the field samples and the manufactured reference sources. It is likely that some systematic error arose from the use of detectors that were not pre-characterised for ISOCS use, and that the gamma detectors used in these surveys were less sensitive than the generalised NaI 3”x3” detector definition that was used to generate the ISOCS efficiencies for calibration of the spectrum analyses. Finally, it could also be partly due to the types of detector that were used. The detector used in Zone 12 and in the experiments described in Chapter 5 was a temperature stabilised unit supplied by Canberra Industries Inc. In contrast, the detector used in the Barrier 31 and the RMT site (*Section 7.*4) was also supplied by Canberra, but was not of the stabilised type. It was noticed that this second detector was subject to considerably more channel drift during operation, with the result that ^{137}Cs peaks were noticeably wider than was the case

with the stabilised detector. Each spectrum was analysed individually and *post hoc* adjustments made to the energy calibration if it was seen that the peaks extended beyond the region-of-interest that had been defined for ^{137}Cs analysis. This was considered to be acceptable because no other peaks were identifiable near this region in any of the measurements, and levels of ^{214}Bi , which has an energy line at 609 keV, were not considered to be sufficient to have had a significant impact on the area of the 662 keV peaks from Barrier 31. The *post hoc* re-calibration procedure discussed above was not necessary in any of the Zone 12 measurements, which were made with a stabilised detector. The greater width of the peaks in individual measurements from Barrier 31 and the reference site may have had some effect on the peak area analysis performed by the Genie 2000 peak analysis software. It is possible that this resulted in an underestimate of activity levels. Ideally, a stabilised detector should be used for contaminated land surveys, and where possible, a recently characterised detector with a dedicated calibration file. This discussion of potential sources of uncertainty also emphasises the need for a method of testing *in situ* measurement results against a reference site with known activity levels (see *Section 8.2.5.1*).

8.2.7 Assessment of Fitness for Purpose (FnFP) of measurements

A method to assess whether measurements are fit for the purpose of describing large-scale geochemical variability was suggested by Ramsey *et al.* (1992). If the variance contributed by the measurement uncertainty was less than 20 % of the overall variance, then the measurements could be considered FFP. These percentages are summarised for both surveys in Table 8.3. According to these criteria, none of the measurements would be FFP in the Zone 12 survey, while only the Canberra *in situ* and the *ex situ* measurements for the 0-100 mm layer would be FFP in Barrier 31. This is an interesting result, as it may be expected that *ex situ* measurements would give more reliable results due to the much longer counting time (3 hours compared to 10 mins for *in situ*). However, the much higher sampling uncertainty for *ex situ* measurements, probably as a result of small scale heterogeneity of ^{137}Cs activity concentrations in the soil, pushes the overall measurement uncertainty above the 20 % threshold. The large mass of soil sampled by the individual *in situ* measurements reduces the sampling uncertainty to 0 % for Zone 12, and 10 % for Barrier 31. Using the same FnFP criteria in Barrier 31, the Canberra *in situ* measurements appear to be the most FFP for assessing variability in activity concentrations across the survey area. In Zone 12, the 10 minute counting time for *in situ* measurements was not sufficient to reduce the analytical uncertainty sufficiently, and resulted in measured activities that were very close to the MDA.

However, this approach to the assesment of FnFP is limited in scope. Both measurement methods used in Zone 12 showed that activity concentrations in all measurements, except the outlier at location E11 (Figs 4.2, 4.3), were only slightly elevated compared to the regional background, and all were below levels of regulatory concern. A more general approach to assessment of fitness-for-purpose of measurements has been suggested, in which minimisation of the combined economic losses due to the missclassification of contamination and the cost of measurement is the target criterion (Thompson and Fearn, 1996). A proposed method of achieving this criterion for high-coverage *in situ* surveys has been described in Chapter 6 and further discussed in *Section 8.3*.

Table 8.3 Components of measurement uncertainty expressed as percentages of the total site variance.

		Contribution to total variance (%)		
		Sampling	Analytical	Measurement
Zone 12	Canberra *in situ*	0	80.3	**80.3**
Detector height	Exploranium *in situ*	54.0	46.0	**100**
= 280mm	*Ex situ* 0-10 cm	34.1	14.2	**48.2**
	Ex situ 10-20 cm	54.6	5.0	**59.6**
	Ex situ 0-20 cm	43.7	18.7	**47.4**
Barrier 31	Canberra *in situ*	0.5	0.3	**0.8**
Detector height	*Ex situ* 0-10 cm	12.6	0.2	**12.8**
= 920mm	*Ex situ 10-20 cm*	43.9	0.1	**44.0**
	Ex situ 0-20 cm	33.2	0.2	**33.4**

8.2.8 Standard error on the mean

The standard error on the mean (**SEM**) for the Zone 12 and Barrier 31 surveys has been calculated (Table 8.4) in order to compare the number (and therefore cost) of *ex situ* measurements required to match the performance of the *in situ* measurements. The SEM for *in situ* measurements made with the Canberra 3”x3” NaI scintillation detector have been calculated in two different ways. Firstly, the SEM has been calculated from the complete measurement datasets for both surveys (88 measurements in Zone 12, and 122 measurements in Barrier 31), using the formula:

$$SEM = \frac{Standard\ Deviation}{\sqrt{Number\ of\ measurements}}$$

For comparison, the SEM has also been calculated based on the measurements that were acquired at the same locations as the *ex situ* measurements. The column on the far right of Table 8.4 shows estimates of the number of *ex situ* measurements (*N*) that would be required

to achieve the same SEM as obtained by the corresponding *in situ* measurements. This calculation assumes that the variance in the *ex situ* measurements remains the same with increasing (or decreasing) *N*. It can be seen that in both surveys, achieving the same SEM as was obtained by the full set of *in situ* measurements would be likely to require a comparatively large number of soil samples (68 in the case of Zone 12, 405 for Barrier 31). This number is likely to be an overestimate, because the variance between the *ex situ* measurements might be expected to decrease as *N* increases above 21 (Zone 12) and 20 (Barrier 31), as it does for the *in situ* measurements.

Table 8.4 Calculation of the standard error on the mean (SEM) for the Zone 12 and Barrier 31 surveys. Values for *in situ* measurements are calculated for the complete measurement set and also for the measurements acquired in the same location as the *ex situ* samples. The right hand column shows an estimate of the number of *ex situ* measurements that would be required to obtain the same SEM as the *in situ* measurement SEMs, assuming that the standard deviation does not change with different numbers of measurements.

Survey	Measurement type	Number of measurements	Standard Deviation Bq g^{-1}	SEM Bq g^{-1}	*Ex situ* N required for SEM
Zone 12	*In situ*	88	0.0153	0.0016	68
	*in situ**	21	0.0239	0.0052	7
	Ex situ	21	0.0134	0.0029	
Barrier 31	*In situ*	122	0.3502	0.0317	405
	*in situ**	20	0.4411	0.0986	42
	Ex situ	20	0.6377	0.1426	

* *In situ* measurements acquired on the ex situ measurement locations

When the estimation of *N* is based on equal numbers of measurement locations, only one third (7 out of 21) of the original *ex situ* measurements would be required in Zone 12, whereas twice as many (42 instead of 20) would be required in Barrier 31. This is a result of the larger small-scale heterogeneity of contaminants in Barrier 31, as indicated by the higher levels of sampling uncertainty for both measurement methods (Table 4.2), and also the greater spatial variation in activity concentrations throughout the Barrier 31 area (see Figs 4.2 and 4.3). A rough approximation of the cost of an *in situ* measurement, based on a 20 minute counting time + 5 minute setup time at £0.50 per minute, plus £2.00 per analysis (Table 6.2) results in a total cost of £9.50 per measurement. Applying this estimate to the data in Table 8.4 results in an estimated measurement cost of approximately £200 for 20-21 *in situ* measurements. The cost of a gamma-spec measurement of a soil sample in the Dounreay laboratory has been estimated at ~£65.00 per sample. So for comparison, the costs of *ex situ* measurements can be estimated as ~£430 for the 7 measurements in Zone 12, and ~£2700 for the 42 measurements in Barrier 31.

8.2.9 Summary of comparison between *in situ* and *ex situ* measurement methods

The relative effectiveness of *in situ* and *ex situ* measurement methods has been discussed in some detail in *Section 8.2* so far, and also in parts of Chapter 4. A traditional view for geochemical measurements is that *ex situ* measurements made in the laboratory are more reliable, however it has recently been argued that *in situ* measurements may be more FFP in some circumstances (Ramsey and Boon, 2012). When applied to the remote detection of gamma emitting radionuclides in land areas, the principal differences between the two measurement methods could be summarised as follows: *Ex situ* measurements are made in controlled conditions on known volumes of material from discretely definable locations, but sample sizes are small and they do not provide any information about the material between the measurement locations; *in situ* measurements are made in environmental conditions on assumed test volumes with assumed depth profiles. In this case the sample sizes are relatively large, and potentially large enough to enable full coverage of a site area. This suggests that *in situ* measurements are capable of giving a more representative picture of the nature and extent of contamination, providing the necessary assumptions are reliable.

These differences in the characteristics of the different measurement techniques imply that neither method is likely to be solely preferable in most surveys of contaminated land. A combination of the methods will be required in most cases in order to perform a characterisation that can give a representative picture of the site with confidence. There is a general imperative to minimise the number of samples that require laboratory analysis, because of the increased costs and turnaround times that are associated with these types of measurements. However, sufficient *ex situ* measurements need to be acquired in order to have confidence in the calibration models that are used to interpret the *in situ* measurements, particularly with respect to the depth profiling of contaminants. An ideal situation could be considered one in which both types of measurements are obtained on the same systematic survey grid. This enables comparisons to be made between the mean activity concentration levels estimated by the two methods. If these are found to be significantly different, then the reasons for this can be further investigated. *Ex situ* measurements may also be used in a targeted way, to investigate anomalous results from an *in situ* survey, or in areas where the *in situ* measurements may have been affected by radiation shine from external sources. *Ex situ* measurements will be needed to characterise activity at depths of more than 500 mm, and they may be the most practical method of detecting activity from depths of more than 200

mm. This makes the assumption, however, that any areas of elevated activity are sufficiently large that there is a high probability that they will be identified by the *ex situ* sampling regime.

However, the remote detection of gamma radiation by *in situ* methods confers a considerable advantage over the use of *ex situ* methods on land areas. *In situ* measurements are significantly less affected by sampling uncertainty than *ex situ* measurements, particularly in areas which are affected by high small-scale heterogeneity of contaminants. High coverage or full coverage surveys are made possible, and this is highly advantageous to the detection of small hotspots of activity, which are very likely to be missed by a systematic soil sampling protocol. Further work to identify suitable reference measurement targets (RMTs) would enable greater confidence in the use of *in situ* measurements for the estimation of average activity concentrations. The optimisation of full coverage *in situ* surveys for the purposes of hotspot identification with known confidence levels is the subject of the next section.

8.3 Optimising the survey parameters of *in situ* investigations

Section 8.3 addresses Objective 2. It further describes some of the assumptions and limitations of the generic models that were tested in Chapter 5, and the application of these to the ROCLI method as described in Chapter 6. The outputs from the optimisation examples in *Section 6.4*, in particular the overall survey times and probabilities of particle detection, are used to discuss the advantages and disadvantages of using portable *in situ* gamma detectors instead of the Groundhog vehicle mounted system.

8.3.1 Overview

It has previously been stated that the remote detection of gamma radiation by *in situ* measurements enables full coverage of a land area. The term ‘full coverage’ has been used here to describe the case where measurements are made in such a way that every part of the ground surface is contained within the FOV of the detector in at least one measurement. This is important for particle detection, because although a significant proportion of the detector response arises from radiation that is received through the walls of the collimator (see *Section 7.2*), the radiation from a particle within the nominal FOV of the collimator will result in a higher detector response than radiation from a particle of the same activity that has to pass through a thickness of lead. The concept of full coverage as used here applies to the ground surface, and does not extend below the surface of the ground without methods such as described in Chapters 5 and 6. These are used to quantify the amount of radiation that would

reach the detector from the minimum activity source at the greatest depth that is expected to be encountered in an investigation. The ROCLI method assumes that full coverage at the ground surface will always be required, and the counting time needed to identify the existence of such a particle is then calculated for various different detector heights. Clearly, there would come a point at which the target particle activity is so low, or the depth so great, that the calculated counting time would be too long for practical purposes. In this case the use of a detector with greater intrinsic efficiency, or alternative methods such as ground scraping to further reduce the detector height, would be required.

Approximately 9.3 % of incident radiation normal to the external surface of a collimator wall will pass though a 20 mm thickness of lead (*Section 7.2.1*). This means that in a full coverage survey, if a single measurement contains a particle of elevated activity wholly within the FOV of the collimator, then adjacent measurements will also show activity levels that are elevated compared to the mean background. The same pattern of measurements could, however, also arise if a larger hotspot of diffuse activity were present, centred on the location of the highest measurement. More detailed investigation in and around this location will be required in order to determine the source of the raised activity levels. This could be carried out by a number of means, but typically a first step would be to perform a scanning survey in and around the area to determine if a high activity particle is present. If no particle is found, then a logical next step would be to conduct a systematic high resolution survey, using an *in situ* detector at low level (see *Section 7.3*). This could be backed up by *ex situ* measurements of extracted soil samples. The objectives would be to delineate the area of raised activity, and to determine the spatial profile of activity concentrations within the area, in order to decide whether remedial action is necessary.

The different circumstances under which a particular pattern of measured results may arise leads to a point that needs some clarification. The ROCLI method described in Chapter 6 is not intended as a definitive approach to particle hunting. Application of the method should enable the optimal identification of any particles within the site area with the stated confidence levels, providing the mean and variance of the local site background have been estimated with sufficient accuracy, and both are reasonably constant throughout the site area. This also assumes that any individual measurements that are found to be above the decision level (calculated by the method) will be investigated. However, measurements obtained in a systematic survey need to be interpreted in relation to each other. This can either be achieved by experienced judgement, or by the use of statistical methods such as Moran's I (Anselin,

1995). Other statistical methods, such as those described on pages 36-37 of Rose *et al.* (1979), can be used to separate anomalous samples from a background distribution. The purpose of the ROCLI method is to estimate settings of optimal experimental parameters, i.e. the detector height, measurement spacing, and counting time, that will enable particle detection against the local site background.

8.3.2 Modelling the effects of experimental parameters

The field experiments described in Chapter 5 were performed in order to investigate the relationships between detector response and three variables of the source/detector geometry: detector height, lateral offset of a particle from the detector axis, and particle depth beneath the ground surface. Calibration software such as ISOCS can be used to calculate detection efficiencies for any combination of these parameters, however doing so would require an ISOCS geometry definition to be built for each scenario. The use of the newly identified set of generic mathematical models to describe these relationships is therefore potentially advantageous to the development of methods for optimising the measurement parameters of a survey. These measurement parameters can be defined as a) detector height; b) measurement spacing; c) counting time.

The mathematical model used for detector height is simply the well known inverse-square relationship. This is a sufficient approximation for ground-based detectors, where the air space between source and detector is too small to make any significant difference due to attenuation of gamma radiation by air. The depth model is based on a more complex mathematical approach, described in *Section 5.2.4*. The model for lateral offset can be derived either from field measurements, or from ISOCS estimates of the **absolute efficiencies** of the detector, for a range of lateral offsets (10 were used in Chapter 5) and at a single detector height. This enables a single model to be defined of the relationship between detector response and the offset of a particle from the detector axis. Although it would be possible to derive a complex mathematical model for this relationship from first principles, it would differ for every detector/collimator configuration. It would also fail to take into account individual properties of a particular detector. An overhead of the approach that has been used is that an individual lateral offset model needs to be defined for every combination of detector and collimator. If this were done using ten ISOCS geometry definitions (as described in Chapter 5), then it could be achieved in a relatively short period of time (e.g. less than 2 hours). However, a potential drawback of using ISOCS to define the lateral offset model is that any bias between

expected counts that were inferred from ISOCS detection efficiencies and the actual counts would be included in the detector count predictions. In the experiments described in Chapter 5, a detector was used that had not been individually characterised for ISOCS. This is considered to be typical of the type of detector that would be used in investigations of land areas on nuclear sites. The experimental bias between measured source activity and the true source activity was estimated at -12.6% (*Section 8.2.5.2*).

The principle objective of the field experiments described in Chapter 5 was to test the generic mathematical models against measurements obtained from field experiments, and also against predictions of detector counts that were calculated from detection efficiencies generated by ISOCS. In order to achieve the second of these, ISOCS geometry definitions had to be built for every combination of the source/detector geometry variables (height, lateral offset and particle depth). An element of uncertainty would have been introduced by random errors in the convergence procedure used by ISOCS to estimate the detection efficiency of each geometry. Other potential sources of uncertainty in the field experiments, particularly relating to variable particle depths, have been described in *Section 5.2.5*. The counts predicted by the generic models were found to be reasonable approximations of the experimental results, and good approximations of counts predicted by ISOCS. The lack of a closer agreement between the ISOCS predicted counts and the measured counts is presumed to have been largely a result of the use of a non-characterised detector in the field experiments.

8.3.3 Optimisation of *in situ* surveys using the ROCLI method, and comparison with other methods.

The ROCLI method (Chapter 6) was developed into a computer program with the objective of optimising the experimental parameters (detector height, measurement spacing and counting time) that would enable particle identification within the FOV of a collimated detector used in a full coverage survey. Estimates of the mean background levels and variance are required in order to use *Equation 6.8* to calculate the counting time necessary to locate a particle of pre-defined activity and depth that is randomly positioned within the coverage square (see *Section 6.3.2*). The probabilities of false measurements, i.e. of false positive or false negative errors, can either be fixed at pre-defined levels, or entered as ranges of possible values. The optimal scenario is identified as the one which results in the lowest cost, which can be defined either as the measurement cost, or as an expectation of financial loss. The latter includes estimates of the probabilistic costs of making incorrect decisions as a result of false measurements.

The ROCLI program includes an option to graphically illustrate the changes in measurement cost or expectation of loss with changing survey parameters. Due to space limitations, this was not included in the paper for publication (Chapter 6). Sample graphics for two of the scenarios reported in Table 6.4 are shown in Fig 8.1.

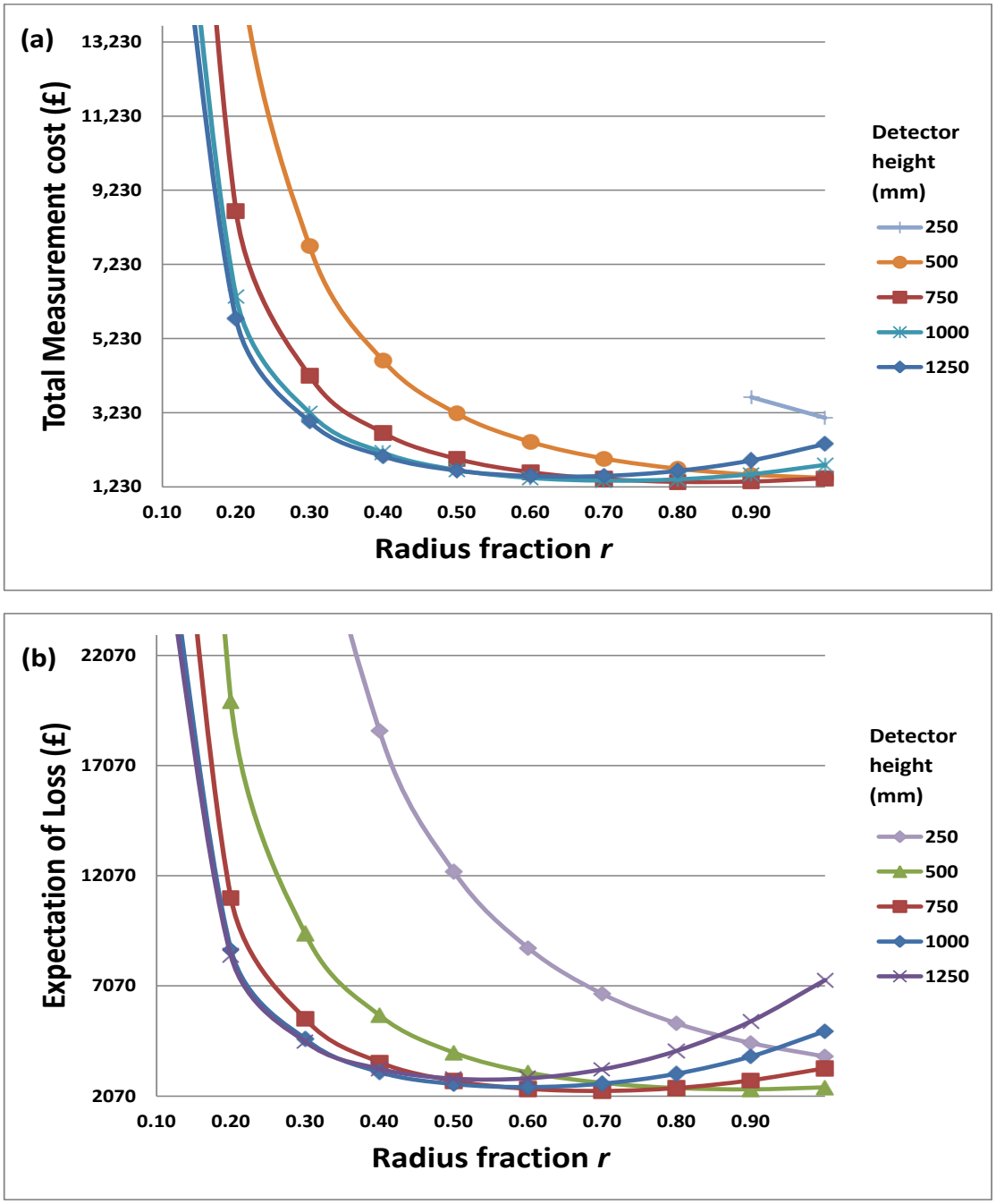

Fig 8.1 Graphic representation of ROCLI optimisation, for Area 1 with a particle depth of 100 mm (See Table 6.4). Fig 8.1a shows the optimisation for minimum measurement cost, Fig 8.1b shows the optimisation for minimum expectation of loss. In each, the five detector heights used in the optimisation program are represented by different lines, plotted against increasing radius fractions. The curve for detector height = 250 mm in Fig 8.1a is incomplete because the program rejects scenarios which result in a measurement counting time of less than 10 seconds.

The scenarios represented in Fig 8.1 are for Area 1 (*Section 6.3.1*), with a particle depth of 100 mm, and for optimisation by minimum measurement cost and minimum expectation of loss. In both cases the optimum detector height was found to be 750 mm, however in the optimisation by expectation of loss (Fig 8.1b) the optimum radius fraction is lowered resulting in a reduced measurement spacing (743 mm compared to 849 mm for optimisation by measurement cost). The counting time is also doubled from 303 s to 605 s (Table 6.4).

A limitation of the method, as it has been applied in the computer program described in Chapter 6, is that counting times and costs are only calculated for fixed values of detector height and measurement spacing. These are defined by the user as ranges of values. The examples in Chapter 6 were optimised for detector heights in steps of 250 mm, and for measurement spacings that were calculated from divisions of 1/10 of the lateral offset. In real surveys, a tripod or trolley with an infinitely variable detector support might be available. It is possible to use repeat runs of the ROCLI optimisation to converge on an optimisation for these parameters down to the nearest centimetre or less, if desired, although this would be a somewhat laborious process. It would also be possible to automate the convergence, either through the development of appropriate algorithms, or by modifying the program to use an iterative method of converging on the optimal scenario. This would have to be the subject of future work.

The example optimisations described in *Section 6.4* are intended to illustrate the outputs of the ROCLI program. They are based on background levels from two surveys that were conducted at the case-study site. The survey identified as *Area 1* was the Zone 12 area already described in *Section 4.3.1*. *Area 2* was on an unused field where an *in situ* survey had been carried out using a 3” x 3” NaI scintillation detector fitted with a 90 degree 20 mm collimator at a height of 920 mm. Using an assumed survey size of 100 m^2, the overall survey times estimated for the scenarios with the minimum measurement costs for a particle of 100 kBq at 100 mm depth were 16-17 hours (Table 6.4). These are long periods of time in comparison to the use of vehicle mounted detector arrays in scanning surveys, such as the Groundhog system.

This is primarily because of the much larger detector volume that is possible with the Groundhog vehicle. The capacity of the 3” x 3” detector used to estimate the background levels in *Area 1* and *Area 2* equates to a detector volume of approximately 0.06 litres. In

contrast, the Groundhog beach monitoring system uses an array of five horizontal NaI detectors, each with a capacity of 0.3 litres.

An evaluation study of the Groundhog vehicle-mounted system has determined that a forward scanning speed of not more than 1.2 ms^{-1} is required to locate a 100 kBq particle at a depth of 100 mm with a 95 % confidence level (SEPA, 2005). The detector array spans a total width of 2 m, and so a full coverage survey of 100 m^2 (as assumed in the ROCLI examples) would be achievable in a few minutes once the machine was on site. The example optimisations quoted for the portable NaI detector are based on a probability of obtaining a false negative that is equal to 1 %, which is lower than the 5% probability of the Groundhog system. Further optimisations at an input probability of 5 % reduce the estimated survey times from 15-17 hours to ~11 hours for both *Area 1* and *Area 2*.

The decision of which is the most cost effective method (or combination of methods) to use in the characterisation of radioactively contaminated land in general depends on the objectives of the survey, and also on the relative costs and practicalities of the various methods. An advantage of the use of *in situ* detection with portable collimated detectors is that the measurements obtained can be used to provide reliable estimate of average activity concentrations across the site, or within defined averaging areas. This is not readily achievable by scanning surveys, which are carried out specifically for the purpose of hotspot detection. However, the large time differentials between using a vehicle mounted system and a portable collimated detector may make a combined approach more cost effective. For example, a portable *in situ* detector could be used to estimate mean values across the site using statistical methods such as described in chapter 5 of the MARSIM guide (USEPA, 2000b). Hotspot detection could then be achieved using the Groundhog system with overlapping coverage swathes (SEPA, 2005). This combined approach may be the most cost-effective in many situations, however it depends on a) the required probability of particle detection being achievable by the scanning survey - A 95 % probability of particle detection is specified in the Groundhog Evaluation Report (SEPA, 2005); b) the site is accessible and the terrain is suitable for operation of the Groundhog vehicle. In situations where these criteria cannot be met then an optimised, full-coverage survey as described in Chapter 6 may be the most suitable option, and is capable of fulfilling both of the objectives that are required in order to determine whether remediation is necessary (*Section 2.2.4*).

Costs of investigations are recognised in the MARSSIM guide, but are considered to be outside the scope of the methodologies used there (USEPA, 2000b). The ROCLI method provides an option to optimise experimental parameters by the minimum expectation of financial loss, and this was used to evaluate the fitness-for-purpose of the measurements (See *Section 6.3.5*). This method calculates the probabilistic consequential costs of obtaining false positive and false negative results in order to also optimise the probabilities of these errors occurring. The probabilistic cost of false positives can be realistically calculated, simply by multiplying the probability of a false positive per measurement by the number of measurement locations, and then multiplying the result by the cost of "following up" on a positive measurement and determining that no further action is required (*Equation 6.10*). Calculating the probabilistic false negative cost is a far more complex issue, because the probability of particle existence is not known *a priori.* The ROCLI method is based on the conservative assumption that a particle is present in every measurement. *Equation 6.11* is then used to calculate the probability that at least one particle will be missed throughout the entire survey area, and this is multiplied by the user defined cost of a false negative. Clearly, this approach has limitations, because it makes an implicit assumption that the total number of particles present throughout the survey area is dependent on the number of measurements. If in practice this number of particles were actually present in the survey area, then an estimate of the local site background that was based on site measurements would be too high for reliable particle identification, and some other means of establishing background levels would be needed. Other methods of estimating false negative costs need to be considered in future work.

In both areas for which the optimisations were carried out, the optimal probability of false negative errors was reduced from 10^{-2} to 10^{-5} (0.001 %), when optimisations were based upon minimum expectation of financial losses. These scenarios result in an increase in the overall survey times by a factor of approximately 2.5, but with a corresponding 95 % reduction in the expectation of losses, from approximately £39,000 – £45,000 to approximately £2,300 - £2,500.

The probabilistic cost of false negative errors for a particle at 100 mm depth was calculated to be £897 in both areas, for the optimum scenarios. This number was added to the probabilistic costs of false positive errors and the measurements costs in order to obtain the total expectations of losses quoted in Table 6.4. For comparison, the same estimation of the probabilistic cost of false negatives (*Section 6.3.5*) can also be applied to a hypothetical

Groundhog vehicle survey of a 100 m^2 area, where measurement costs can be estimated at £5.00 - £20.00 plus mobilisation (Heathcote, 2013). The parameters defined in the Groundhog evaluation report are as follows (SEPA, 2005):

Width of detector = 2 m
Scanning overlap between swathes = 0.3 m
Ground speed = 1.2 m
Counting time interval = 1s
Probability of particle detection per measurement = 0.05 (100 kBq at 100 mm depth)

From these parameters, the number of measurements obtained in a 100 m^2 area can be estimated:

$100 / ((2 – 0.3) \times 1.2) = 49$ measurements

Applying *Equation 6.11*, the probabilistic cost of false negative errors can then be calculated using the same cost of a false negative per site of £50,000 that was used in the ROCLI optimisations (See *Section 6.3.5*):

$£50{,}000 \times (1 – (1 – 0.05)^{49}) = £45{,}950$

This cost estimate, which is much higher than the £897 that was estimated for the optimum scenarios using the portable collimated detectors, is partly a result of the stringent approach used by the ROCLI method in determining the probabilistic cost of a false negative measurement. However, it suggests that if the location of particles is a high priority, then the use of portable, stationary detectors that are set up to record for a pre-determined counting time in an optimised survey strategy, may have an overall cost advantage over Groundhog surveys that are carried out at a speed of 1.2 ms^{-1}. Hand portable Groundhog scanning surveys (i.e. not vehicle mounted) do not reliably provide confidence levels of 95 % of particle detection (SEPA, 2005).

Using this method of calculating the expectation of financial loss for small particle detection cannot be readily applied to the case of *ex situ* measurements, because in this case a full coverage survey is practically unachievable. Assuming a sampling tool with a diameter of approximately 10 cm, the area covered by each measurement would be less than one hundredth of a square metre. So even in the case of a very high density survey, e.g. where 1 soil sample is acquired in every square metre, the probability of missing a small particle of activity contained within the survey area would approach 100 % using *ex situ* methods. The

probabilistic cost of a false negative measurement based on the criteria used above would then be ~£50,000.

8.4 Discussion of the findings of this project in a broader context

The work that has been presented so far has centred on the detection of the gamma-emitting radionuclide ^{137}Cs in areas of uncovered ground with a soil layer extending to at least 100-200 mm. This was considered to be the most useful approach to gathering data in the field experiments, because ^{137}Cs contamination is widely encountered in this situation as part of the contamination inventory at nuclear sites (See *Section 4.2.3*). Also, its presence can be inferred from gamma emissions at a characteristic energy level from its short-lived progeny ^{137m}Ba. It was therefore possible to obtain a larger number of both *in situ* and *ex situ* measurements than would have been achievable had the target radionuclide been less frequently encountered, or had required a more expensive measurement method. Caesium is also well retained by micas and clays in the soil matrix, and has a relatively long half-life (about 30 years) and so is likely to still be detectable in soil for several decades following deposition.

It is assumed that the main conclusions of Chapters 4, 5, 6 and 7 will be broadly applicable to investigations for other target radionuclides that can be identified by gamma spectroscopy. However, the different spectral peaks that are used to identify them vary considerably in their energy levels. For example, ^{241}Am (a progeny of ^{241}Pu) is identifiable by a gamma energy line at 59.5 keV, whereas characteristic energy lines for ^{60}Co exist at 1173 keV and 1332 keV. The degree of transmission of gamma energy through absorbing media such as soil, concrete or air is energy-dependent, and so the actual sample volumes (and hence sample masses) of *in situ* measurements will differ between different radionuclides. This would result (for example) in different dimensions of the sample mass for ISOCS interpretation as described in *Section 7.2.* The ROCLI method (Chapter 6) depends on a characterisation of a specific detector at a specific energy level, obtained either through experiment with a known source, or by using ISOCS efficiency estimates, again at specific energy levels. Re-calculating the example scenarios shown in *Section 6.4* would result in longer survey times if the target were ^{241}Am, and shorter survey times if it were ^{60}Co. The levels of heterogeneity of contamination may also be different for radionuclides other than ^{137}Cs. It was found that ^{137}Cs exhibited significant levels of heterogeneity over relatively small spatial scales. This was estimated using the relative standard deviation of the sampling duplicates, for example an RSD_{samp} % of 21.8 % was found

in the *ex situ* measurements in Barrier 31, where the sampling duplicates were separated by 0.13 m (*Section 7.3.4*). It has been implied that there may be a significant advantage to the use of *in situ* measurements for the estimation of mean activity concentrations and the identification of particulate activity (*Sections 4.5.3, 4.5.5* and *4.5.6*). The applicability of this finding to other radionuclides will be partly dependent on their degree of heterogeneity in contaminated areas. This would be expected to depend on a combination of the method of deposition, and also on the degree of retention by components of the soil or other media in which they have been deposited. This work provides a generalised method of evaluating that heterogeneity (described in *Section 2.3.5*) which is relatively easy to apply, however its applicability to other radionuclides in contaminated land areas, and also the evaluation of heterogeneity using *in situ* methods, would need to be the subject of future work.

It also needs to be stated that some radionuclides are not practically identifiable by gamma spectroscopy, due to the fact that they are not themselves gamma-emitters, or they lack a short-lived gamma emitting progeny in a convenient part of their decay chain. In these cases, *in situ* field measurements are not generally practical. An exception to this is where high-energy beta emitters produce beta-particles with sufficient energy that they can be detected (in sufficient numbers) by large-area beta detectors that are placed very close (~ 10 mm) to a prepared soil surface. This method has been used to measure activity levels of the alpha-emitter ^{238}U, from the high-energy beta emissions of one of its progeny radionuclides ^{234}Pa (EA, 1999). It should be noted that the presence of high energy beta-emitters would lead to **Bremsstrahlung** radiation being detected by a lead-collimated detector that was placed very close to the beta source (as could potentially occur in the experimental setup described in *Section 7.3*). This would have the effect of increasing the background continuum, especially at lower energy levels, and so make it harder to resolve peaks of interest, particularly at the lower energy levels, e.g. at 59.5 keV for ^{241}Am. Other beta-emitters that could be encountered in contaminated land areas include ^{90}Sr and Tritium (^{3}H). Measurement of these would need to be carried out after chemical processing of soil samples in a laboratory (EA, 1999). The methods that have been described in *Sections 2.3.4* and *2.3.5* could usefully be applied in order to understand how the uncertainties in such measurements affect inferences that are made about the concentrations and distributions of these contaminants, and the potential impact that these uncertainties have on subsequent decisions making. Relatively complex laboratory procedures are required to chemically extract some beta-emitters, which increases the measurement costs. When alpha-emitting radionuclides are the target, then the measurement cost can greatly increase, e.g. up to ~£1000 per sample (Heathcote, 2013), due

to the processes needed to quantify activities of these low-penetration particles. It is suggested that the use of the new unbalanced robust ANOVA method that is described in Chapter 3 will be particularly applicable to quantifying uncertainty and *in situ* heterogeneity in a cost-effective way for these types of investigations. This is because the number of additional measurements required for uncertainty estimation is reduced by one third, compared to the number required for the previously published balanced design.

Investigations of the radionuclide content of land areas that have been covered by concrete or tarmac may also be required. A common example of this type of investigation on a decommissioning nuclear site is the need for characterisation of the floor space of a condemned or demolished building. If the building has not been demolished, or is surrounded by other structures, then it may not be possible to use vehicle mounted systems, and the use of hand-portable detection equipment may be the only method of obtaining *in situ* measurements. The general principles of uncertainty estimation and the findings described in this thesis in relation to the suitability of the different measurement methods are assumed to apply equally to the characterisation of hard standings. A potentially important difference between such surveys and surveys on uncovered ground areas would be an increased cost of the acquisition and analyses of the *ex situ* samples, which would be in the form of concrete cores. This will clearly be highly dependent on the available facilities and procedures at individual sites. Example costs from previous surveys are give here as a cost of concrete core extraction of ~£1500 per metre length, and an analysis cost of ~£200 per sample, compared to estimated costs of £10 for extraction of a soil sample and £60-£70 per gamma-spec analysis in the on-site laboratory.

During the course of this project (not reported elsewhere in this thesis), a concrete floor slab was investigated by personnel at the case study site, using a combination of *in situ* measurements and *ex situ* methods. Uncertainty was estimated for the *in situ* measurements, using the duplicate method with a balanced design (See *Sections 2.3.4* and Fig 3.1). The *in situ* survey was carried out using the same detector configuration and measurement spacing as was used in the Barrier 31 survey (Table 4.1), i.e. with a NaI 3”x3” detector with 90 degree collimation, at a detector height of 920 mm and 1300 mm measurement spacing, although a shorter counting time of 30 seconds was used. The expanded relative uncertainty for *in situ* measurements of ^{137}Cs was then estimated at 47 %, and was composed entirely of analytical uncertainty. The uncertainty for other target radionuclides (^{235}U, ^{228}Ac, ^{60}Co) was estimated to be much higher (over 250 %), however the counts obtained for these radionuclides were less

than 33 % of the MDA reported by the spectrum analysis software (Genie 2000, using the Currie MDA algorithm) in every measurement. The high analytical uncertainty in the *in situ* measurements of ^{137}Cs suggest that a longer counting time would have been needed to obtain a reliable characterisation of the spatial distribution of this radionuclide. This preliminary experiment demonstrates the broader applicability of the techniques that are described in the thesis to media other than soil.

Chapter 9 – Conclusions and recommendations for further work

9.1 Introduction: innovative aspects of this research

Below is a brief summary of the new findings from this research (described in more detail in *Section 9.2*):

1. Estimates of the random components of measurement uncertainty were made using a published empirical method on measurements from two radioactively contaminated land areas. These estimates include the contributions from the sampling as well as the analytical processes. The first of these areas (Zone 12) had been chosen to be representative of an area with low levels of contamination, while the second area (Barrier 31) was known to have moderate contamination levels. To the author's knowledge this is the first time that an empirical method of uncertainty estimation, which also accounts for sampling uncertainty, has been used on land at a decommissioning nuclear site.
2. Empirical estimates of the random component of analytical uncertainty in the *in situ* measurements were found to be 2-4 times higher than that which would be expected from Poisson counting statistics.
3. Measurement results from two surveys indicate that contamination by ^{137}Cs was highly heterogeneous on a relatively small scale in these areas (e.g. RSD_{samp} = 21.8 % on a scale of 0.12 m, measured from *ex situ* duplicate samples). This finding applies both to contamination that is thought to have arisen from aerial deposition from authorised discharges (Zone 12), and also from historic leaks and spills (Barrier 31). Measurements from a high-resolution *in situ* survey also indicate significant heterogeneity at a very small scale (<= 25 mm).
4. The systematic component of uncertainty in measurements made *in situ* was estimated by comparing individual and mean values to the results of *ex situ* measurements. Additionally, an area was chosen as a reference measurement target (RMT) for *in situ* measurements, where estimates of activity concentrations across the RMT were compared to a nationally traceable gamma standard source.
5. A refinement to an existing method of estimating the random component of measurement uncertainty has been developed using an unbalanced design, which enables these estimates to be made at reduced cost. This was applied in the high density survey experiment described in *Section 7.3*.

6. A generic mathematical method has been derived that enables estimation of the detector response to a buried particle at different positions with respect to an *in situ* detector, once an initial characterisation of the detector has been carried out for a limited number (e.g. 10) measurements or modelled estimations of the response for different source/detector offsets. This has been shown to give predictions that are very good estimates of those obtained by time-consuming, detailed geometry modelling.
7. A new method (ROCLI) for optimising *in situ* investigations of land areas has been designed. This enables *in situ* surveys of land contaminated by small hotspots of gamma-emitting radionuclides to be conducted with optimal settings of the experimental parameters. These optimised settings are intended to minimise the costs incurred, which could either be the measurement costs only, or the measurement costs plus the projected overall costs of an investigation. Example optimisations have been produced for two case-study sites.
8. Evaluations of the fitness-for-purpose of the measurements have been made, based on minimised costs, in order to compare the relative effectiveness of the different measurement methods.

Detailed conclusions are presented below, followed by recommendations for future research work that have been identified from consideration of the findings. Where applicable, the title of each section specifies the relevant research objective from *Section 1.2.2*.

9.2 Estimates of the random component of uncertainty. Effects of contaminant heterogeneity

(Objectives 1a, 1c)

There is a considerable body of evidence from two surveys (Zone 12 and Barrier 31, Chapter 4) that suggests significant *in situ* heterogeneity of the target radionuclide (^{137}Cs) in these areas. Firstly, this is suggested by the high levels of the random component of sampling uncertainty in the *ex situ* measurements. The expanded relative sampling uncertainty was estimated for the 0-200 mm soil layer at 43.6 % in Zone 12 and 72.5 % in Barrier 31. In contrast, the sampling uncertainty in the *in situ* measurements was estimated at 0 % in Zone 12 and 10.2 % in Barrier 31. The large difference in sampling uncertainty between the two measurement methods is likely to be a result of the different masses of the primary samples. *Ex situ* soil samples had a combined average mass of approximately 0.5 kg for a soil depth of 0-200 mm. This is

compared to a total soil mass of 40 kg (Zone 12) and 269 kg (Barrier 31) that was defined by the FOV of the collimator to a depth of 200 mm in the *in situ* measurements, based on a soil density of 1.6 g cm^{-3}. This greater mass potentially results in an averaging out of some of the small-scale heterogeneity that has been shown to be present. However, it has been seen that the total soil mass from which emitted radiation causes ~95 % of the detector response is very much larger, due to transmission of radiation through the components of the collimator. This total mass has been estimated to be up to ~160 tonnes in these experiments.

Further evidence of heterogeneity of contaminants is provided by the results of *in situ* measurements that were made with a detector positioned very close to the ground surface. Sampling uncertainty for the Exploranium detector used in Zone 12 was estimated at 34.5 %, and a sampling uncertainty of 17.5-20.5 % was estimated for the high resolution (0.25 m spacing) survey in Barrier 31 (*Section 7.3*). In the latter case, comparisons between the random components of analytical uncertainty estimated using the balanced design with those estimated using the unbalanced design also suggest heterogeneity on a very small scale (<=25 mm).

In both surveys, the random component of analytical uncertainty was found to be higher in the *in situ* measurements than in the *ex situ* measurements. This is to be expected, because the counting time used in the laboratory (3 hours) was substantially longer than that used in the field (10 minutes). In Zone 12, the random component of analytical uncertainty for the *in situ* measurements was estimated to be 42.6 %, which is approximately twice as high as the 18.7 % estimate for *ex situ* measurements. The difference is less pronounced in the Barrier 31 data (7.5 % compared to 5.1 %). However, the analytical uncertainty was found to be higher in Zone 12 than in Barrier 31 for all measurement methods, because of the relatively low levels of ^{137}Cs activity in Zone 12. The mean value of the *in situ* measurements made with the collimated Canberra detector in Zone 12 is 0.043 Bq g^{-1}, which is less than a factor of two above the average MDA of these measurements (0.026 Bq g^{-1}) (*Section 4.3.3*). The analytical uncertainty was estimated to be approximately 6 times lower in the Barrier 31 measurements, because although the same 10 minute counting time was used, the mean site activity concentration (0.49 Bq g^{-1}) was approximately 10 times higher than in Zone 12.

The large differences between the random components of sampling uncertainty in the *in situ* and the *ex situ* measurements strongly suggests that *in situ* measurements (with a collimated detector) are able to give less uncertain estimates of average activity concentrations, provided the analytical uncertainty is taken into account. This is because *in situ* measurements are less

affected by small scale heterogeneity of contaminants, which is a direct result of the significantly larger primary sample mass. Comparisons of estimates of the SEM between *in situ* and *ex situ* methods suggest that *in situ* measurements can achieve the same confidence levels on the mean value of an averaging area at a lower cost than *ex situ* measurements, especially where there is significant variation of activity levels across the site.

9.3 Systematic differences between *in situ* and *ex situ* measurements

(Objectives 1b, 1d)

Comparisons of the site mean values revealed no significant differences between *in situ* and *ex situ* measurements, once single judgementally positioned high values were removed from the datasets from both (otherwise non-judgemental) surveys. The large differences between the primary sample masses of *in situ* and *ex situ* measurements means that comparisons of the two methods at individual measurement locations are of limited applicability, however a reasonable correlation ($r^2 = 0.64$) was found in the case of Barrier 31. No significant correlation was found between the *in situ* and the *ex situ* measurements in Zone 12, even though the mean values are similar (0.043 Bq g^{-1} for in situ, 0.047 Bq g^{-1} for *ex situ* depth 0-100 mm, 0.066 Bq g^{-1} for *ex situ* depth 0-200 mm). The non-significant correlation between *in situ* and *ex situ* measurements at individual locations is probably due to the high random uncertainty levels in the data from both measurement methods.

Although no significant differences were found between the mean activity concentration levels, there is some evidence throughout these experiments to suggest that the *in situ* measurements were underestimating the *ex situ* measurements, by as much as 25 % in some cases. There is therefore a need for a reliable method of calibrating *in situ* measurements of land areas, estimating their bias, and establishing their traceability.

Experiments to estimate the systematic differences between mean activity concentrations made by *in situ* measurements and *ex situ* measurements of a suitable reference measurement target were made (*Section 7.4*). For this purpose a pre-existing area of concrete was selected, based on assumptions about its homogeneity and thickness. *In situ* measurements acquired in the centre of the concrete area were found to be significantly lower (by about 25 %) than the mean value of the *ex situ* measurements of extracted core samples. However, it was found that two of the basic requirements of the site were not met. These were a) homogeneity of natural radionuclide content, and b) a sufficient depth of concrete (at

least 200 mm). These shortcomings limit the value of this particular area as a designated Reference Measurement Target (RMT). The principal value of these experiments is in highlighting the requirements and the likely difficulties of establishing such RMTs in the future.

9.4 Reducing the cost of estimating the random component of uncertainty

(Objective 2a)

Evaluation of the fitness-for-purpose of measurements in contaminated land investigations requires estimates to be made of the uncertainty in the measurements. It is also important to minimise the costs of contaminated land investigations, so far as is practicable. This is of particular importance to investigations of radioactively contaminated land, where measurement costs of laboratory samples are often relatively high, e.g. £60 - £190 per sample (Heathcote, 2013). A statistical method of estimating the random components of sampling and analytical uncertainty using an un-balanced experimental design has been built into a new computer program (Chapter 3). This reduces the cost of the additional analyses that are required for the uncertainty estimation by 33 %. In order to validate this method, estimates of robust standard deviations were compared with those estimated by a previously published method, which had been based on the balanced design (Ramsey and Ellison, 2007). A set of 1000 simulated base populations was used in the validation. It was found that calculations of the robust mean values differed by less than 1 % between the two methods, and the maximum difference between the robust standard deviations was 6.1 %, on estimates of sampling standard deviation alone. Differences greater than 5 % only occurred when the analytical standard deviation in the simulated base population was set to be equal to, or higher than, the sampling standard deviation.

9.5 Optimising the experimental parameters of full coverage *in situ* surveys

(Objectives 2b, 2c)

A novel approach to optimising the experimental parameters of full coverage *in situ* investigations made with portable, collimated gamma detectors has been designed (ROCLI). This was based on a newly developed generic mathematical model. Prior to development of the ROCLI method, this model was validated by comparison with the results of field experiments, and also against predictions made using a Monte-Carlo method of calculating

absolute detection efficiencies (ISOCS). The model predicts the expected numbers of detector counts that would be recorded from small activity hotspots (particles), when they are positioned at different offsets, distances and depths with respect to a detector. It was found to give good predictions of the detector response when compared to field experiments using a 40.6 kBq source, and results that were extremely close to predictions made using individual ISOCS geometry definitions (Chapter 5). Rotational biases between modelled counts and measured counts were non-significant when regressions were performed on the complete set of data obtained in the experiments. Some high biases did exist for individual experiments, e.g. generic model counts showed a rotational bias of -45 % against measured counts when lateral offset was increased with the source at a depth of 200 mm. However, the rotational biases were less than 10 % in 67 % of the different experiments, and with the exception of this one high bias, were all lower than 25 %.

Example optimisations were generated using the ROCLI method for two areas with previously measured background levels, one in which ^{137}Cs activity was recorded throughout the site, and one in which it was not. The optimal scenarios were considered to be the ones with the lowest measurement costs. It was predicted that with optimal settings of the detector height, measurement spacing and counting time, a systematic, full coverage survey of an area of 100 m^2 would require approximately 3.5 hours to locate a 100 kBq particle on the ground surface in both areas. These survey times increased to ~17 hours when the maximum particle depth was set to 100 mm (Table 6.4).

9.6 Evaluating the fitness for purpose (FnFP) of measurements (Objective 2d)

Evaluation of the FnFP of measurements using criteria proposed by Ramsey *et al.* (1992) suggest that the *in situ* measurements and the *ex situ* measurements for the 0-100 mm soil layer in Barrier 31 could be considered fit for the purpose of mapping the geochemical variation of ^{137}Cs activity within the sites. The remaining *ex situ* measurements in Barrier 31, and all the measurements in Zone 12, were not FFP by these criteria. This is due to the relatively high levels of measurement uncertainty in comparison to the spatial variability of ^{137}Cs levels in the ground. For example, the random component of measurement uncertainty in the *ex situ* measurements made in Zone 12 was found to contribute 52-83 % of the total variance (Table 8.3). However, these criteria are limited in scope, and it is considered that the

combined *in situ* and *ex situ* measurements in Zone 12 were successful in demonstrating that the contaminant levels on the site were below anything of regulatory concern.

A refined definition of FnFP, based on the method first proposed by Thompson and Fearn (1996), was built into the ROCLI optimisation method. This new approach selects the experimental parameters that minimise an estimate of the total expectation of financial loss, which includes the probabilistic costs of misclassification as well as the measurement cost. Using such an approach may be particularly applicable to investigations on radioactively contaminated land, where these costs are potentially high compared to those that would typically be encountered in chemically contaminated land investigations. Compared to the results of the optimisations based on minimum measurement cost (*Section 9.5*), optimisations based on minimum expectation of loss resulted in an increase in overall survey times of approximately 150 %, with a consequential increase in measurement costs, but with an accompanying decrease in the total expectation of loss of approximately 95 %.

9.7 Comparisons between *in situ* and *ex situ* measurement methods

(Objective 3)

Characterisation of radioactively contaminated land on a decommissioning nuclear site usually requires estimates of mean activities or mean activity concentration levels over a defined area, and also the maximum activity within that area (EA, 1999). Individual *in situ* measurements of land areas are substantially less expensive (e.g. by around 90 %) than the analysis of *ex situ* soil samples, and a faster turnaround time is usually possible. The experiments at the case-study site suggest that *in situ* measurements are able to give reliable estimates of mean levels of activity concentrations in land areas with radionuclides up to a depth of approximately 200 mm. In order to do so, sufficient information is required about the depth profile of activities in the ground. Also, any external sources of radiation at the site, which may add to the measured detector counts (shine), need to be taken into consideration. Advanced spectral analysis of *in situ* measurements may enable depth profiling, however it is likely that some data from *ex situ* measurements will usually be required in order to have confidence in the depth distributions of activity.

Within these constraints, the evidence from the experiments in Chapter 4 suggests that correctly calibrated *in situ* measurements are able to give estimates of mean activity concentrations that are at least as reliable as those obtained from *ex situ* measurements. This

has been shown to be the case for ^{137}Cs contamination on two areas of land that were contaminated by different sources, and which were affected by high levels of contaminant heterogeneity on a small scale (i.e. heterogeneity levels of more than 20 % RSD_{samp}). Ideally, these measurements should be made using a temperature stabilised *in situ* detector that has recently been characterised for ISOCS use, and that has also been calibrated on a suitable reference measurement target, with traceability to certified reference materials. However the experiments described in Chapter 5 suggest that the use of an "off-the-shelf" detector can be fit for the purpose of reliably identifying small particles of activity, if suitable calibrations are first performed.

The large primary sample mass of *in situ* measurements implies that with the detector at a height of 0.25 – 1.0 m there is limited ability to delineate the boundaries of large activity hotspots, because of the low spatial resolution. Experiments with a collimated *in situ* detector at ground level, however, suggest that this approach would enable the spatial mapping of areas of activity with a resolution on a scale of a few centimetres. This would be prohibitively expensive to achieve using *ex situ* methods only, because of the large number of samples that would need to be analysed.

The detection of small hotspots of activity (e.g. particles) cannot be reliably achieved with *ex situ* measurements of soil samples alone, because of the low areal coverage that is achievable by this method. This can be achieved quickly using *in situ* scanning surveys (e.g. Groundhog) with confidence levels of around 95 %. Scanning surveys with vehicle mounted detectors can be limited by access and terrain, however, and do not give reliable estimates of activity concentrations for individual measurements. Hand portable scanning surveys are less restricted by access, but these typically do not achieve confidence levels of at least 95 % (SEPA, 2005). New methods developed for this project suggest that particle detection can be achieved with higher confidence levels by using hand portable, stationary detectors, where these are set up to record measurements in a systematic, full coverage sampling pattern, and where the mean and variance of the local site background radiation levels has been estimated (Chapter 6). The generic mathematical models of detector response that are necessary for the design of such surveys have been tested and compare reasonably well with field measurements (Chapter 5). This further suggests that full coverage *in situ* surveys with relatively inexpensive portable equipment can be designed to produce measurements that are fit for the purpose of detecting particles, while simultaneously providing reliable estimates of activity concentrations.

9.8 – Recommendations for future work

9.8.1 – Further development of the ROCLI method (Objectives 2e, 2f)

The ROCLI method described in Chapter 6 calculates the counting times that would be required to identify the presence of a small hotspot of activity for ranges of discrete measurement parameters. The optimal measurement parameters are then determined as those which would result in minimum cost, whether that is the total measurement cost or the overall expectation of financial loss. The examples presented in Chapter 6 were based on a range of detector heights in divisions of 250 mm, and measurement spacings that were calculated from lateral offset divisions of 0.1 x the maximum radius of the nominal FOV. In many cases, however, a trolley or tripod mount for the collimated gamma detector could be used, which would potentially allow infinitely variable setting of the detector height. Future developments of the ROCLI method may allow for finer adjustments of the parameters, by using a programmed convergence to achieve the optimal settings, to (e.g.) the nearest 100 mm for both parameters.

The development of a decision support tool (**DST**) for fulfilling the objectives of a contaminated land investigation would require consideration of the measurement costs, or the expectations of financial losses, for alternative methods of characterisation. For example, in some cases it would be advantageous to use scanning surveys (e.g. vehicle mounted detectors such as Groundhog, *Section 4.5.5*) to identify activity hotspots, and also a number of *in situ* or *ex situ* measurements for the estimation of average activity concentrations within a defined area. Vehicle mounted surveys are, however, limited by access issues, the nature of the terrain, and the required probabilities of detection. When any of these limitations apply, then the use of optimised *in situ* surveys with portable gamma detectors may be the least cost, fit-for-purpose option. Further work is needed to build a DST that is capable of balancing the costs of scanning surveys, *in situ* surveys with portable detectors, and *ex situ* measurements, in order to determine the least cost means of characterising specific sites with specific objectives.

9.8.2 – Characterisation of spatial distributions of radionuclides

This study has shown that radioactive contamination in land areas can be highly heterogeneous (e.g. $RSD_{samp} > 20$ %). The relatively high sampling uncertainty in the *ex situ*

measurements in the Zone 12 and Barrier 31 surveys (Chapter 4), compared with that estimated for *in situ* measurements, suggested that heterogeneity of ^{137}Cs activity existed on a larger scale than the ~100 mm diameter of the device used to extract the soil samples. The high-resolution survey conducted in Barrier 31 further suggested that significant heterogeneity (RSD % = 8.7 %) was present on an even smaller scale of around 25 mm (*Section 7.3.4*). Heterogeneity had a high impact on the uncertainty of individual *ex situ* measurements because of the small mass of the primary sample.

Regardless of the source of contamination, contemporary distributions of contaminants will have been complicated by processes within the soil over time, e.g. the sorption of ^{137}Cs onto clay minerals. However, it would be reasonable to assume that the spatial distribution of any contaminant will be partially dependent on the nature of its original deposition. It is considered likely that the average background levels of ^{137}Cs levels measured in Zone 12 were a result of aerial deposition arising from spray being blown back from the sea following authorised discharges. In contrast, the Barrier 31 survey area was not expected to have been subjected to significant aerial deposition from authorised discharges. The most likely sources of raised concentrations of ^{137}Cs in Barrier 31 were historic leaks from the active drains alongside the area, and accidental spills of material during previous discharges to the ILW store (*Section 4.3.1*).

It may be that some generalisations could be made about the heterogeneity of contaminants that have been deposited by different processes. This could be achieved by acquiring a number of measurements over different spatial scales. These could then be analysed either by variography, which plots inter-measurement variance against spatial separation, or by using the regression method for the evaluation of heterogeneity proposed by Ramsey *et al.* (2013). This has the potential to provide information that would be useful to the design of future surveys. Predictions of the levels of heterogeneity at different measurement spacings could enable better informed decisions to be made about the most appropriate measurement methods for a particular site.

9.8.3 – Traceability of *in situ* measurements

The importance of using an adequate calibration model for the interpretation of *in situ* measurements, and the practical difficulties to overcome, have been discussed in *Sections 7.2*, *7.4* and *8.2.5*. Because of the challenges involved in constructing a reference measurement

target of the appropriate dimensions, a more practical scenario would be the identification of a pre-existing area of concrete of sufficient extent and depth, which is also homogeneous with respect to its content of a natural radionuclide such as ^{40}K. *Ex situ* measurements could then be acquired in a systematic pattern and compared to measurements of a certificated reference source. This would provide traceability of *in situ* measurements on land areas, although this makes the assumption that the distribution of activity is not subject to systematic variability on a scale that is comparable to the dimensions of the *in situ* primary sample. The attempt to establish a reference measurement target near the case-study site met with difficulties that are described in detail in *Section 7.4.*

There are three encompassing potential sources of systematic uncertainty between the measurements obtained by an *in situ* detector, and *ex situ* measurements of activity levels on a homogeneous reference measurement target of suitable dimensions, which can then be traced to a reference source:

1. Uncertainty in the laboratory measurements. This includes uncertainties in measurements of the *ex situ* core samples, and also of the reference source. It also includes uncertainty in the composition of the reference source in comparison to the composition of the processed core samples;

2. Uncertainty in the analyses of the *in situ* measurements, including uncertainties in estimating peak areas in the resulting energy spectra, and uncertainties in the calibration model. Programs such as ISOCS use Monte-Carlo methods of calculating the detection efficiencies of a defined source size and shape. Random uncertainty in the laboratory version of ISOCS (LabSOCS) has been estimated at up to 10 % (Gilmore (2008);

3. Uncertainty in the detector response to photons arriving from different directions to different components of the detector.

The first of these can largely be controlled by good practice in sample collection and laboratory procedure, e.g. appropriate sampling protocols and estimation of the random components of uncertainty through the use of replicate measurements. However, some level of systematic uncertainty will inevitably arise because the composition of the reference source will never be exactly the same as the composition of the processed core samples.

The objective of setting up a reference measurement target for *in situ* measurements is to be able to estimate the systematic uncertainties arising due to (2) and (3) above. It has been seen that with a source depth of 0.5 m, approximately 97 % of the detector response to activity at an energy level of 662 keV comes from within a source diameter of 25 m, using a detector height of 920 mm (*Section 7.2*). A concrete source of these dimensions may be hard to find. Two alternatives would be a) to use a collimator with thicker side walls, which would reduce the proportion of detector response that is due to radiation from outside the FOV; b) acquire the test measurements with the detector on or very close to the surface of the RMT, thus limiting the size of the sampling volume (See *Section 7.3*). Either of these approaches would reduce the sample volume of the detector and hence enable a physically smaller RMT to be used. Desk experiments using ISOCS suggest that approximately 96 % of the detector response to radiation at 1461 keV (corresponding to an energy line of the natural radionuclide ^{40}K) comes from within an area of 5 m diameter when a collimator with 50 mm sidewalls is used. If a site of these dimensions were located, and shown through the use of *ex situ* measurements to be sufficiently homogeneous in activity levels of a natural radionuclide such as ^{40}K, then measurements with an *in situ* detector fitted with 50 mm collimation would enable quantification of the combined uncertainty due to the sources of uncertainty (2) and (3) above. Changing back to a 20 mm collimator for ease of use in the field would introduce uncertainty in the calibration model. However this approach would enable greater confidence in measurements taken in the field with different detector types, especially if these are of the un-stabilised type and have not been individually characterised.

9.8.4 – Evaluation of uncertainty due to small scale heterogeneity in soil samples

It has previously been suggested that heterogeneity of the radionuclide content of soil may occur on a very small scale, e.g. ~25 mm (*Section 7.3.4*). This is smaller than the dimensions of the coring tool that was used in these experiments, and also of the sample pots that were used to store the soil samples. These were placed unopened in the laboratory detectors for measurements of gross gamma activity. Therefore, heterogeneity of contaminants is potentially an additional source of random uncertainty in gross gamma measurements of *ex situ* soil samples. This is because of the differential attenuation that will occur for radiation emanating from a small particle of activity that is positioned differently within the sample. One approach to reducing this uncertainty would be to dry, grind and homogenise the samples

prior to measurement. This has two drawbacks. Firstly, it would increase the costs of measurements. Secondly, the measurements will be less representative of actual site conditions. It also may not solve the problem, if a small number of active particles exist with dimensions that are less than or equal to the particulate size after grinding.

A future study to estimate the random component of uncertainty due to soil sample heterogeneity could be based on the balanced design methodology already described in Chapter 3. This would require a total of four measurements to be made on a percentage of the soil samples. First, two measurements would be made on each sample as received. The container would then be opened, the sample removed, mixed, and repacked into the same container. A further two measurements would then be made, using the same detector. Robust analysis of variance could then be used to estimate the random component of analytical uncertainty, as well as the random component of uncertainty due to heterogeneity of radionuclide content. A diagram of this experimental design is shown in Fig 9.1. It was initially intended to perform this experiment with soil samples from Barrier 31, but for logistical reasons it was not possible to complete during the project period.

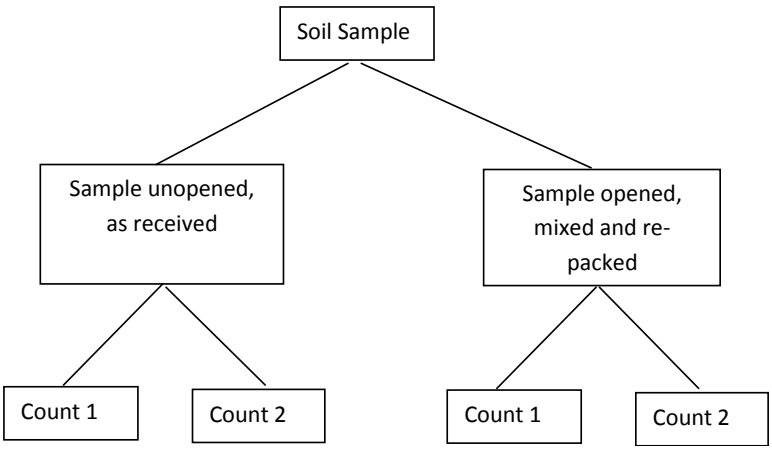

Fig 9.1 - Analysis protocol of soil samples for estimation of the random component of uncertainty due to internal heterogeneity. Each sample will be placed on the detector as received, and counted twice. The sample container will then be opened, the contents mixed, the lid replaced, and the sample container positioned in the same detector, and again counted twice.

References and bibliography

AMC (1989) 'Robust statistics - how not to reject outliers. Part1, basic concepts'. *Analyst.* **114**, 1693-1697.

AMC (2001) *Analytical Methods Committee AMC tech brief 6: Robust statistics: A method of coping with outliers.* Royal Society of Chemistry, URL accessed 16 April 2013: http://www.rsc.org/images/robust-statistics-technical-brief-6_tcm18-214850.pdf

Anselin, L. (1995) 'Local Indicators of Spatial Association – LISA'. *Geographical Analysis.* **27**, 93-115.

Back, P. (2007) 'A model for estimating the value of sampling programs and the optimal number of samples for contaminated soil'. *Environmental Geology.* **52**, 573-585.

Baeza, A., Corbacho, J.A. (2010) 'In situ determination of low-level concentrations of 137Cs in soils'. *Applied Radiation and Isotopes*. **68**, 812-815.

Beresford, N.A. (2006) 'Land contaminated by radioactive materials'. *Soil Use and Management*, **21**, 468-474.

Boon, K.A., Taylor, P.D., Ramsey, M.H. (2007). 'Estimating and Optimising Analytical and Sampling Uncertainty in Environmental Investigations: Application and Evaluation'. *Geostandards and Geoanalytical Research*. **31**, 237-249.

Boon, K.A., Rostron, P., Ramsey, M.H. (2011) 'An Exploration of the Interplay between the Measurement Uncertainty and the Number of Samples in Contaminated Land Investigations'. *Geostandards and Geoanalytical Research,* **35, 3**, 353-367.

Boudreault, J-P., Dubé, J-S., Sona, M., Hardy, É. (2012) 'Analysis of procedures for sampling contaminated soil using Gy's Sampling Theory and Practice'. *Science of the Total Environment,* **425**, 199-207.

Brown, J., Etherington, G. (2011) *Health risks from Radioactive Objects on Beaches in the Vicinity of the Sellafield Site.* Health Protection Agency. URL accessed 16 April 2013: http://www.hpa.org.uk/Publications/Radiation/CRCEScientificAndTechnicalReportSeries/HPACRCE018/

Brus, D.J., Gruijter, J.J. (1997) 'Choosing between design-based and model-based sampling strategies for soil (with Discussion)'. *Geoderma.* **80**, 1-44.

Buczko, U., Kuchenbuch, R.O., Übelhör, W., Nätscher, L. (2012) 'Assessment of sampling and analytical uncertainty of trace element contents in arable field soils'. *Environmental Monitoring and Assessment.* **184**, 4517-4538.

Canberra (2009a) Genie 2000 Gamma Acquisition and Analysis, Version 2.3. Software supplied by Canberra Industries Inc.

Canberra (2009b) ISOCS Geometry Composer version 4.2. Software supplied by Canberra Industries Inc.

Canberra (2013) *ISOCS datasheet.* Canberra Industries Inc. URL accessed 15 April 2013: http://www.canberra.com/products/insitu_systems/isocs.asp

Casanovas, R., Morant, J.J., Salvado, M. (2012) 'Temperature peak-shift correction methods for NaI(Tl) and $LaBr_3$ (Ce) gamma-ray spectrum stabilisation'. *Radiation Measurements*. 47, 588-595.

Currie, L.A. (1999) 'Nomenclature in evaluation of analytical methods including detection and quantification capabilities (IUPAC recommendations 1995)'. *Analytica Chimica Acta.* **391**, 105-126.

Dale, P., Robertson, I., Toner, M. (2008) 'Radioactive particles in dose assessments'. *Journal of Environmental Radioactivity*. **99**, 1589-1595.

DEFRA (2011) *Guidance on the scope of and exemptions from the radioactive substances legislation in the UK.* URL accessed 16 April 2013: http://www.defra.gov.uk/publications/2011/09/14/pb13624-ep-guidance-radioactive/

Dennis, F., Morgan, G., Henderson, F. (2007) 'Dounreay hot particles: the story so far'. *Journal of Radiological Protection*. **27**, A3-A11.

de Zorzi, P. (2002) 'A practical approach to assessment of sampling uncertainty'. *Accreditation in Quality Assurance.* **7**, 182-188.

DPAG (2006) *Dounreay Particles Advisory Group - Third Report*. SEPA. URL accessed 16 April 2013: http://www.google.co.uk/url?sa=t&rct=j&q=)%20dounreay%20particles%20advisory%20group%20-%20third%20report.%20sepa&source=web&cd=2&cad=rja&ved=0CDgQFjAB&url=http%3A%2F%2Fwww.sepa.org.uk%2Fradioactive_substances%2Fpublications%2Fidoc.ashx%3Fdocid%3D7f3bf06c-75f0-4735-9467-182d4a1bc65b%26version%3D-1&ei=_vhsUaXPD4aZO_TzgegM&usg=AFQjCNE7B0ofiAWazCTs32IUnjehSOLvQw

EA (2012) *Sites we Regulate.* Environment Agency. URL accessed 5 Feb 2013: http://www.environment-agency.gov.uk/homeandleisure/110310.aspx

EA (1999) *R&D Technical Report P307. Technical Support Materials for the Regulation of Radioactively Contaminated Land*. Environment Agency, Bristol.

Eisenbud, M., Gesell, T. (1997) *Environmental Radioactivity from natural, industrial & military sources.* Fourth edition., Academic Press, San Diego, California.

Euratom (2000) *Radiation protection 122: Practical use of the concepts of clearance and exemption Part 1.* URL accessed 15 Nov 2013: http://ec.europa.eu/energy/nuclear/radiation_protection/doc/publication/122_part1.pdf

Euratom (1996) *Council Directive 96/29Euratom - laying down basic safety standards for the protection of the health of workers and the general public against the dangers arising from ionizing radiation.* URL accessed 15 Nov 2013: http://ec.europa.eu/energy/nuclear/radioprotection/doc/legislation/9629_en.pdf

Europa (2007) Summaries of EU legislation - Treaty establishing the European Atomic Energy Community (Euratom). URL accessed 15 Nov 2013:

http://europa.eu/legislation_summaries/institutional_affairs/treaties/treaties_euratom_en.htm

Fearn, T., Fisher, S.A., Thompson, M., Ellison, S.L.R. (2002) 'A decision theory approach to fitness for purpose in analytical measurement'. *Analyst*. **127**, 818-824.

Ferguson, C.C. (1992) 'The statistical basis for spatial sampling of contaminated land'. *Ground Engineering*. **25**, 34-38.

Garrett, R.G. (1969) 'The determination of sampling and analytical errors in exploration geochemistry'. *Economic Geology.* **64**, 568-569.

Garrett, R.G., Goss, T.I. (1980) 'UANOVA: A Fortran iv program for unbalanced nested analysis of variance'. *Computers & Geosciences.* **6**, 35-60.

Gilmore, G. (2008) *Practical Gamma-ray Spectroscopy*. John Wiley & Sons, Oxford.

Goovearts, P. (1999) 'Geostatistics in soil science: state-of-the-art and perspectives'. *Geoderma.* **89**, 1-45.

Golosov, V.N., Walling, D.E., Kvasnikova, E.V., Stukin, E.D., Nikolaev, A.N., Panin, A.V. (2000) Application of a field-portable scintillation detector for studying the distribution of ^{137}Cs inventories in a small basin in Central Russia'. *Journal of Environmental Radioactivity*. **48**, 79-94.

Goss, O.E., Liddiard, M. (2007) 'Management of particles on the Dounreay site'. *Journal of Radiological Protection* **27**, A89-A96.

Gy, P. (2004) 'Sampling of discrete materials – a new introduction to the theory of sampling – 1. Qualitative approach'. *Chemometrics and Intelligent Laboratory Systems.* **74**, 7-24.

He, Q., Walling, D.E. (2000) 'Calibration of a field-portable gamma detector to obtain in situ measurements of the ^{137}Cs inventories of cultivated soils and floodplain sediments'. *Applied Radiation and Isotopes*. **52**, 865-872.

Heathcote, J.A. (2013) Personal communication to Dr. John Heathcote, Dounreay Site Restoration Ltd, 2 May 2013.

Hill, M. (2010), *Safegrounds – The UK regulatory framework for contaminated land on nuclear licensed sites and defence-sites,* Ciria, Classic House, 174-180 Old Street, London. URL accessed 22 May 2013:
http://www.safegrounds.com/pdfs/W36_UK_Framework_pp1-53_v3.pdf

HSE (2005) HSE Criterion for delicensing nuclear sites. Health and Safety Executive. URL accessed 16 April 2013:
http://www.hse.gov.uk/nuclear/delicensing.pdf

HSE (2010) The management of higher activity radioactive waste on nuclear licensed sites - Part 2 Radioactive waste management cases. Health and Safety Executive. URL accessed 16 April 2013:
http://www.hse.gov.uk/nuclear/wastemanage/rwm-part2.pdf

HSE (2013) Website of the UK Health and Safety Executive. URL accessed 16 April 2013: http://www.hse.gov.uk/

HSE/Environment Agencies (2001) *HSE information sheet. Control of radioactive substances. Ionising radiation protection series No 8.* URL accessed 17 April 2013: http://www.hse.gov.uk/pubns/irp8.pdf

IAEA (1998) *TECDOC-1017. Characterization of radioactively contaminated sites for remediation purposes.* International Atomic Energy Agency, Vienna. URL accessed 16 April 2013: http://www-pub.iaea.org/MTCD/publications/PDF/te_1017_prn.pdf

IAEA (1999) *TECDOC-1148. Site characterization techniques used in environmental restoration activities.* International Atomic Energy Agency, Vienna. URL accessed 16 April 2013: http://www-pub.iaea.org/MTCD/Publications/PDF/te_1148_prn.pdf

IAEA (2003) *TECDOC-1415. Soil sampling for environmental contaminants.* International Atomic Energy Agency, Vienna. URL accessed 16 April 2013: http://www-pub.iaea.org/MTCD/publications/PDF/te_1415_web.pdf

IAEA *(2004a) Application of the concepts of exclusion, exemption and clearance, IAEA Safety Standards Series, No. RS-G-1.7.* International Atomic Energy Agency, Vienna. URL accesses 22 May 2013: http://www-pub.iaea.org/MTCD/Publications/PDF/Pub1202_web.pdf

IAEA (2004b) *IAEA TECDOC-1415. Soil sampling for environmental contaminants.* International Atomic Energy Agency, Vienna. URL accessed 16 April 2013: http://www-pub.iaea.org/MTCD/Publications/PDF/te_1415_web.pdf

IAEA (2011) *TECDOC-1663. Radioactive particles in the Environment: Sources, Particle Characterization and Analytical Techniques.* International Atomic Energy Agency, Vienna. URL accessed 16 April 2013: http://www-pub.iaea.org/MTCD/Publications/PDF/TE_1663_web.pdf

IAEA (2013) *Regulatory control of nuclear power plants (glossary)*. URL accessed 17 April 2013: http://www.iaea.org/ns/tutorials/regcontrol/intro/glossarya.htm

ICRU (1998) *Fundamental quantities and units for ionizing radiation.* International Commission on Radioactive Units and Measurements. URL accessed 16 April 2013: http://web.engr.oregonstate.edu/~higley/rbe%20references/RBE%20Copy.Data/PDF/icru%2060-4008143401/icru%2060.pdf

IUPAC (1990) 'Nomenclature for sampling in analytical chemistry (Recommendations 1990)' *Pure and Applied Chemistry.* **62,** 1193-1208.

JCGM (2008a) *International vocabulary of metrology – Basic and general concepts and associated terms (VIM).* Bureau International des Poids et Mesures (BIPM). URL accessed 16 April 2013: http://www.bipm.org/utils/common/documents/jcgm/JCGM_200_2008.pdf

JCGM (2008b) *Evaluation of measurement data – Guide to the expression of uncertainty in measurement.* Bureau International des Poids et Mesures (BIPM). URL accessed 16 April 2013: http://www.bipm.org/utils/common/documents/jcgm/JCGM_100_2008_E.pdf

Jones, D (2012) Personal communication to Dr. D. Jones, British Geological Survey, 18 October 2012.

Li, J., Li, Y., Wang, Y., Wu, J. (2010) 'Applicability study of using in-situ gamma-ray spectrometry technique for 137Cs and 210Pbex inventories measurement in grassland environments'. *Applied Radiation and Isotopes* **68**, 1143-1149.

Kalb, P., Luckett, L., Miller, K., Gogolak, C., Milian, L. (2000) *Comparability of ISOCS instrument in characterization at Brookhaven National Laboratory.* Brookhaven National Laboratory, New York. URL accessed 16 April 2013: http://www.orau.gov/ddsc/ret/BNL-ISOCS-report.pdf

Kastlander, J., Bargholtz, C. (2005) 'Efficient in situ method to determine radionuclide concentration in soil'. *Nuclear Instruments and Methods in Physics Research A.* **547**, 400-410.

Knoll, G.F. (2000), *Radiation Detection and Measurement.* Third Ed, John Wiley & Sons, USA.

Korun, M., Likar, A., Lipoglavšek, M., Martinčič, R., Pucelj, B. (1994) 'In-situ measurement of Cs distribution in the soil'. *Nuclear Instruments and Methods in Physics Research B*. **93**, 485-491.

Korun, M., Martinčič, R., Pucelj, B. (1991) 'In-situ measurements of the radioactive fallout deposit'. *Nuclear Instruments and Methods in Physics Research A*. **300**, 611-615.

Kurfurst, U., Desaules, A., Rehnert, A., Muntau, H. (2004) 'Estimation of measurement uncertainty by the budget approach for heavy metal content in soils under different land use'. *Accreditation and Quality Assurance.* **9**, 64-75.

Lettner, H., Andrasi, A.K., Hubmer, A.K., Lovranich, E., Steger, F., Zombori, P. (1996) 'In situ gamma-spectrometry intercomparison exercise in Salzburg, Austria'. *Nuclear Instruments and Methods in Physics Research A*. **369**, 547-551.

Li, C., Ma, T., Shi, J. (2003) 'Application of a fractal method relating concentrations and distances for separation of geochemical anomalies from background'. *Journal of Geochemical Exploration.* **77**, 167-175.

Li, C., Ma, T., Cheng, J. (2004) 'A fractal interploratory approach to geochemical exploration data processing'. *Mathematical Geology.* **36, 5**, 593-606.

Long, S., Martin, L. (2007) 'Optimisation of systems to locate discrete gamma-ray sources within a large search area'. *Journal of environmental radioactivity*. **94**, 41-53.

Longworth, G. (ed) (1998), *The radiochemical manual.* AEA Technology plc, Harwell.

Lyn, J.A., Ramsey, M.H., Coad, D.S., Damant, A.P., Wood, R., Boon, K.A. (2007) 'The duplicate method of uncertainty estimation: Are eight targets enough?'. *Analyst.* 132, 1147-1152.

MacDonald, J., Gibson, C.J., Fish, P.J., Assinder, D.J. (1997) 'A theoretical comparison of methods of quantification of radioactive contamination in soil using in situ gamma spectrometry'. *Journal of Radiological Protection*, **17**, 3-15.

MacDonald, J., Smith, P.H., Assinder, D.J. (1996) 'The development and use of an in situ gamma-ray spectrometry system in North Wales'. *Journal of Radiological Protection.* **16**, 115-127.

MARTAC (2003) *Rehabilitation of a former nuclear test site at Emu and Maralinga (Australia) 2003.* Report by the Maralinga Rehabilitation Technical Advisory Committee. URL accessed 16 April 2013:
http://www.ret.gov.au/resources/Documents/radioactive_waste/martac_report.pdf

Myers, J.C. (1997) *Geostatistical error management.* Van Nostrand Reinhold, New York.

National Archives (1965) *Nuclear Installations Act 1965.*URL accessed 22 April 2013:
http://www.legislation.gov.uk/ukpga/1965/57/contents

National Archives (1995) *Environment Act 1995. Part IIA Contaminated Land.* URL accessed 16 April 2013:
http://www.legislation.gov.uk/ukpga/1995/25/section/57

National Archives (2006a) *No. 1379 ENVIRONMENTAL PROTECTION, ENGLAND. The Radioactive Contaminated Land (Modification of Enactments)(England) Regulations 2006.*
URL accessed 16 April 2013:
http://www.legislation.gov.uk/2006/1379

National Archives (2006b) *No. 2988 (W.277), ENVIRONMENTAL PROTECTION, WALES*
The Radioactive Contaminated Land (Modification of Enactments) (Wales) Regulations 2006.
URL accessed 16 April 2013:
http://www.legislation.gov.uk/2006/2988

National Archives (2006c) *No. 345, RADIOACTIVE SUBSTANCES, ENVIRONMENTAL PROTECTION*
The Radioactive Contaminated Land Regulations (Northern Ireland) 2006.
URL accessed 16 April 2013:
http://www.legislation.gov.uk/2006/345

National Archives (2007) *No. 179, ENVIRONMENTAL PROTECTION, The Radioactive Contaminated Land (Scotland) Regulations 2007.*
URL accessed 16 April 2013:
http://www.legislation.gov.uk/2007/179

NDA (2006) Strategy (of the Nuclear Decommissioning Authority). Nuclear Decommissioning Authority. URL accessed 16 April 2013:
http://www.nda.gov.uk/documents/upload/NDA_Final_Strategy_published_7_April_2006.pdf

NDA (2013) Website of the Nuclear Decommissioning Authority. URL accessed 16 April 2013:
http://www.nda.gov.uk/

ONR (2013) Website of the Office for Nuclear Regulation. URL accessed 16 April 2013:
http://www.hse.gov.uk/nuclear/contaminatedland.htm

OSPAR (1992) *Annex 30* of *Convention for the protection of the marine environment of the North-East Atlantic.* URL accessed 15 Nov 2013: www.**ospar**.org/documents/dbase/decrecs/**decisions**/od98-02e.doc

OSPAR (1992) *Convention for the protection of the marine environment of the North-East Atlantic.*URL accessed 15 Nov 2013: http://www.ospar.org/html_documents/ospar/html/ospar_convention_e_updated_text_2007.pdf

Poston, T.M., Peterson, R.E., Cooper, A.T. (2007) 'Past radioactive particle contamination in the Columbia river at the Hanford site, USA'. *Journal of Radiological Protection.* **27**, A45-A50.

Potts, P (2013) Personal communication with Prof. Phil Potts, Department of Environment, Earth & Ecosystems at The Open University, November 2013.

Ramsey MH (1998) 'Sampling as a source of measurement uncertainty: Techniques for quantification and comparison with analytical sources'. *Journal of Analytical Atomic Spectrometry*. **13**, 97-104.

Ramsey, M.H. (2004) *Improving the Reliability of Contaminated Land Assessment using Statistical Methods: Part 1 - Basic Principles and Concepts*. *CL:AIRE Technical Bulletin.* URL accessed 16 April 2013: http://www.sussex.ac.uk/cer/documents/paper94_tb704.pdf

Ramsey, M.H., Argyraki, A. (1997) 'Estimation of measurement uncertainty from field sampling: Implications for the classification of contaminated land.' *Science of the Total Environment*. **198**, 243-257.

Ramsey, M.H., Boon, K.A. (2010) 'New approach to geochemical measurement: Estimation of measurement uncertainty from sampling, rather than an assumption or representative sampling'. *Geoanalytical Research.* **34, 3**, 293-304.

Ramsey, M.H., Boon, K.A. (2012) 'Can *in situ* geochemical measurements be *more* fit-for-purpose than those made *ex situ*?'. *Applied Geochemistry.* **27**, 969-976.

Ramsey, M.H., Ellison, S.L.R. (eds.) (2007). Eurachem/EUROLAB/CITAC/Nordtest/AMC Guide: Measurement uncertainty arising from sampling: a guide to methods and approaches Eurachem (2007). Available from the Eurachem secretariat. URL last accessed 16 April 2013: http://www.eurachem.org/images/stories/Guides/pdf/UfS_2007.pdf

Ramsey, M.H., Geelhoed, B., Wood, R., Damant, A.P. (2011) 'Improved evaluation of measurement uncertainty from sampling by inclusion of between-sampler bias using sampling proficiency testing'. *Analyst.* **136**, 1313-1321.

Ramsey, M.H., Squire, S., Gardner, M.J. (1999) ' Synthetic reference sampling target for the estimation of measurement uncertainty'. *Analyst.* **124**, 1701-1706.

Ramsey, M.H., Solomon-Wisdom, G., Argyraki, A. (2013) 'Evaluation of *in situ* heterogeneity of elements in solids: implications for analytical geochemistry'. *Unpublished manuscript.* Under review by Geostandards and Geoanalytical Research (April 2013).

Ramsey, M.H., Taylor, P.D., Lee, J.C. (2002) 'Optimised contaminated land investigation at minimum overall cost to achieve fitness-for-purpose.' *Journal of Environmental Monitoring*. **4**, 809-814.

Ramsey, M.H., Thompson, M., Hale, M. (1992) 'Objective evaluation of precision requirements for geochemical analysis using robust analysis of variance'. *Geochemical Exploration.* **44**, 23-36.

Rose, A. W., Hawkes, H. E. and Webb, J. S. (1979) *Geochemistry in Mineral Exploration.* Second edition. Academic Press Inc. (London).

Rostron, P., Heathcote, J.A., Ramsey, M.H. (submitted-a). 'Optimisation of *in situ* measurement strategies for the characterisation of radioactively contaminated land that includes the presence of small particles'. **Submitted to Journal of Radiological Protection June 2013.**

Rostron, P., Heathcote, J.A., Ramsey, M.H. (submitted-b). *In situ* detection of 'hot' particles by portable gamma-ray devices: modelling the effects of experimental parameters**. Submitted to Journal of Radiological Protection June 2013.**

Rousseeuw PJV, Verboven, S. (2002) 'Robust estimation in very small samples'. *Computational Statistics and Data Analysis.* **40**, 741-758

Sadremomtaz, A., Moghaddam, M.V., Khoshbinfar, S., Moghaddasi, A. (2010) 'A Comparative Study of Field Gamma-ray Spectrometry by NaI(Tl) and HPGe Detectors in the South Caspian Region'. *Caspian Journal of Environmental Science.* **8**, 203-210.

Salbu, B., Lind, O.C. (2005) 'Radioactive particles released from various nuclear sources'. *Radioprotection.* **Supplement 1 40**, S27-S32.

Scottish Executive (2006) *Paper SE/2006/44: Environmental Protection Act 1990 - Part IIA: Contaminated Land - Statutory Guidance: Edition 2.* URL accessed: 21 May 2013: http://www.scotland.gov.uk/Resource/Doc/127825/0030600.pdf

Scottish Government (2010) *Guidance document on the Radioactive Contaminated Land (Scotland) Amendment Regulations 2009.* URL accessed 22 April 2013: http://www.scotland.gov.uk/Publications/2010/03/19125743/0

Scottish Government (2011) *Radioactive Substances Act 1993 Amendment (Scotland) Regulations 2011*. URL accessed 20 May 2013: http://www.legislation.gov.uk/ssi/2011/207/contents/made

SEPA *(2005) An Evaluation of the Sensitivity of the Groundhog Evolution™ Beach Monitoring System*. URL accessed 16 April 2013: http://www.google.co.uk/url?sa=t&rct=j&q=an%20evaluation%20of%20the%20groundhog&source=web&cd=2&cad=rja&ved=0CDQQFjAB&url=http%3A%2F%2Fwww.sepa.org.uk%2Fradioactive_substances%2Fpublications%2Fidoc.ashx%3Fdocid%3Dadf9a85a-1345-4805-aaab-59cb009ee30d%26version%3D-1&ei=gFRcUd3yKsjrOoamgOgI&usg=AFQjCNGyN97xXhsjSzL4qWzhsKNK_cOeAw

SEPA (2009), *Decommissioning (Page on the Scottish Environmental Protection Agency website.* URL accessed 16 April 2013:

http://www.sepa.org.uk/radioactive_substances/decommissioning/nuclear_decommissioning_author.aspx

Squire, S., Ramsey, M.H., Gardner, M.J. & Lister, D. 'Sampling proficiency test for the estimation of uncertainty in the spatial delineation of contamination'. *Analyst*. **125**, 2026-2031.

Taylor, P.D., Ramsey, M.H., Potts, P. J. (2004) 'Balancing measurement uncertainty against financial benefits: Comparison of *in situ* and *ex situ* analysis of contaminated land'. *Environmental Science and Technology*. **38**, 6824-6831.

Taylor, P.D., Ramsey, M.H., Potts, P. J. (2005) 'Spatial contaminant heterogeneity: quantification with scale of measurement at contrasting sites'. *Journal of Environmental Monitoring.* **7**, 1364-1370.

Thompson, M. (1982) 'Regression Methods in the Comparison of Accuracy'. *Analyst.* **107**, 1169-1180.

Thompson, M. (1995) 'Uncertainty in an uncertain world'. *Analyst.* **120**, 117N-118N.

Thompson, M., Fearn, T. (1996) 'What exactly is fitness for purpose in analytical measurement?' *Analyst*. **121**, 275-278.

Thompson, M., Ramsey, M.H. (1995) 'Quality concepts and practices applied to sampling – an exploratory study'. *Analyst*. **120**, 261-270.

Towler, P., Rankine, A., Kruse, P., Eslave-Gomez, A. (2009) 'Good practice guidance for site characterization, SAFEGROUNDS.' Ciria, London. URL last accessed 16 April 2013: http://www.safegrounds.com/pdfs/w30_safegrounds_site_characterisation.pdf

Tyler, A.N., Sanderson, D.C.W., Scott, E.M. (1996a) 'Estimating and Accounting for ^{137}Cs Source Burial through In-Situ Gamma Spectrometry in Salt Marsh Environments.' *Journal of Environmental Radioactivity*. **3**, 195-212.

Tyler, A.N., Sanderson, D.C.W., Scott, E.M., Allyson, J.D. (1996b) 'Accounting for Spatial Variability and Fields of View in Environmental Gamma Ray Spectrometry' *Journal of Environmental Radioactivity*. **3**, 213-235.

USEPA (2000a) *Guidance for the Data Quality Objectives Process EPA QA/G-4,* United States Environmental Protection Agency. URL Accessed 16 April 2013: http://www.epa.gov/osw/hazard/correctiveaction/resources/guidance/qa/epaqag4.pdf

USEPA (2000b) *Multi-Agency Radiation Survey And Site Investigation Manual (MARSSIM), Available on the website of the U.S. Environmental Protection Agency.* URL accessed 16 April 2013:
http://www.epa.gov/rpdweb00/marssim/obtain.html

USNRC (2013) *Website of the United States Nuclear Regulatory Commission.* URL accessed 27 March 2013:
http://www.nrc.gov/reading-rm/doc-collections/cfr/part020/

WNA (2013) *Website of the World Nuclear Association.* URL accessed 21 May 2013: http://www.world-nuclear.org/info/Safety-and-Security/Radiation-and-Health/Naturally-Occurring-Radioactive-Materials-NORM/

Appendix 1 (Table A1.1) - Raw data for U-RANOVA test

See Chapter 3. All data in appendixes is also included on the enclosed data disk.

Table A1.1 Original simulated data populations for testing of robust ANOVA, as used by Ramsey *et al.*, 1992. Both comprise of 4 columns of 100 random numbers drawn from a normal distribution: Trial 1 = no outliers, Trial 2 = 5 % of analytical duplicates overwritten with high-value outliers (highlighted). Used in U-RANOVA Test 1 (*Section 3.3.1*)

Trial 1 – no outliers			
104.69	101.4	108.72	106.3
93.614	98.761	94.693	95.544
103.84	105.04	92.097	88.522
118.7	116.36	110.44	109.14
100.67	100.48	103.25	103.96
98.452	97.688	92.595	98.266
105.22	110.11	102.81	97.649
99.767	96.734	96.19	96.111
105.26	106.34	98.338	102.57
116.27	117.67	119.83	119.83
113.27	111.09	109.26	111.6
82.31	86.122	90.558	88.697
101.82	108	104.54	103.66
78.551	78.124	89.681	87.409
116.74	116.37	117.64	122.46
92.294	88.589	93.025	94.815
129.64	132.89	122.81	121.76
96.433	93.677	106.84	108.53
99.247	101.36	96.023	96.228
103.63	102.43	96.065	98.905
126.67	125.14	114.69	112.64
107.52	107.97	103.02	105.41
106.02	106.29	103.23	106.23
89.265	86.459	97.1	96.759
97.171	98.218	99.646	98.44
99.992	100.49	99.365	97.33
102.09	100.96	89.438	91.601
92.681	91.54	99.404	98.232
92.962	94.467	87.523	87.692
94.311	91.628	77.407	81.355
96.542	94.689	96.33	95.489
122.46	118.49	108.68	109.91
93.173	91.179	91.255	91.743
104.9	107.37	105.12	103.88
106.87	109.64	99.754	102.11
95.553	91.71	97.53	95.553
88.974	88.439	92.883	95.857
81.014	80.255	84.516	84.092
82.17	83.965	86.347	87.46
102.6	100.82	99.796	97.175
103.35	98.188	95.717	95.176
110.15	115.97	107.47	103.22
86.027	89.084	79.01	79.383

Trial 2 - analytical outliers			
104.69	101.4	108.72	106.3
93.614	98.761	94.693	95.544
103.84	105.04	92.097	88.522
118.7	116.36	110.44	109.14
100.67	100.48	103.25	103.96
98.452	97.688	92.595	98.266
105.22	110.11	102.81	97.649
99.767	96.734	96.19	96.111
105.26	106.34	98.338	102.57
116.27	117.67	119.83	119.83
113.27	111.09	109.26	111.6
82.31	86.122	90.558	88.697
101.82	108	104.54	103.66
78.551	78.124	89.681	87.409
116.74	116.37	117.64	122.46
92.294	88.589	93.025	94.815
129.64	132.89	122.81	121.76
96.433	93.677	106.84	108.53
99.247	101.36	96.023	96.228
103.63	102.43	96.065	98.905
126.67	125.14	114.69	112.64
107.52	107.97	103.02	105.41
106.02	106.29	103.23	106.23
89.265	86.459	97.1	96.759
97.171	98.218	99.646	98.44
99.992	100.49	99.365	97.33
102.09	100.96	89.438	91.601
92.681	91.54	99.404	98.232
92.962	94.467	87.523	87.692
94.311	91.628	77.407	81.355
96.542	94.689	96.33	95.489
122.46	118.49	108.68	109.91
93.173	91.179	91.255	91.743
104.9	107.37	105.12	103.88
106.87	109.64	99.754	102.11
95.553	91.71	97.53	95.553
88.974	88.439	92.883	95.857
81.014	80.255	84.516	84.092
82.17	83.965	86.347	87.46
102.6	100.82	99.796	97.175
103.35	98.188	95.717	95.176
110.15	115.97	107.47	103.22
86.027	89.084	79.01	79.383

92.652	93.453	99.879	93.961	92.652	93.453	99.879	93.961
95.84	93.824	90.382	87.414	95.84	93.824	90.382	87.414
116.37	117.15	113.2	115.44	116.37	117.15	113.2	115.44
92.714	89.217	87.188	86.624	92.714	89.217	87.188	86.624
93.85	95.829	94.559	97.055	93.85	95.829	94.559	97.055
101.19	98.951	109.05	102.5	101.19	98.951	109.05	102.5
99.422	97.093	104.35	100.79	99.422	97.093	104.35	100.79
123.78	125.76	112.82	112.72	123.78	125.76	112.82	112.72
119.54	117.14	115.43	117.95	119.54	117.14	115.43	117.95
98.484	102.58	92.861	92.549	98.484	102.58	92.861	92.549
104.41	100.62	98.201	96.462	104.41	100.62	98.201	96.462
100.33	102.86	102.28	100.53	100.33	102.86	102.28	100.53
97.389	90.876	95.337	95.943	97.389	90.876	95.337	95.943
99.004	96.112	92.752	91.895	99.004	96.112	92.752	91.895
104.9	104.06	99.678	95.579	104.9	104.06	99.678	95.579
85.429	84.406	89.513	86.977	85.429	84.406	89.513	86.977
104.65	111.01	103.07	101.5	104.65	111.01	103.07	101.5
97.852	101.2	96.226	97.15	97.852	101.2	96.226	97.15
114.87	117.41	101.59	98.957	114.87	117.41	101.59	98.957
129.09	129.35	120.89	117.94	129.09	129.35	120.89	117.94
100.29	100.37	97.516	96.075	100.29	100.37	97.516	96.075
108.7	105.73	117.66	117.82	108.7	105.73	117.66	117.82
92.909	91.862	96.225	97.073	92.909	91.862	96.225	97.073
106.88	104.89	104.28	106.69	106.88	104.89	104.28	106.69
88.228	85.303	88.286	85.809	88.228	85.303	88.286	85.809
92.697	96.809	94.939	100.74	92.697	96.809	94.939	100.74
100.56	101.75	98.23	94.733	100.56	101.75	98.23	94.733
117.38	115.58	121.99	118.38	117.38	115.58	121.99	118.38
105.85	107.7	101.42	100.06	105.85	107.7	101.42	100.06
104	100.58	94.212	93.034	104	100.58	94.212	93.034
89.715	88.771	78.987	80.737	89.715	88.771	78.987	80.737
85.056	83.713	86.535	86.902	85.056	83.713	86.535	86.902
93.845	95.666	82.743	83.952	93.845	95.666	82.743	83.952
91.132	91.705	94.352	95.018	91.132	91.705	94.352	95.018
86.821	86.891	97.715	96.23	86.821	86.891	97.715	96.23
110.54	112.6	100.58	99.562	110.54	112.6	100.58	99.562
101.52	99.247	107.21	108.61	101.52	99.247	107.21	108.61
105.99	107.13	107.23	107.51	105.99	107.13	107.23	107.51
98.125	99.605	109.05	108.84	98.125	99.605	109.05	108.84
95.737	99.006	87.312	92.503	95.737	99.006	87.312	92.503
101.49	103.72	108.75	111.24	101.49	103.72	108.75	111.24
109.48	106.44	108.85	114.64	109.48	106.44	108.85	114.64
106.45	103.34	117.64	117.09	106.45	103.34	117.64	117.09
106.27	100.47	104.1	106.43	106.27	100.47	104.1	106.43
117.92	118.72	112.87	110.7	117.92	118.72	112.87	110.7
92.919	89.953	93.136	92.373	92.919	89.953	93.136	92.373
102.36	99.469	111.14	112.43	102.36	99.469	111.14	112.43
81.423	82.055	90.477	87.235	81.423	82.055	90.477	**187.23**
76.779	74.422	87.253	88.654	76.779	74.422	87.253	**188.65**
107.41	106.3	99.763	101.1	107.41	106.3	99.763	**201.1**
62.89	67.339	77.66	81.813	62.89	67.339	77.66	**181.81**
100.91	95.623	98.088	97.658	100.91	95.623	98.088	**197.66**
105.55	104.19	106.34	103.94	105.55	104.19	106.34	**203.94**
112.76	110.54	98.468	101	112.76	110.54	98.468	**201**
96.147	97.735	116.55	112.9	96.147	97.735	116.55	**212.9**

122.27	122.84	114.82	119.92	122.27	122.84	114.82	**219.92**
91.665	95.648	104.58	105.62	91.665	95.648	104.58	**205.62**

Table A1.2 Original simulated data populations for testing of robust ANOVA, as used by Ramsey *et al.*, 1992. Both comprise of 4 columns of 100 random numbers drawn from a normal distribution: Trial 1 = 5 %of sampling duplicates overwritten with high values; Trial 2 = 10% of between-target values overwritten with high-value outliers. Overwritten values have been highlighted.

Trial 3 - sampling outliers				**Trial 4 - between-target outliers**			
104.69	101.4	108.72	106.3	104.69	101.4	108.72	106.3
93.614	98.761	94.693	95.544	93.614	98.761	94.693	95.544
103.84	105.04	92.097	88.522	103.84	105.04	92.097	88.522
118.7	116.36	110.44	109.14	118.7	116.36	110.44	109.14
100.67	100.48	103.25	103.96	100.67	100.48	103.25	103.96
98.452	97.688	92.595	98.266	98.452	97.688	92.595	98.266
105.22	110.11	102.81	97.649	105.22	110.11	102.81	97.649
99.767	96.734	96.19	96.111	99.767	96.734	96.19	96.111
105.26	106.34	98.338	102.57	105.26	106.34	98.338	102.57
116.27	117.67	119.83	119.83	116.27	117.67	119.83	119.83
113.27	111.09	109.26	111.6	113.27	111.09	109.26	111.6
82.31	86.122	90.558	88.697	82.31	86.122	90.558	88.697
101.82	108	104.54	103.66	101.82	108	104.54	103.66
78.551	78.124	89.681	87.409	78.551	78.124	89.681	87.409
116.74	116.37	117.64	122.46	116.74	116.37	117.64	122.46
92.294	88.589	93.025	94.815	92.294	88.589	93.025	94.815
129.64	132.89	122.81	121.76	129.64	132.89	122.81	121.76
96.433	93.677	106.84	108.53	96.433	93.677	106.84	108.53
99.247	101.36	96.023	96.228	99.247	101.36	96.023	96.228
103.63	102.43	96.065	98.905	103.63	102.43	96.065	98.905
126.67	125.14	114.69	112.64	126.67	125.14	114.69	112.64
107.52	107.97	103.02	105.41	107.52	107.97	103.02	105.41
106.02	106.29	103.23	106.23	106.02	106.29	103.23	106.23
89.265	86.459	97.1	96.759	89.265	86.459	97.1	96.759
97.171	98.218	99.646	98.44	97.171	98.218	99.646	98.44
99.992	100.49	99.365	97.33	99.992	100.49	99.365	97.33
102.09	100.96	89.438	91.601	102.09	100.96	89.438	91.601
92.681	91.54	99.404	98.232	92.681	91.54	99.404	98.232
92.962	94.467	87.523	87.692	92.962	94.467	87.523	87.692
94.311	91.628	77.407	81.355	94.311	91.628	77.407	81.355
96.542	94.689	96.33	95.489	96.542	94.689	96.33	95.489
122.46	118.49	108.68	109.91	122.46	118.49	108.68	109.91
93.173	91.179	91.255	91.743	93.173	91.179	91.255	91.743
104.9	107.37	105.12	103.88	104.9	107.37	105.12	103.88
106.87	109.64	99.754	102.11	106.87	109.64	99.754	102.11
95.553	91.71	97.53	95.553	95.553	91.71	97.53	95.553
88.974	88.439	92.883	95.857	88.974	88.439	92.883	95.857
81.014	80.255	84.516	84.092	81.014	80.255	84.516	84.092
82.17	83.965	86.347	87.46	82.17	83.965	86.347	87.46
102.6	100.82	99.796	97.175	102.6	100.82	99.796	97.175
103.35	98.188	95.717	95.176	103.35	98.188	95.717	95.176
110.15	115.97	107.47	103.22	110.15	115.97	107.47	103.22
86.027	89.084	79.01	79.383	86.027	89.084	79.01	79.383
92.652	93.453	99.879	93.961	92.652	93.453	99.879	93.961

95.84	93.824	90.382	87.414
116.37	117.15	113.2	115.44
92.714	89.217	87.188	86.624
93.85	95.829	94.559	97.055
101.19	98.951	109.05	102.5
99.422	97.093	104.35	100.79
123.78	125.76	112.82	112.72
119.54	117.14	115.43	117.95
98.484	102.58	92.861	92.549
104.41	100.62	98.201	96.462
100.33	102.86	102.28	100.53
97.389	90.876	95.337	95.943
99.004	96.112	92.752	91.895
104.9	104.06	99.678	95.579
85.429	84.406	89.513	86.977
104.65	111.01	103.07	101.5
97.852	101.2	96.226	97.15
114.87	117.41	101.59	98.957
129.09	129.35	120.89	117.94
100.29	100.37	97.516	96.075
108.7	105.73	117.66	117.82
92.909	91.862	96.225	97.073
106.88	104.89	104.28	106.69
88.228	85.303	88.286	85.809
92.697	96.809	94.939	100.74
100.56	101.75	98.23	94.733
117.38	115.58	121.99	118.38
105.85	107.7	101.42	100.06
104	100.58	94.212	93.034
89.715	88.771	78.987	80.737
85.056	83.713	86.535	86.902
93.845	95.666	82.743	83.952
91.132	91.705	94.352	95.018
86.821	86.891	97.715	96.23
110.54	112.6	100.58	99.562
101.52	99.247	107.21	108.61
105.99	107.13	107.23	107.51
98.125	99.605	109.05	108.84
95.737	99.006	87.312	92.503
101.49	103.72	108.75	111.24
109.48	106.44	108.85	114.64
106.45	103.34	117.64	117.09
106.27	100.47	104.1	106.43
117.92	118.72	112.87	110.7
92.919	89.953	93.136	92.373
102.36	99.469	111.14	112.43
81.423	82.055	**190.48**	**187.23**
76.779	74.422	**187.25**	**188.65**
107.41	106.3	**199.76**	**201.1**
62.89	67.339	**177.66**	**181.81**
100.91	95.623	**198.09**	**197.66**
105.55	104.19	**206.34**	**203.94**
112.76	110.54	**198.47**	**201**
96.147	97.735	**216.55**	**212.9**
122.27	122.84	**214.82**	**219.92**

95.84	93.824	90.382	87.414
116.37	117.15	113.2	115.44
92.714	89.217	87.188	86.624
93.85	95.829	94.559	97.055
101.19	98.951	109.05	102.5
99.422	97.093	104.35	100.79
123.78	125.76	112.82	112.72
119.54	117.14	115.43	117.95
98.484	102.58	92.861	92.549
104.41	100.62	98.201	96.462
100.33	102.86	102.28	100.53
97.389	90.876	95.337	95.943
99.004	96.112	92.752	91.895
104.9	104.06	99.678	95.579
85.429	84.406	89.513	86.977
104.65	111.01	103.07	101.5
97.852	101.2	96.226	97.15
114.87	117.41	101.59	98.957
129.09	129.35	120.89	117.94
100.29	100.37	97.516	96.075
108.7	105.73	117.66	117.82
92.909	91.862	96.225	97.073
106.88	104.89	104.28	106.69
88.228	85.303	88.286	85.809
92.697	96.809	94.939	100.74
100.56	101.75	98.23	94.733
117.38	115.58	121.99	118.38
105.85	107.7	101.42	100.06
104	100.58	94.212	93.034
89.715	88.771	78.987	80.737
85.056	83.713	86.535	86.902
93.845	95.666	82.743	83.952
91.132	91.705	94.352	95.018
86.821	86.891	97.715	96.23
110.54	112.6	100.58	99.562
101.52	99.247	107.21	108.61
105.99	107.13	107.23	107.51
98.125	99.605	109.05	108.84
95.737	99.006	87.312	92.503
101.49	103.72	108.75	111.24
109.48	106.44	108.85	114.64
106.45	103.34	117.64	117.09
106.27	100.47	104.1	106.43
117.92	118.72	112.87	110.7
92.919	89.953	93.136	92.373
102.36	99.469	111.14	112.43
81.423	82.055	90.477	87.235
76.779	74.422	87.253	88.654
107.41	106.3	99.763	101.1
62.89	67.339	77.66	81.813
100.91	95.623	98.088	97.658
105.55	104.19	106.34	103.94
112.76	110.54	98.468	101
96.147	97.735	116.55	112.9
122.27	122.84	114.82	119.92

91.665	95.648	**204.58**	**205.62**

91.665	95.648	104.58	105.62
1437.7	**1563.8**	**1265.5**	**1370**
597.01	**627.2**	**707.98**	**720.11**
1106.8	**1170.1**	**1172.1**	**1036.9**
495.38	**489.73**	**692.58**	**643.48**
1605.2	**1694.6**	**1732.4**	**1522.3**
666.41	**607.45**	**528.7**	**506.31**
1702.4	**1768.4**	**1871.4**	**1759.2**
1108.8	**1130.4**	**931**	**946.38**
1046.9	**970.24**	**927.08**	**947.9**
940.91	**997.5**	**1079.7**	**1056.5**

Source data for U-RANOVA Test 2 (*Section 3.3.2*) is on the enclosed data disk only.

Appendix 2 (Tables A2.1 to A2.8) - Raw data from the Zone 12 and Barrier 31 surveys

See Chapter 4. All data in appendixes is also included on the enclosed data disk.

Table A2.1 Zone 12 raw data for in situ measurements. Canberra detector measurements have been converted to mass activity concentrations using an ISOCS circular plane geometry definition of 25 m diameter and 0.2 m depth. Values for duplicate measurement locations have been averaged across all four measurements at each location. Pertains to *Section 4.4.2.*

ID	Canberra (Bq g^{-1})	Exploranium (Counts)	ID	Canberra (Bq g^{-1})	Exploranium (Counts)	ID	Canberra (Bq g^{-1})	Exploranium (Counts)
A2	0.063502	240	C9	0.05043	333	F5	0.057972	333
A3	0.049563	372	C10	0.043111	374	F6	0.056665	215
A4	0.058931	363	C11	0.04913575	375	F7	0.0441	231
A5	0.050211	255	C12	0.039623	422	F8	0.046762	422
A6	0.03915	284	D2	0.050702	372	F9	0.044384	250
A7	0.026521	311	D3	0.040716	228	F10	0.041037	346
A8	0.010431	294	D4	0.048566	253	F11	0.040842	240
A9	0.031003	257	D5	0.032623	333	F12	0.026588	ND
A10	0.019455	ND	D6	0.047035	338	G2	0.044155	357
A11	0.027701	234	D7	0.041883	382	G3	0.036398	338
A12	0.040775	341	D8	0.048965	504	G4	0.036816	333
B2	0.05093	226	D09	0.035599	333	G5	0.049902	253
B3	0.037815	386	D10	0.049788	215	G6	0.045753	328
B4	0.045414	381	D11	0.036395	231	G7	0.050301	533
B5	0.04147	355	D12	0.03026	250	G8	0.050931	238
B6	0.035703	ND	E2	0.048069	380	G9	0.022237	404
B7	0.037388	369	E3	0.069781	533	G10	0.04783225	333
B8	0.045312	361	E4	0.04068	238	G11	0.033436	376
B9	0.048819	394	E5	0.046648	404	G12	0.032525	353
B10	0.037304	359	E6	0.042793	376	H2	0.0493355	271
B11	0.038293	271	E7	0.055548	452	H3	0.043257	318
B12	0.038174	ND	E8	0.034797	306	H4	0.047261	489
C2	0.049043	412	E9	0.04467	252	H5	0.0428235	327
C3	0.03438	295	E10	0.052444	362	H6	0.053141	398
C4	0.054489	348	E11	0.1484035	2525	H7	0.042104	293
C5	0.042188	243	E12	0.012674	ND	H8	0.040281	437
C6	0.045346	305	F2	0.047477	285	H9	0.04045225	324
C7	0.050528	327	F3	0.052858	382	H10	0.027603	450
C8	0.03624	303	F4	0.051316	504	H11	0.028498	317
						H12	0.019793	423

Table A2.2 Zone 12 raw data for duplicate *in situ* measurements. Pertains to *Section 4.4.1*.

Canberra 3" x 3" NaI detector (collimated)				
Duplicate	**Activity Concentration (Bq g^{-1})**			
Measurement location	**S1A1**	**S1A2**	**S2A1**	**S2A2**
B4	0.045315	0.045388	0.042592	0.048361
B8	0.051058	0.034729	0.048651	0.04681
C3	0.031419	0.039614	0.044928	0.03438
C11	0.052702	0.030343	0.055687	0.057811
E11	0.24756	0.27194	0.053744	0.02037
G10	0.042483	0.054586	0.040998	0.053262
H2	0.059282	0.043958	0.046247	0.047855
H5	0.043975	0.047695	0.041922	0.037702
H9	0.031704	0.048529	0.037505	0.044071

Exploranium 2" x 2" NaI detector (un-collimated)				
Duplicate	**Activity Concentration (raw counts)**			
Measurement location	**S1A1**	**S1A2**	**S2A1**	**S2A2**
B4	321	357	384	462
B8	434	378	334	297
C3	347	270	256	308
C11	465	394	284	357
D2	303	378	435	371
E11	2450	2424	2555	2672
G10	368	316	268	378
H5	260	272	486	291
H9	319	385	292	299

Table A2.3 Zone 12 raw data for *ex situ* measurements of soil samples, made in the on-site laboratory. Values for duplicate measurement locations have been averaged across all four measurements at each location. Pertains to *Section 4.4.2*.

	Laboratory measurement (Bq g^{-1})	
ID	**0-10cm**	**10-20cm**
A5T	0.03642	
B3T	0.04236	
B4T	0.043385	0.062
B8T	0.04053	0.0471525
B9T	0.04611	
C10T	0.05053	
C11T	0.0474525	0.072995
C3T	0.040085	0.0462475
D12T	0.04208	
D2T	0.0474725	0.0459325
D4T	0.04221	
D9T	0.03554	
E11T	0.098175	0.059695
E3T	0.04576	
E7T	0.05539	
G10T	0.0610175	0.3176775
G5T	0.03877	
G8T	0.05119	
H5T	0.047465	0.0401475
H7T	0.04221	
H9T	0.033145	0.033125

Table A2.4 Zone 12 raw data for duplicate *ex situ* measurements for both the 0-100 mm and the 100-200 mm soil layers. Pertains to *Section 4.4.1*.

***Ex situ* soil sample measurements 0-10cm**				
Duplicate	**Activity Concentration (Bq g^{-1})**			
Measurement location	**S1A1**	**S1A2**	**S2A1**	**S2A2**
B4T	0.03736	0.04054	0.04882	0.04682
B8T	0.04438	0.041	0.04282	0.03392
C3T	0.04473	0.0381	0.03598	0.04153
C11T	0.04776	0.04062	0.04973	0.0517
D2T	0.04695	0.04589	0.04733	0.04972
E11T	0.1752	0.1219	0.04667	0.04893
G10T	0.07368	0.06453	0.04987	0.05599
H5T	0.03699	0.04591	0.05763	0.04933
H9T	0.03046	0.02741	0.03896	0.03575

***Ex situ* soil sample measurements 10-20cm**				
Duplicate	**Activity Concentration (Bq g^{-1})**			
Measurement location	**S1A1**	**S1A2**	**S2A1**	**S2A2**
B4B	0.07513	0.07995	0.04339	0.04953
B8B	0.04891	0.04738	0.0478	0.04452
C3B	0.04798	0.0502	0.04646	0.04035
C11B	0.06599	0.06378	0.07111	0.0911
D2B	0.05347	0.04947	0.04239	0.0384
E11B	0.07225	0.0732	0.04392	0.04941
G10B	0.5603	0.5788	0.06179	0.06982
H5B	0.03274	0.03639	0.04901	0.04245
H9B	0.02556	0.02858	0.04588	0.03248

Table A2.5 Barrier 31 raw data for *in situ* measurements. Canberra detector measurements have been converted to mass activity concentrations using an ISOCS circular plane geometry definition of 25 m diameter and 0.2 m depth. Values for duplicate measurement locations have been averaged across all four measurements at each location. Pertains to *Section 4.4.2*.

ID	Canberra (Bq g^{-1})	ID	Canberra (Bq g^{-1})	ID	Canberra (Bq g^{-1})	ID	Canberra (Bq g^{-1})
0y2	0.49249	C4	0.92008	G6	0.24228	L4	0.63775
0y3	0.54856	C5	0.369038	G7	0.20068	L5	0.52817
0y4	0.42068	C6	0.3608	G8	0.18032	L6	0.48968
0y5	0.302903	C7	0.24276	H2	1.1145	L7	0.21754
0y6	0.23226	C8	0.14481	H3	0.76991	L8	0.16845
0y7	0.16108	D2	1.2446	H4	0.80975	M3	0.7025
0y8	0.14603	D3	1.3672	H5	0.41014	M4	0.3867
0z2	0.32395	D4	1.0105	H6	0.26137	M5	0.638893
0z3	0.66984	D5	0.51285	H7	0.20495	M6	0.31138
0z4	0.422728	D6	0.31833	H8	0.18056	M7	0.23774
0z5	0.31282	D7	0.2219	I2	0.97864	M8	0.19574
0z6	0.22538	D8	0.18643	I3	0.741093	N3	0.8309
0z7	0.098491	E2	1.0526	I4	0.71943	N4	0.36478
0z8	0.14128	E3	1.006	I5	0.43438	N5	0.39263
A2	0.45142	E4	0.87756	I6	0.28815	N6	0.54182
A3	0.93019	E5	0.17312	I7	0.17838	N7	0.5026
A4	0.72232	E6	0.2861	I8	0.14443	N8	0.2281
A5	0.18093	E7	0.21275	J2	0.919133	O3	0.35004
A6	0.27332	E8	0.20948	J3	1.0171	O4	0.23336
A7	0.058727	F2	0.91995	J4	0.64283	O5	0.295778
A8	0.10834	F3	0.88689	J5	0.40799	O6	0.38649
B2	0.49064	F4	0.93221	J6	0.28202	O7	0.46914
B3	1.3068	F5	0.45954	J7	0.16763	O8	0.2408
B4	0.73721	F6	0.28462	J8	0.16038	P3	0.85475
B5	0.36977	F7	0.20901	K3	0.80782	P4	0.19464
B6	0.29466	F8	0.20397	K4	0.66759	P5	0.18012
B7	0.12159	G2	0.6906	K5	0.43286	P6	0.22372
B8	0.111802	G3	0.87237	K6	0.32319	P7	0.36821
C2	1.3788	G4	0.971345	K7	0.20177	P8	0.31465
C3	1.9239	G5	0.42589	K8	0.16976	Q3	1.4193
				L3	0.68145	Q4	0.2196

Table A2.6 Barrier 31 raw data for *ex situ* measurements of soil samples, made in the on-site laboratory. Values for duplicate measurement locations have been averaged across all four measurements at each location. Pertains to *Section 4.4.2*.

	Activity concentration (Bq g^{-1})		
ID	**0-10cm**	**10-20cm**	**Mean (0-20cm)**
A2	0.134433	0.090077	0.112255
B8	0.030758	0.057598	0.044177917
C3	3.937	2.04	2.9885
C5	0.583625	0.39145	0.4875375
E3	0.9577	0.8309	0.8943
E5	0.29275	0.26605	0.2794
E6	0.1069	0.18035	0.143625
G4	0.839825	0.667075	0.75345
G8	0.49675	0.601325	0.5490375
H2	0.9716	0.75755	0.864575
H3	0.3439	0.18185	0.262875
H6	0.11665	0.13935	0.128
I3	0.70015	0.8146	0.757375
I5	0.4323	0.3557	0.394
J2	1.03575	1.08025	1.058
M5	0.740625	0.73345	0.7370375
N6	0.5948	0.34955	0.472175
P3	0.648675	0.547125	0.5979
Z3	0.396243	0.387885	0.39206375
Z7	0.080135	0.06577	0.0729525

Table A2.7 Barrier 31 raw data for duplicate measurements for the Canberra *in* situ detector, and the ex *situ* measurements for both the 0-100 mm and the 100-200 mm soil layers. Pertains to *Section 4.4.1*.

Canberra 3" x 3" NaI detector (collimated)				
Duplicate	**Activity Concentration (Bq g^{-1})**			
Measurement location	**S1A1**	**S1A2**	**S2A1**	**S2A2**
0y5	0.31453	0.29388	0.27331	0.32989
0z4	0.41627	0.43961	0.41598	0.41905
B8	0.1164	0.14691	0.045476	0.13842
C5	0.54827	0.53028	0.18563	0.21197
E5	0.18705	0.17974	0.16698	0.15871
G4	0.95259	0.97314	0.99587	0.96378
G8	0.17667	0.17885	0.18711	0.17865
I3	0.72095	0.75237	0.77012	0.72093
J2	0.91517	0.9416	0.91191	0.90785
L4	0.57989	0.59988	0.69199	0.67924
M5	0.61748	0.6184	0.66327	0.65642
O5	0.31469	0.32869	0.28262	0.25711

***Ex situ* soil sample measurements 0-10cm**				
Duplicate	**Activity Concentration (Bq g^{-1})**			
Measurement location	**S1A1**	**S1A2**	**S2A1**	**S2A2**
B8	0.02488	0.02246	0.03987	0.03387
C5	0.6756	0.6438	0.5006	0.5145
E5	0.2577	0.2553	0.3239	0.3341
G4	1.517	1.529	0.1508	0.1625
G8	0.1204	0.1334	0.8629	0.8703
I3	0.7618	0.7388	0.6605	0.6395
J2	1.088	0.955	1.064	1.036
M5	0.8043	0.7849	0.7007	0.6726

***Ex situ* soil sample measurements 0-20cm**				
Duplicate	**Activity Concentration (Bq g^{-1})**			
Measurement location	**S1A1**	**S1A2**	**S2A1**	**S2A2**
B8	0.04157	0.04257	0.07568	0.07057
C5	0.4762	0.4888	0.303	0.2978
E5	0.2401	0.2552	0.2791	0.2898
G4	1.244	1.194	0.1202	0.1101
G8	0.1588	0.1495	1.054	1.043
I3	0.9815	0.9367	0.6368	0.7034
J2	1.151	1.128	1.021	1.021
M5	0.5525	0.5504	0.8872	0.9437

Table A2.8 Barrier 31 raw data for measurement of shine. Measured activity concentrations shown were obtained with the collimated Canberra *in situ* detector placed on the trolley (height 920 mm) on top of four lead bricks of total thickness 60 mm, and which completely obscured the collimator aperture. Pertains to *Section 4.5.4*.

ID	Distance from centre silo (m)	Measured activity concentration (Bq g^{-1})
H2	7.8	0.32999
H3	9.1	0.32318
H4	10.4	0.29774
H5	11.7	0.23731
H7	14.3	*0.1135*
C2	9.5	0.21868
C3	10.5	0.19355
C4	11.6	0.20203
C5	12.8	0.17142
C6	14	0.14841
C7	15.2	0.11274
C8	16.5	0.10494

Appendix 3 (Figs A3.1 to A3.3) – Regressions from detector modelling experiments

These are additional regressions from the source/detector modelling experiments described in Chapter 5. All the data in the appendixes is also included on the enclosed data disk.

Detector height = 215 mm

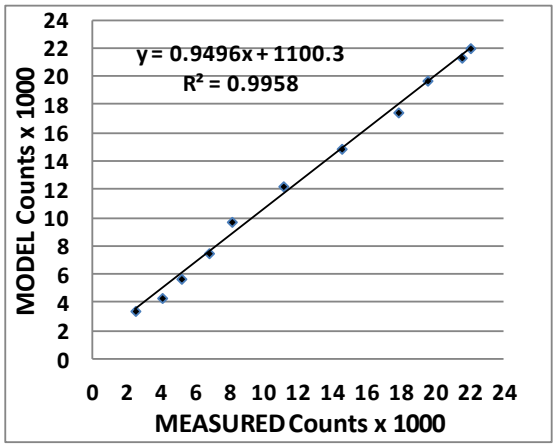

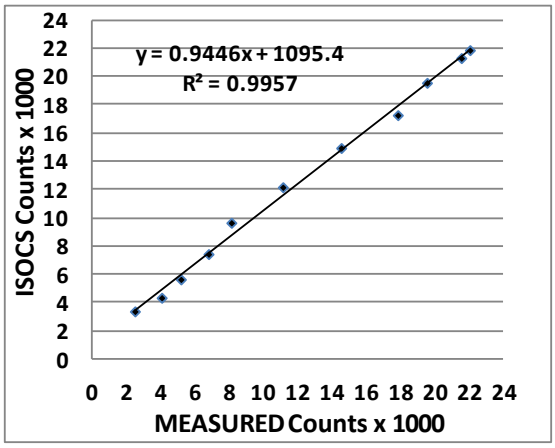

Detector height = 445 mm

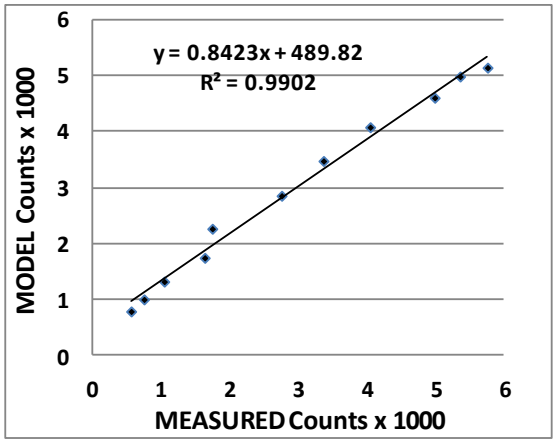

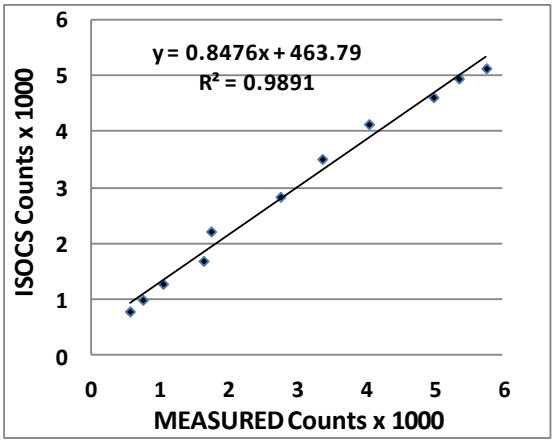

Detector height = 661 mm

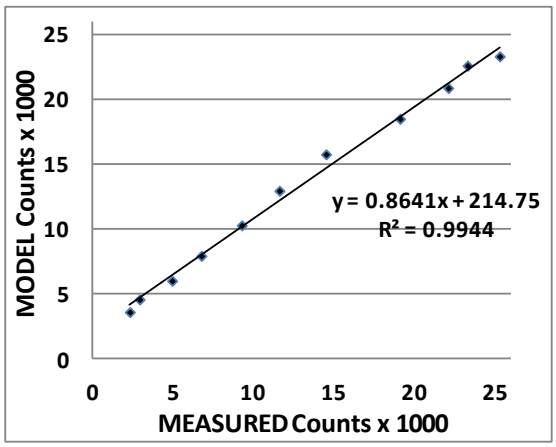

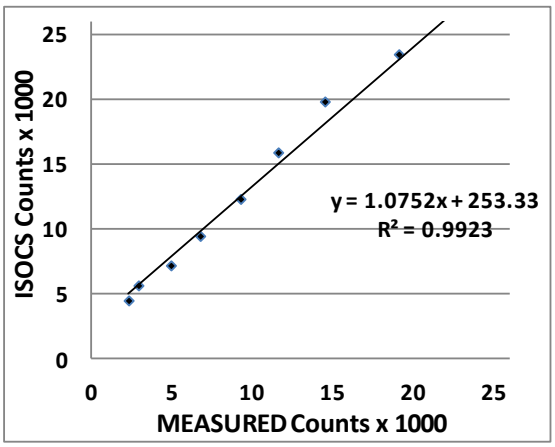

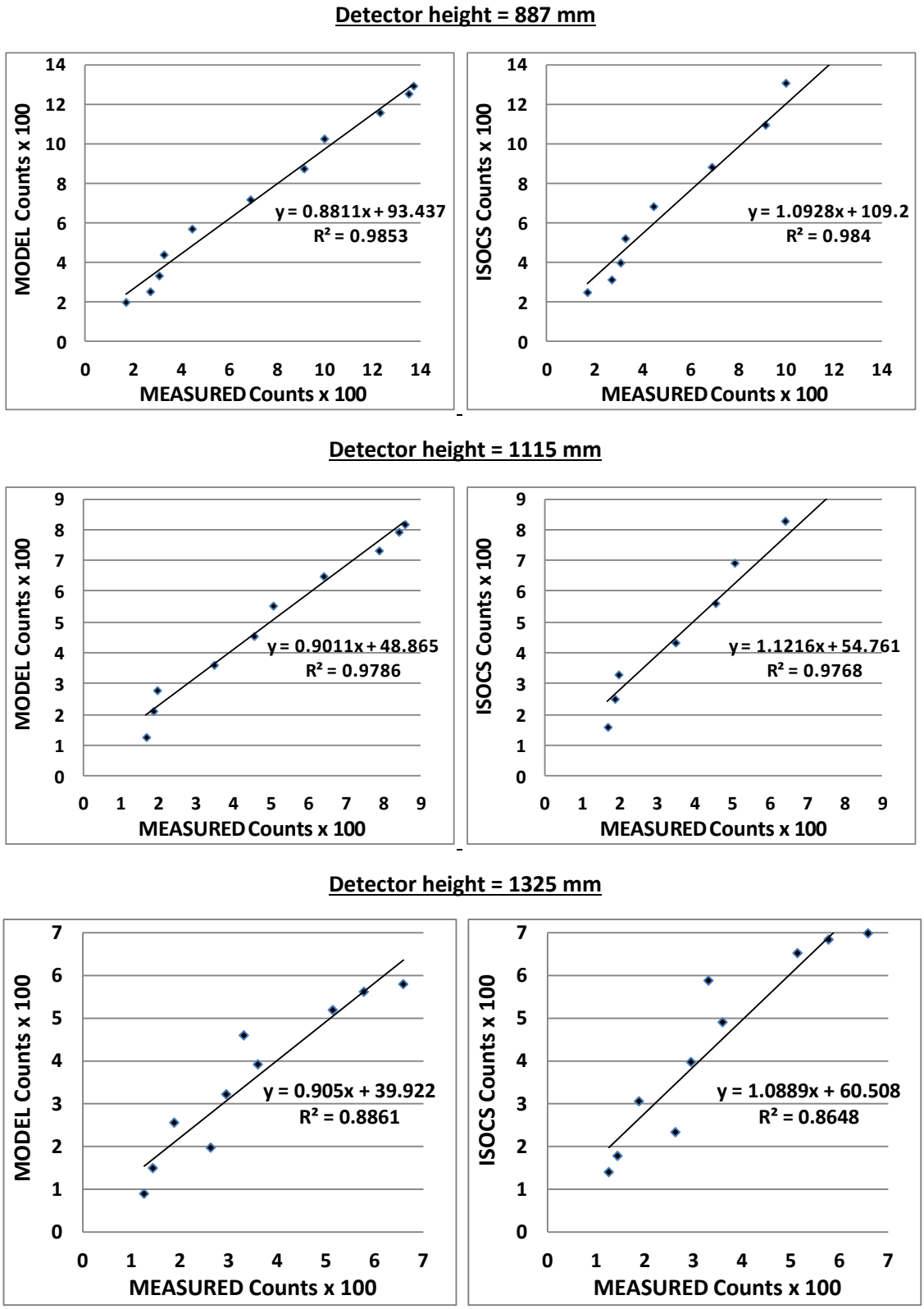

Fig A3.1 Regressions of counts predicted by the generic model (graphs on left) and ISOCS predicted counts (graphs on right) against measured counts, for increasing LATERAL OFFSET for different detector heights and with the source at zero depth.

Detector height = 215 mm, lateral offset = 0.0

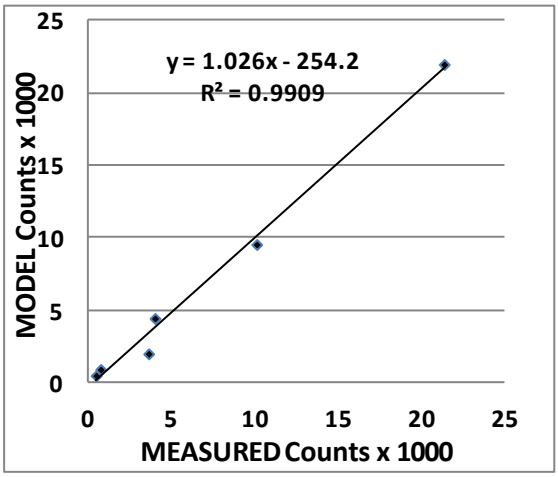

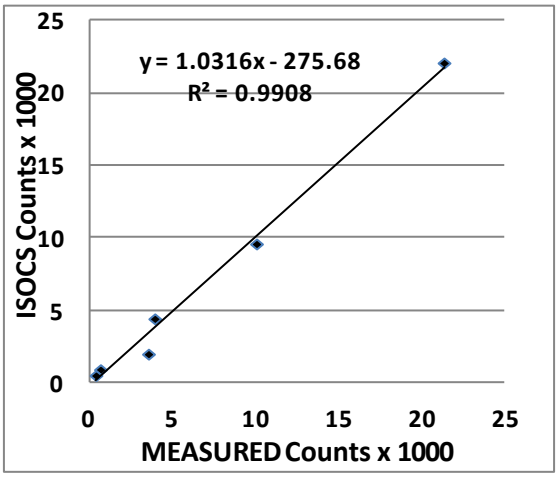

Detector height = 215 mm, lateral offset = 0.3

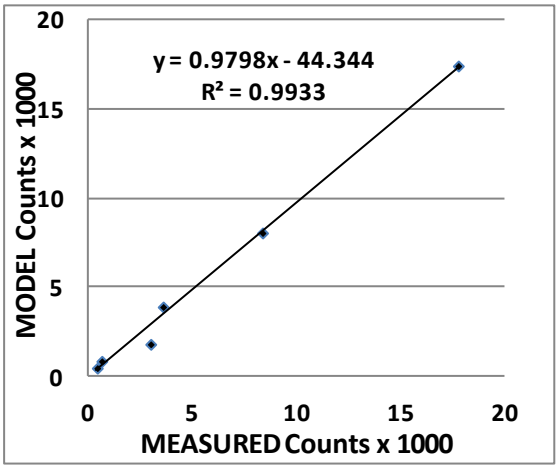

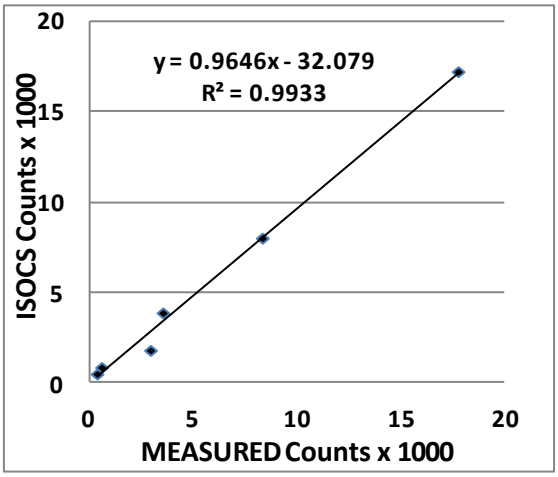

Detector height = 215 mm, lateral offset = 0.5

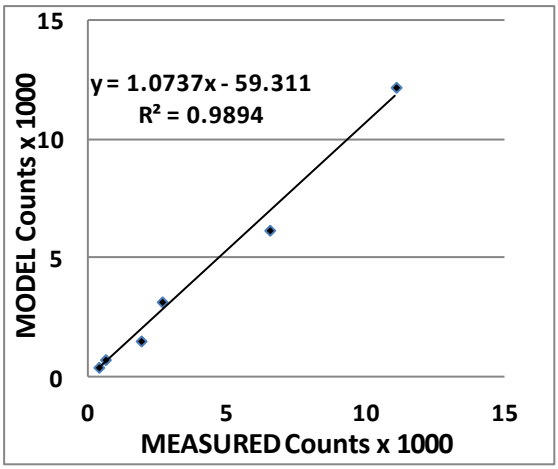

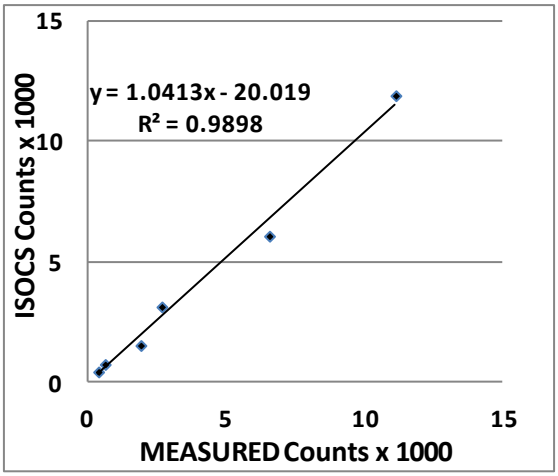

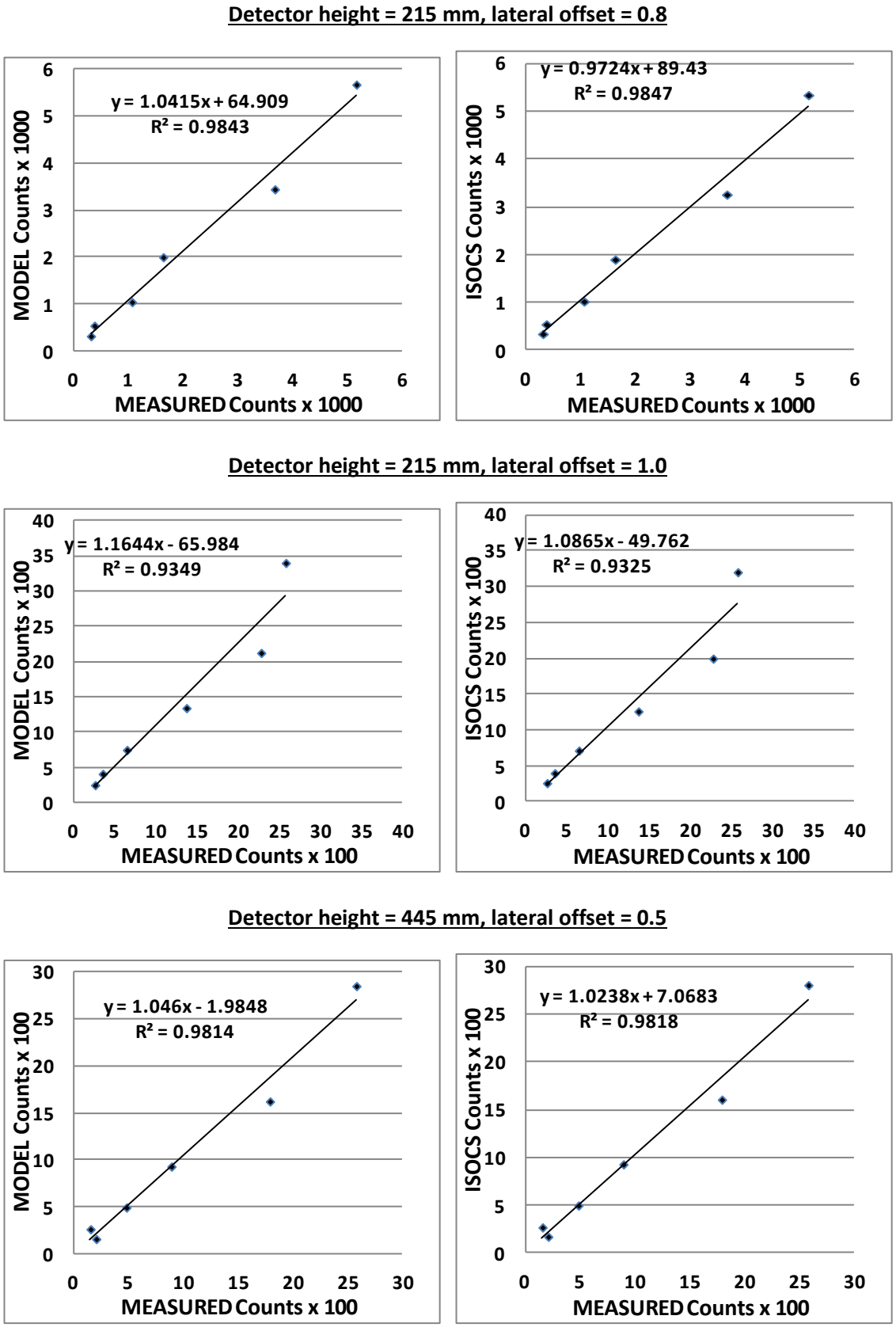

Fig A3.2 Regressions of counts predicted by the generic model (graphs on left) and ISOCS predicted counts (graphs on right) against measured counts, for increasing SOURCE DEPTH with fixed values of detector height and lateral offset.

Detector height = 215 mm, Source depth = 50 mm

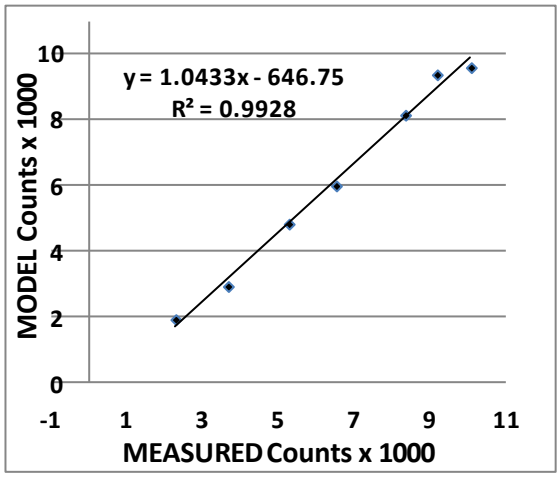

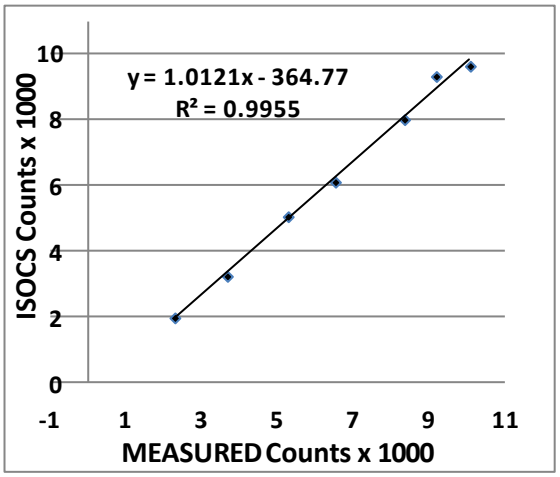

Detector height = 215 mm, Source depth = 100 mm

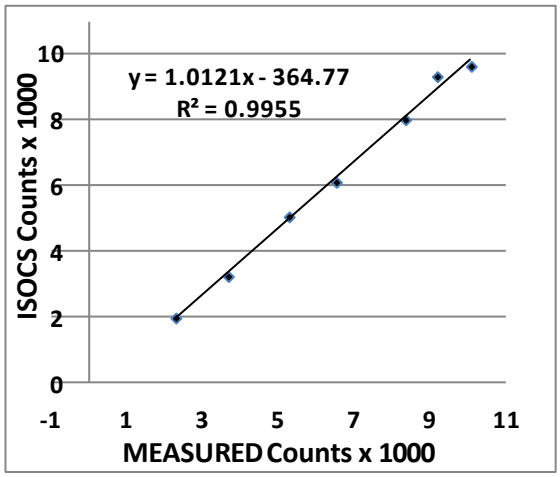

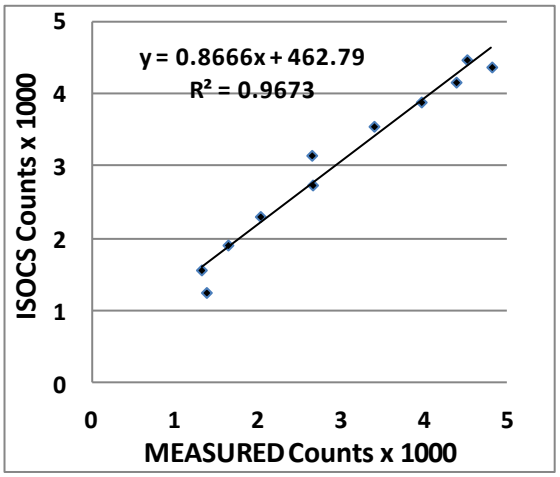

Detector height = 215 mm, Source depth = 150 mm

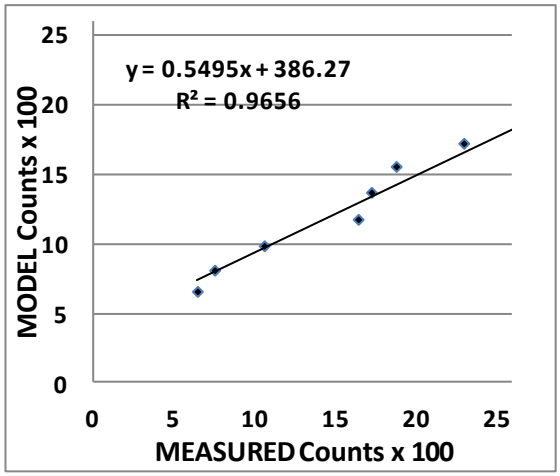

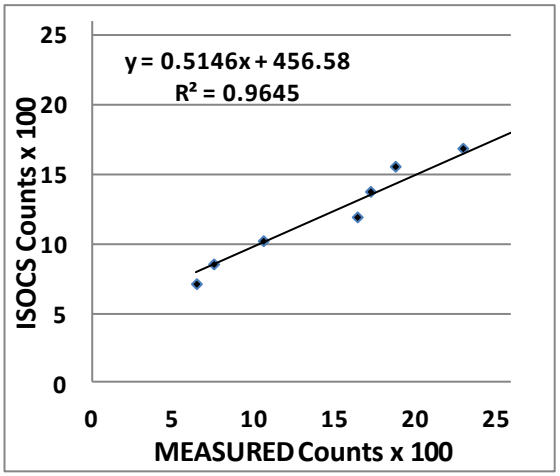

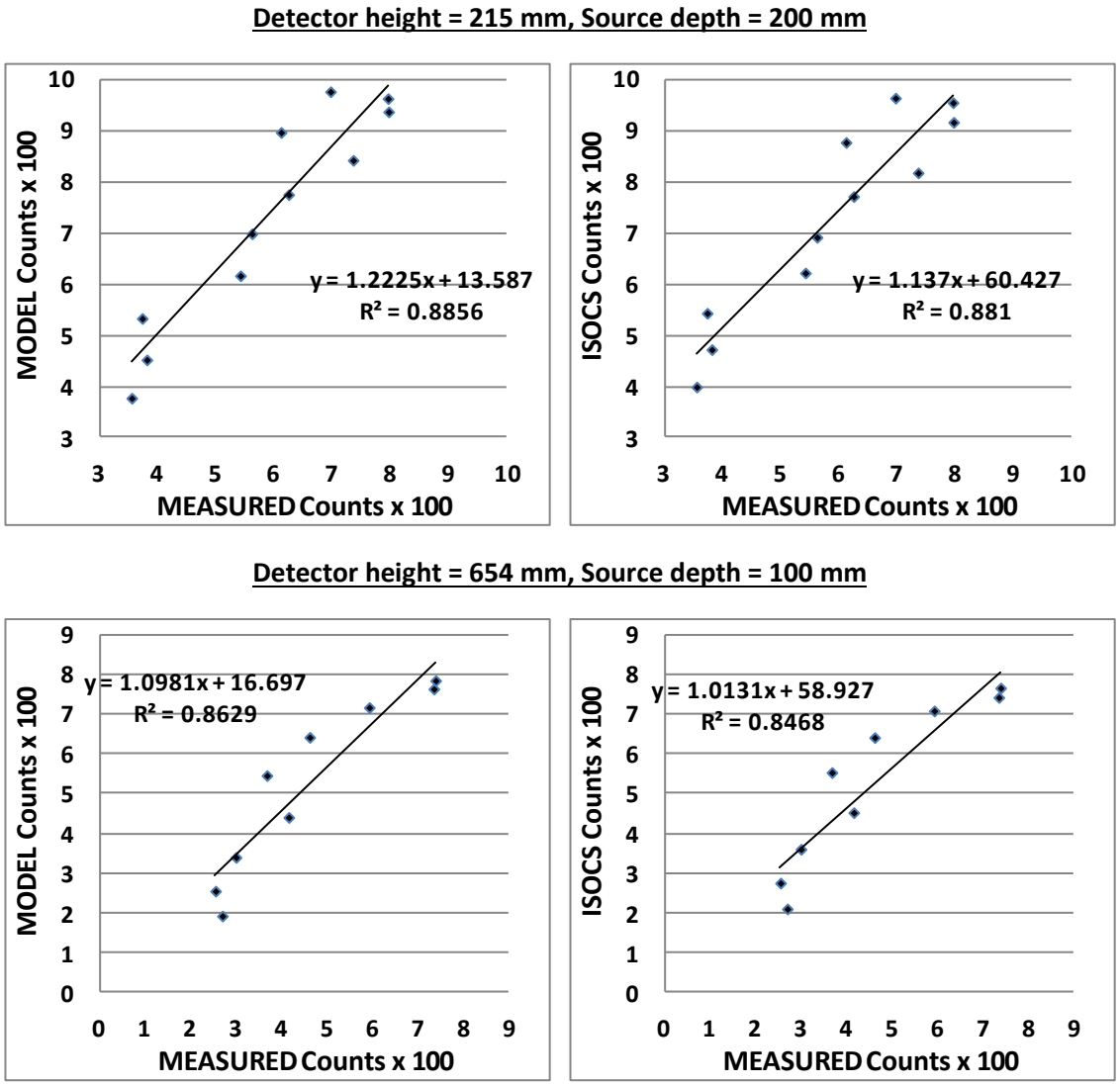

Fig A3.3 Regressions of counts predicted by the generic model (graphs on left) and ISOCS predicted counts (graphs on right) against measured counts, for increasing LATERAL OFFSET with fixed values of detector height, and with the source at a fixed depth beneath the ground surface.

Appendix 4 (Tables A4.1 to A4.3) - Raw data from the RMT experiments

See Chapter 7. All data in appendixes is also included on the enclosed data disk.

Table A4.1 West runway core (*ex situ*) measurements, showing GPS positions, depths, activities and uncertainties as reported by the external laboratory, including summary statistics. Pertains to *Section 7.4.4.*

Core ID	Easting	Northing	Depth (mm)	Activity conc Bq g^{-1}	Uncertainty Bq g^{-1}
WRW/C01	299172.113	966799.559	135	0.601	0.04
WRW/C02	299172.113	966802.059	98	0.546	0.043
WRW/C03	299172.113	966812.059	170	0.52	0.037
WRW/C04	299175.6485	966803.0945	115	0.856	0.053
WRW/C05	299179.1841	966806.6301	78	0.69	0.12
WRW/C06	299174.613	966799.559	120	0.638	0.042
WRW/C07	299179.613	966799.559	112	0.783	0.053
WRW/C08	299182.113	966799.559	100	0.691	0.048
WRW/C09	299184.613	966799.559	140	0.888	0.055
WRW/C10	299177.4163	966794.2557	60	0.962	0.061
WRW/C11	299179.1841	966792.4879	135	0.672	0.052
WRW/C12	299172.113	966797.059	140	0.828	0.052
WRW/C13	299172.113	966794.559	90	0.625	0.05
WRW/C14	299172.113	966787.059	140	0.632	0.044
WRW/C15	299170.3452	966797.7912	105	0.627	0.049
WRW/C16	299166.8097	966794.2557	98	0.643	0.051
WRW/C17	299167.113	966799.559	80	1.05	0.12
WRW/C18	299164.613	966799.559	112	0.739	0.051
WRW/C19	299168.5775	966803.0945	95	0.815	0.055
WRW/C20	299165.0419	966806.6301	100	0.762	0.048
		Mean	111.15	0.73	
		Standard Dev	26.38	0.14	
		Minimum	60	0.52	
		Maximum	170	1.05	
		Standard err		0.031	

Table A4.2 ANOVA of the five groups of *in situ* measurements from positions 1,3,9,14 and 21 (Fig 7.8), analysed using the 111 mm depth ISOCS model, and showing that there is no evidence of a significant difference between the mean measurements at each of the five locations ($p>0.05$). This suggests that the concrete area proposed as a RMT has no significant large-scale variation in ^{40}K activity. Pertains to *Section 7.4.4.*

Anova: Single Factor						
SUMMARY						
Position	*Count*	*Sum*	*Bq/g*	*Variance*		
1	10	5.54394	0.554394	0.000825		
3	10	5.48401	0.548401	0.001597		
14	10	5.6533	0.56533	0.001772		
21	10	5.81494	0.581494	0.000673		
9	10	5.59291	0.559291	0.000393		
ANOVA						
Source of Variation	*SS*	*df*	*MS*	*F*	*P-value*	*F crit*
Between Groups	0.00641	4	0.001602	1.522982	0.211607	2.578739
Within Groups	0.047349	45	0.001052			
Total	0.053759	49				

Table A4.3 *In situ* measurements of ^{40}K activity concentration with detector in position 01 (the centre point of the reference site) using an ISOCS circular plane model of diameter of 25 m, and two depths of 111 mm (the mean core depth) and 500 mm (the standard model depth). Pertains to *Section 7.4.4.*

Model dia=25000mm, **depth=111mm**			
In Situ ID	Activity conc Bq g^{-1}		Activity conc Bq g^{-1}
01-1	0.57445	Mean	**0.557**
01-2	0.57251	Stdev	0.032
01-3	0.55375	Min	0.483
01-4	0.58749	Max	0.587
01-5	0.52873	SE	0.0100
01-6	0.48338		
01-7	0.56625		
01-8	0.54622		
01-9	0.5872		
01-10	0.57251		

Model dia=25000mm, **depth=500mm**			
In Situ ID	Activity conc Bq g^{-1}		Activity conc Bq g^{-1}
01-1	0.49419	Mean	**0.495**
01-2	0.51434	Stdev	0.026
01-3	0.49337	Min	0.435
01-4	0.51747	Max	0.519
01-5	0.47643	SE	0.0081
01-6	0.43478		
01-7	0.5032		
01-8	0.48502		
01-9	0.51869		
01-10	0.51434		

Table A4.4 *In situ* measurements of ^{40}K activity concentrations at the four measurement positions at the periphery of the proposed RMT (Fig 7.8), using an ISOCS circular plane model of diameter of 25 m and a depth of 111 mm. Pertains to *Section 7.4.4.*

		Sampling location			
		03	09	14	21
Count sequence	1	0.60705	0.55205	0.57841	0.5824
	2	0.50641	0.55408	0.47635	0.58302
	3	0.52841	0.56968	0.58938	0.54841
	4	0.5855	0.58322	0.59775	0.54581
	5	0.56063	0.54324	0.51961	0.60958
	6	0.54895	0.52108	0.5708	0.59181
	7	0.57848	0.54887	0.53524	0.60559
	8	0.56656	0.55949	0.57699	0.55389
	9	0.52858	0.57595	0.60762	0.61909
	10	0.47344	0.58525	0.60115	0.57534

Appendix 5 – List of files on enclosed data disk.

INDEX OF FILES ON DATA DISK

File name	Description of content	Thesis section
A1.1	Original test data – input data to Test 1, Table A1.1	3.3.1
A1.2	Folder containing input data for Chapter 3 Test 2 (Not supplied in printed form)	3.3.2
A1.3	Visual Basic program for Chapter 3 Test 2	3.3.1, 3.4.2
A2.1	*In situ* measurements for Zone 12	4.4.2
A2.2	*In situ* duplicate measurements for Zone 12	4.4.1
A2.3	*Ex situ* measurements for Zone 12	4.4.2
A2.4	*Ex situ* duplicate measurements for Zone 12	4.4.1
A2.5	*In situ* measurements for Barrier 31	4.4.2
A2.6	*Ex situ* measurements for Barrier 31	4.4.2
A2.7	*In situ* and *ex situ* duplicate measurements for Barrier 31	4.4.1
A2.8	*In situ* shine measurements from Barrier 31	4.5.4
A3.1	Regressions of counts predicted by the generic model against measured counts, for increasing lateral offset with the source at zero depth	5.4.5
A3.2	Regressions of counts predicted by the generic model against measured counts, for increasing source depth with fixed lateral offset	5.4.5
A3.3	Regressions of counts predicted by the generic model against measured counts, for increasing lateral offset with the source at a fixed depth beneath the ground surface	5.4.5
A4.1	*Ex situ* measurements of K-40 activity from the RMT cores	7.4.4
A4.2	ANOVA of the five different sets of *in situ* measurements from the centre and circumference of the proposed RMT site	7.4.4
A4.3	*In situ* measurements of K-40 activity concentrations modelled for depths of 111 mm and 500 mm	7.4.4
A4.4	*In situ* measurements at the 4 points on the periphery of the proposed RMT site	7.4.4

Appendix 6 - List of presentations and publications

Presentations

1. Oral presentation: **"A simulation technique for the optimisation of contaminated land investigations"** at Society of Environmental Geochemistry and Health (SEGH), Dublin (2009). *Based on the conclusions of a final year undergraduate project, preparatory to the work presented in this thesis.*

2. Poster presentation **"In situ investigation of radioactively contaminated land"** at Society of Environmental Geochemistry and Health (SEGH), Galway (2010).

3. Oral presentation: "**Relative effectiveness of *in* situ and *ex* situ measurement methods for the characterisation of radioactively contaminated land"** at Society of Environmental Geochemistry and Health (SEGH), Edge Hill (2011).

4. Oral presentation: **"Comparison between measurement methods for the characterisation of radioactively contaminated land"** at the Workshop on Radiological Characterisation and Decommissioning, Studsvik, Sweden, 2012.

5. Oral presentation: **"Optimised investigation of radioactively contaminated land"** at the International Symposium on Environmental Geochemistry, Aveiro, Portugal, 2012.

Publications

1. Boon, K.A., Rostron, P., Ramsey, M.H. (2011) 'An Exploration of the Interplay between the Measurement Uncertainty and the Number of Samples in Contaminated Land Investigations'. *Geostandards and Geoanalytical Research,* **35, 3**, 353-367. *Based on the conclusions of a final year undergraduate project, preparatory to the work presented in this thesis.*

2. Rostron, P., Ramsey, M.H. (2012) "Cost effective, robust estimation of measurement uncertainty from sampling using unbalanced ANOVA, *Accreditation and Quality Assurance*, **17,** 7-14.

3. Rostron, P., Heathcote, J.A., Ramsey, M.H. (2012) 'Comparison between measurement methods for the characterisation of radioactively contaminated land', Workshop on Radiological Characterisation for Decommissioning, Page on OECD Nuclear Energy Website, URL: http://www.oecd-nea.org/rwm/wpdd/rcd-workshop/index.html

4. Rostron, P., Heathcote, J.A., Ramsey, M.H. (2013) 'Advantages of *in situ* over *ex situ* radioactivity measurements for the characterisation of land on a decommissioning nuclear site.' **Revision submitted to Journal of Environmental Radioactivity February 2013.**

5. Rostron, P., Heathcote, J.A., Ramsey, M.H. (submitted-a). 'Optimisation of *in situ* measurement strategies for the characterisation of radioactively contaminated land that includes the presence of small particles'. **Submitted to Journal of Radiological Protection June 2013.**

6. Rostron, P., Heathcote, J.A., Ramsey, M.H. (submitted-b). *In situ* detection of 'hot' particles by portable gamma-ray devices: modelling the effects of experimental parameters**. Submitted to Journal of Radiological Protection June 2013.**